Tuned Mass Dampers for Seismic Response Control of Building Structures: Toward Innovative Applications and Developments

同調質量ダンパーによる建築構造物の地震応答制御：

新たな応用と開発に向けた提案

Ping XIANG

項　平

February 2014
2014 年 02 月

Tuned Mass Dampers for Seismic Response Control of Building Structures:

Toward Innovative Applications and Developments

同調質量ダンパーによる建築構造物の地震応答制御：

新たな応用と開発に向けた提案

Ping XIANG

項　平

Waseda University

Graduate School of Creative Science and Engineering

Major in Architecture, Research on Structural Response Control

February 2014

ABSTRACT

In corporation with advanced technologies, how to conduct "response control" has become a very important issue in designing anti-seismic building structures. Structural response control aims at not only the earthquake resistance improvement, but also the comfort enhancement. Currently, vibration control can be mainly classified into three categories: active, semi-active and passive control. Active control could achieve the best control performance, but it requires external energy supply and sometimes lacks of reliability. Semi-active control utilizes the change of mechanical characteristics of a control device and does not require large external energy supply, and it has much less potential of injecting vibration energy to a structure. Passive control schemes are widely adopted in practice because of their relatively simple, maintenance-easy mechanisms that could reduce the seismic responses of structures with relative ease at low cost.

Widely recognized as one of the representative passive control schemes, tuned mass dampers (TMDs) have been regarded to be effective in mitigating structural vibrations under wind, harmonic excitations and human movements. However, the effectiveness of TMDs for seismic response control applications is still a topic of controversial discussion. The objective of this study is to present the optimal design frameworks for traditional and non-traditional TMDs for seismic response control and propose a novel multiple TMD floor system together with its optimum design schemes. The proposed design schemes for traditional and non-traditional TMDs aim at compensating the vulnerability of base-isolated buildings to large-amplitude, long-period and pulse-like ground motions. On the other hand, the proposed multiple TMD floor system is implemented into mid- or high-rise buildings to provide an innovative structural control scheme. This system would

bring about a large TMD mass ratio and exhibit less sensitive control performance to the natural frequency of a main oscillator.

This dissertation consists of six chapters.

In Chapter 1, the background of tuned systems for vibration control is firstly discussed, and then the motivation, objectives and scope of this study is stated. Pertinent works with respect to the design methods of traditional TMDs, new types of TMDs and large mass ratio TMD systems are reviewed.

In Chapter 2, a hybrid control strategy based on the combination of a traditional TMD and a semi-actively controlled variable slip-force level damper is proposed, and it is applied to a base-isolated structure. A general framework for the optimization design of traditional TMDs is presented and demonstrated to be validated for the heavily-damped primary system integrated with the variable slip-force level damper. Through the numerical simulations of the hybrid-controlled system under different types of ground excitations, the performance of the hybrid control strategy is demonstrated to be superior to TMD based passive control and VSFLD based semi-active control, especially for protecting the base-isolated structure from low-frequency resonance induced by long period ground motions.

A non-traditional TMD in which the dashpot is directly connected to the ground instead of the primary structure is studied in Chapters 3 and 4. It is adopted so as to mitigate the

seismic vibrations of base-isolated structures utilizing two different design criteria, respectively, in Chapters 3 and 4.

Chapter 3 proposes an optimum design method of non-traditional TMDs based on the criterion for obtaining wider suppression frequency bandwidths than traditional TMDs, since the fixed points theory assumption cannot provide the global minimum value of objective functions for the case of non-traditional TMD systems. Conducted numerical simulations demonstrate that, compared to the traditional TMD, the control effect of the optimally designed non-traditional TMD is significantly improved and furthermore the stroke length is greatly reduced, during long period earthquakes.

In Chapter 4, the stability maximization criterion for designing non-traditional TMD systems is discussed, and the largest degree of stability is achieved compared with the traditional TMDs designed by the quasi-fixed points theory and the stability maximization criterion, and non-traditional TMD based on the quasi-fixed points theory. It is demonstrated that non-traditional TMDs provide better performance than traditional TMDs via either the quasi-fixed points theory or the stability maximization criterion in terms of both the response of the primary structure and stroke length of TMD. The free vibration response of the primary structure decays the most quickly in the non-traditional TMD system designed by the stability maximization criterion. Though the non-traditional TMD attached system designed by the method proposed in Chapter 3 achieves the minimum values of the maximum relative displacement of the primary structure as well as the stroke length of the TMD, the stability maximization criterion is still recommended

as a design criterion because the required stiffness and damping coefficient are smaller than those designed by the method proposed in Chapter 3.

In Chapter 5, a new vibration control system with multiple TMD floors integrated is proposed for mid- or high-rise buildings. This system takes advantages of both the benefits of floor isolation systems and multiple TMDs, in which both of the absolute accelerations of floors and inter-storey drift displacements of storeys are significantly mitigated. Since the floor components themselves serve as TMDs in this scheme, the system does not need any additional masses for TMDs, but achieves larger mass ratios than a common TMD system. To validate the effectiveness of the TMD floor system, a shaking table test on a small-scaled frame model has been carried out. Numerical simulation conducted to reproduce the experimental result has also been carried out. The obtained numerically-simulated results agree with the scale model experimental results with favorable accuracy. Moreover, the problem of selecting the optimum locations of TMD floors, if not all the floors can serve as TMDs, has also been investigated by employing the so-called multimode approach. All the performance of the TMD floor systems designed based upon H_∞, H_2 and stability maximization criteria has been demonstrated to be effective for different types of seismic excitations, indicating that the proposed TMD floor system has a great potential of achieving very satisfactory, innovative vibration control effect for building structures. The comparison of the performance based on the employed design criteria indicates that the TMD floor system designed via the stability maximization criterion can achieve smaller stroke lengths of TMD floors and quicker decay of free vibrations than the system designed via H_∞ or H_2

criterion.

Chapter 6 lists some of the important conclusions drawn from the present research.

NOMENCLATURE

Symbols Nomenclature

$\mathbf{A}_g$ steady-state amplitude of harmonic acceleration excitation

B_A^* suppression bandwidth for traditional tuned mass damper system

B_B^* suppression bandwidth for non-traditional tuned mass damper system

$\mathbf{C}$ damping matrix

$\mathbf{E}$ unit vector

F_D dynamic friction force

F_e external force

F_S static friction force

$\mathbf{G}$ dynamic flexibility matrix

$\mathbf{H}$ transfer function vector

H_{As} frequency response function of absolute accelerarion of structure

H_{Xb} frequency response function of deformation of base isolators

H_{Xs} frequency response function of relative displacement of structure

$\mathbf{I}$ identity matrix

J objective function

$\mathbf{K}$ stiffness matrix

$\mathbf{M}$ mass matrix

M_s lumped mass of primary structure

M_n lumped mass of n-th storey

$\mathbf{P}_i$ Lagrange's interpolation polynomial

Q_d non-linear damping force of variable slip-force level damper

T_{is}	fundamental natural period of base-isolated structure
T_s	fundamental natural period of superstructure
$\mathbf{X}_s$	steady-state amplitude of relative displacement for primary structure
$\mathbf{X}_T$	steady-state amplitude of relative displacement for tuned mass damper
a_b	absolute acceleration of base isolation layer
a_g	ground motion acceleration
a_s	absolute acceleration of superstructure
a_T	absolute acceleration of tuned mass damper
c_{deq}	equivalent linear viscous damping coefficient of damper
c_{is}	linear viscous damping coefficient of base isolators
c_s	linear viscous damping coefficient of primary structure
c_T	linear viscous damping coefficient of tuned mass damper
c_{Tf}	equivalent linear viscous damping coefficient of friction
c_{Td}	linear viscous damping coefficient of airpot dashpot
d_b	deformation of base isolators
d_s	displacement of superstructure relative to base isolation layer
d_T	stroke length of tuned mass damper
$\mathbf{e}_i$	mass matrix normalized eigenvector corresponding to i-th eigenvalue
k	stiffness of coil extension spring
k_d	linear stiffness of damper

k_{deq}	equivalent linear stiffness of damper
k_{is}	linear stiffness of base isolators
k_{s}	linear stiffness of primary structure
k_{seq}	equivalent linear stiffness of system
k_{T}	linear stiffness of tuned mass damper
l_{0}	original length of coil extension spring
m_{b}	lumped mass of base isolation layer
m_{s}	lumped mass of structure
m_{T}	lumped mass of tuned mass damper
$\mathbf{q}_i$	displacement eigenvector corresponding to i-th eigenvalue
r	circular frequency ratio of harmonic excitation to primary structure
$\mathbf{r}_i$	participation vector corresponding to i-th eigenvalue
s	Laplace operator
t	dimension time
u	scalar-input
v	velocity of TMD floor relative to primary structure
$\mathbf{v}$	eigenvector
$\mathbf{x}$	relative displacement vector or state vector
$\dot{\mathbf{x}}$	relative velocity vector
$\ddot{\mathbf{x}}$	relative acceleration vector
x_{1abs}	absolute displacement of primary structure
$\dot{x}_{1abs}$	absolute velocity of primary structure

$\ddot{x}_{1\mathrm{abs}}$	absolute acceleration of primary structure
x_{b}	deformation of base isolators
$\dot{x}_{\mathrm{b}}$	velocity of base isolators relative to ground
$\ddot{x}_{\mathrm{b}}$	acceleration of base isolators relative to ground
x_{g}	ground displacement input
$\dot{x}_{\mathrm{g}}$	ground velocity input
$\ddot{x}_{\mathrm{g}}$	ground acceleration input
x_{m}	relative displacement amplitude of steady-state resonant vibration
x_{s}	displacement of primary structure relative to ground
x_{st}	statical deflection of primary structure
$\dot{x}_{\mathrm{s}}$	velocity of primary structure relative to ground
$\ddot{x}_{\mathrm{s}}$	acceleration of primary structure relative to ground
x_{T}	displacement of tuned mass damper relative to ground
$\dot{x}_{\mathrm{T}}$	velocity of tuned mass damper relative to ground
$\ddot{x}_{\mathrm{T}}$	acceleration of tuned mass damper relative to ground
x_{y}	elastic limit displacement or yielding displacement
z	product of υ and ζ_{T}
Δl	initial tensile length of coil extension spring
Δt	sampling time
Λ	degree of stability

α ratio of k_{d} to k_{seq}

β one parameter in Newmark-β method

β_i opposite value of real part of i-th eigenvalue or i-th participation factor

γ one parameter in Newmark-β method

ζ_{eq} equivalent damping ratio of system

ζ_{eqr} equivalent damping ratio of system for resonant case

ζ_{is} damping ratio of base isolators

ζ_{s} damping ratio of primary structure

ζ_{T} damping ratio of tuned mass damper

$\zeta_{\mathrm{T}}^{\mathrm{opt}}$ optimal damping ratio of tuned mass damper

η ductility factor

θ_i absolute value of imaginary part of i-th eigenvalue

λ_i i-th eigenvalue of system

μ mass ratio of tuned mass damper to primary structure

τ dimensionless time

υ tuning ratio

υ^{opt} optimal tuning ratio

ω circular frequency of harmonic excitation

ω_{l} fundamental natural circular frequency of base-isolated structure or uncontrolled building

ω_i i-th resonant frequency

$\bar{\omega}_i$ i-th anti-resonance frequency

$\hat{\omega}_i$ i-th new resonant frequency

ω_s fundamental natural circular frequency of primary structure

ω_{seq} equivalent natural circular frequency of system

ω_T natural circular frequency of tuned mass damper

Math Symbols Nomenclature
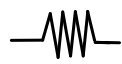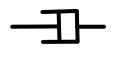
[ ]   Matrix

{ }   Vector

j imaginary unit

Acronyms Nomenclature

Acc.   absolute acceleration

Disp.   displacement

DOF   degree-of-freedom

DVA   dynamic vibration absorber

FIS   floor isolation system

FRF   frequency response function

GA   genetic algorithm

LC   location candidate

LQG   Linear Quadratic Gaussian

Max   maximum value

MDOF   multi-degree-of-freedom

MTMDs	multiple-tuned mass dampers
OL	optimal location
PGA	peak ground acceleration
QFPT	quasi-fixed points theory
RMS	root mean square
SDOF	single-degree-of-freedom
SMC	stability maximization criterion
STMD	single-tuned mass damper
TLCD	tuned liquid column damper
TLD	tuned liquid damper
TMD	tuned mass damper
TMDFS	tuned mass damper floor system
VD	viscous damper
VED	visco-elastic damper
VSFLD	variable slip-force level damper
WSB	wide suppression bandwidth
w/	with
w/o	without

Graphic Symbols Nomenclature

	linear spring
	linear viscous damper
	variable slip-force level damper

OPERATIONS

| | | magnitude or absolute value

$| \; |_2$ | 2-norm value

Re( ) | real part

sgn( ) | signum function

$\tilde{x}$ | x in dimensionless time domain

$\dot{x}$ | derivative of x with respect to dimension time t

$\tilde{\dot{x}}$ | derivative of x with respect to dimensionless time τ

$\mathbf{x}^{\mathrm{T}}$ | conjugate transpose of a matrix or vector $\mathbf{x}$

TABLE OF CONTENTS

1. INTRODUCTION

1.1 Tuned Systems for Vibration Control

Seismic vibration control of structures is a relatively new research field in civil engineering. It aims at not only the earthquake resistance improvement, but also the comfort enhancement. Currently, vibration control can be classified into four categories: active control, semi-active control, passive control and hybrid control. Active control could achieve the best control performance, but it requires external energy supply and sometimes lacks of reliability, and thus it is not very widely applied in the world. Semi-active control utilizes the change of mechanical characteristics of a control device and does not require large external energy supply, and it has much less potential of integrating vibration energy to a structure. Passive control schemes are widely adopted in practice because of their simplicity and reliability, which generally include two groups: passive dampers and tuned systems. Hybrid control is the combination of at least two of the above control schemes, which can take advantages of the benefits of multiple control schemes. In this section tuned systems are discussed, which comprise tuned mass dampers, tuned liquid dampers and tuned liquid column dampers, etc.

1.1.1 Tuned mass dampers

A tuned mass damper (TMD) is one of the simplest and most reliable structural control devices in terms of reducing the resonant vibration of a primary structure. A TMD is also named as a dynamic vibration absorber (DVA) in many literatures. Frahm (1911) firstly proposed the un-damped tuned mass system, in which a secondary oscillator is attached

to an un-damped primary oscillator by a linear spring with its frequency tuned to the natural frequency of the primary oscillator, as shown in Figure 1.1.
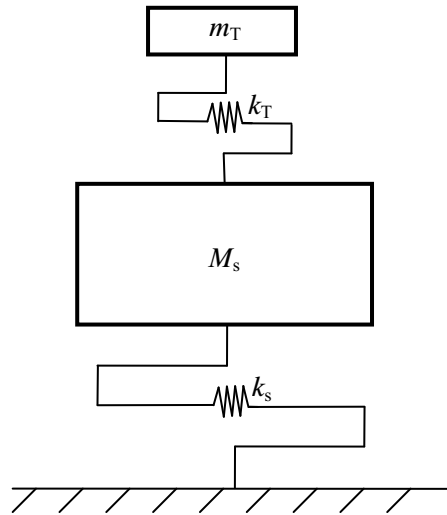

Figure 1.1 Un-damped linear TMD attached to un-damped linear primary structure

The vibration response of the primary structure at the natural frequency is reduced to zero (anti-resonance of the tuned mass system), while resonances occur at the two new resonant frequencies lying in the left-hand and right-hand side neighborhood of the anti-resonance frequency. The magnitude of a frequency response function (FRF) is presented in Figure 1.2. It can be found from the figure that the vibration magnitude of the primary structure will be significantly amplified with an un-damped TMD if the input frequency is not close to the natural frequency of the primary structure, or if the natural frequency of the primary structure fluctuates. This phenomenon implies the tuned mass system lacks of frequency robustness and its effectiveness is limited. For the purpose of reducing the responses at the two new resonant frequencies, as shown in Figure 1.3, an energy dissipation damper connected between the secondary and primary oscillators is

supplemented in the tuned mass system by Ormondroyd and Den Hartog (1928), while at the expense of increasing the response at the anti-resonance frequency as referring to Figure 1.4. This system is referred to as a traditional TMD system in this study. When the primary structure is subjected to external excitations, the attached TMD is excited and the kinetic energy is transferred from the primary structure to the TMD, and then the transferred energy is dissipated by the damping device. Traditional TMDs usually exhibit large stroke length.
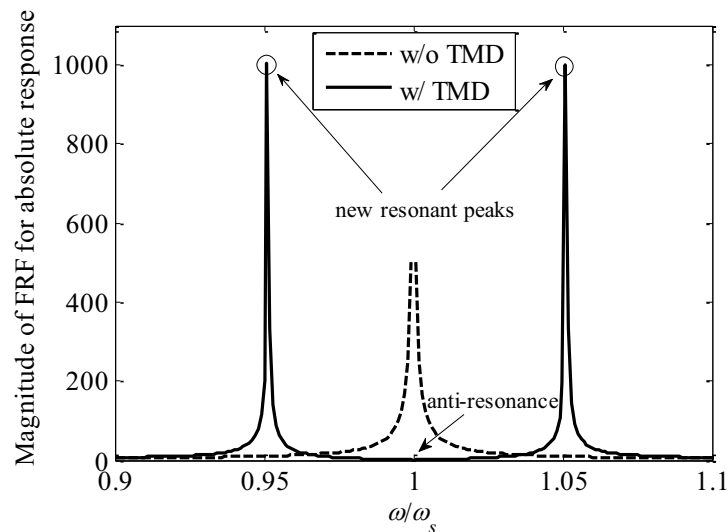

Figure 1.2 FRF magnitudes for un-damped SDOF primary structure w/ and w/o TMD
(TMD mass ratio of 0.01, un-damped TMD with $\omega_T = \omega_s$)

TMDs have been mainly applied to mechanical systems, and have also been implemented in high-rise building structures primarily for reducing wind-induced vibrations. Several examples are as follows (Lee *et al.*, 2006). Two TMDs of each weigh 2700 kN consisting of a lead-filled steel box have been installed in the 60-storey John Hancock Tower in Boston for reducing wind gust induced vibration. A concrete mass block of 3660 kN has been implemented in the 279-metre high Citicorp Center building in Manhattan as a TMD for mitigating the building sway amplitude. Two lead dampers are utilized for
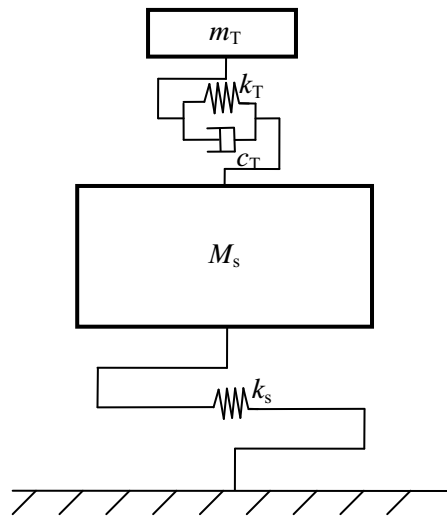
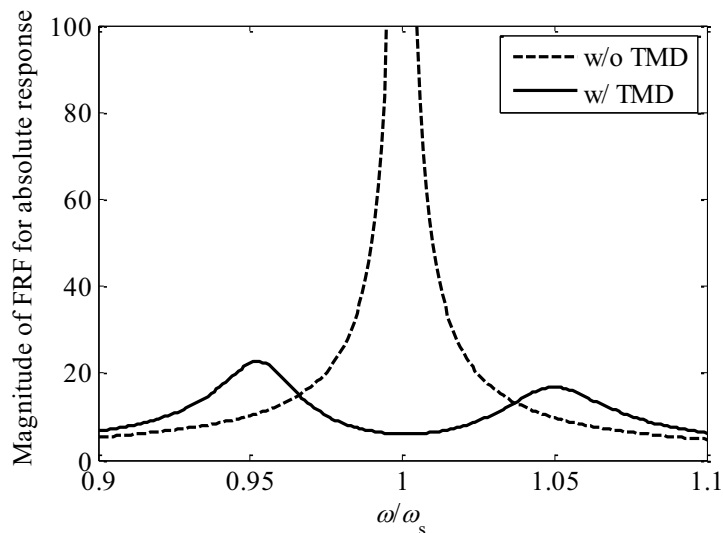Figure 1.3 Damped linear TMD attached to un-damped linear primary structure

Figure 1.4 FRF magnitudes for un-damped SDOF primary structure w/ and w/o TMD
(TMD mass ratio of 0.01, damped TMD with damping ratio of 0.03 and $\omega_T = \omega_s$)

preventing the deflection of antenna which is on the top of the 535-metre high Canadian National Tower in Toronto. Chiba Port Tower is the first tower equipped with a TMD for increasing the first modal damping in both the x and y directions in Japan. The aforementioned TMDs are all classified into the translational TMDs. Pendulum TMDs are of another typical type. Air cooling and heating ice thermal storage tanks are used as

4

pendulum TMDs in the Crystal Tower in Osaka, Japan for mitigating wind-induced vibration. A 6600 kN TMD system is installed in the 508-metre high Taipei 101 tower for reducing the effects of wind-induced vibration and withstanding forces in a 2500-year recurrence interval seismic event.

1.1.2 Tuned liquid dampers

Tuned liquid dampers (TLDs) are also a typical tuned system, in which a rigid tank contained with shallow liquid is utilized instead of steel, concrete or lead blocks of TMD systems. The sloshing motion absorbs the energy and viscous characteristic of the liquid dissipates it in a TLD system. The frequencies of TLDs can be adjusted by changing the dimensions of the tanks. The effects of TLDs on the responses of structures subjected to excitations are not as well understood as TMDs because of the complexity of liquid sloshing motions. The studies of TLD systems have been carried out by some researchers (Sun *et al.*, 1989; Fujino *et al.*, 1992; Wakahara *et al.*, 1992; Banerji *et al.*, 2000). TLDs have been implemented in the Shin Yokohama Prince Hotel and the control tower at the Narita Airport in Japan (Tamura *et al.*, 1992).

1.1.3 Tuned liquid column dampers

Tuned liquid column dampers (TLCDs) utilize U-tube-like containers with liquid filled, which are attached rigidly to structures. Liquid moves through the orifice in the tube and dissipates energy. The frequency and damping of a TLCD can be adjusted by changing the liquid column length and the orifice opening, respectively. In a tall building, the container can be used as the water supply. Studies on TLCDs were carried out by some

researchers (Sakai and Takaeda, 1989; Xu *et al.*, 1992; Abe *et al.*, 1996; Gao *et al.*, 1997; Sadek *et al.*, 1998; Yalla and Kareem, 2000). TLCDs have been implemented in the deck of the Higashi Kobe cable stayed bridge in Japan.

1.2 Research Motivation, Objectives, and Scope

The number of base-isolated structures has significantly increased in Japan since the 1995 Kobe earthquake at a speed of more than 150 buildings per year (Pan *et al.*, 2005). Base isolation systems are very effective in reducing the responses of buildings, while the base isolation layer itself undergoes a relatively large displacement when subjected to large-amplitude, long period, and pulse-like ground motions, i.e., near-field motions in the forward directivity (Wongprasert and Symans, 2005). Possible damage can be induced, e.g., collision with the surrounding retaining walls, which remains not fully resolved (Pan *et al.*, 2005). High damping devices are incorporated in base isolation systems for reducing large deformation of isolation layers, while at the expense of increasing inter-storey drifts and floor accelerations of superstructures (Kelly, 1999).

For the last decade, it has been frequently warned that high-rise buildings would exhibit long-lasting vibrations due to the effect of resonances under the excitations of long period earthquake ground motion. At the occasion of the occurrence of the 3.11 earthquake at the Tohoku (north-east) area in Japan in the year of 2011, unfortunately or rather anticipatorily, the phenomena of long-lasting vibrations were recognized in quite a few high-rise buildings which were far away from the Tohoku area. A piece of TV news

6

visually reported how one of the high-rise buildings in Tokyo exhibited several-minute lasting vibration responding to the seismic wave propagated a long distance from the epicenter. Installing auxiliary damping devices is an efficient strategy to resolve tall building motion problems (Ali and Moon, 2007). Simple passive dampers, such as viscous, friction or viscoelastic dampers, rely on relative motions between the two components they are mounted to dissipate vibration energy. As the major component of the deformation associated with the fundamental mode of high-rise buildings is the bending deformation, damping devices utilizing shear deformation would not be very effective.

TMDs have been verified to be effective in mitigating structural vibrations under wind excitations (McNamara, 1977; Luft, 1979; Kwok and MacDonald, 1990), harmonic excitations (Den Hartog, 1956) and human movements (Setareh and Hanson, 1992). However, the effectiveness of TMDs for seismic applications is still a topic of controversial discussion. Some researchers reported TMDs are not effective for seismic vibration mitigation (Kaynia *et al.*, 1981; Sladek and Klingner, 1983; Lee *et al.*, 2012), while some researchers held the opposite opinion (Wirsching, 1974; Jagadish *et al.*, 1979; Pinkaew *et al.*, 2003; Hoang *et al.*, 2008).

The objective of this study is to formulate frameworks for the optimal design of TMDs and propose innovative structural control schemes of applying TMDs to mitigating vibrations of base-isolated buildings and high-rise buildings, which are vulnerable to different types of long period ground motions, such as some famous earthquakes, Landers

(1992), Northridge (1994), Kobe (1995), and Chi-Chi (1999), characterized by pulse-type wave shape, long pulse period, abundant long period components, high ratio of peak ground velocity to peak ground acceleration, or large permanent ground displacement (Li *et al.* 2007; Makris 1997), due to resonant behaviors (Heaton *et al.* 1995; Takewaki *et al.* 2011; Ribakov 2010).

1.3 Literature Review of Pertinent Works

1.3.1 Design methods of tuned mass dampers

The design parameters of a TMD system are tuning ratio υ (frequency ratio of the natural frequency of TMD to the dominant natural frequency of a primary structure) and damping ratio ζ_T (the ratio of TMD's damping coefficient to its critical damping coefficient). They need to be optimally designed so as to obtain the best control effect. Design methods of TMDs in the literature can be generally classified into two main categories: one is based on approximate or exact algebraic design formulae; and the other is to use numerical searching methods.

(1) Algebraic design formulae

The formulae for TMDs are only available to the cases in which the primary structure is simplified as a single-degree-of-freedom (SDOF) structure. The most famous formulae were derived originally by Hahnkamm (1932) and Brock (1946), which are presented in a well-known textbook *Mechanical Vibrations* by Den Hartog (1956). The derivation

method is called the fixed points theory. For an un-damped SDOF primary structure, the FRFs pass through two fixed or invariant points which are independent of the damping ratio of a TMD. The optimal tuning ratio, υ^{opt}, is obtained by making the magnitudes of the two fixed points equal to each other, and then two damping ratios which make the FRF curve pass through the two fixed points with a horizontal tangent can be derived. The root mean square (RMS) value of the two possible damping ratios is taken to be the optimal damping ratio, $\zeta_{\mathrm{T}}^{\mathrm{opt}}$. The optimum parameters are formulated as:

$$\upsilon^{\mathrm{opt}} = \frac{1}{1+\mu} \tag{1.1}$$

$$\zeta_{\mathrm{T}}^{\mathrm{opt}} = \sqrt{\frac{3\mu}{8(1+\mu)}} \tag{1.2}$$

where μ is the mass ratio of the TMD to the primary structure.

The above formulae are derived with the performance index set as the maximum value of the dimensionless FRF magnitude ratio of the primary structure's absolute displacement, x_{1abs}, to the statical deflection, x_{st}, in the case of a force excitation, i.e., $\left| x_{\mathrm{1abs}} / x_{\mathrm{st}} \right|$. For un-damped SDOF primary structure systems, the fixed points theory formulae are also applicable to the optimum design of TMDs for ground motion excitations if the performance index is set as the maximum value of the dimensionless FRF magnitude ratio of the primary structure's absolute response to the ground input, i.e., $\left| x_{\mathrm{1abs}} / x_{\mathrm{g}} \right|$, or $\left| \dot{x}_{\mathrm{1abs}} / \dot{x}_{\mathrm{g}} \right|$, or $\left| \ddot{x}_{\mathrm{1abs}} / \ddot{x}_{\mathrm{g}} \right|$ (x_{1abs}, $\dot{x}_{\mathrm{1abs}}$, and $\ddot{x}_{\mathrm{1abs}}$ respectively denote the absolute

displacement, velocity and acceleration of the primary structure, and x_{g}, $\dot{x}_{\mathrm{g}}$, and $\ddot{x}_{\mathrm{g}}$ represent the ground displacement, velocity and acceleration, respectively), because the formulae of the FRF magnitude ratios are the same both for the force excitation and ground motion excitation cases. Following the procedure of the fixed points theory, Warburton (1982) derived the optimum parameter design formulae for the cases with various combinations of excitation and performance indices. For instance, Equations (1.3) and (1.4) are the design formulae for a TMD system subjected to a ground motion excitation, and the performance index is set as the maximum FRF magnitude of the relative displacement of the un-damped SDOF primary structure with respect to the ground acceleration.

$$\upsilon^{\mathrm{opt}} = \frac{\sqrt{1-\mu/2}}{1+\mu} \tag{1.3}$$

$$\zeta_{\mathrm{T}}^{\mathrm{opt}} = \sqrt{\frac{3\mu}{8(1+\mu)(1-\mu/2)}} \tag{1.4}$$

For a damped primary structure, the fixed points theory is not applicable, because the two fixed or invariant points do not exist anymore. The quasi-fixed points theory, which is constructed by regarding as if the two fixed points still existed for lightly or even moderately damped primary structures, was employed by Ghosh and Basu (2007), and a closed-form formula for the optimum tuning ratio of a TMD has been derived as

$$\upsilon^{\text{opt}} = \sqrt{\frac{1 - 4\zeta_{\text{s}}^2 - \mu\left(2\zeta_{\text{s}}^2 - 1\right)}{\left(1 + \mu\right)^3}}$$ (1.5)

where ζ_{s} denotes the damping ratio of the primary structure.

Anh and Nguyen (2012) proposed another closed-form expression for the optimum tuning ratio, which is obtained based on the equivalent linearization method by replacing the damped primary structure with an equivalent un-damped primary structure and utilizing Equation (1.1), as follows

$$\upsilon^{\text{opt}} = \frac{1}{\left(1 + \mu\right)\left(\sqrt{1 + \frac{4}{\pi^2}\zeta_{\text{s}}^2} + \frac{2}{\pi}\zeta_{\text{s}}\right)}$$ (1.6)

The derived formulae for damped SDOF primary structures for the force excitation cases are not applicable to optimal design of TMDs under ground motion excitations.

A lot of researches have been carried out to derive the optimum design formulae of TMDs attached to un-damped or damped SDOF primary structures for different combinations of excitations and performance indices. Three criteria, termed as H_∞-norm, H_2-norm and stability maximization, are the representative optimization criteria. For H_∞ optimization, the objective is to minimize the maximum magnitude of an FRF, which is the same as that of the fixed points theory. However, even for a TMD attached to an un-damped SDOF primary structure, the optimum parameters in the fixed points theory are only the approximate solution of H_∞ optimization, because the damping ratios that

make the curve horizontally pass through the fixed points obtained by the fixed points theory are not identical, and their RMS value is approximately taken as the optimum damping ratio as mentioned before. For un-damped SDOF primary structures under either force or ground motion excitations, the accurate solutions of H_∞ optimization for different objective FRFs have been derived by Asami and Nishihara (2003). However, closed-form solutions of H_∞ optimization cannot be obtained for damped SDOF primary structures. The series solutions for optimum parameters of a TMD obtained by using a perturbation method were proposed by Asami *et al.* (Asami *et al.*, 2002).

While the H_∞ optimization criterion is stick to the resonant frequency response, H_2 optimization aims to reduce the total vibration energy for all the frequency range of the primary structure subjected to a random excitation with infinitely frequencies. The area under the FRF curve is minimized in this criterion. The H_2 optimization criterion for TMD design was firstly proposed by Crandall and Mark (1963). The exact solutions for both un-damped and damped SDOF primary structures subjected to a force excitation or ground motion excitation have been derived by Asami *et al.* (2002), and they also derived the approximate solutions, which are more convenient to utilize, by using a perturbation method. Tigli (2012) derived the accurate optimum parameters of TMDs with the performance index set as the variance of the velocity of the primary structure subjected to a force excitation, and also obtained the solutions of the optimum tuning ratios as functions of optimum damping ratios for mitigating the displacement and acceleration variances, respectively.

Both of the H$_\infty$ and H$_2$ optimization criteria are based on the FRFs. This fact implies that the steady-state responses are the performance indices to be minimized. The stability maximization criterion is employed to decay free vibration responses in the minimum duration. The criterion was firstly proposed by Yamaguchi (1988), and developed by Nishihara and Matsuhisa (1997) for demonstrating the stability maximization criterion optimization can be achieved by maximizing the minimum absolute value of the real parts of the system eigenvalues. The closed-form solutions of the stability maximization criterion have been derived for both un-damped (Equations (1.7) and (1.8)) and damped (Equations (1.9) and (1.10)) SDOF primary structures as follows:

For un-damped primary structures

$$\upsilon^{\text{opt}} = \frac{1}{1+\mu} \tag{1.7}$$

$$\zeta_{\text{T}}^{\text{opt}} = \sqrt{\frac{\mu}{1+\mu}} \tag{1.8}$$

For damped primary structures

$$\upsilon^{\text{opt}} = \frac{1}{1+\mu}\left(1 - \zeta_{\text{s}}\sqrt{\frac{\mu}{1+\mu-\zeta_{\text{s}}^2}}\right) \tag{1.9}$$

$$\zeta_{\text{T}}^{\text{opt}} = \frac{1}{1+\mu}\left(\sqrt{\left(1+\mu-\zeta_{\text{s}}^2\right)\mu} + \zeta_{\text{s}}\right) \tag{1.10}$$

On the other hand, Villaverde *et al.* (Villaverde, 1985; Villaverde and Koyama, 1993; Villaverde and Martin, 1995) suggested that TMDs performed well for seismic vibration

mitigation when the first two modal damping ratios of the single-TMD (STMD) attached

SDOF primary system have the same values. Sadek *et al.* (1997) pointed out Villaverde's

formula does not result in equal damping in the first two modes, especially for the cases

of large mass ratios, and they improved the research results of Villaverde *et al.* by giving

the following two equations

$$\upsilon^{\mathrm{opt}} = \frac{1}{1+\mu}\left(1-\zeta_{\mathrm{s}}\sqrt{\frac{\mu}{1+\mu}}\right) \tag{1.11}$$

$$\zeta_{\mathrm{T}}^{\mathrm{opt}} = \frac{\zeta_{\mathrm{s}}}{1+\mu} + \sqrt{\frac{\mu}{1+\mu}} \tag{1.12}$$

In fact, the essence of the method proposed to achieve equal and large modal damping in

the first two modes is the stability maximization. It is obvious that the formulae

(Equations (1.11) and (1.12)) proposed by Sadek *et al.* are approximate to the exact

solutions of the stability maximization criterion (Equations (1.9) and (1.10)) derived by

Nishihara and Matsuhisa.

(2) Numerical searching methods

To obtain the accurate optimal solutions of TMD parameters for multi-degree-of-freedom

(MDOF) primary structures in a variety of specific cases, i.e., specific excitations or

outputs (performance indices), numerical searching methods by using optimization

techniques were employed by some researchers. Linear Quadratic Gaussian (LQG)

control method was employed to design active TMDs for MDOF primary structures subjected to a Gaussian random excitation with a dominant frequency by Nishimura *et al.* (1989). Genetic algorithm (GA) developed by Holland (1975) was applied to designing TMDs in recent years. GA searches the possible solutions from many different points and finds a nearly global optimum solution. Hadi and Arfiadi (1998) employed GA to design an STMD attached to the top of damped MDOF primary structures, with the objective function set as the H_2-norm value of the frequency transfer function from an unit intensity and zero mean white noise to the top displacement relative to the ground. Singh *et al.* (2002) applied GA to the optimization of TMDs for response control of torsional building systems subjected to bi-directional seismic excitations. Desu *et al.* (2006) used GA for optimal design of coupled TMDs attached to asymmetric buildings to control the lateral-and-torsional coupled vibrations. Pourzeynali *et al.* (2007) investigated the combined applications of GA and fuzzy logic to design active TMD control systems under seismic excitations. Gradient-based algorithms with initial values given by the analytical formulae of the fixed points theory were adopted by some researchers (Rana and Soong, 1998; Zuo and Nayfeh, 2005). For optimization problems with non-smooth objective functions, such as maximization of the minimum damping, sub-gradient optimization method was adopted (Zuo and Nayfeh, 2004). Hoang and Warnitchai (2005) utilized a numerical optimizer that followed the Davidon-Fletcher-Powell algorithm (Davidon, 1959; Fletcher and Powell, 1963) to design multiple TMDs for SDOF structures subjected to wide-band excitations. Lee *et al.* (2006) proposed a step-by-step iteration method integrating the golden section search method (Mathews, 1992) to search the optimal design parameters with the objective function set as the mean square value of

the structural responses in the frequency domain. Leung *et al.* (Leung *et al.*, 2008; Leung and Zhang, 2009) applied particle swarm optimization algorithm to the design of TMDs attached to a viscously damped SDOF primary structure under non-stationary excitations, with the objective function set as the mean square response of either displacement or acceleration. Bekdas and Nigdeli (2011; 2013) utilized the harmony searching method (Geem *et al.*, 2001) to design TMD parameters (mass, stiffness and damping) with the objective to reduce the peak values of the first storey displacement and acceleration transfer functions.

1.3.2 New types of tuned mass dampers

A traditional TMD, comprising of a mass, a linear spring and a linear damper, is usually not very effective for vibration mitigation of a system. Accordingly, new types of TMDs have been proposed by some researchers.

(1) Non-passive tuned mass dampers

TMDs integrated with active or semi-active control strategies, possibly would improve the performance. Active or semi-active TMDs require prescribed control algorithms and external power supplies for on-line analyses and generation of driving forces. Active TMD was firstly presented by Morison and Karnopp (1973), and then the studies of active TMDs in civil engineering began from 1980 (Chand and Soong, 1980; Udwadia and Tabaie, 1981). Semi-active TMDs with variable stiffness and/or damping characteristics were also investigated to mitigate vibration responses induced by winds

and earthquakes (Hrovat *et al.*, 1983; Abe, 1996). In addition to that, many studies focusing on non-passive TMDs were conducted. Aldemir (2003) incorporated a magnetorheological damper in a TMD to semi-actively control the peak responses of an SDOF structure subjected to a broad class of seismic inputs. Rüdinger (2006) proposed a TMD with the damping governed by a nonlinear viscous power law, where the law is dependent on both the structural damping and excitation intensity. Cheung *et al.* (2012) proposed a hybrid control (active-passive) TMD to minimize the velocity response of a structure based on the H_2 optimization criterion by using displacement and velocity feedback.

(2) Multiple tuned mass dampers

Single-tuned mass damper (STMD) installed on the top floor is usually used to control the fundamental vibration mode of a building, indicating that an STMD system is effective only when the dominant frequency of a narrow-banded earthquake excitation is close to the fundamental frequency of the structure. Thus, STMD is not always effective in reducing vibrations induced by various kinds of earthquakes. On the other hand, multiple-tuned mass dampers (MTMDs) with distributed natural frequencies have been confirmed to be robust for excitations with wide spectrum of frequency components (Xu and Igusa, 1992; Yamaguchi and Harnpornchai, 1993; Abe and Fujino, 1994; Igusa and Xu, 1994 ;Kareem and Kline, 1995; Joshi and Jangid, 1996; Strasberg and Feit, 1996; Li, 2000; Park and Reed, 2001), and be able to moderately reduce peak responses even under impulsive earthquakes (Chen and Wu, 2001). MTMDs have been recently employed to solve multimodal vibration problems in bridge engineering (Kwon and Park, 2004; Li *et*

al., 2010; Daniel *et al.*, 2012).

(3) Non-traditional tuned mass dampers

A new type of TMD was recently proposed by Ren (2001), in which the dashpot is directly connected to the ground instead of the primary structure, and it can achieve a larger suppression of the maximum magnitude of FRFs for primary structures than a traditional TMD with the same mass ratio. This type of TMDs may provide an inexpensive and convenient solution to the TMD-based vibration suppression issue in some cases, such as when a damper is too massive to be attached between the primary structure and TMD. Further studies on this new type of TMD, termed as "non-traditional TMD", have been conducted by some other researchers (Liu and Liu, 2005; Wong and Cheung, 2008; Liu and Coppola, 2010; Cheung and Wong, 2011). Figure 1.5 presents the comparison of the analytic model between the non-traditional TMD system and the traditional TMD system.
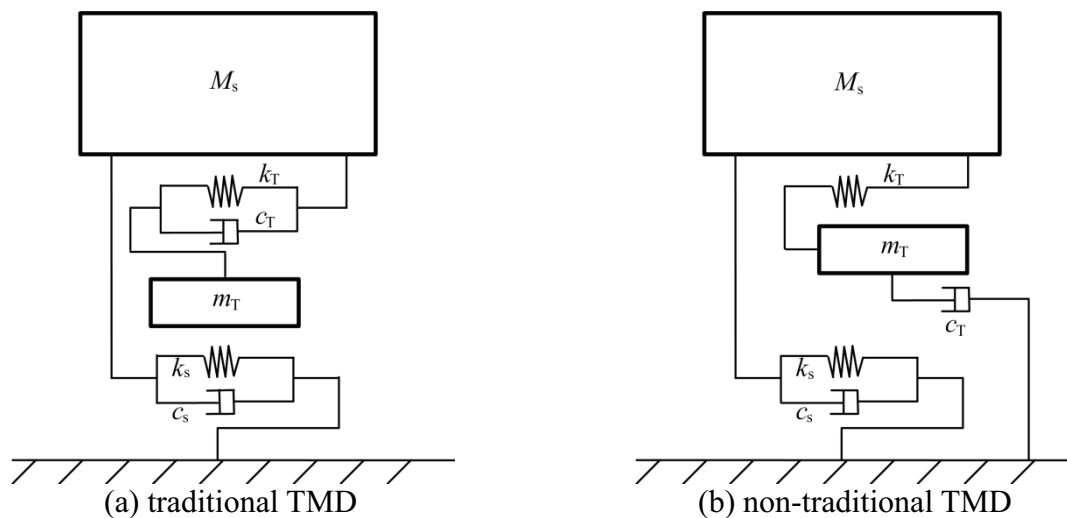
(a) traditional TMD   (b) non-traditional TMD
Figure 1.5 Analytic model comparison of two systems

For un-damped SDOF primary structures with non-traditional TMDs attached, two fixed points of FRFs also exist where their magnitudes are independent of the TMD damping. Ren (2001) derived design formulae for the optimum parameters of such a non-traditional TMD that is attached to an un-damped SDOF primary structure under a force excitation, utilizing the fixed points theory with the performance index set as the maximum magnitude of the normalized displacement FRF. The formulae are as follows

$$\upsilon^{\mathrm{opt}} = \frac{1}{\sqrt{1-\mu}} \tag{1.13}$$

$$\zeta_{\mathrm{T}}^{\mathrm{opt}} = \sqrt{\frac{3\mu}{8(1-0.5\mu)}} \tag{1.14}$$

Cheung and Wong (2009) proposed design formulae of non-traditional TMDs for minimizing the normalized velocity FRF magnitude of a force excited un-damped SDOF primary structure, as shown in the following

$$\upsilon^{\mathrm{opt}} = \sqrt{\frac{1-\sqrt{1-2\mu}}{\mu\sqrt{1-2\mu}}} \tag{1.15}$$

$$\zeta_{\mathrm{T}}^{\mathrm{opt}} = \sqrt{\frac{A\sqrt{1-2\mu}+B}{8\mu^2\sqrt{1-2\mu}\left(-7\mu^2-2\mu+4+\left(3\mu^2-2\mu-4\right)\sqrt{1-2\mu}\right)}} \tag{1.16}$$

where $A = 16 - 48\mu - 12\mu^2 + 84\mu^3 + 3\mu^4 - 15\mu^5$,

$B = -16 + 64\mu - 28\mu^2 - 112\mu^3 + 61\mu^4 + 38\mu^5$.

Wong and Cheung (2008) derived the formulae of optimum parameters in the case in which a non-traditional TMD is attached to an un-damped SDOF primary structure under a ground motion excitation, where the same procedures as Ren were employed. The derived optimum tuning condition is the same as Equation (1.13), while the optimum damping ratio is

$$\zeta_{\mathrm{T}}^{\mathrm{opt}} = \sqrt{\frac{\mu(3-\mu)}{8}} \qquad (1.17)$$

Cheung and Wong (2011) investigated the optimum tuning and damping of a non-traditional TMD attached to an un-damped SDOF primary structure under a force excitation, where the performance index is the mean square value of the normalized displacement FRF magnitude. Higher tuning ratio is preferable, because the global optimum tuning ratio does not exist. For $\mu < 2 - 4\sqrt{2}/3$ (note an error in the reference on Page 1043), the optimum damping ratio is related to the tuning ratio as

$$\zeta_{\mathrm{T}}^{\mathrm{opt}} = \sqrt{\frac{\upsilon^4 + (\mu-2)\upsilon^2 + 1}{4\upsilon^2}} \qquad (1.18)$$

Cheung and Wong (2011) pointed out that the optimum parameters of non-traditional TMDs, which are derived based on the fixed-points theory, i.e., Equations (1.13) and (1.14), do not lead to the global minimum FRF magnitude. They proposed a new set of optimum tuning and damping ratios as follows

$$\upsilon^{\text{opt}} = \sqrt{\frac{2(1-\mu)}{\mu}} \tag{1.19}$$

$$\zeta^{\text{opt}} = \sqrt{\frac{1-2\upsilon^2(1-\mu)+\upsilon^4(1+\mu+\mu^2)-(1-\upsilon^2(1-\mu))\sqrt{1-2(1-\mu)\upsilon^2+(1+\mu^2)\upsilon^4}}{4\upsilon^2\left(1+\upsilon^2+\mu\upsilon^2-\sqrt{1-2(1-\mu)\upsilon^2+(1+\mu^2)\upsilon^4}\right)}} \tag{1.20}$$

It can be found that a very high TMD damping ratio is required in the proposed design method (it becomes larger than 1 when the mass ratio is smaller than 0.2).

For a damped SDOF primary structure subjected to a force excitation, Liu and Coppola (2010) derived the optimum tuning ratio of non-traditional TMDs based on the assumption proposed by Ghosh and Basu (2007). In the assumption, the FRF magnitude curves are postulated to join at two points when a damped TMD with a small mass ratio is attached to a lightly or moderately damped primary structure. The derived optimum tuning ratio is as shown in Equation (1.21).

$$\upsilon^{\text{opt}} = \sqrt{\frac{1-4\zeta_s^2}{1-\mu}} \tag{1.21}$$

where ζ_s denotes the damping ratio of the damped SDOF primary structure.

Anh and Nguyen (2013) derived the following approximate analytical formula of the tuning ratio of a non-traditional TMD attached to a damped SDOF primary structure under a force excitation, by replacing the original damped structure by an equivalent un-damped structure and utilizing Equation (1.13).

$$\upsilon^{opt} = \cfrac{1}{\sqrt{1-\mu}\left(\sqrt{1 + \cfrac{\pi^2}{\left(\pi^2 - 2\right)^2}\zeta_s^2} + \cfrac{\pi}{\pi^2 - 2}\zeta_s\right)} \qquad (1.22)$$

1.3.3 Large mass ratio tuned mass damper systems

A TMD usually requires a large mass to achieve a better control effect (Rana and Soong, 1998; De Angelis *et al.*, 2012). A TMD with a large mass ratio has been found to be able to function properly even if its parameters shift away from the optimally designed values. In this regard, a TMD with a larger mass ratio would be robust with respect to the variations in the structural properties (Hoang *et al.*, 2008). From this point of view, those TMD systems with large mass ratios, have been proposed by some researchers, in which a part of a building is utilized as TMD for vibration control while it can still retain the structural and architectural functions of the buildings.

Feng and Mita (1995) proposed a mega-subcontrol system for super tall buildings by utilizing the substructures as TMDs, which takes advantages of the mega-substructure configuration of super tall buildings. The mass ratio in the system can reach as much as 1.0. As the substructures naturally have several vibration modes, energy in a broad frequency range can be absorbed accordingly, which cannot be realized by the traditional TMD system.

Tian *et al.* (2008) proposed a sliding roof system, in which the roof acts as the mass of TMD. Springs implemented between the roof and the supporting beams provide lateral

stiffness, and the friction force between the roof beams and the supporting beams supplies damping. A mass ratio of 23% was achieved in the sliding roof system.

Matta and De Stefano (2009) proposed a roof garden TMD system, which combines the dynamic response mitigation ability of traditional TMDs with the environmental advantages of traditional roof gardens. The ratio of TMD's mass to total structural mass was 17.1% in the study.

Ziyaeifar and Noguchi (1998) firstly proposed an idea to isolate a part of a tall building by an isolator layer located in the height of the building. This system is termed as "middle-storey isolation system" (Murakami *et al.*, 2000; Sueoka *et al.*, 2004) or "segmented upper storeys system" (Chey *et al.*, 2010). Chey *et al.* (2010) developed the segmented upper storeys system by integrating a semi-active TMD for providing robust adaptability to broader ranges of the structural response. In the study, the ratios of the segmented upper storey mass to the lower storey mass are 24.4% and 59.4%, respectively, for the 10+2 and 8+4 models.

Fu and Johnson (2011) proposed a shading fin mass damper system to improve buildings both structurally and environmentally. External shading fins can adjust the amount of sunlight entering a building, and meanwhile act as TMDs to dissipate energy during strong earthquakes or winds. The TMDs are distributed along the height of a building with the mass ratio of 5%.

1.4 Dissertation Organization

This dissertation aims to study and develop innovative applications of TMDs for mitigation of building structural responses under seismic excitations.

In Chapter 2, a hybrid control strategy based on the combination of a traditional TMD and a damper with variable slip-force level, is presented, and is applied to a base-isolated structure. A general framework for optimization design of TMDs is presented and verified to be validated for the heavily-damped primary system integrated with the variable slip-force level damper. Based on numerical simulation results, the hybrid control strategy is demonstrated to be effective for both harmonic excitations and non-stationary seismic excitations, and can effectively protect base-isolated structures from low-frequency resonance induced by long period ground motions.

In Chapters 3 and 4, the non-traditional TMD introduced in Section 1.3.2 (3) is discussed for the purpose of adopting it to mitigate the seismic vibrations of base-isolated structures via two different design criteria, respectively.

In Chapter 3, an optimum design method is proposed to obtain a wide suppression bandwidth based on frequency response functions, since the fixed points assumption cannot provide the global minimum value of objective function for non-traditional TMD systems. Numerical simulations demonstrate that the control effect of the optimally designed non-traditional TMD is significantly improved by the proposed design method, and furthermore the stroke length is greatly reduced, compared with the traditional TMD

during near-field long period earthquake ground motions. In Chapter 4, the stability maximization criterion for designing non-traditional TMD systems is discussed. The free vibration response of a primary structure decays the most quickly in the optimally designed non-traditional TMD system.

In Chapter 5, a concept of a TMD floor system is proposed, in which building floors serve as TMDs is proposed. This system takes advantages of the characteristics of both the floor isolation system and MTMDs. Since the floor components themselves serve as TMD in this scheme, the system does not need any additional masses for TMDs, and also achieves larger TMD mass ratios than a common TMD system. To validate the effectiveness of the TMD floor system, a shaking table test on a small-scaled model is carried out. Numerical simulation demonstrates that the numerical results agree with the experimental results with favorable accuracy. Moreover, the problem of how to select the optimum locations of TMD floors if not all the floors can serve as TMDs, is also investigated by employing the so-called multimode approach. The performance of the TMD floor systems designed via different criteria have been compared and demonstrated to be effective for different types of seismic excitations, indicating that the TMD floor systems have a great potential of achieving very satisfactory, innovative vibration control effect for building structures.

Chapter 6 gives some of the important conclusions drawn from this research.

2. HYBRID STRUCTURAL CONTROL COMBINING TRADITIONAL TUNED MASS DAMPER AND VARIABLE SLIP-FORCE LEVEL DAMPER

2.1 Introduction

As is mentioned in Chapter 1, TMD is one of the simplest and most reliable structural control devices in terms of reducing the resonant vibration of a primary structure. For achieving superior control performance, hybrid control schemes integrating TMDs have been proposed by some researchers. Loh and Chao (1996) investigated the control effect of active TMD located between the basement and foundation of base-isolated structures. The weighting matrix in the optimal algorithm was determined by the pole assignment method. The hybrid control system was verified to have good control performance especially for reducing isolator deformation. Mitchell *et al.* (2012) proposed a hybrid control system consisting of a TMD and an actuator placed on the top of a building, and viscous liquid dampers located on each floors. The system adopts an algorithm which combines the fuzzy logic theory and neural networks to create an adaptive neuro-fuzzy inference system, and then is combined with wavelet theory to filter the response data. Numerical simulations demonstrate that though the proposed control system uses fewer sensors in the building than full state feedback controllers, less computation time than adaptive neuro-fuzzy inference system is required with comparable resulting responses. Bozer and Altay (2013) studied a combined structure/un-damped TMD system which is equipped with an active controller to track the response of an oscillator with natural frequency set to the operating frequency of the TMD unit. This tracking type controller is formulized by both linear quadratic regulator and H_∞ control schemes. The response of the controlled structure matches the desired operating frequency of the un-damped TMD

27

unit even if the structure is excited by a broadband input, and thus supports the un-damped TMD unit to function effectively. Nishitani and Inoue (2001) summarized the information of buildings integrating hybrid TMDs in Japan. The hybrid TMD integrates certain active control operation into passive TMD movement, and can work more effectively employing a smaller driving force.

Variable slip-force level damper (VSFLD), firstly proposed by Nishitani *et al.* (2003), is a semi-actively controlled damper which provides an elastic-perfectly plastic hysteresis with variable slip-force levels. It can be controlled so as to maintain a ductility factor of two responding to harmonic excitations. The ductility factor of two can be the optimum value in mitigating the relative displacement amplitude of steady-state resonant vibrations. By hybrid-combining TMD and VSFLD, enhancement of response control performance for different types of seismic excitations can be achieved.

In this chapter, first of all, it is theoretically demonstrated that, an elastic-perfectly plastic hysteresis would be the most effective in mitigating the steady-state resonant vibration to harmonic excitations, with the ductility factor of two. Secondly, an optimization method is presented to determine the optimum parameters of an STMD. Then, the hybrid control strategy is applied to a base-isolated structure, and the dynamic iterative equation of the hybrid-controlled nonlinear system is derived. Through numerical simulations of the hybrid-controlled system under different types of seismic excitations, the effectiveness of the hybrid control strategy is demonstrated by comparing with the un-controlled, passive control based on only TMD and semi-active control based on only VSFLD.

2.2 Variable Slip-Force Level Dampers

A VSFLD is a semi-actively controlled damper which provides an elastic-perfectively plastic hysteresis with variable slip-force levels. Its concept has been proposed by Nishitani *et al.* (2000, 2003). It is controlled so as to maintain a ductility factor of two responding to harmonic excitations. It has been demonstrated that, with the ductility factor of two, an elastic-perfectly plastic hysteresis would be the most effective in mitigating steady-state vibrations to harmonic excitations (Tajimi, 1965; Nishitani *et al.*, 2009). Herein, however, a different way is employed to demonstrate that a ductility factor of two is the optimum value for mitigating the relative displacement amplitude of steady-state resonant vibrations.

In the hysteresis loop of an elastic-perfectly plastic damper shown in Figure 2.1, k_{d} represents the stiffness of the damper, k_{seq} denotes the required equivalent linear stiffness of the system, and α is the ratio of k_{d} to k_{seq}. x_{y} and η are the elastic limit displacement and ductility factor, respectively. The equivalent linear stiffness, k_{deq}, and equivalent viscous damping coefficient, c_{deq}, of the damper can be obtained as

$$k_{\text{deq}} = \frac{k_{\text{d}}}{\eta} = \frac{\alpha k_{\text{seq}}}{\eta} \tag{2.1}$$

$$c_{\text{deq}} = \frac{4(\eta-1)\alpha k_{\text{seq}}}{\pi \eta^2 \omega} \tag{2.2}$$

where ω is circular frequencies of harmonic excitations.
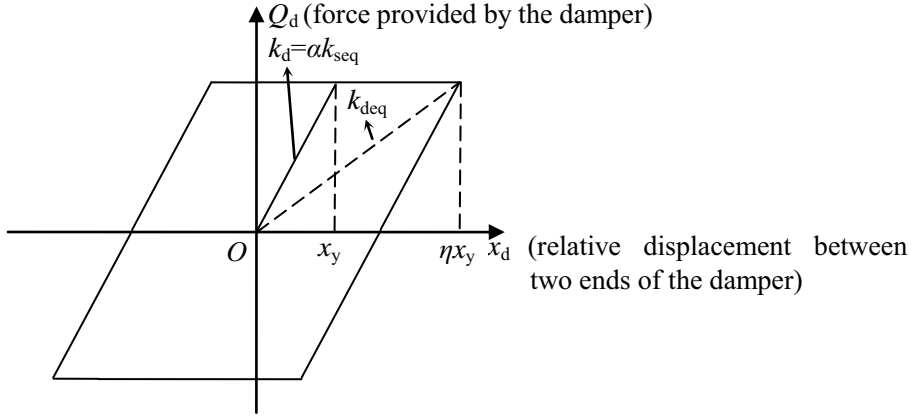
Figure 2.1 Elastic-perfectly plastic hysteresis loop

Under the condition that the total equivalent linear stiffness, k_{seq}, of the structure incorporating with the damper is a constant, the stiffness of the structure, k_s, and the equivalent damping ratio, ζ_{eq}, of the whole system can be obtained as Equations (2.3) and (2.4), respectively.

$$k_s = k_{seq} - k_{deq} = \frac{\eta - \alpha}{\eta} k_{seq} \tag{2.3}$$

$$\zeta_{eq} = \sqrt{\frac{\eta - \alpha}{\eta}} \zeta_s + \frac{2(\eta - 1)\alpha \omega_{seq}}{\pi \eta^2 \omega} \tag{2.4}$$

where ζ_s and ω_{seq} denote the damping ratio of the structure and equivalent linear natural circular frequency of the whole system, respectively, and ζ_s is approximately in the range of 0.01~0.02 for most building structures.

The relative displacement amplitude, x_m, of the steady-state resonant vibration for the damper attached structure is

$$x_{\mathrm{m}} = \frac{m_{\mathrm{s}}A_{\mathrm{g}}/\left(2k_{\mathrm{seq}}\right)}{\zeta_{\mathrm{eqr}}} = \frac{m_{\mathrm{s}}A_{\mathrm{g}}/\left(2k_{\mathrm{seq}}\right)}{\sqrt{\dfrac{\eta-\alpha}{\eta}}\zeta_{\mathrm{s}} + \dfrac{2\left(\eta-1\right)\alpha\omega_{\mathrm{seq}}}{\pi\eta^2\omega_{\mathrm{seq}}}} = \frac{m_{\mathrm{s}}A_{\mathrm{g}}/\left(2k_{\mathrm{seq}}\right)}{\sqrt{\dfrac{\eta-\alpha}{\eta}}\zeta_{\mathrm{s}} + \dfrac{2\left(\eta\text{-}1\right)\alpha}{\pi\eta^2}} \qquad (2.5)$$

where m_{s} denotes the mass of the structure, ζ_{eqr} represents the equivalent damping ratio of the system consisted of the structure and VSFLD in the case of resonance, and A_{g} is the amplitude of a harmonic excitation.

It can be found that x_{m} is the minimum when ζ_{eqr} is the maximum. In other words, the minimum value of x_{m} can be obtained when the first and second order derivatives of ζ_{eqr} with respect to η are equal to zero and negative, respectively. The equation of the first order derivative of ζ_{eqr} is

$$(16 - \pi^2\zeta_{s}^{2})\eta^3 - 16\left(4+\alpha\right)\eta^2 + 64\left(1+\alpha\right)\eta - 64\alpha = 0 \qquad (2.6)$$

The coefficient, $\pi^2\zeta_{s}^{2}$, in Equation (2.6) can be neglected compared with the coefficient 16, thus the following formulation can be obtained.

$$\left(\eta\text{-}2\right)^2\left(\eta-\alpha\right) = 0 \qquad (2.7)$$

It can be found from Equation (2.7) that two is the optimum value of the ductility factor η, otherwise k_{s} will be zero. On the other hand, it can be easily proved that the second

order derivative of ζ_{eqr} with respect to η is negative when η equals two. Therefore, when the ductility factor of the elastic-perfectly plastic damper is equal to two, the relative displacement amplitude of the steady-state resonant vibration can be maximally mitigated, which is the same as the conclusion drawn by Tajimi (1965). In addition, it is found from the denominator of Equation (2.5) that the equivalent linear damping ratio for resonant vibrations, i.e. ζ_{eqr}, is equal to $1/2\pi$ that is approximately 16% corresponding to the ductility factor of two if only the VSFLD is taken into consideration (without considering the primary structure), which is the same as the numerical result obtained by Tajimi (1965). In the case of steady-state harmonic oscillations, zero displacement occurs when velocity reaches its peak value. Therefore, VSFLD is designed so as to slip when the peak velocity is reached, and then the ductility factor of two will be automatically satisfied.

The behavior of the hysteresis illustrated in Figure 2.1 could be compared with that of a visco-elastic damper (VED). Figure 2.2 shows the hysteresis loops of a VSFLD and its corresponding VED when responding to a harmonic excitation with increasing amplitudes. It can be found that the relative displacements are identical to each other for the two hystereses, while the maximum force required by the equivalent VED is larger than the VSFLD by 19%. Additionally, in consideration of such a fact for VEDs that properties are temperature-dependent, the design is in general complex and cumbersome, and visco-elastic materials are possibly de-bonding and tearing, VSFLDs could be idealistic alternatives of VEDs.

2.3 Design of Tuned Mass Dampers

In this section, the optimum design for the hybrid-controlled system consisting of a TMD and VSFLD is discussed. The system is shown schematically in Figure 2.3. The VSFLD is installed between the primary structure and ground. The symbols M or m, k, and c denote the mass, stiffness, and damping coefficient, respectively, with the subscripts s and T representing the primary structure and TMD, and a_g denotes the ground motion acceleration.
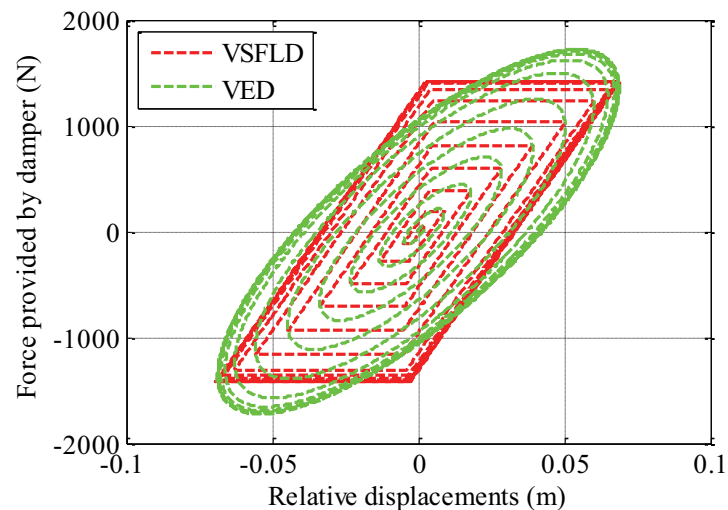
Figure 2.2 Hysteresis loops for VSFLD and equivalent VED

If structures are lightly-damped, such as damping ratios of 0.01~0.02, these damping ratios have practically very little influence on the optimum parameters of linear TMDs (Ankireddi and Yang, 1996; Rüdinger, 2006). Accordingly, it is reasonable to neglect the damping ratios in determining the optimum parameters of TMDs based on the fixed points theory (Den Hartog, 1956). Even for those moderately-damped structures, to which the fixed points theory can be no longer applied, the quasi-fixed points theory has
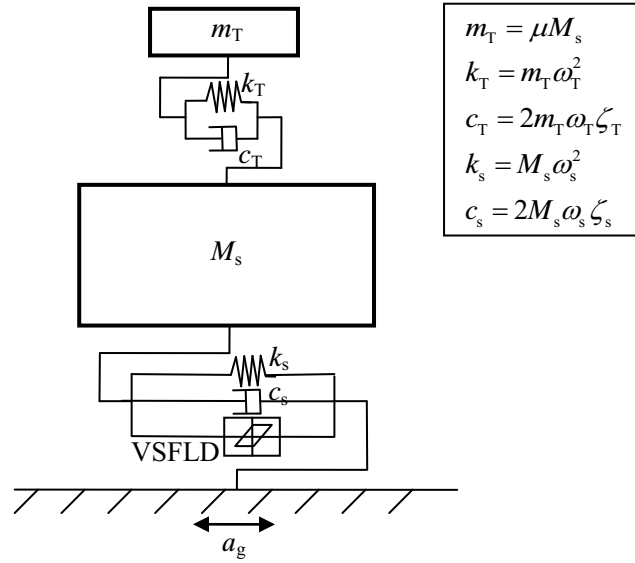
Figure 2.3 Analytic model of hybrid-controlled system

been employed by some researchers (Tsai *et al.*, 1993; Asami *et al.*, 1995; Ghosh *et al.*, 2007) as mentioned in Section 1.3.1 (1). As also stated in Section 1.3.1 (2), numerical searching procedures can be employed for the optimal design of TMDs corresponding to each specific situation. In this dissertation, a gradient-based optimization analysis method is employed. The optimization problem can be formulated to search the optimal set of the design variables over an admissible domain so as to minimize the objective function. Herein, the design variables are the tuning ratio which is the frequency ratio of TMD to primary structure, υ, and the damping ratio of TMD, ζ_{T}, within the admissible domains which are respectively $0 < \upsilon \leq 1/\sqrt{\mu}$ and $0 < \zeta_{\mathrm{T}} \leq 1.00$ (Bakre and Jangid, 2007). It should be noted that the gradient-based method requires a set of initial values with respect to the design variables, and the method efficiency and accuracy are quite sensitive to these initial values. The numerical method is thus classified into the local optimum method category rather than the global optimum method category. However, if

the initial values are given properly, gradient-based methods can be more accurate and efficient than those global optimum design methodologies such as the genetic algorithm (GA). To derive a global optimization result, a number of sets of initial values are given in terms of random numbers (e.g., using *rand* function in MATLAB), and then the global optimum parameters υ^{opt} and $\zeta_{\text{T}}^{\text{opt}}$ are searched. The values of υ and ζ_{T} that would provide the global minimum objective function would be the global optimum parameters υ^{opt} and $\zeta_{\text{T}}^{\text{opt}}$. Since there are only two design variables to be considered in the present study, it is not time-consuming to carry out the above analysis. The flowchart for the gradient-based optimization method is shown in Figure 2.4, and the corresponding MATLAB program is given in Appendix A.

In designing a TMD for this hybrid-controlled system, the equivalent damping ratio, ζ_{eqr}, of the combination of the primary structure and the VSFLD for the case of resonance is regarded as the damping ratio of the primary structure.

The circular frequency and damping coefficient of TMD can be obtained as

$$\omega_{\text{T}} = \upsilon^{\text{opt}} \omega_{\text{seq}} \tag{2.8}$$

$$c_{\text{T}} = 2m_{\text{T}} \zeta_{\text{T}}^{\text{opt}} \omega_{\text{T}} \tag{2.9}$$

where $m_{\text{T}} = \mu m_{\text{s}}$.

```
                        ┌──────────────┐
                        │    START     │
                        └──────────────┘
                               │
                   ┌───────────────────────┐
                   │ Define mass ratio, μ   │
                   └───────────────────────┘
                               │
        ┌─────────────────────────────────────────────────┐
        │ Define set number of initial values for design    │
        │ variables, NUM                                    │
        └─────────────────────────────────────────────────┘
                               │
                          ┌─────────┐
                          │   n=1   │
                          └─────────┘
                               │
```

Define initial values of design variables: $\upsilon = rand(1) \times \left(1\big/\sqrt{\mu}\,\right)$ and $\zeta = rand(1)$

Define objective function (O.F.)

Call MATLAB function: *fmincon*

Record local minimum value of O.F. and corresponding local optimum design variables

n=n+1   Yes $n < NUM$

No

Obtain global optimum design variables υ^{opt} and ζ_T^{opt} which correspond to the global minimum O.F.

END

Figure 2.4 Flowchart of gradient-based optimization method

The dimensionless FRF magnitudes of the equivalent linear primary structure from the ground harmonic acceleration input to the relative displacement response (denoted as $|H_{Xs}|$), are shown in Figure 2.5 (a) and (b), respectively, with respect to η and α. The dashed lines in the figures represent the cases without TMD, while the solid lines correspond to the cases with TMD. In Figure 2.5 (a), the optimum ductility factor is found to be two, which is consistent with the result discussed in Section 2.2. On the other hand, Figure 2.5 (b) demonstrates the effectiveness of the employed hybrid control strategy, where the maximum magnitudes of the FRFs are significantly mitigated. The

larger the stiffness of VSFLD is, the larger mitigation can be achieved, whereas TMD is less effective.
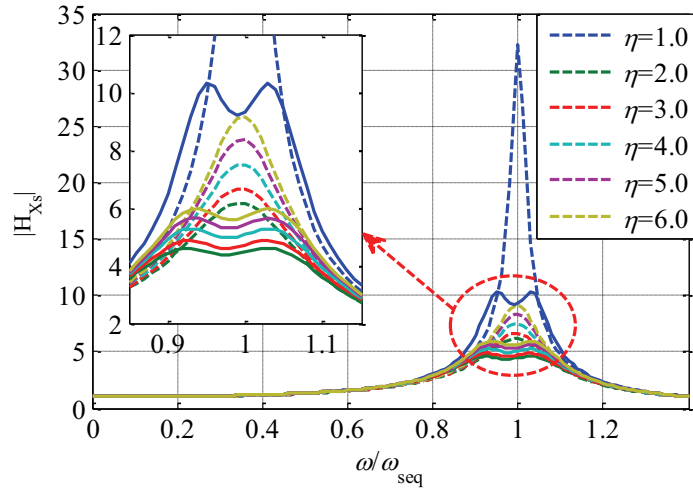
(a) $\mu = 0.01$, $\zeta_s = 0.02$ and $\alpha = 0.4$
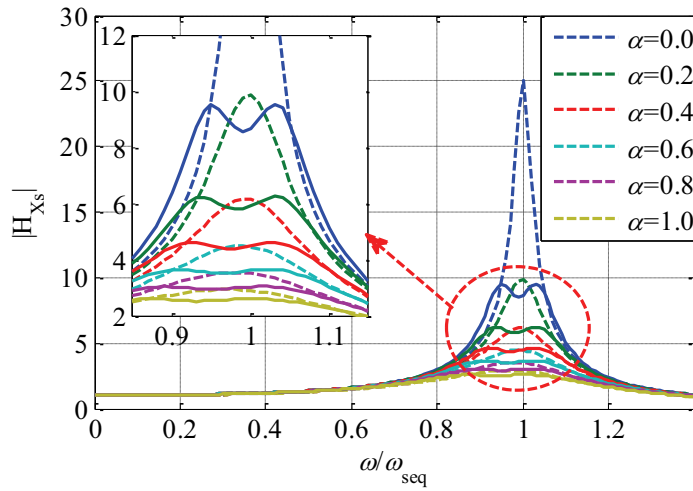
(b) $\mu = 0.01$, $\zeta_s = 0.02$ and $\eta = 2$

Figure 2.5 Magnitudes of dimensionless FRF from harmonic acceleration input to relative displacement of primary structure: '---' without TMD, '—' with TMD.

2.4 Analysis of Hybrid-Controlled Base-Isolated Structure

2.4.1 Analytic model and method

In the following, the hybrid control strategy is applied to a base-isolated structure. The structural model is schematically illustrated in Figure 2.6. The mass M_s, natural period T_s and damping ratio ζ_s of the superstructure are 1.0×10^6 kg, 1.0 s and 0.02, respectively. The mass of the base isolation layer m_b is 5.0×10^4 kg, and the natural period T_{is} and viscous damping ratio ζ_{is} of the base isolators are assumed to be 4.0 s and 0.10, respectively, and α is set to be 0.76 to achieve an equivalent damping ratio, ζ_{eqr}, of 0.2. The mass ratio of TMD to the primary structure μ is 0.1.
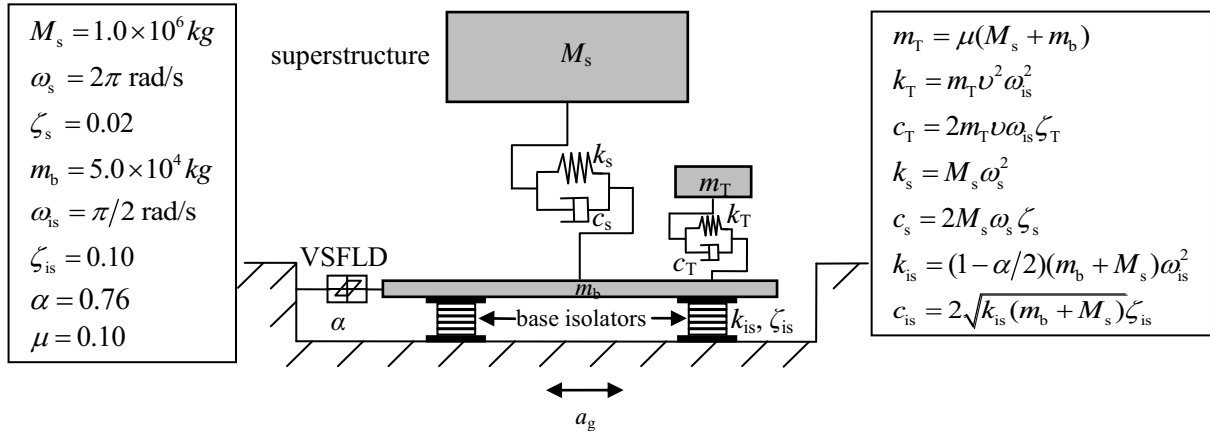
Figure 2.6 Hybrid-controlled base-isolated structural analytic model

Figure 2.7 (a) and (b) show, respectively, the FRF magnitudes of deformations for base isolators (denoted as $|H_{Xb}|$), and absolute accelerations for the superstructure (denoted as $|H_{As}|$) from the ground harmonic acceleration input. The parameters of TMD are determined by using both the quasi-fixed points theory (QFPT in the figure) and the gradient-based optimization method (O.F. in the figure) discussed in Section 2.3. ω_1

denotes the fundamental natural circular frequency of the base-isolated primary structure, which is 1.53 rad/s. It can be found from the figures that, for the cases in which primary structures are MDOF systems or the objective functions are set differently (e.g., Max$|H_X|$), the design formulae of quasi-fixed points theory is not available anymore, while the gradient-based optimization method can be conveniently used to obtain the optimum parameters for TMD design in different cases.
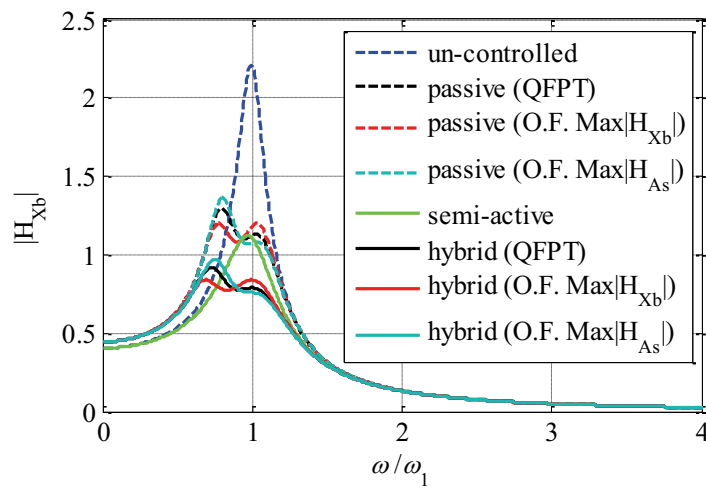
(a) deformation of base isolators
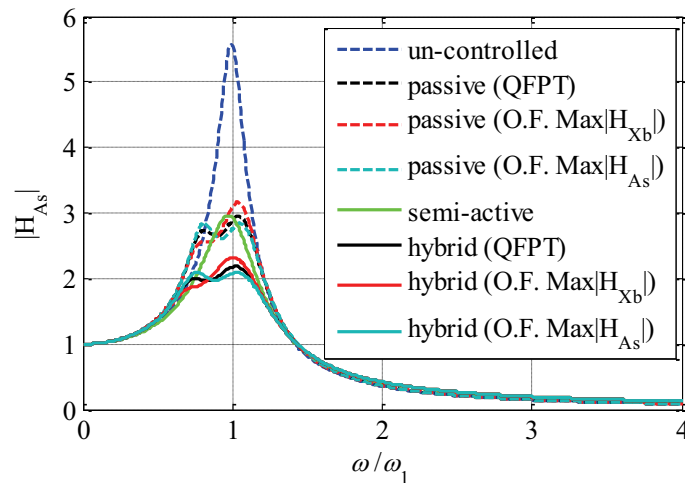
(b) absolute acceleration of superstructure

Figure 2.7 Magnitudes of FRFs from harmonic acceleration input to structural responses for different control strategies

Figure 2.8 shows the optimization results by the gradient-based optimization method corresponding to ten different sets of initial values in the case of hybrid control with the objective function of Max|H_{Xb}|, for instance. It can be seen from the figure that the stability of the optimization method is satisfying.
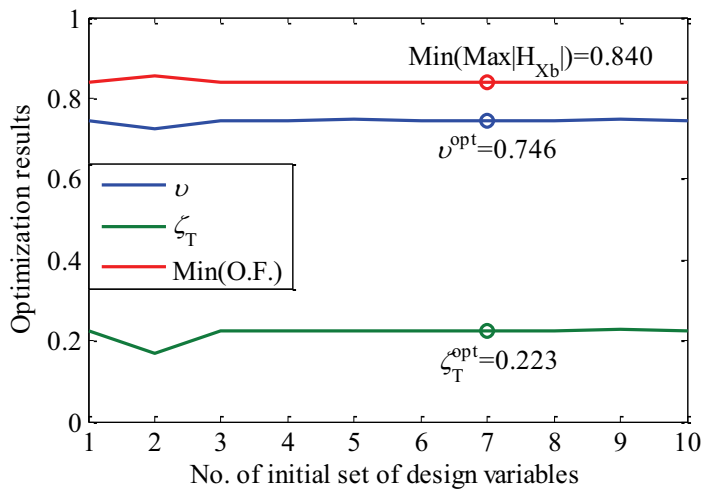
Figure 2.8 Optimum results obtained by gradient-based optimization method

As the control of large base isolator deformation is a critical concern for base-isolated structures, the parameters of TMD obtained by the gradient-based optimization method with the objective function set as Max|H_{Xb}|, corresponding to the red lines in Figure 2.7 (a), are adopted in the following time domain analysis. The optimal parameters of the TMD are υ^{opt} =0.83 and ζ_T^{opt} =0.20 for the passive control, and υ^{opt} =0.75 and ζ_T^{opt} =0.22 corresponding to the hybrid control.

The VSFLD is treated as a nonlinear element in the following time domain discussion, although the effect of the VSFLD was approximately estimated by the equivalent

linearization method in the above frequency domain discussion.

With a_g representing the ground acceleration, the equation of motion for the 3DOF system shown in Figure 2.6 can be written as

$$\mathbf{M\ddot{x}} + \mathbf{C\dot{x}} + \mathbf{Kx} + \mathbf{r}_1 Q_d = -\mathbf{Mr}_2 a_g \tag{2.10}$$

where $\mathbf{M} = \begin{bmatrix} m_b & 0 & 0 \\ 0 & M_s & 0 \\ 0 & 0 & m_T \end{bmatrix}$, $\mathbf{C} = \begin{bmatrix} c_{is} + c_s + c_T & -c_s & -c_T \\ -c_s & c_s & 0 \\ -c_T & 0 & c_T \end{bmatrix}$,

$\mathbf{K} = \begin{bmatrix} k_{is} + k_s + k_T & -k_s & -k_T \\ -k_s & k_s & 0 \\ -k_T & 0 & k_T \end{bmatrix}$,

$\mathbf{r}_1 = \begin{Bmatrix} 1 \\ 0 \\ 0 \end{Bmatrix}$, $\mathbf{r}_2 = \begin{Bmatrix} 1 \\ 1 \\ 1 \end{Bmatrix}$, $\mathbf{\ddot{x}} = \begin{Bmatrix} \ddot{x}_b \\ \ddot{x}_s \\ \ddot{x}_T \end{Bmatrix}$, $\mathbf{\dot{x}} = \begin{Bmatrix} \dot{x}_b \\ \dot{x}_s \\ \dot{x}_T \end{Bmatrix}$, $\mathbf{x} = \begin{Bmatrix} x_b \\ x_s \\ x_T \end{Bmatrix}$, with x_b, x_s and x_T respectively

denoting deformation of base isolators, displacements of the superstructure and TMD relative to the ground, and Q_d represents the damping force of the VSFLD.

Solving Equation (2.10) based on the Newmark-β method, the dynamic iterative equation expressed by the variable, $\mathbf{x}$, can be obtained as

$$\mathbf{x}_{n+1} = \left[\frac{1}{\beta(\Delta t)^2}\mathbf{M} + \mathbf{K} + \frac{\gamma}{\beta\Delta t}\mathbf{C} \right]^{-1} \cdot$$

$$\left\{ \left[\left(\frac{1}{2\beta} - 1 \right)\mathbf{M} - \left(1 - \frac{\gamma}{2\beta} \right)\Delta t\mathbf{C} \right]\ddot{\mathbf{x}}_n + \left[\frac{1}{\beta\Delta t}\mathbf{M} - \left(1 - \frac{\gamma}{\beta} \right)\mathbf{C} \right]\dot{\mathbf{x}}_n \right.$$

$$\left. + \left[\frac{1}{\beta(\Delta t)^2}\mathbf{M} + \frac{\gamma}{\beta\Delta t}\mathbf{C} \right]\mathbf{x}_n - \mathbf{M}\mathbf{r}_2 a_{g,n+1} - \mathbf{r}_1 Q_{d,n+1} \right\} \tag{2.11}$$

where, $\mathbf{x}_n$, $\dot{\mathbf{x}}_n$ and $\ddot{\mathbf{x}}_n$ are displacement, velocity and acceleration vectors at the time instant $n(\Delta t)$ (Δt is the sampling time); and $\mathbf{x}_{n+1}$, $a_{g,n+1}$ and $Q_{d,n+1}$ are the displacement vector, ground acceleration scalar and VSFLD force scalar at the time instant $(n+1)(\Delta t)$, respectively. $\gamma = 0.5$ and $\beta = 0.25$ are employed. $\mathbf{x}_{n+1}$ can be solved iteratively during the time period $n(\Delta t) \sim (n+1)(\Delta t)$ from Equation (2.11), and then $\dot{\mathbf{x}}_{n+1}$ and $\ddot{\mathbf{x}}_{n+1}$ can be obtained by the following formulations:

$$\dot{\mathbf{x}}_{n+1} = \frac{\gamma}{\beta\Delta t}(\mathbf{x}_{n+1} - \mathbf{x}_n) + \left(1 - \frac{\gamma}{\beta} \right)\dot{\mathbf{x}}_n + \left(1 - \frac{\gamma}{2\beta} \right)\Delta t\ddot{\mathbf{x}}_n \tag{2.12}$$

$$\ddot{\mathbf{x}}_{n+1} = -\mathbf{M}^{-1}(\mathbf{C}\dot{\mathbf{x}}_{n+1} + \mathbf{K}\mathbf{x}_{n+1} + \mathbf{r}_1 Q_{d,n+1}) - \mathbf{r}_2 a_{g,n+1} \tag{2.13}$$

Subsequently, $\mathbf{x}$, $\dot{\mathbf{x}}$ and $\ddot{\mathbf{x}}$ at the next time step can be obtained from Equations (2.11)~(2.13).

2.4.2 Numerical simulations

With the computer program written based on the above formulation, the hybrid controlled system is analyzed in different excitation situations. The sampling time is set to be 0.01 s.

(1) Harmonic resonant excitation

The case in which the frequency of a harmonic excitation is equal to the fundamental natural frequency of the base-isolated structure is considered. In Figure 2.9 two different hysteresis loops of VSFLD are presented. The green and red lines, respectively, correspond to the case when only the VSFLD is attached to the primary structure (referred to as "semi-active" in the figure), and the case of the combination of the TMD and the VSFLD (referred to as "hybrid" in the figure). It is evident from the figure that the algorithm of the VSFLD exhibits satisfactory hysteresis in both cases when the base-isolated structural system is subjected to the harmonic excitation.
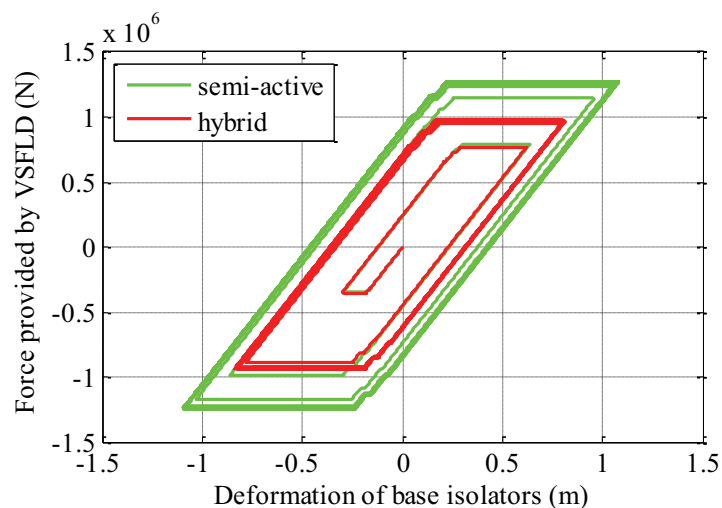
Figure 2.9 Hysteresis loops of VSFLD

The response time histories (deformations of the base isolators, absolute accelerations of the base isolation layer, relative displacements and absolute accelerations of the superstructure) are shown in Figure 2.10. In the figure, the blue dashed, black solid, green dashed and red solid lines correspond to the un-controlled (base-isolated), passive-controlled (base-isolated with TMD), semi-active-controlled (base-isolated with VSFLD), and hybrid-controlled (base-isolated with both TMD and VSFLD) responses, respectively. To make a quantitative evaluation of the control effects of these control schemes, Figure 2.11 gives the response ratios of the three control schemes to the un-controlled case, with respect to the maximum deformation of base isolators (Max.d_b), maximum and root mean square values of absolute acceleration of the superstructure (Max.a_s and RMS.a_s). It can be seen from the figure that, by incorporating both the TMD and the VSFLD into the system, all the responses are mitigated. Among the schemes, the hybrid control achieves the best control effect. Compared with the responses of the un-controlled case, i.e., simple base-isolated system, the responses are reduced by 40~46% for the passive control system with only the TMD; A reduction of 40~50% is achieved for the semi-active control with only the VSFLD; and they are reduced by 52~62% for the hybrid control with both the TMD and the VSFLD.

(2) Earthquake excitations

The effect of the hybrid control strategy is investigated by using four un-scaled near-fault earthquake records from the PEER Ground Motion Database (http://peer.berkeley.edu/peer_ground_motion_database): the 1952 Kern County (TAF111), the 1995 Kobe (KJM000), the 1999 Chi-chi (TCU068EW) and the 2011

Tohoku (TKY007EW). These seismic records are chosen as representatives of distinct classes of earthquakes (Hisada, 2004; Takewaki *et al.*, 2011). Figure 2.12 shows the hysteresis loops of the VSFLD for the case of the four different ground motions. It can be seen from the figure that plumpness of the hysteresis loops of VSFLD is favorable even under random excitations either in pure VSFLD or in hybrid scheme.
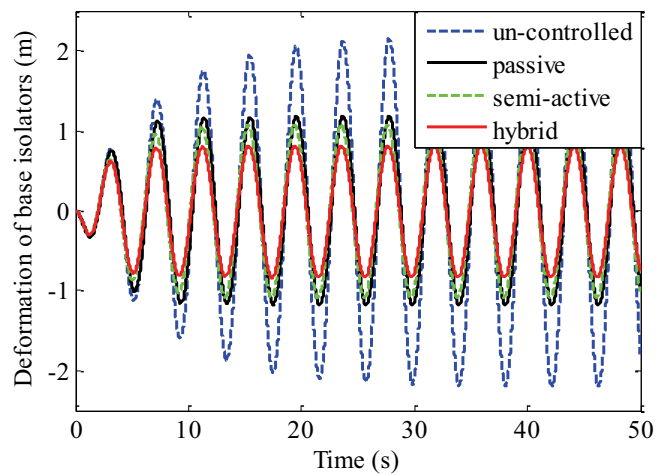
(a) deformation of base isolators
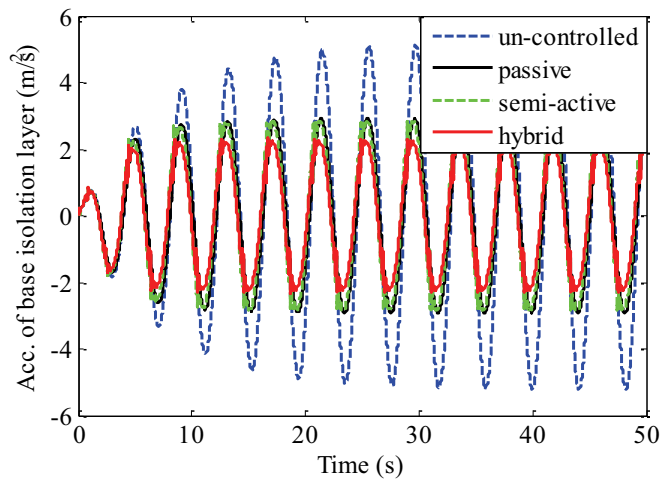
(b) absolute acceleration of base isolation layer

Figure 2.10 Time histories of responses
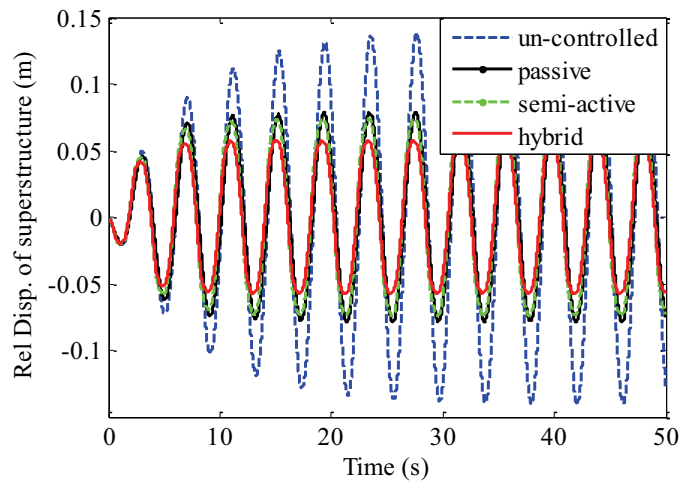
(c) displacement of superstructure relative to base isolation layer
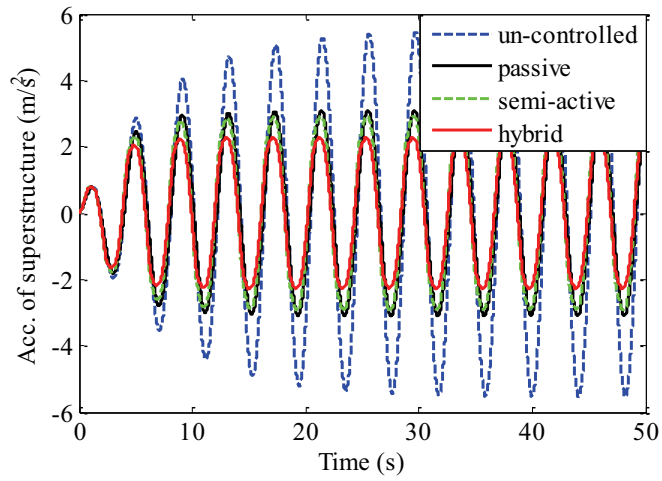
(d) absolute acceleration of superstructure

Figure 2.10 Continued
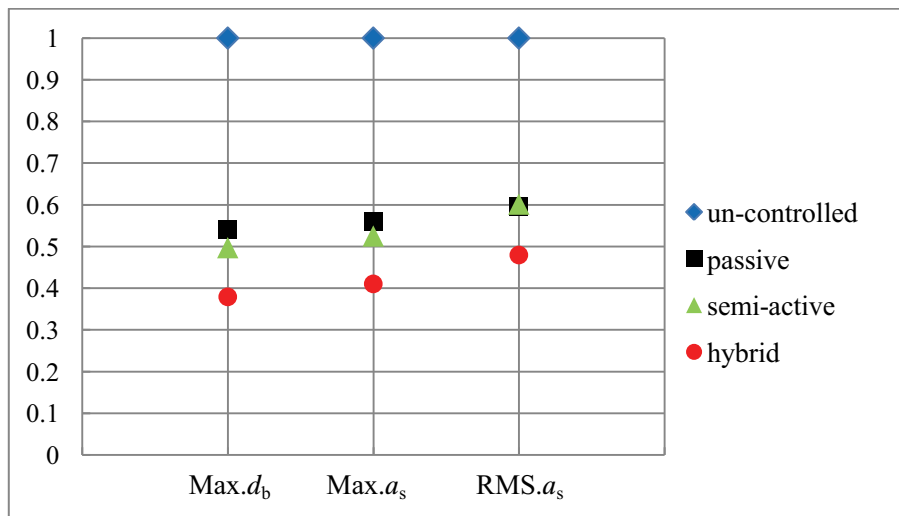
Figure 2.11 Response ratios of different control strategies: 'd_b' deformation of base isolators, 'a_s' absolute acceleration of superstructure.
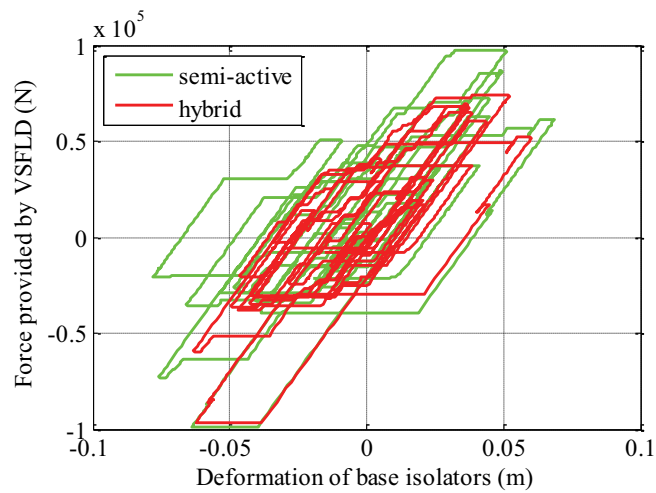
(a) Kern County (TAF111)

Figure 2.12 Hysteresis loops of VSFLD
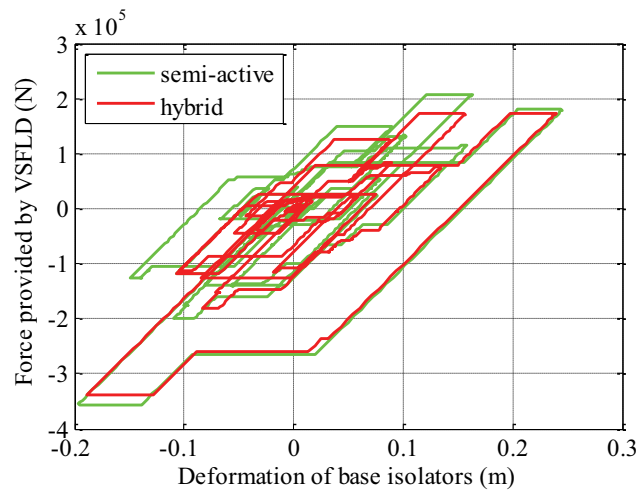
(b) Kobe (KJM000)
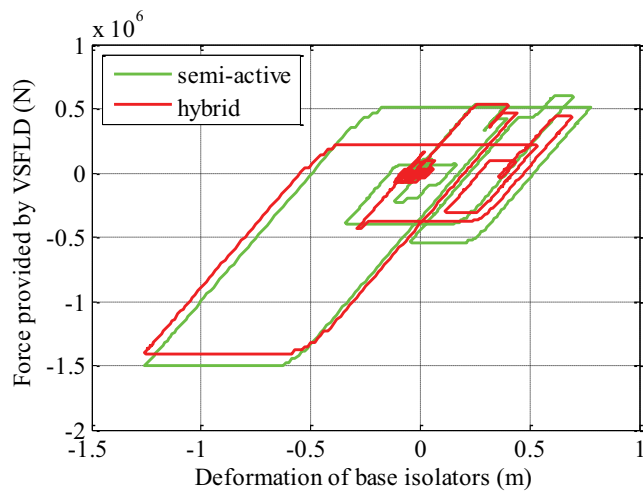
(c) Chi-chi (TCU068EW)
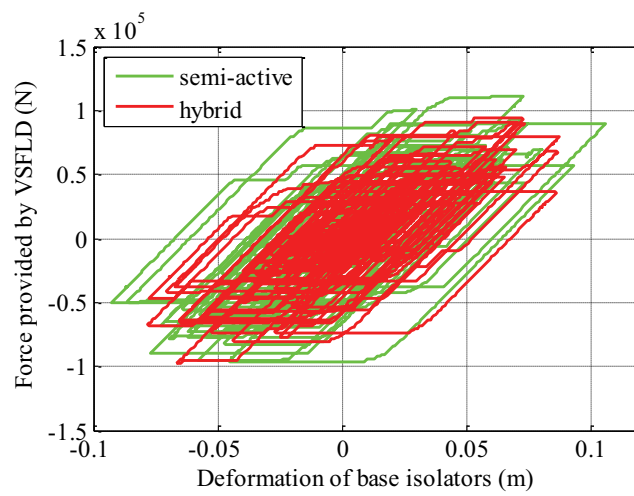
(d) Tohoku (TKY007EW)

Figure 2.12 Continued

48

Figures 2.13 and 2.14 show the FRF magnitudes for the deformation of base isolators in the passive and hybrid control cases, respectively. The FRFs are the ratio of the Fourier spectra of the deformation responses of the base isolators to the Fourier spectra of the earthquake excitations. The flowchart for the calculation procedure of FRF magnitude is given in Appendix B. From Figure 2.13 it can be found that in the passive control case, the FRF magnitudes obtained by the Fourier transform of the responses in the time domain are well close to the theoretical FRF magnitudes in the frequency domain, as illustrated by the red solid line in Figure 2.13 or the red dashed line in Figure 2.7 (a). This fact also indicates the accuracy of the time domain analyses. For the VSFLD integrated hybrid control on the other hand, the FRF magnitudes corresponding to the low frequencies, do not agree well with the frequency domain results, while corresponding to high frequencies, the FRF magnitudes obtained from the time domain analysis, agree relatively well with the frequency domain results. The reason for the inconsistency is due to the nonlinearity characteristic of the VSFLD.
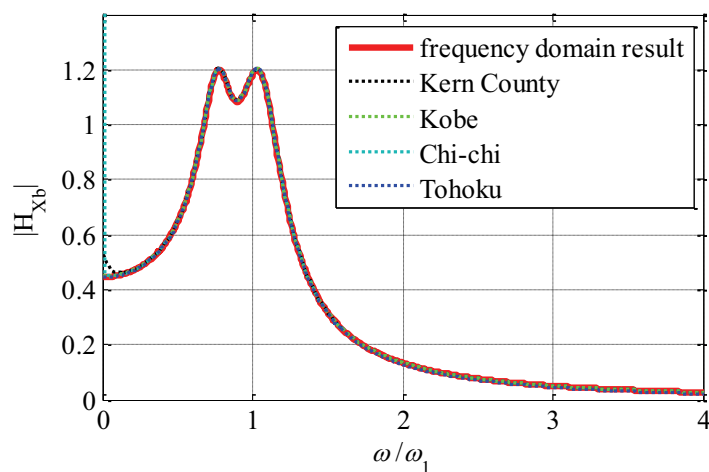
Figure 2.13 FRF magnitudes for deformation responses of base isolators from random earthquakes in passive control strategy
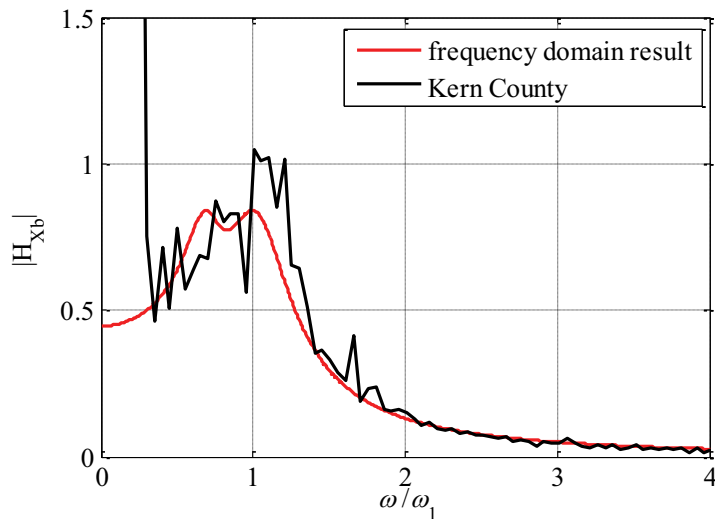
(a) Kern County (TAF111)
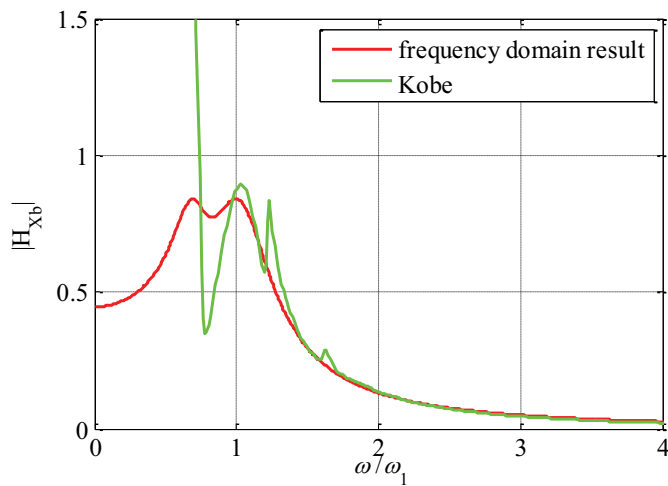
(b) Kobe (KJM000)

Figure 2.14 FRF magnitudes for deformation responses of base isolators from random

earthquakes in hybrid control strategy
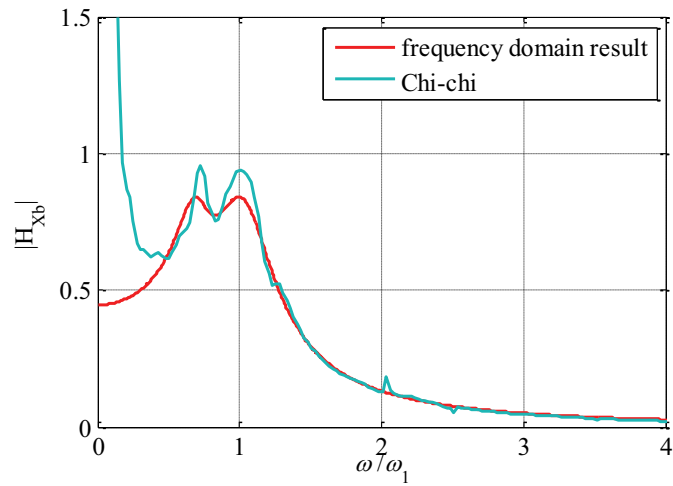
(c) Chi-chi (TCU068EW)
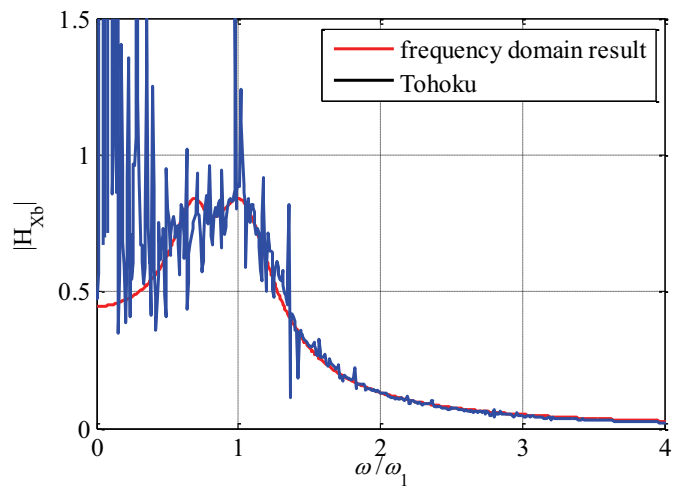
(d) Tohoku (TKY007EW)

Figure 2.14 Continued

Figure 2.15 gives the response ratios of the three control schemes to the un-controlled case for the four earthquakes. It can be seen from the figure that, the hybrid control strategy generally achieves the best control performance. Figure 2.15 (a) indicates that, by the hybrid control, the reductions of Max.d_b are 7% for Kobe (KJM000), which are mainly comprised of short-period components; while 19~36% for Kern County (TAF111), Chi-chi (TCU068EW) and Tohoku (TKY007EW) which contain fairly large long period

components. It can be seen from Figure 2.15 (b) and (c) that, the reduction of the deformation of base isolators will not be at the expense of increasing the responses of the superstructure. Max.d_b, Max.a_s and RMS.a_s can be respectively mitigated by 36%, 36% and 32% in the hybrid strategy for Tohoku (TKY007EW) excitation. The reason for the relatively large improvement achieved for Tohoku earthquake is that, the periods of 4 and 6 seconds are the predominant periods of the Tohoku earthquake from the view point of input energy of earthquakes (Takewaki *et al*. 2011), which are close to the natural period of the base-isolated primary structure.

(a) Max.d_b
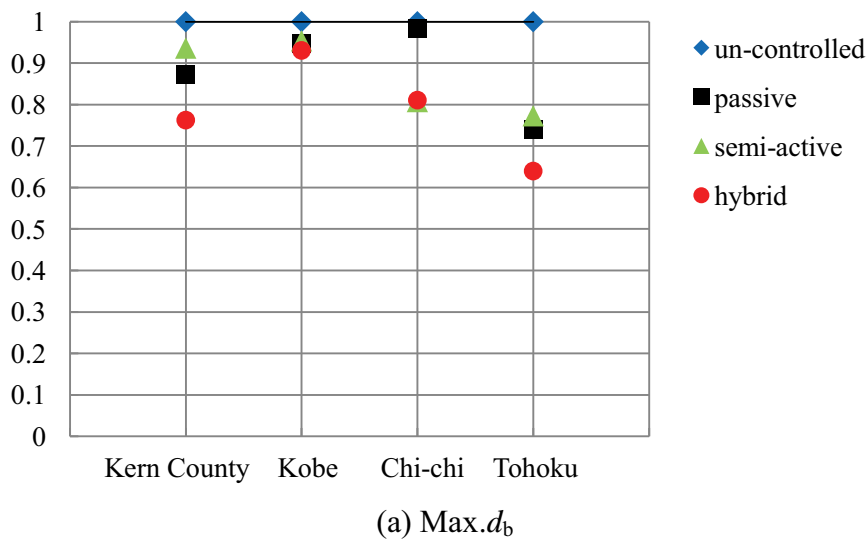
Figure 2.15 Response ratios of different control strategies
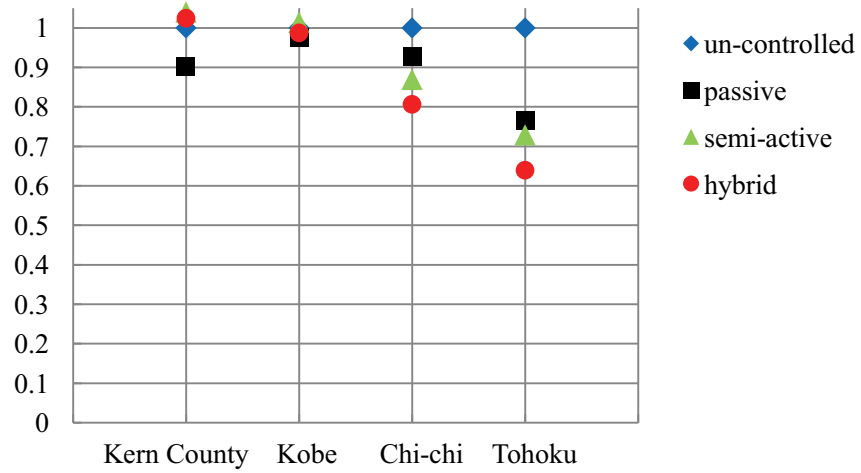
(b) Max.a_s
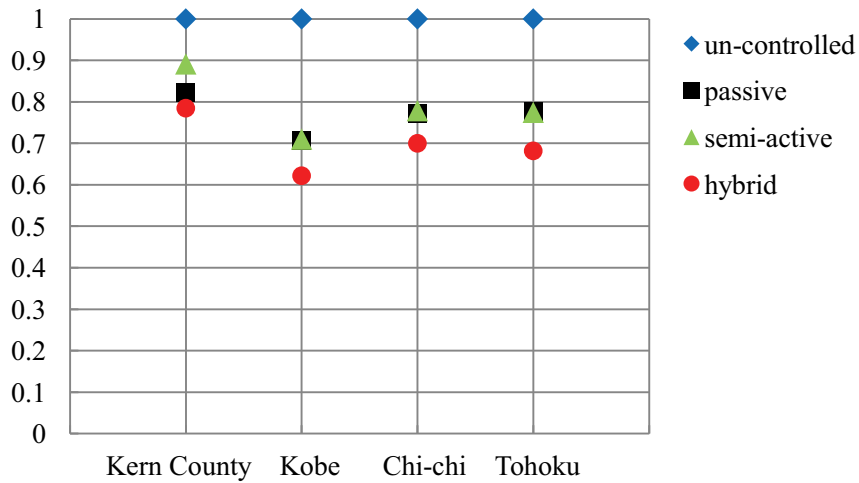
(c) RMS.a_s

Figure 2.15 Continued

2.5 Conclusions

This chapter presents a hybrid control strategy based on the combination of a tuned mass damper (TMD) and a variable slip-force level damper (VSFLD). It is theoretically demonstrated that, with a ductility factor of two, an elastic-perfectly plastic hysteresis would be the most effective in mitigating the steady-state resonant vibrations. The hybrid

control strategy is then applied to a base-isolated structure. A gradient-based optimization method for designing the parameters of the TMD in the hybrid-controlled system is proposed, and the dynamic iterative equation of the nonlinear system is also presented. Through the numerical simulations of the hybrid-controlled system under different types of ground excitations, the performance of the hybrid control strategy is demonstrated to be superior compared with TMD based passive control and VSFLD based semi-active control, especially for protecting the base-isolated structure from low-frequency resonance induced by long period ground motions.

3. OPTIMUM DESIGN OF NON-TRADITIONAL TUNED MASS DAMPER SYSTEM FOR WIDER SUPPRESSION BANDWIDTHS

3.1 Introduction

Base isolation systems are very effective in reducing the seismic responses of buildings, while the base isolation itself undergoes a relatively large displacement. They are vulnerable to long period ground motions due to resonant behaviors. Some researchers proposed and studied the hybrid control strategy of combining traditional TMDs with base isolation systems, and demonstrated the effectiveness of TMDs (Yang *et al.*, 1991; Tsai, 1995; Palazzo *et al.*, 1997; Taniguchi *et al.*, 2008; Petti *et al.*, 2010). However, a traditional TMD would need a large stroke to diminish the large responses of the primary structure in the event of resonance, and thus a large clearance is needed to accommodate the large stroke. In addition, a traditional TMD is less effective for broad banded ground motions or ineffective for those narrow banded ground motions of which the predominant frequencies are not close to the natural frequency of the primary structure. To overcome this kind of drawback, new types of TMDs have been proposed which involve either weakly or strongly nonlinear characteristics (Nissen *et al.*, 1985; Natsiavas, 1992; Vakakis *et al.*, 2003). For those TMDs which nonlinear elements are involved into, however, additional attention should be paid to the instability problems, such as chaos, limit cycles and bifurcations. As mentioned in Section 1.3.2 (3), a new type of TMD systems termed as "non-traditional TMDs" was recently proposed and studied by some researchers (Ren, 2001; Liu and Liu, 2005; Wong and Cheung, 2008; Liu and Coppola, 2010; Cheung and Wong, 2011). Such a non-traditional TMD is directly connected to the ground with a dashpot. It may provide an inexpensive and convenient solution to the

TMD-based vibration suppression issue. Furthermore, a non-traditional TMD would achieve a larger suppression of the maximum FRF magnitude than a traditional TMD.

From the standpoint of ensuring a wide frequency suppression range, this chapter intends to address the issue of optimum design for the aforementioned non-traditional TMD which is attached to a damped primary structure excited by ground motions and also investigates the combination effect of the non-traditional TMD and base isolation systems. First the analytic model of the non-traditional TMD system is given, and the formulae for the magnitudes of the FRFs are presented. Then it is demonstrated that the optimum parameters of the non-traditional TMD derived based on the quasi-fixed points theory are not the global optimal solutions. And an optimum design method of a non-traditional TMD is proposed, which can ensure the suppression covering a wider frequency range than a traditional TMD. Finally, numerical simulations are carried out, which demonstrate the improvement of control effect achieved by combining a non-traditional TMD with a base-isolated structure.

3.2 Frequency Response Functions of Systems with Tuned Mass Dampers

Consider the traditional and non-traditional TMDs attached to a damped SDOF system which is subjected to ground acceleration inputs. These two systems are schematically illustrated in Figure 3.1, where M or m, k and c are the mass, stiffness and damping coefficient, respectively, with the subscripts s and T denoting the primary structure and TMD, and a_g represents the ground motion acceleration.

$$\mu = m_T / M_s$$
$$\omega_s = \sqrt{k_s / M_s}$$
$$\omega_T = \sqrt{k_T / m_T}$$
$$\zeta_s = c_s / (2\sqrt{M_s k_s})$$
$$\zeta_T = c_T / (2\sqrt{m_T k_T})$$
$$\upsilon = \omega_T / \omega_s$$
$$r = \omega / \omega_s$$

(a) traditional TMD   (b) non-traditional TMD
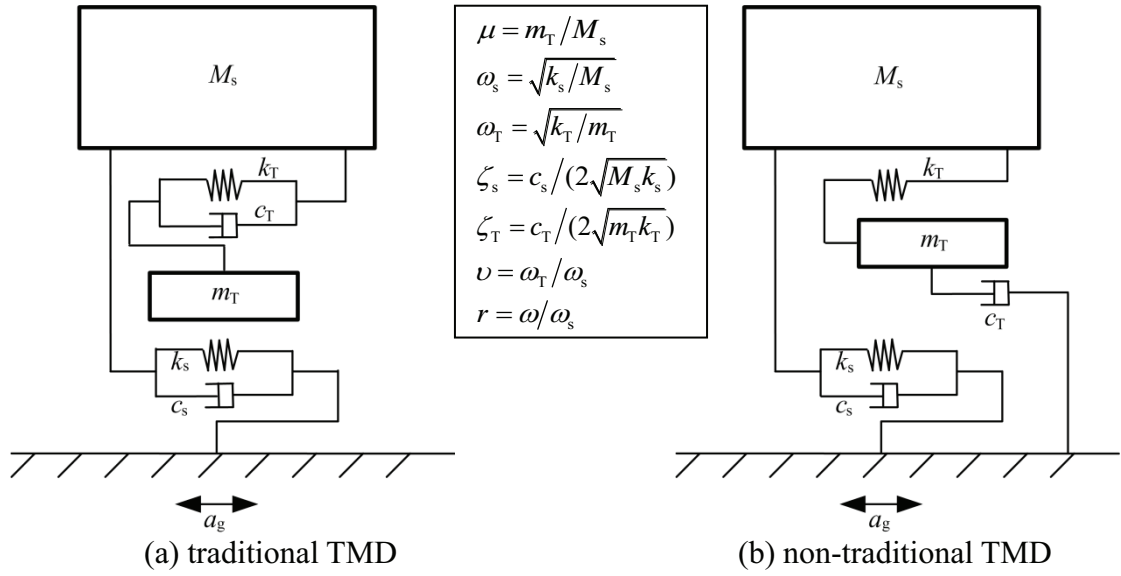
Figure 3.1 Analytic models of two systems

The FRFs of the absolute accelerations of the primary structures are obtained in the following manner. The equations of motion for the structural systems integrating the traditional and non-traditional TMDs can be represented by Equations (3.1) and (3.2), respectively.

$$\begin{cases} M_s \ddot{x}_s + (c_s + c_T)\dot{x}_s + (k_s + k_T)x_s - c_T \dot{x}_T - k_T x_T = -M_s a_g \\ m_T \ddot{x}_T + c_T \dot{x}_T + k_T x_T - c_T \dot{x}_s - k_T x_s = -m_T a_g \end{cases} \tag{3.1}$$

$$\begin{cases} M_s \ddot{x}_s + c_s \dot{x}_s + (k_s + k_T)x_s - k_T x_T = -M_s a_g \\ m_T \ddot{x}_T + c_T \dot{x}_T + k_T x_T - k_T x_s = -m_T a_g \end{cases} \tag{3.2}$$

where x_s and x_T are the relative displacements of the primary structure and TMD to the base, respectively, and the dot over the symbol denotes the derivative with respect to time.

Assuming such a harmonic ground acceleration as $a_g = \mathbf{A}_g e^{j\omega t}$, where $\mathbf{A}_g$ and ω are respectively the amplitude and circular frequency of the harmonic ground acceleration input, the steady-state responses may be written as

$$x_s = \mathbf{X}_s e^{j\omega t}, \quad \dot{x}_s = j\omega \mathbf{X}_s e^{j\omega t}, \quad \ddot{x}_s = -\omega^2 \mathbf{X}_s e^{j\omega t} \tag{3.3}$$

$$x_T = \mathbf{X}_T e^{j\omega t}, \quad \dot{x}_T = j\omega \mathbf{X}_T e^{j\omega t}, \quad \ddot{x}_T = -\omega^2 \mathbf{X}_T e^{j\omega t} \tag{3.4}$$

where $\mathbf{X}_s$ and $\mathbf{X}_T$ are the steady-state amplitudes of the relative displacements for the primary structure and TMD to the base, respectively.

Substituting Equations (3.3) and (3.4) into Equations (3.1) and (3.2), the equations of motion of the two structural systems can be obtained in the frequency domain as follows:

$$\begin{cases} \left[-\omega^2 + j2(\omega_s \zeta_s + \mu \omega_T \zeta_T)\omega + \omega_s^2 + \mu \omega_T^2 \right] \dfrac{\mathbf{X}_s}{\mathbf{A}_g} - \left(\mu \omega_T^2 + j2\mu\omega_T\zeta_T\omega \right) \dfrac{\mathbf{X}_T}{\mathbf{A}_g} = -1 \\[2ex] \qquad -\left(\omega_T^2 + j2\omega_T\zeta_T\omega \right) \dfrac{\mathbf{X}_s}{\mathbf{A}_g} + \left(-\omega^2 + j2\omega_T\zeta_T\omega + \omega_T^2 \right) \dfrac{\mathbf{X}_T}{\mathbf{A}_g} = -1 \end{cases} \tag{3.5}$$

$$\begin{cases} \left(-\omega^2 + j2\omega_s\zeta_s\omega + \omega_s^2 + \mu \omega_T^2 \right) \dfrac{\mathbf{X}_s}{\mathbf{A}_g} - \mu \omega_T^2 \dfrac{\mathbf{X}_T}{\mathbf{A}_g} = -1 \\[2ex] \qquad -\omega_T^2 \dfrac{\mathbf{X}_s}{\mathbf{A}_g} + \left(-\omega^2 + j2\omega_T\zeta_T\omega + \omega_T^2 \right) \dfrac{\mathbf{X}_T}{\mathbf{A}_g} = -1 \end{cases} \tag{3.6}$$

where $\omega_s = \sqrt{\dfrac{k_s}{M_s}}$, $\omega_T = \sqrt{\dfrac{k_T}{m_T}}$, $\zeta_s = \dfrac{c_s}{2\sqrt{M_s k_s}}$, $\zeta_T = \dfrac{c_T}{2\sqrt{m_T k_T}}$ and $\mu = \dfrac{m_T}{M_s}$.

The FRF magnitudes of the absolute accelerations for the primary structures in the two systems can be solved in a straightforward manner from Equations (3.5) and (3.6) as:

$$\left|H_{Acc}\left(\omega\right)\right|_A = \left|-\omega^2 \frac{\mathbf{X}_s}{\mathbf{A}_g}\left(\omega\right)+1\right|_A$$

$$= \sqrt{\frac{\left[1-\left(4\zeta_s\zeta_T\upsilon+1\right)\dfrac{r^2}{\upsilon^2}\right]^2 + 4r^2\left(\dfrac{\zeta_s r^2}{\upsilon^2}-\zeta_s-\dfrac{\zeta_T}{\upsilon}\right)^2}{\left[\dfrac{r^4}{\upsilon^2}-\left(1+\mu+4\dfrac{\zeta_s\zeta_T}{\upsilon}+\dfrac{1}{\upsilon^2}\right)r^2+1\right]^2 + 4r^2\left[\left(\dfrac{(1+\mu)\zeta_T}{\upsilon}+\dfrac{\zeta_s}{\upsilon^2}\right)r^2-\zeta_s-\dfrac{\zeta_T}{\upsilon}\right]^2}} \qquad (3.7)$$

$$\left|H_{Acc}\left(\omega\right)\right|_B = \left|-\omega^2 \frac{\mathbf{X}_s}{\mathbf{A}_g}\left(\omega\right)+1\right|_B$$

$$= \sqrt{\frac{\left[1-\left(4\zeta_s\zeta_T\upsilon+1\right)\dfrac{r^2}{\upsilon^2}\right]^2 + 4r^2\left(\dfrac{\zeta_s r^2}{\upsilon^2}-\zeta_s-\dfrac{\zeta_T}{\upsilon}-\mu\zeta_T\upsilon\right)^2}{\left[\dfrac{r^4}{\upsilon^2}-\left(1+\mu+4\dfrac{\zeta_s\zeta_T}{\upsilon}+\dfrac{1}{\upsilon^2}\right)r^2+1\right]^2 + 4r^2\left[\left(\dfrac{\zeta_T}{\upsilon}+\dfrac{\zeta_s}{\upsilon^2}\right)r^2-\zeta_s-\dfrac{\zeta_T}{\upsilon}-\mu\zeta_T\upsilon\right]^2}} \qquad (3.8)$$

where H_{Acc} denotes the FRF from the ground accelerations to the absolute accelerations of the primary structure, with $\upsilon=\dfrac{\omega_T}{\omega_s}$ and $r=\dfrac{\omega}{\omega_s}$. And the terms related to the traditional and non-traditional TMDs are denoted by the subscripts A and B, respectively.

3.3 Optimum Design of Non-traditional Tuned Mass Dampers

As stated already in Section 1.3.1, there are two main methods for the optimum design of traditional TMD systems: one is the optimization analysis method and the other is the

fixed-points or quasi-fixed points theory. For non-traditional TMD systems, the fixed points or quasi-fixed points theory, which assumes that the maximum FRF magnitude occurs at two points of frequencies, has been also adopted to obtain υ^{opt} and ζ_T^{opt} by some researchers (Ren, 2001; Liu and Liu, 2005; Wong and Cheung, 2008). It has been proved that a non-traditional TMD provides a larger suppression of steady-state resonant vibration amplitude of the primary structure than a traditional TMD does. Figure 3.2 shows the comparison between the traditional and non-traditional TMDs, both of which employ the optimum value sets of υ and ζ_T obtained by the quasi-fixed points theory. It can be seen from Figure 3.2 (a) that, with a small value of mass ratio μ=0.01, very limited improvement can be achieved by the non-traditional TMD system compared with the traditional TMD system. Herein, the suppression bandwidth is defined as the frequency range in which the response magnitude ratio of the system with a TMD to the one without a TMD is not greater than unity. Even for such a large mass ratio μ=0.2 as shown in Figure 3.2 (b), the maximum FRF magnitude is reduced to some extent in the non-traditional TMD system, but the suppression bandwidths for the traditional and non-traditional TMD systems (denoted as B_A^* and B_B^*, respectively, in Figure 3.3) are almost the same.
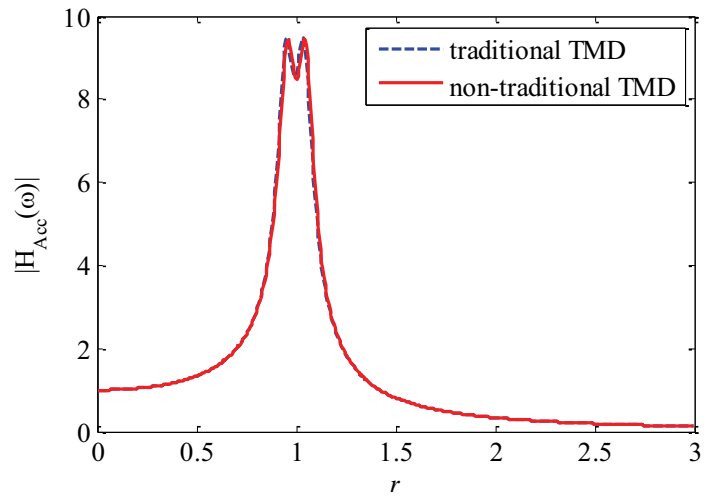
(a) $\mu = 0.01$, $\zeta_s = 0.02$, $\upsilon_A^{opt} = 0.987$, $\zeta_{TA}^{opt} = 0.064$, $\upsilon_B^{opt} = 1.003$, $\zeta_{TB}^{opt} = 0.064$
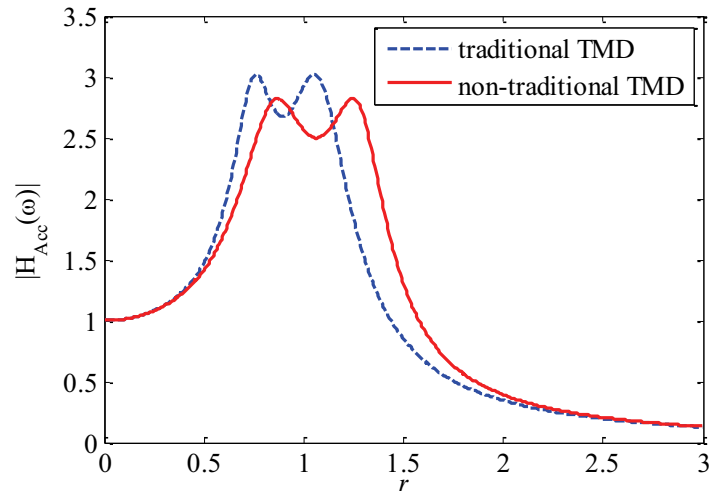
(b) $\mu = 0.2$, $\zeta_s = 0.02$, $\upsilon_A^{opt} = 0.823$, $\zeta_{TA}^{opt} = 0.253$, $\upsilon_B^{opt} = 1.118$, $\zeta_{TB}^{opt} = 0.280$

Figure 3.2 Magnitudes of FRF from harmonic acceleration input to absolute acceleration

of primary structure
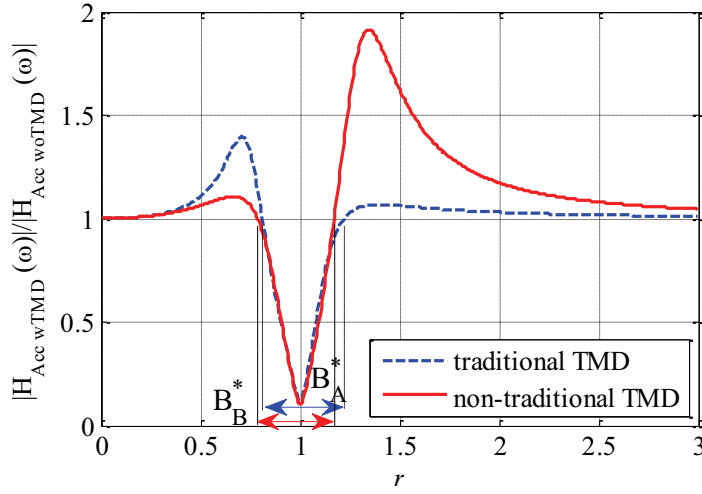
Figure 3.3 Comparison of maximum suppression bandwidths for traditional and

non-traditional TMDs

(μ =0.2, ζ_s =0.02, $\upsilon_A^{\mathrm{opt}}$ =0.823, $\zeta_{TA}^{\mathrm{opt}}$ =0.253, $\upsilon_B^{\mathrm{opt}}$ =1.118, $\zeta_{TB}^{\mathrm{opt}}$ =0.280)

Actually, by using the gradient-based optimization method as mentioned in Section 2.3, it is found that the maximum FRF magnitude of the non-traditional TMD system designed by the quasi-fixed points theory is not the global minimum solution. The maximum FRF magnitude which occurs at only one point of frequency is smaller than the magnitude at the two peak points obtained by the quasi-fixed points theory if υ is larger than a certain value. However, such a phenomenon is not found for the traditional TMD system. This can be also indicated from Figure 3.4. Figure 3.4 (a) indicates that the maximum FRF magnitude of the traditional TMD system will be minimum when υ is near the value of 1, while Figure 3.4 (b) signifies that the maximum FRF magnitude of the non-traditional TMD system is a local minimum value when υ is near the value of 1 and the maximum FRF magnitude could be smaller if υ is a large value.

(a) traditional TMD system

(b) non-traditional TMD system
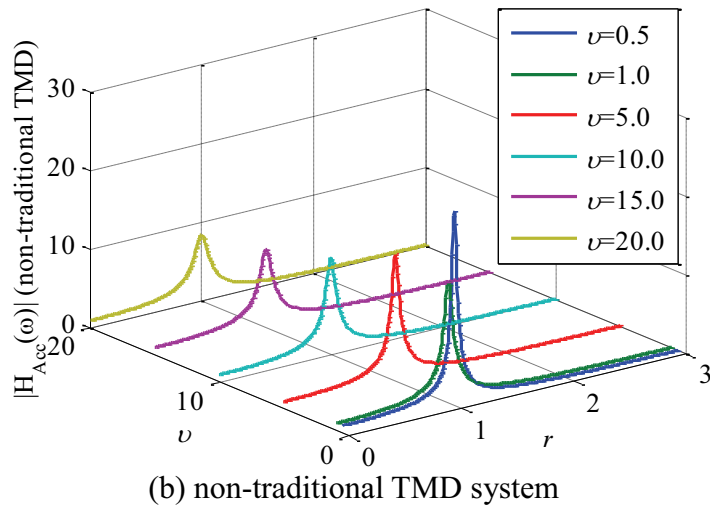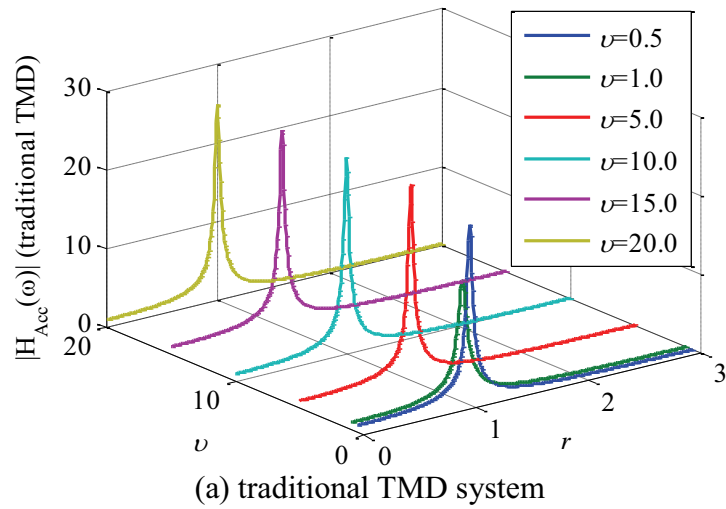
Figure 3.4 Magnitudes of FRFs from harmonic acceleration input to absolute acceleration

of primary structure in traditional and non-traditional TMD systems

(μ =0.01, ζ_s =0.02, ζ_T =0.2)

Figure 3.5 (a) and (b) show the relationships between the FRF magnitude and ζ_T, respectively, for the traditional and non-traditional TMD systems when υ is equal to 6 for instance. It can be found from the figures that the maximum FRF magnitude can be regarded as independent of ζ_T for a traditional TMD system. For a non-traditional

TMD system, on the other hand, the larger the value of ζ_T is, the smaller the maximum

FRF magnitude can be obtained.
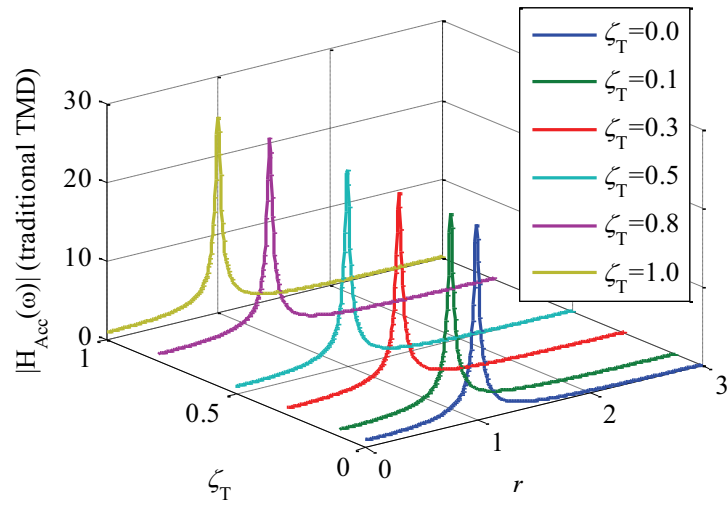
(a) traditional TMD system
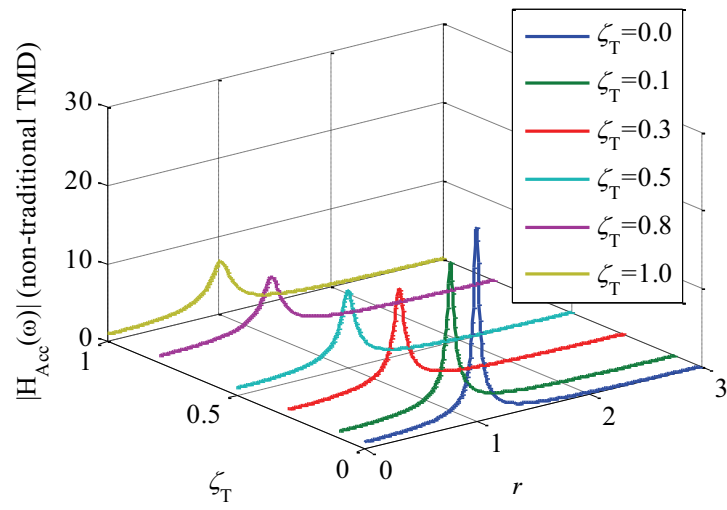
(b) non-traditional TMD system

Figure 3.5 Magnitudes of FRFs from harmonic acceleration input to absolute acceleration

of primary structure in traditional and non-traditional TMD systems

($\mu = 0.01$, $\zeta_s = 0.02$, $\upsilon = 6$)

An optimum design method for a non-traditional TMD is proposed to obtain wider suppression bandwidths. By substituting υ_A^{opt} and ζ_{TA}^{opt} into Equation (3.7), differentiating Equation (3.7) with respect to r, and then making thus-obtained equation equal to zero, the coordinates of the three extreme points p1, p2, and p3 (as shown in Figure 3.6) can be derived.
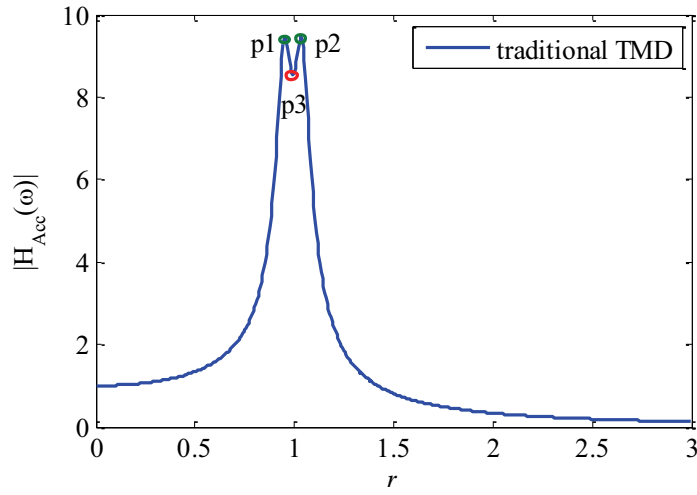
Figure 3.6 Three extreme points in optimally designed traditional TMD system

(μ =0.01, ζ_s =0.02, υ_A^{opt} =0.987, ζ_{TA}^{opt} =0.064,

p1 (0.953, 9.473), p2 (1.033, 9.473), p3 (0.992, 8.543))

By employing the constraints that the values of the parameters are: $0 < \upsilon_B \leq 1/\sqrt{\mu}$ and $0 \leq \zeta_{TB} \leq 1$ (Bakre and Jangid, 2007) for a non-traditional TMD, the global minimum value of the maximum FRF magnitude for the absolute acceleration of the primary structure can be obtained by using the gradient-based optimization method with respect to each value of $\upsilon_B \in \left(0, 1/\sqrt{\mu}\right]$, with the result shown in Figure 3.7. The following can be

seen from the figure: when υ_B=3.900 and ζ_{TB}=1.0, the maximum FRF magnitude for the non-traditional TMD system equals the magnitude value at points p1 and p2 of the traditional TMD system; and when υ_B=4.456 and ζ_{TB}=1.0, it equals the corresponding value at point p3 of the traditional TMD system. By setting the parameters υ_B and ζ_{TB} equal to the two sets of the above values, the FRF magnitudes for the non-traditional TMD system are obtained as shown in Figure 3.8. From the figure, it can be found that in the frequency range of $r \leq 1.15$, the control effect is improved for the non-traditional TMD system, while in the frequency range of $r > 1.15$, the FRF magnitudes for the non-traditional TMD system are a bit larger than those for the traditional TMD system. This is due to the fact that when $r > 1$, the value of $\left|H_{Acc}(\omega)\right|$ for the traditional TMD system decreases monotonically with respect to ζ_T when ζ_T is a large value, while the value of $\left|H_{Acc}(\omega)\right|$ for the non-traditional TMD system increases monotonically with respect to ζ_T. In other words, larger ζ_{TB} will result in a larger FRF magnitude in the high frequency range for a non-traditional TMD system. Therefore, too large values of ζ_{TB} are unfavorable. For achieving better performance than traditional TMD with respect to both maximum FRF magnitude and frequency suppression bandwidth, the optimum value of ζ_{TB} is obtained when the maximum FRF magnitude is equal to the magnitude at p3.

66
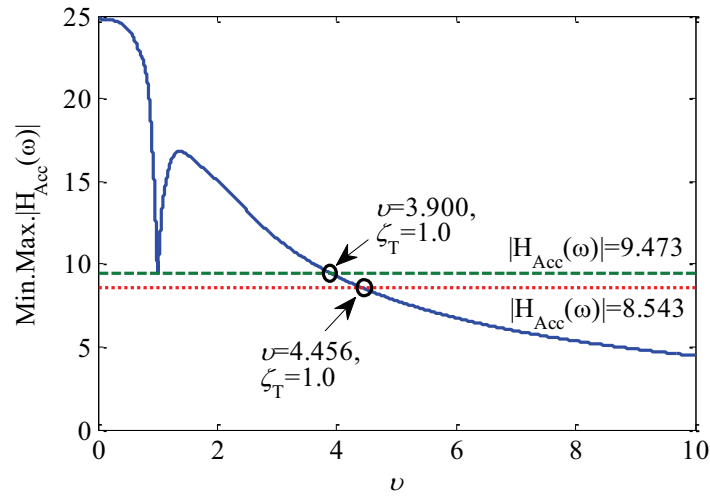
Figure 3.7 Global minimum values of maximum FRF magnitude for absolute acceleration

of primary structure in non-traditional TMD system

$(\mu=0.01, \zeta_s=0.02)$
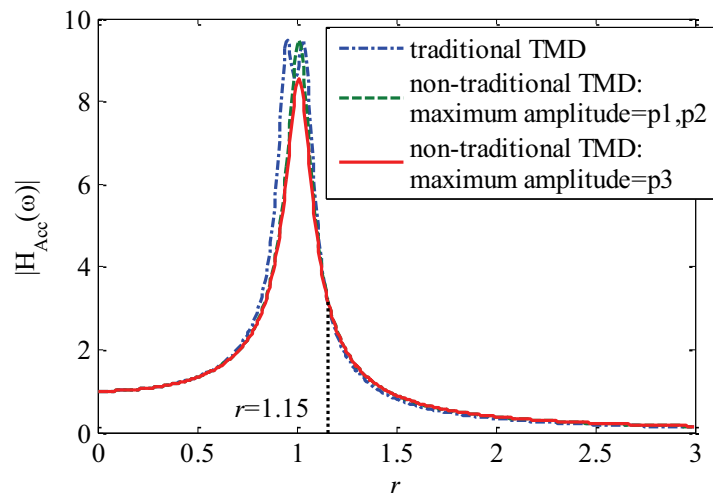

Figure 3.8 Magnitudes of FRFs from harmonic acceleration input to absolute acceleration

of primary structure ($\mu=0.01$, $\zeta_s=0.02$, $\upsilon_A^{opt}=0.987$, $\zeta_{TA}^{opt}=0.064$, $\upsilon_{B(p1,p2)}^{opt}=3.900$,

$\zeta_{TB(p1,p2)}^{opt}=1$, $\upsilon_{B(p3)}^{opt}=4.456$, $\zeta_{TB(p3)}^{opt}=1$)

Based on the above discussion, an optimum design method for a non-traditional TMD system is proposed as follows. Firstly, choose a practical value of υ_B as large as possible. When μ=0.01 and ζ_s=0.02, referring to Figure 3.7, it can be seen that: if the practical value of υ_B is in the range from 0 to 3.9, the optimum values of υ_B and ζ_{TB} can be determined by the quasi-fixed points theory; if υ_B is in the range from 3.9 to 4.5, ζ_{TB} should be set as large as possible under the constraint; and if υ_B can be larger than 4.5, ζ_{TB} can be set so as to make the maximum FRF magnitude equal to the magnitude at point p3 in Figure 3.6. For base-isolated structures, it would be possible to set the stiffness of the attached non-traditional TMD equal to the stiffness of base isolation bearings, i.e., $\upsilon_B = 1/\sqrt{\mu}$. If μ=0.01 and ζ_s=0.02, for instance, then υ_B=10 and ζ_{TB} can be obtained as 0.390 as illustrated in Figure 3.9.
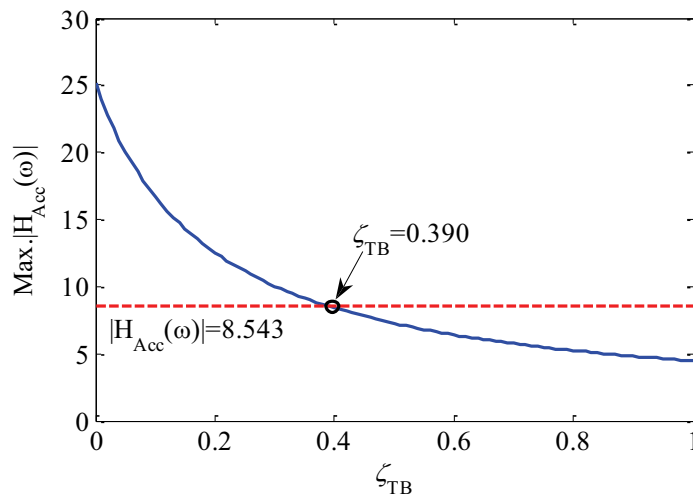
Figure 3.9 Relationship between maximum FRF magnitude for absolute acceleration of primary structure and ζ_{TB} (μ=0.01, ζ_s=0.02, υ_B=10)

The design method of traditional TMDs based on the stability maximization criterion, which ensures the same damping ratios in the first two vibration modes, has been verifed to be effective in seismic applications by Sadek (Sadek *et al.*, 1997). Traditional TMDs designed according to the quasi-fixed points theory and the stability maximization criterion are compared with the non-traditional TMD designed according to the method proposed in this chapter. The FRF magnitudes and maximum suppression bandwidths are shown in Figures 3.10 and 3.11, respectively. It can be found from Figures 3.10 (a) and 3.11 (b) that, the maximum FRF magnitude, i.e., $\text{Max}|H_{Acc}(\omega)|$ in the stability maximization criterion (referred to as SMC in the figures) is larger than that in the quasi-fixed points theory method (referred to as QFPT in the figures), whereas $|H_{Acc}(\omega)|$ in the stability maximization criterion are always smaller than that in the quasi-fixed points theory method except for the vicinity of the frequency range between the two fixed points. However, $|H_{Acc}(\omega)|$ in the traditional TMD system are larger than that in the non-traditional TMD system in the frequency range $r=0\sim1.497$. Moreover, it can be seen from Figure 3.11 (a) and (b) that, the suppression bandwidths in the stability maximization criterion are almost the same as those in the quasi-fixed points theory method for the traditional TMD system, and they are much narrower than those in the non-traditional TMD system. From Figure 3.10 (b), it can be found that though the stroke length of the traditional TMD designed by the stability maximization criterion is reduced compared with that in the quasi-fixed points theory method, it is still much larger than the stroke length of the non-traditional TMD.
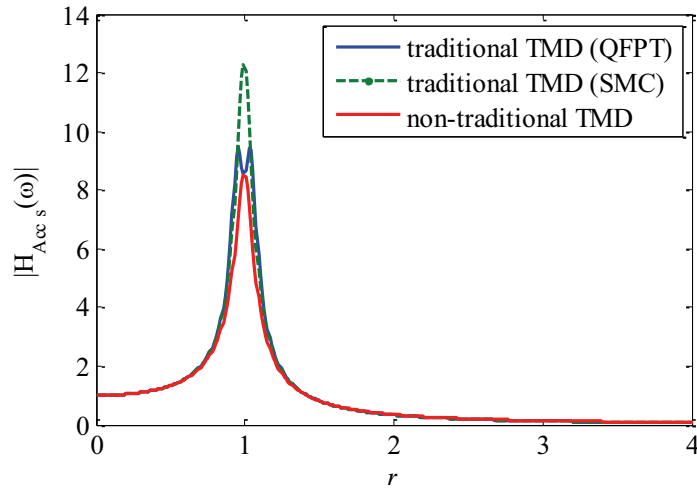
(a) absolute acceleration of primary structure
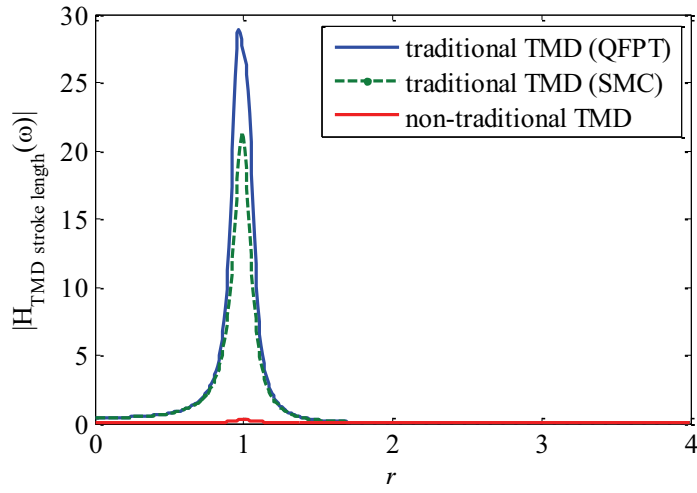
(b) stroke length of TMD

Figure 3.10 Magnitudes of FRFs from harmonic acceleration input to absolute

acceleration of primary structure and stroke length of TMD

(μ =0.01, ζ_s =0.02, $\omega_s = 2\pi/4$, $\upsilon_A^{opt(QFPT)}$ =0.987, $\zeta_{TA}^{opt(QFPT)}$ =0.064, $\upsilon_A^{opt(SMC)}$ =0.988,

$\zeta_{TA}^{opt(SMC)}$ =0.119, υ_B^{opt} =10, ζ_{TB}^{opt} =0.390)

(a) relative displacement of primary structure
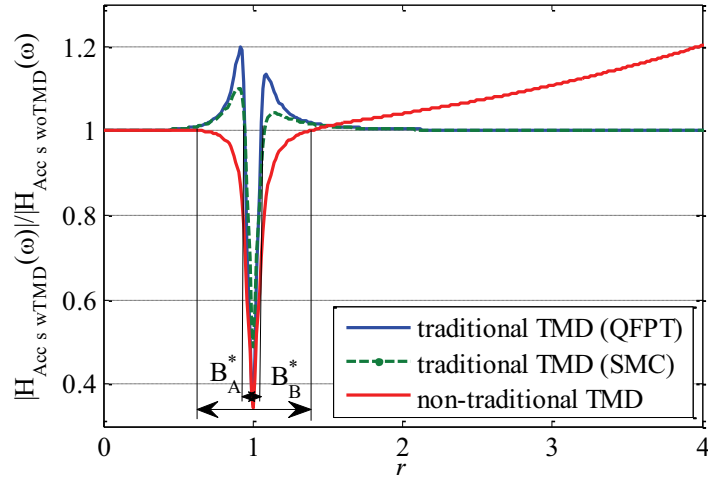
(b) absolute acceleration of primary structure

Figure 3.11 Suppression bandwidths for structural responses

(μ =0.01, ζ_{s} =0.02, $\omega_{\mathrm{s}}=2\pi/4$, $\upsilon_{\mathrm{A}}^{\mathrm{opt\,(QFPT)}}$ =0.987, $\zeta_{\mathrm{TA}}^{\mathrm{opt\,(QFPT)}}$ =0.064, $\upsilon_{\mathrm{A}}^{\mathrm{opt\,(SMC)}}$ =0.988,

$\zeta_{\mathrm{TA}}^{\mathrm{opt\,(SMC)}}$ =0.119, $\upsilon_{\mathrm{B}}^{\mathrm{opt}}$ =10, $\zeta_{\mathrm{TB}}^{\mathrm{opt}}$ =0.390)

It should be noted that the values of $\upsilon_{\mathrm{B}}^{\mathrm{opt}}$ and $\zeta_{\mathrm{TB}}^{\mathrm{opt}}$ based on the above-presented optimum design method are only related to the two parameters μ and ζ_{s}. Table 3.1 gives the values of $\zeta_{\mathrm{TB}}^{\mathrm{opt}}$ for different values of μ and ζ_{s} under the condition of

$v_{\mathrm{B}} = 1/\sqrt{\mu}$.

Table 3.1 Optimum values of ζ_{TB} $(v_{\mathrm{B}} = 1/\sqrt{\mu})$

		ζ_{s}						
		0.02	0.04	0.06	0.08	0.10	0.15	0.20
	0.01	0.390	0.378	0.372	0.369	0.370	0.390	0.437
	0.02	0.394	0.386	0.382	0.380	0.380	0.392	0.419
	0.03	0.395	0.390	0.387	0.386	0.387	0.398	0.422
	0.04	0.396	0.392	0.390	0.391	0.392	0.404	0.427
	0.05	0.396	0.393	0.393	0.394	0.396	0.410	0.433
	0.06	0.395	0.394	0.394	0.396	0.399	0.414	0.438
μ	0.07	0.394	0.394	0.395	0.398	0.402	0.418	0.443
	0.08	0.393	0.394	0.396	0.399	0.404	0.421	0.448
	0.09	0.392	0.393	0.396	0.400	0.405	0.424	0.452
	0.10	0.391	0.393	0.396	0.401	0.407	0.427	0.455
	0.15	0.384	0.389	0.395	0.402	0.410	0.436	0.471
	0.20	0.376	0.383	0.391	0.400	0.410	0.441	0.481
	0.25	0.368	0.377	0.386	0.396	0.408	0.443	0.489
	0.30	0.361	0.370	0.381	0.392	0.405	0.438	0.469

3.4 Numerical Example

For simplicity in evaluating the efficiency and performance of an optimum non-traditional TMD attached to a base-isolated structure, the entire structural system including the base isolation system is assumed to be linear elastic. A 3-DOF linear model shown in Figure 3.12 represents the system by simplifying the superstructure as an SDOF system. The mass M_{s}, natural period T_{s} and damping ratio ζ_{s} of the superstructure are 1.0×10^{6} kg, 1.0 s and 0.02, respectively. The mass of the base isolation layer m_{b} is 5.0×10^{4} kg, and the fundamental natural period of the base-isolated structure T_{is} is 4.0 s. The equivalent viscous damping ratios of the base isolators (ζ_{is}) are assumed to be 0.05 and 0.10 in the following analyses. Accordingly, the first modal damping ratios of the base-isolated structures are 0.0461 and 0.0920, respectively.
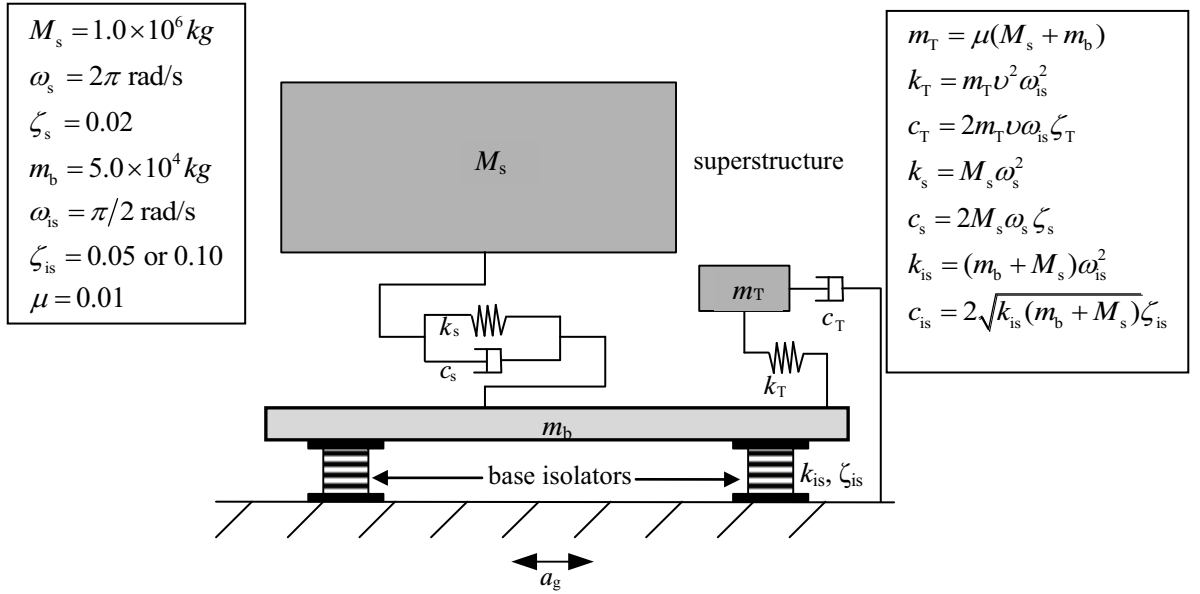
Figure 3.12 Analytic model of hybrid controlled system

The control effect of the optimum-designed non-traditional TMD (μ =0.01, υ_B =10, and

ζ_{TB}^{opt} =0.376 for ζ_{is} =0.05 and ζ_{TB}^{opt} =0.369 for ζ_{is} =0.10, which are obtained by applying

the linear interpolation method to the values in Table 3.1) is investigated by conducting

time-domain analyses with selected near- and far-field un-scaled earthquake records from

the PEER Berkeley database (http://peer.berkeley.edu/peer_ground_motion_database):

Kern County (TAF111, PEL090, in 1952), Kobe (KJM000, KAK000, in 1995) and

Landers (LCN260, BRS000, in 1992) which represent the three different kinds of

earthquakes (they are, respectively, classified into short period random phase type,

mid-long period pulse type and long period fling step type (Hisada, 2004)), and are

compared with the control effect of the optimum-designed traditional TMD (μ =0.01,

υ_A^{opt} =0.982 and ζ_{TA}^{opt} =0.0671 for ζ_{is} =0.05, υ_A^{opt} =0.969 and ζ_{TA}^{opt} =0.0705 for ζ_{is} =0.10,

which are obtained by the quasi-fixed points theory method). The velocity response

spectra ($\zeta_{structure} = 0.05$) of these selected records are shown in Figure 3.13. It is found

that the velocity responses for KJM000 and LCN260 are larger than those for the other excitations.
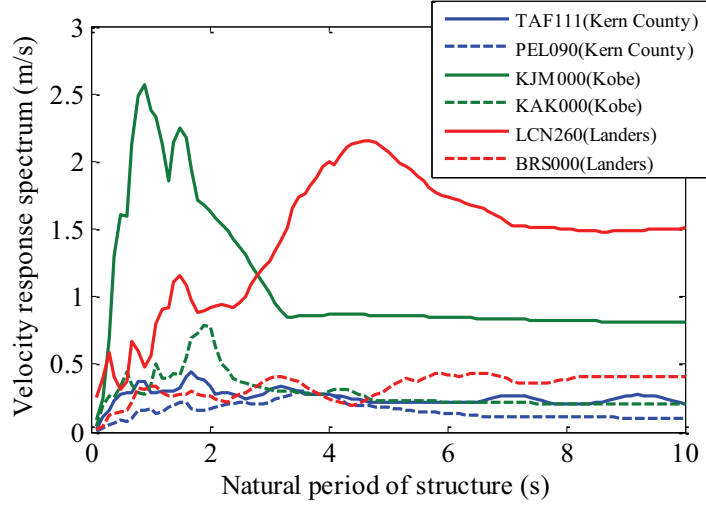
Figure 3.13 Velocity response spectra ($\zeta_{\text{structure}}$=0.05)

Figure 3.14 shows the time histories of damping forces resulting from the damping coefficient ($c_{\text{is}} = 2\sqrt{k_{\text{is}}(m_{\text{b}} + M_{\text{s}})}\zeta_{\text{is}}$) of base isolators in the base-isolation system, the damping coefficient ($c_{\text{TA}} = 2m_{\text{T}}\upsilon_{\text{A}}^{\text{opt}} \dfrac{2\pi}{T_{\text{is}}} \zeta_{\text{TA}}^{\text{opt}}$) of the traditional TMD attached to the base-isolation system and the damping coefficient ($c_{\text{TB}} = 2m_{\text{T}}\upsilon_{\text{B}} \dfrac{2\pi}{T_{\text{is}}} \zeta_{\text{TB}}^{\text{opt}}$) of the non-traditional TMD attached to the base-isolation system for the cases of KJM000 and LCN260. It is found that the maximum damping forces required by the non-traditional TMD could be practically realized though they are larger than those required by the traditional TMD.

(a) Kobe KJM000; ζ_{is} =0.05

Max(base-iso)=1.330x10⁵
Max(tra)=0.049x10⁵
Max(non-tra)=0.902x10⁵

(b) Kobe KJM000; ζ_{is} =0.10

Max(base-iso)=2.651x10⁵
Max(tra)=0.035x10⁵
Max(non-tra)=0.888x10⁵

(c) Landers LCN260; ζ_{is} =0.05
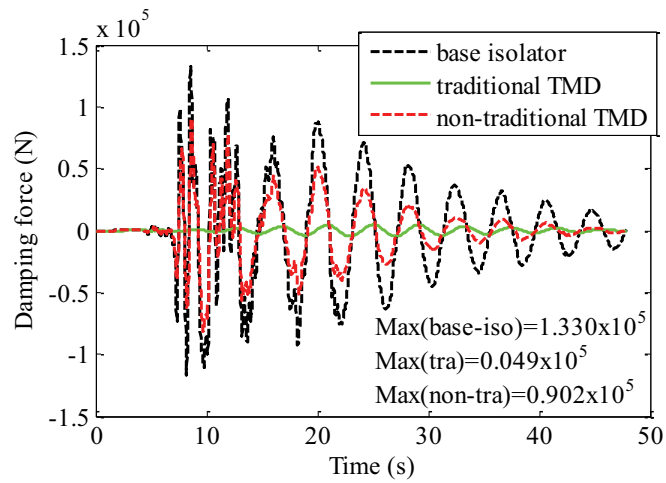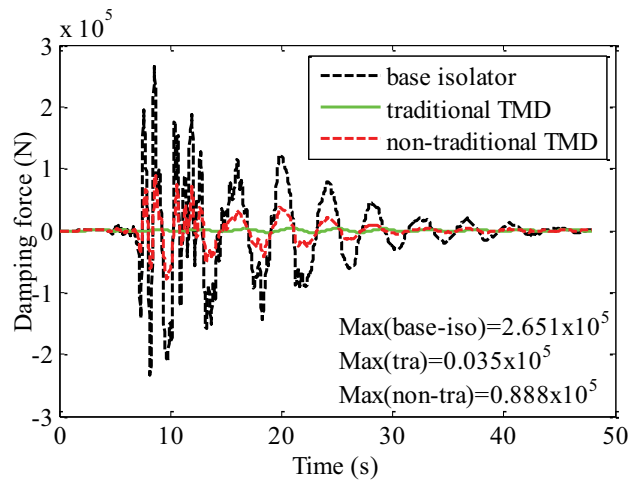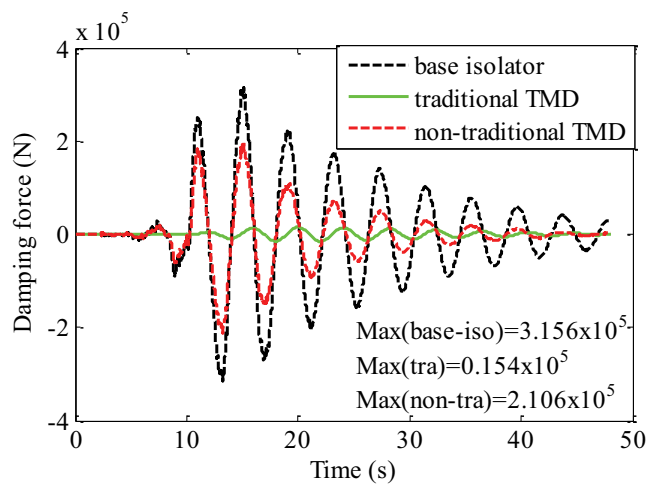
Max(base-iso)=3.156x10⁵
Max(tra)=0.154x10⁵
Max(non-tra)=2.106x10⁵

Figure 3.14 Time histories for damping forces
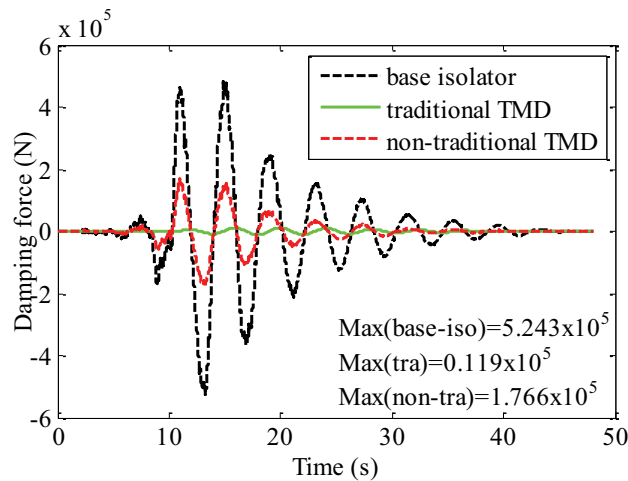
(d) Landers LCN260; ζ_{is} =0.10

Figure 3.14 Continued

The response ratios of the traditional TMD system to the system without a TMD, those of the non-traditional TMD system to the system without a TMD and those of the non-traditional TMD system to the traditional TMD system are plotted in Figure 3.15 (a)~(f), respectively, for the six earthquake records. In the figures, d_b represents deformation of the base isolators; d_s and a_s denote displacements of the superstructure relative to the base-isolation layer and absolute accelerations of the superstructure, respectively; d_T and a_T represent stroke length and absolute accelerations of the TMDs; and 'w/o TMD' is the abbreviation of without a TMD. It is noted that the response ratios for d_s and a_s are the same according to the results of numerical simulations. This fact can be demonstrated by the results in the frequency domain. It is found that for either traditional or non-traditional TMD system, the FRF magnitude ratios are exactly the same for d_s and a_s. It is predicted that the response ratios in the time domain also will be the same for d_s and a_s. Figure 3.16 is the combination of the figures in Figure 3.15 for response ratios of Max. d_b, Max. d_s or a_s, and RMS. d_s or a_s.

Ratio of Max. d_b with respect to w/o TMD

■ traditional TMD   ■ non-traditional TMD

$\zeta$is=0.05   0.940 / 0.832
$\zeta$is=0.10   0.966 / 0.877

Ratio of Max. d_s or a_s with respect to w/o TMD

■ traditional TMD   ■ non-traditional TMD

$\zeta$is=0.05   0.937 / 0.859
$\zeta$is=0.10   0.969 / 0.989

Ratio of RMS. d_s or a_s with respect to w/o TMD

■ traditional TMD   ■ non-traditional TMD

$\zeta$is=0.05   0.895 / 0.800
$\zeta$is=0.10   0.960 / 0.886

Ratio of Max. d_T and a_T of non-traditional TMD to traditional TMD

■ d_T ■ a_T

$\zeta$is=0.05   0.037 / 1.194
$\zeta$is=0.10   0.049 / 1.712

(a) Kern County TAF111

Ratio of Max. d_b with respect to w/o TMD

■ traditional TMD   ■ non-traditional TMD

$\zeta$is=0.05   0.975 / 0.873
$\zeta$is=0.10   0.975 / 0.884

Ratio of Max. d_s or a_s with respect to w/o TMD

■ traditional TMD   ■ non-traditional TMD

$\zeta$is=0.05   0.973 / 0.880
$\zeta$is=0.10   0.973 / 0.887

Ratio of RMS. d_s or a_s with respect to w/o TMD

■ traditional TMD   ■ non-traditional TMD

$\zeta$is=0.05   0.828 / 0.743
$\zeta$is=0.10   0.932 / 0.857

Ratio of Max. d_T and a_T of non-traditional TMD to traditional TMD

■ d_T ■ a_T

$\zeta$is=0.05   0.025 / 0.335
$\zeta$is=0.10   0.031 / 0.493

(b) Kern County PEL090

Figure 3.15 Comparison of responses of three different systems under earthquakes

Ratio of Max. d_b with respect to w/o TMD

■ traditional TMD ■ non-traditional TMD

$\zeta$is=0.05
- 0.895
- 0.786

$\zeta$is=0.10
- 0.996
- 0.958

Ratio of Max. d_s or a_s with respect to w/o TMD

■ traditional TMD ■ non-traditional TMD

$\zeta$is=0.05
- 0.883
- 0.856

$\zeta$is=0.10
- 0.995
- 0.992

Ratio of RMS. d_s or a_s with respect to w/o TMD

■ traditional TMD ■ non-traditional TMD

$\zeta$is=0.05
- 0.839
- 0.740

$\zeta$is=0.10
- 0.902
- 0.856

Ratio of Max. d_T and a_T of non-traditional TMD to traditional TMD

■ d_T ■ a_T

$\zeta$is=0.05
- 0.039
- 1.570

$\zeta$is=0.10
- 0.058
- 2.425

(c) Kobe KJM000

Ratio of Max. d_b with respect to w/o TMD

■ traditional TMD ■ non-traditional TMD

$\zeta$is=0.05
- 0.911
- 0.783

$\zeta$is=0.10
- 0.927
- 0.842

Ratio of Max. d_s or a_s with respect to w/o TMD

■ traditional TMD ■ non-traditional TMD

$\zeta$is=0.05
- 0.911
- 0.826

$\zeta$is=0.10
- 0.942
- 0.890

Ratio of RMS. d_s or a_s with respect to w/o TMD

■ traditional TMD ■ non-traditional TMD

$\zeta$is=0.05
- 0.841
- 0.747

$\zeta$is=0.10
- 0.920
- 0.864

Ratio of Max. d_T and a_T of non-traditional TMD to traditional TMD

■ d_T ■ a_T

$\zeta$is=0.05
- 0.032
- 1.029

$\zeta$is=0.10
- 0.039
- 1.487

(d) Kobe KAK000

Figure 3.15 Continued

Ratio of Max. d_b with respect to w/o TMD

■ traditional TMD   ■ non-traditional TMD

	traditional TMD	non-traditional TMD
$\zeta_{is}=0.05$	0.972	0.850
$\zeta_{is}=0.10$	0.993	0.925

Ratio of Max. d_s or a_s with respect to w/o TMD

■ traditional TMD   ■ non-traditional TMD

	traditional TMD	non-traditional TMD
$\zeta_{is}=0.05$	0.964	0.857
$\zeta_{is}=0.10$	0.987	0.929

Ratio of RMS. d_s or a_s with respect to w/o TMD

■ traditional TMD   ■ non-traditional TMD

	traditional TMD	non-traditional TMD
$\zeta_{is}=0.05$	0.842	0.732
$\zeta_{is}=0.10$	0.919	0.837

Ratio of Max. d_T and a_T of non-traditional TMD to traditional TMD

■ d_T ■ a_T

	d_T	a_T
$\zeta_{is}=0.05$	0.026	0.351
$\zeta_{is}=0.10$	0.030	0.495

(e) Landers LCN260

Ratio of Max. d_b with respect to w/o TMD

■ traditional TMD   ■ non-traditional TMD

	traditional TMD	non-traditional TMD
$\zeta_{is}=0.05$	1.004	0.944
$\zeta_{is}=0.10$	1.015	0.938

Ratio of Max. d_s or a_s with respect to w/o TMD

■ traditional TMD   ■ non-traditional TMD

	traditional TMD	non-traditional TMD
$\zeta_{is}=0.05$	1.011	0.958
$\zeta_{is}=0.10$	1.015	0.963

Ratio of RMS. d_s or a_s with respect to w/o TMD

■ traditional TMD   ■ non-traditional TMD

	traditional TMD	non-traditional TMD
$\zeta_{is}=0.05$	1.015	0.952
$\zeta_{is}=0.10$	1.014	0.960

Ratio of Max. d_T and a_T of non-traditional TMD to traditional TMD

■ d_T ■ a_T

	d_T	a_T
$\zeta_{is}=0.05$	0.049	1.242
$\zeta_{is}=0.10$	0.053	1.509

(f) Landers BRS000

Figure 3.15 Continued

79

Figure 3.16 Response ratios with respect to w/o TMD under earthquakes

From the figures, it is found that both the traditional and non-traditional TMDs are more effective for lightly damped isolators. For the traditional TMD, it is not effective in reducing the responses for Landers BRS000 which has abundant very long period predominant components (See Figure 3.13), and the maximum deformation of the base isolators (denoted as Max. d_b) can be reduced by 3%-10% for ζ_{is} =0.05, and 0.4%-7.0%

for ζ_{is}=0.10 except for BRS000. The maximum relative displacements and absolute accelerations of the superstructure (denoted as Max.d_s and Max.a_s, respectively) can be reduced by 3%-12% for ζ_{is}=0.05, and 0.5%-6.0% for ζ_{is}=0.10 except for BRS000. The root mean square (RMS) values of relative displacements and absolute accelerations of the superstructure (denoted as RMS.d_s and RMS.a_s, respectively) can be reduced by 10%-17% for ζ_{is}=0.05, and 4%-10% for ζ_{is}=0.10 except for BRS000. For the non-traditional TMD, though it is less effective for Landers BRS000 compared with other excitations, certain control effect for Landers BRS000 is still achieved. Except for the case of BRS000, the maximum deformation of the base isolators (denoted as Max. d_b) can be reduced by 13%-22% for ζ_{is}=0.05, and 4%-16% for ζ_{is}=0.10; the maximum relative displacements and absolute accelerations of the superstructure (denoted as Max.d_s and Max.a_s, respectively) can be reduced by 12%-17% for ζ_{is}=0.05, and 0.8%-11.0% for ζ_{is}=0.10; the RMS values of relative displacements and absolute accelerations of the superstructure (denoted as RMS.d_s and RMS.a_s, respectively) can be reduced by 20%-27% for ζ_{is}=0.05, and 11%-16% for ζ_{is}=0.10. It can be concluded that the non-traditional TMD is always much more effective than the traditional TMD in mitigating the responses of the base isolators and superstructure under the different types of seismic excitations. Furthermore, it is shown in Figure 3.17 that the stroke length of the traditional TMD is very large when the structural system is excited by the large near-field ground motions, i.e., Kobe (KJM000) or Landers (LCN260). For the non-traditional TMD, however, the stroke length is much smaller, which indicates that the required accommodation space of the TMD is greatly reduced.
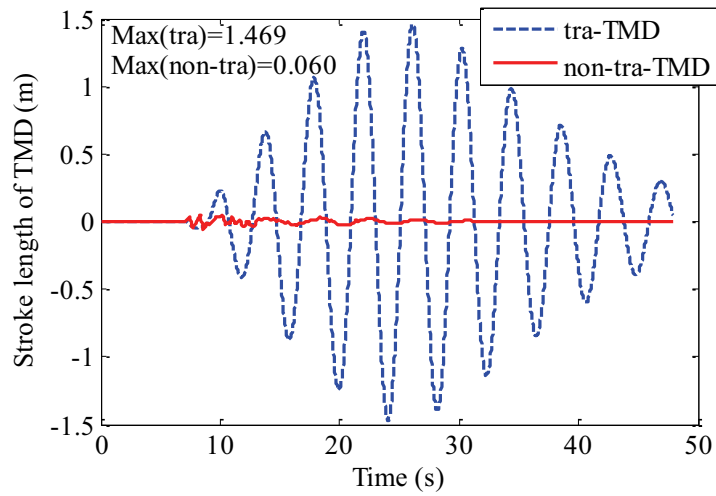
(a) Kobe KJM000; ζ_{is}=0.05
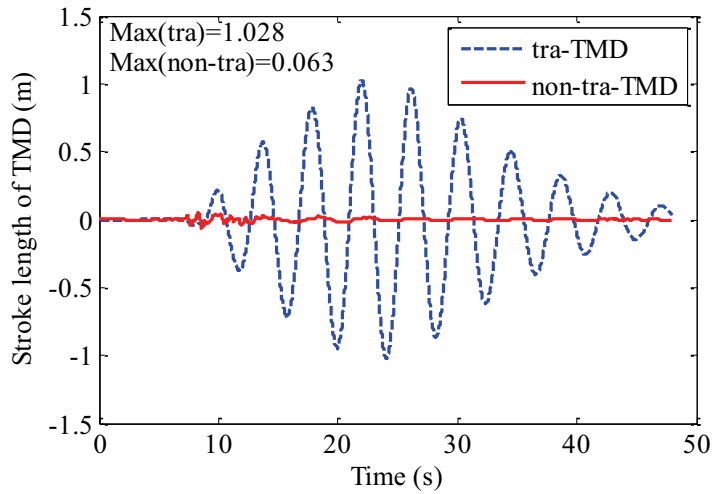
(b) Kobe KJM000; ζ_{is}=0.10

Figure 3.17 Time histories for stroke length of TMDs
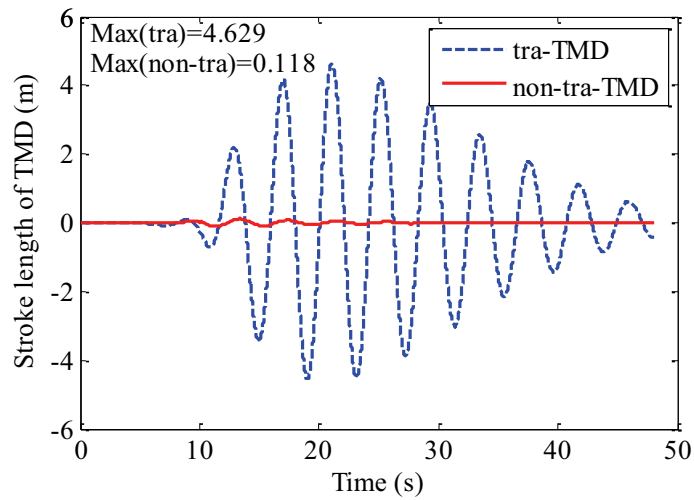
(c) Landers LCN260; ζ_{is} =0.05
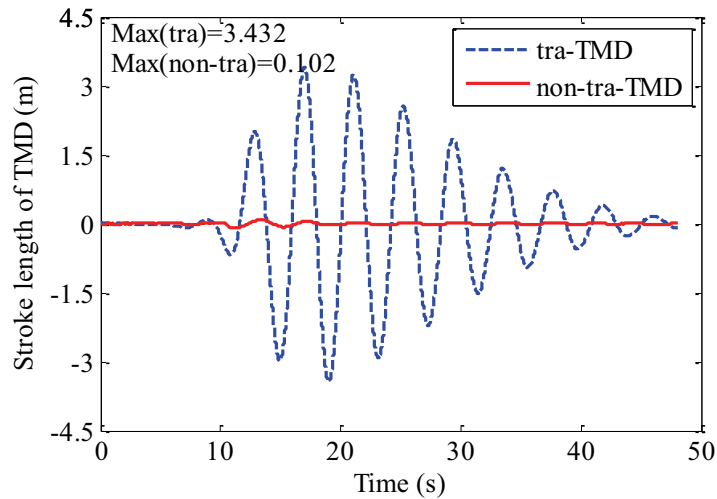
(d) Landers LCN260; ζ_{is} =0.10

Figure 3.17 Continued

The non-traditional TMD has its dashpot directly connected to the ground, and in the following it is compared to the system in which just pure dashpot with the same damping coefficient as the non-traditional TMD is connected between the base isolation layer and the ground. It is found that the responses of the superstructure are similar in the two systems as well as the deformation of the base isolators. However, the absolute accelerations of the base isolation layer (denoted as a_b) in the non-traditional TMD

system are much smaller than those in the pure dashpot system under all the six earthquakes, which indicates that the non-traditional TMD system provides higher human comfortability to the ground floor. In addition, it is beneficial to protect rubbers in the base isolators from damage. Figure 3.18 (a)~(f) show the ratios of the maximum and RMS values of a_b (denoted as Max. a_b and RMS. a_b, respectively) of the non-traditional TMD system to those of the pure dashpot system for the six earthquake records, respectively. It is found that the Max. a_b can be reduced by 6%-28% and 6%-21% in the non-traditional TMD system compared with the pure dashpot system for ζ_{is}=0.05 and ζ_{is}=0.10, respectively. RMS. a_b can be reduced by 1%-18% and 2%-18% in the non-traditional TMD system compared with the pure dashpot system for ζ_{is}=0.05 and ζ_{is}=0.10, respectively. Figure 3.19 is the combination of Figure 3.18 (a)~(f).

To compare the differences of the responses of the superstructure between the non-traditional TMD system and the pure dashpot system, a parametric analysis is conducted with different combinations of mass ratios μ and damping ratios ζ_{is}. The FRF magnitudes, $|H_{Acc}(\omega)|$, of the superstructure in the non-traditional TMD system are compared with those in the pure dashpot system during the frequency range of $0.6 \leq r \leq 1.6$. The 2-norm value of $|H_{Acc}(\omega)|$ which can generally represent the area under the frequency response curve, and the maximum value of $|H_{Acc}(\omega)|$ which indicates the resonant vibration amplitude are used as the two performance indices in the comparison. In Figure 3.20 (a), the ratios of the 2-norm values of $|H_{Acc}(\omega)|_B$ (magnitudes of the FRF $H_{Acc}(\omega)$ in the non-traditional TMD system) to those of $|H_{Acc}(\omega)|_{VD}$ (magnitudes of the FRF $H_{Acc}(\omega)$ in the pure dashpot system) are presented for μ=0.01, 0.05, 0.10, 0.15, 0.20,

84

0.25, 0.30, with the parameters of ζ_{is}=0.02, 0.06, 0.10 and 0.20, respectively. In Figure 3.20 (b), the ratios of the maximum values of $|H_{Acc}(\omega)|_B$ to those of $|H_{Acc}(\omega)|_{VD}$ are given. It can be seen from Figure 3.20 that the 2-norm values and maximum values of $|H_{Acc}(\omega)|_B$ are all smaller than those in the pure dashpot system, and the ratios decrease monotonically with respect to μ when ζ_{is}=0.02. For the cases with ζ_{is}=0.06, the 2-norm values of $|H_{Acc}(\omega)|_B$ are smaller than those of $|H_{Acc}(\omega)|_{VD}$ when μ is larger than 0.15, while the maximum values of $|H_{Acc}(\omega)|_B$ are always smaller than those of $|H_{Acc}(\omega)|_{VD}$ and the ratios decrease monotonically with respect to μ. For ζ_{is}=0.10, the 2-norm values of $|H_{Acc}(\omega)|_B$ are larger than those of $|H_{Acc}(\omega)|_{VD}$ for all the seven values of μ, while the maximum values of $|H_{Acc}(\omega)|_B$ are smaller than those of $|H_{Acc}(\omega)|_{VD}$ when μ is larger than 0.15. When ζ_{is} is 0.20, the 2-norm values and maximum values of $|H_{Acc}(\omega)|_B$ are larger than those of $|H_{Acc}(\omega)|_{VD}$ for all the seven mass ratios. In conclusion, the non-traditional TMD system has better performance than the pure dashpot system when mass ratio μ is large (e.g., larger than 0.15 in the numerical example), and damping ratio ζ_{is} is small (e.g., less than 0.06 in the numerical example).

3.5 Conclusions

For non-traditional TMD systems, it has been demonstrated that the conventional design method based on the quasi-fixed points theory cannot provide the global minimum value of the maximum FRF magnitude for responses of primary structures. This fact is different from traditional TMD systems. An optimum design method of non-traditional TMDs has been presented from the standpoint of obtaining much wider suppression bandwidths in this chapter. On the basis of the optimum-designed TMD discussion, a base-isolated

structural system with a non-traditional TMD combined is proposed. The control effect of the optimally designed non-traditional TMD integrated to a base-isolated structure under different types of earthquake excitations have been investigated and compared with that of the optimally designed traditional TMD. It is found that the control effect of the non-traditional TMD is significantly improved compared with the traditional TMD, in particular in terms of significant reduction of TMD stroke length. There is no need to consider the problem of stroke length exceeding the limitation for non-traditional TMDs, whereas traditional TMDs may exceed space limitations when systems are subjected to near-field long period earthquake ground motions. Compared with the pure dashpot system which has the same damping coefficient as the corresponding non-traditional TMD, the accelerations of the base isolation layer in the non-traditional TMD system are much smaller, which can prevent the base-isolation bearings from damage and also ensure human comfortability of the ground floor. In this regard, non-traditional TMDs may provide a better solution for either retrofitting or constructing base-isolated structures.
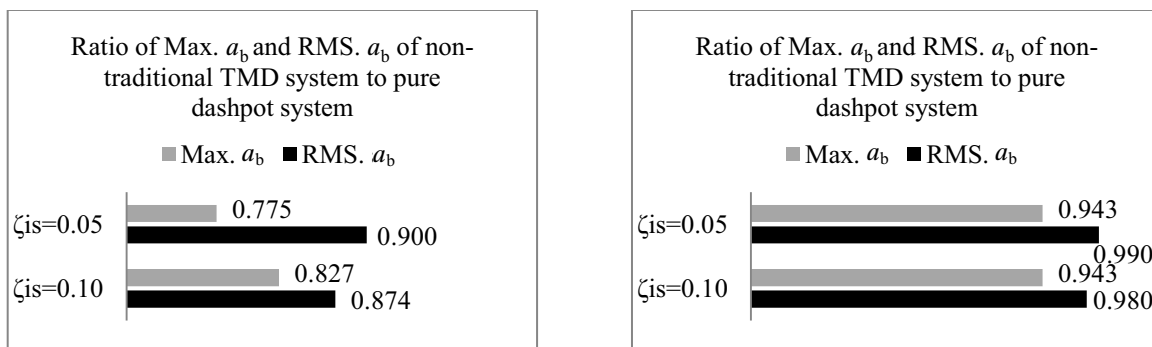
(a) Kern County TAF111   (b) Kern County PEL090

Figure 3.18 Comparison of accelerations of base isolation layer in non-traditional TMD and pure dashpot systems under earthquakes
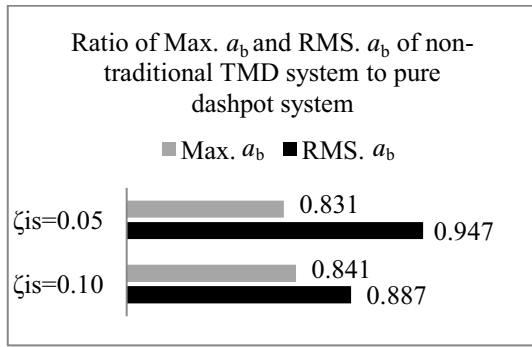
(c) Kobe KJM000
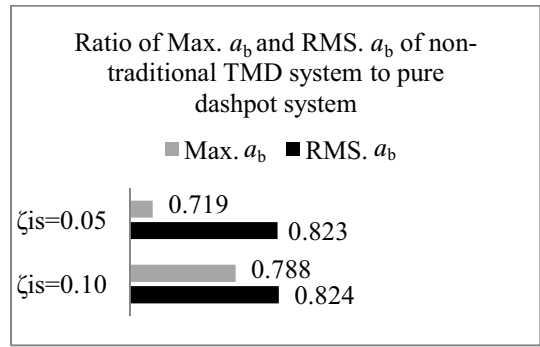
(d) Kobe KAK000
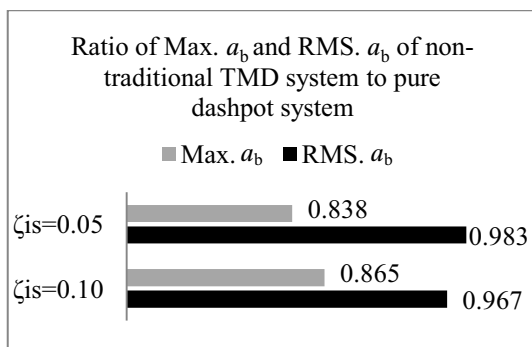
(e) Landers LCN260
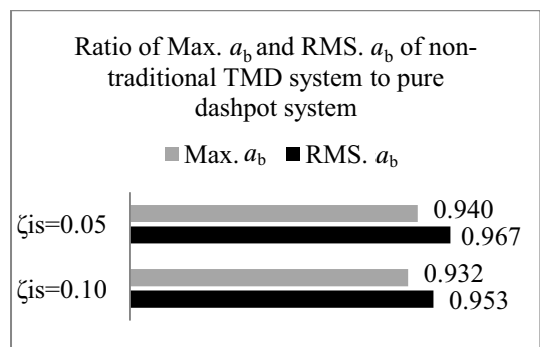
(f) Landers BRS000

Figure 3.18 Continued
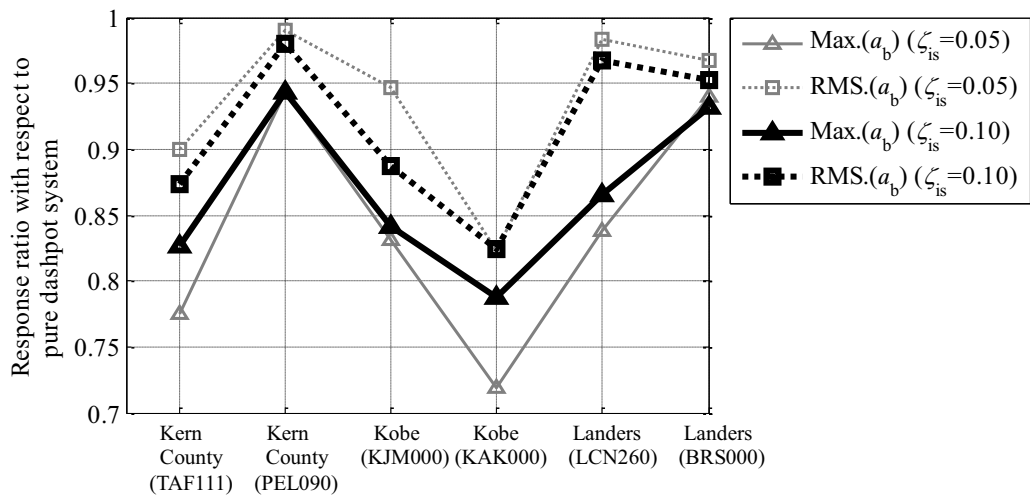
Figure 3.19 Response ratios of absolute accelerations of base isolation layer in

non-traditional TMD system with respect to those in pure dashpot system under

earthquakes
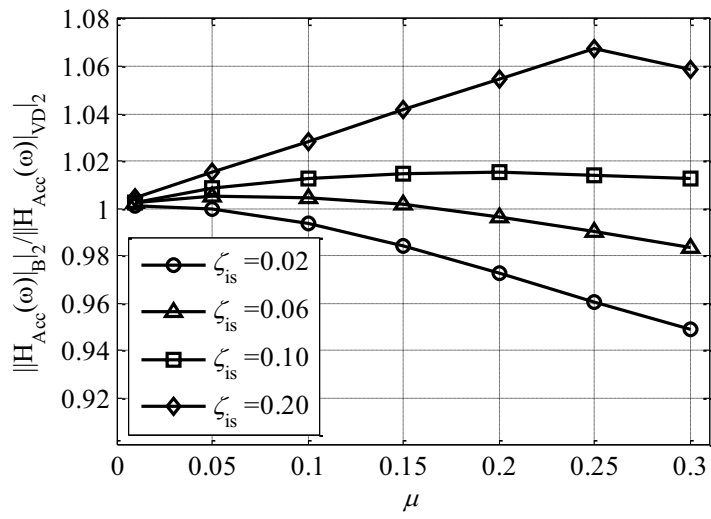
(a) ratios for 2-norm value of FRF magnitudes
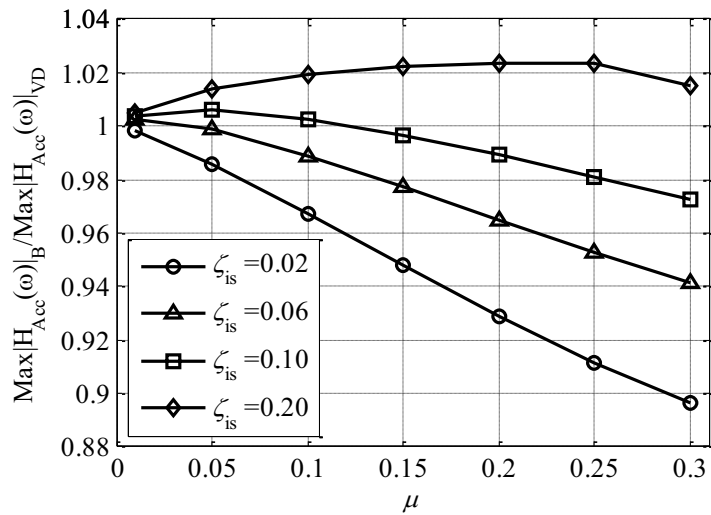
(b) ratios for maximum value of FRF magnitudes

Figure 3.20 Comparison of FRF magnitudes between non-traditional TMD system and

pure dashpot system

4. OPTIMUM DESIGN OF NON-TRADITIONAL TUNED MASS DAMPER VIA STABILITY MAXIMIZATION CRITERION

4.1 Introduction

A non-traditional TMD system has been designed for reducing steady state responses for wider suppression bandwidths in the frequency domain in Chapter 3. Stability maximization criterion has been employed to design traditional TMDs by some researchers as mentioned in Section 1.3.1 (1). In this chapter, stability maximization criterion is employed to design non-traditional TMD systems for decaying free vibration responses in the minimum duration.

4.2 Stability Maximization Criterion

The state space model of a scalar-input linear system of order N is written as

$$\dot{\mathbf{x}} = \mathbf{A}\mathbf{x} + \mathbf{B}u \tag{4.1}$$

where $\mathbf{x}$ and u are the state vector and input, respectively. The response of this system is given by

$$\mathbf{x}(t) = \mathrm{e}^{\mathbf{A}(t-t_0)}\mathbf{x}(t_0) + \int_{t_0}^{t} \mathrm{e}^{\mathbf{A}(t-\tau)}\mathbf{B}u(\tau)d\tau \tag{4.2}$$

If λ_i ($i = 1, \cdots, N$) are defined as the eigenvalues of the system and all of them are singular, then $\mathbf{A}$ is diagonalizable and semisimple, and the free vibration response term in Equation (4.2) can be given in terms of the spectral resolution as

$$e^{\mathbf{A}(t-t_0)}\mathbf{x}(t_0) = \sum_{i=1}^{N} \mathbf{P}_i \mathbf{x}(t_0) e^{\lambda_i(t-t_0)} \tag{4.3}$$

where $\mathbf{P}_i$ is given by Lagrange's interpolation polynominal as

$$\mathbf{P}_i = \frac{(\mathbf{A} - \lambda_1\mathbf{I})\cdots(\mathbf{A} - \lambda_{i-1}\mathbf{I})(\mathbf{A} - \lambda_{i+1}\mathbf{I})\cdots(\mathbf{A} - \lambda_n\mathbf{I})}{(\lambda_i - \lambda_1)\cdots(\lambda_i - \lambda_{i-1})(\lambda_i - \lambda_{i+1})\cdots(\lambda_i - \lambda_n)} \tag{4.4}$$

The degree of stability is defined as the absolute value of the maximum real part of the eigenvalues:

$$\Lambda = -\max_i \mathrm{Re}(\lambda_i) \tag{4.5}$$

where $\Lambda > 0$, and the following inequality holds:

$$\left| e^{\mathbf{A}(t-t_0)}\mathbf{x}(t_0) \right| \le \sum_{i=1}^{N} \left| \mathbf{P}_i \mathbf{x}(t_0) \right| e^{-\Lambda(t-t_0)} \tag{4.6}$$

Thus Λ indicates the speed of convergence of the free vibration response.

The objective of this criterion is to decay the free vibration response of a system in the minimum duration. The optimization can be achieved when the degree of stability Λ is maximized. In other words, all the eigenvalues are located far from the imaginary axis in the left-half s-plane.

4.3 Optimum Design of Non-traditional Tuned Mass Dampers

If there is a ground motion applied to the non-traditional TMD system as shown in Figure 4.1, the equations of motion of the system are

$$\begin{cases} M_s \ddot{x}_s + c_s \dot{x}_s + \left(k_s + k_T \right) x_s - k_T x_T = -M_s \ddot{x}_g \\ m_T \ddot{x}_T + c_T \dot{x}_T + k_T x_T - k_T x_s = -m_T \ddot{x}_g \end{cases} \tag{4.7}$$

where x denotes the displacement relative to the ground, the dot over the symbol denotes the derivative with respect to time t, and $\ddot{x}_g$ represents the ground acceleration which can also be denoted as a_g.
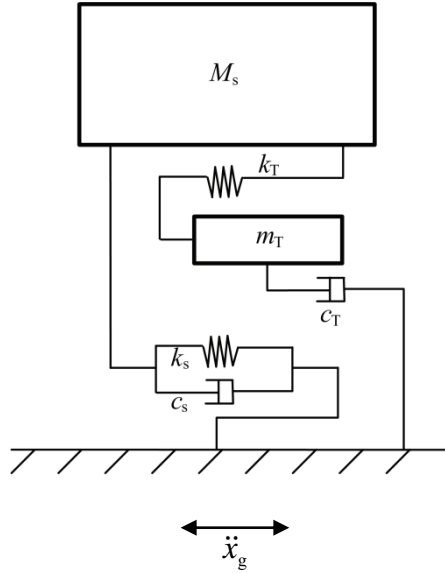
Figure 4.1 Non-traditional TMD system

If τ is defined as $\tau = \omega_s t$, where $\omega_s = \sqrt{k_s/M_s}$, then $d/dt = \omega_s \left(d/d\tau \right)$, $d^2/dt^2 = \omega_s^2 \left(d^2/d\tau^2 \right)$, Equation (4.7) becomes

$$\begin{cases} \ddot{\tilde{x}}_s + 2\zeta_s\dot{\tilde{x}}_s + \left(1 + \mu\upsilon^2\right)\tilde{x}_s - \mu\upsilon^2\tilde{x}_T = -\ddot{\tilde{x}}_g \\ \ddot{\tilde{x}}_T + 2\upsilon\zeta_T\dot{\tilde{x}}_T + \upsilon^2\tilde{x}_T - \upsilon^2\tilde{x}_s = -\ddot{\tilde{x}}_g \end{cases} \tag{4.8}$$

where $\tilde{x} = x(\tau)$, $\dot{\tilde{x}} = \mathrm{d}\tilde{x}/\mathrm{d}\tau$, $\ddot{\tilde{x}} = \mathrm{d}^2\tilde{x}/\mathrm{d}\tau^2$, $\upsilon = \sqrt{k_T/m_T}\big/\sqrt{k_s/M_s}$, $\zeta_s = c_s\big/\left(2\sqrt{M_s k_s}\right)$,

$\zeta_T = c_T\big/\left(2\sqrt{m_T k_T}\right)$ and $\mu = m_T/M_s$.

If the state vector $\mathbf{x}$ is defined as $\mathbf{x} = [\dot{\tilde{x}}_s, \dot{\tilde{x}}_T, \tilde{x}_s, \tilde{x}_T]^T$, then the matrix $\mathbf{A}$ corresponding to

Equation (4.1) in this system can be obtained as

$$\mathbf{A} = \begin{bmatrix} -2\zeta_s & 0 & -\left(1 + \mu\upsilon^2\right) & \mu\upsilon^2 \\ 0 & -2\upsilon\zeta_T & \upsilon^2 & -\upsilon^2 \\ 1 & 0 & 0 & 0 \\ 0 & 1 & 0 & 0 \end{bmatrix} \tag{4.9}$$

Accordingly, the characteristic equation can be obtained as

$$\lambda^4 + 2(z + \zeta_s)\lambda^3 + \left(\upsilon^2 + 4\zeta_s z + 1 + \mu\upsilon^2\right)\lambda^2 + 2\left(\zeta_s\upsilon^2 + z + \mu z\upsilon^2\right)\lambda + \upsilon^2 = 0 \tag{4.10}$$

where $z = \upsilon\zeta_T$.

Assuming the solutions of Equation (4.10), i.e., four eigenvalues in complex conjugate

pairs, are $\lambda_{1,2} = -\beta_1 \pm i\theta_1$ and $\lambda_{3,4} = -\beta_2 \pm i\theta_2$, and thus the characteristic equation

should satisfy

$$(\lambda + \beta_1 - i\theta_1)(\lambda + \beta_1 + i\theta_1)(\lambda + \beta_2 - i\theta_2)(\lambda + \beta_2 + i\theta_2) = 0 \tag{4.11}$$

The following equations can be obtained by comparing the coefficients of λ in Equations (4.10) and (4.11):

$$2(z + \zeta_s) = 2(\beta_1 + \beta_2) \tag{4.12}$$

$$\upsilon^2 + 4\zeta_s z + 1 + \mu\upsilon^2 = r_1^2 + r_2^2 + 4\beta_1\beta_2 \tag{4.13}$$

$$2(\zeta_s\upsilon^2 + z + \mu z\upsilon^2) = 2(\beta_1 r_2^2 + \beta_2 r_1^2) \tag{4.14}$$

$$\upsilon^2 = r_1^2 r_2^2 \tag{4.15}$$

where $r_1^2 = \beta_1^2 + \theta_1^2$ and $r_2^2 = \beta_2^2 + \theta_2^2$.

For a certain value of z, it can be seen from Equation (4.12) that the degree of stability will be maximized if β_1 and β_2 are equal to each other, because the degree of stability is equal to the smaller value of β_1 and β_2. Accordingly, by replacing both β_1 and β_2 by β, and then substituting Equations (4.12) and (4.15) into Equations (4.13) and (4.14), the following two equations are obtained:

$$r_1^2 r_2^2 + 4\zeta_s(2\beta - \zeta_s) + 1 + \mu r_1^2 r_2^2 = r_1^2 + r_2^2 + 4\beta^2 \tag{4.16}$$

$$\zeta_s r_1^2 r_2^2 + 2\beta - \zeta_s + \mu\left(2\beta - \zeta_s\right) r_1^2 r_2^2 = \beta\left(r_1^2 + r_2^2\right) \tag{4.17}$$

By substituting $r_2^2 = \upsilon^2 / r_1^2$ into Equation (4.17), υ can be obtained as

$$\upsilon = r_1 \sqrt{\frac{\beta\left(r_1^2 - 2\right) + \zeta_s}{\left[\left(1 - \mu\right)\zeta_s + 2\mu\beta\right] r_1^2 - \beta}} \tag{4.18}$$

Correspondingly,

$$r_2 = \sqrt{\frac{\beta\left(r_1^2 - 2\right) + \zeta_s}{\left[\left(1 - \mu\right)\zeta_s + 2\mu\beta\right] r_1^2 - \beta}} \tag{4.19}$$

Substituting Equations (4.18) and (4.19) into Equation (4.16), we get

$$a r_1^4 + b r_1^2 + c = 0 \tag{4.20}$$

where $a = \left(1 - \mu\right)$, $b = -2\left[1 + 2\left(\beta - \zeta_s\right)\left(\zeta_s + 2\mu\beta - \mu\zeta_s\right)\right]$ and $c = 1 + 4\beta\left(\beta - \zeta_s\right)$.

The following inequality should be satisfied to ensure that r_1 is a positive real value,

$$b^2 - 4ac \geq 0 \tag{4.21}$$

In the special case when $\zeta_s = 0$, i.e., the primary structure has no damping, the upper

limit value of β can be obtained in the following fashion:

$$\beta \leq \frac{1}{2\mu} \sqrt{\frac{1 - 3\mu - (1-\mu)\sqrt{1-4\mu}}{2}} \text{ , where } 0 < \mu \leq 0.25 \tag{4.22}$$

And β equals the upper limit value when

$$\upsilon = \frac{1 - \sqrt{1-4\mu}}{2\mu} \tag{4.23}$$

and

$$\zeta_T = \frac{\sqrt{2}}{1 - \sqrt{1-4\mu}} \sqrt{1 - 3\mu - (1-\mu)\sqrt{1-4\mu}} \tag{4.24}$$

Equation (4.23) is obtained from Equations (4.18) and (4.20) with the upper limit value

of β combined, and Equation (4.24) is derived from Equation (4.12) and the relationship

of $z = \upsilon\zeta_T$.

In the general case when $\zeta_s \neq 0$, constraints can be obtained by solving Equation (4.21)

as $0 < \mu \leq 0.25$ and

$$0 \leq \zeta_s \leq \frac{1}{1+\mu} \sqrt{\frac{2 - \mu(5-4\mu)\sqrt{5-4\mu} + 5\mu(-1+4\mu)}{2(1+\mu)}} \tag{4.25}$$

By selecting μ and ζ_s in these ranges and substituting them into Equation (4.21), the corresponding upper limit value of β can be obtained. Then the parameters, υ and ζ_T, can be solved via Equations (4.20), (4.18) and (4.12). Table 4.1 gives the values of υ and ζ_T for different cases. According to Equation (4.25), solutions cannot be obtained for μ equals 0.2 and 0.25, if ζ_s is larger than 0.151 and 0, respectively.

Table 4.1 Optimum values of υ and ζ_T

			ζ_s				
			0	0.05	0.10	0.15	0.20
μ	0.05	υ	1.056	1.070	1.084	1.100	1.118
		ζ_T	0.230	0.280	0.329	0.378	0.426
	0.10	υ	1.127	1.153	1.181	1.213	1.250
		ζ_T	0.336	0.386	0.436	0.485	0.534
	0.15	υ	1.225	1.270	1.323	1.389	1.475
		ζ_T	0.429	0.481	0.534	0.586	0.639
	0.20	υ	1.382	1.477	1.621	2.034	-
		ζ_T	0.526	0.586	0.651	0.751	
	0.25	υ	2.000	-	-	-	-
		ζ_T	0.707				

4.4 Numerical Example

In the following, five systems consisting of an SDOF primary structure and an STMD based on different design methods are investigated. The five different TMDs are, respectively, a non-traditional TMD using the design method proposed in Chapter 3 for wide suppression bandwidth (WSB), a non-traditional TMD via stability maximization criterion (SMC) discussed in this chapter, a non-traditional TMD utilizing quasi-fixed points theory (QFPT), a traditional TMD designed by stability maximization criterion (SMC), and a traditional TMD employing quasi-fixed points theory (QFPT). The

parameters of the non-traditional and traditional TMDs are listed in Table 4.2, where μ

and ζ_s are set to be 0.1 and 0.2, respectively, as an illustration. Figure 4.2 shows the

corresponding FRF magnitude curves. It can be found that, either designed by the

quasi-fixed points theory or the stability maximization criterion, the maximum FRF

magnitudes of the non-traditional TMD systems are smaller than those of the traditional

TMD systems, and the non-traditional TMD system designed by the method proposed in

Chapter 3 is the best for both the relative displacement of the primary structure and the

stroke length of the TMD.

Table 4.2 Parameters of TMDs (μ =0.1 and ζ_s =0.2)

	non-traditional TMD			traditional TMD	
	WSB	SMC	QFPT	SMC	QFPT
υ	3.162	1.250	0.906	0.853	0.713
ζ_T	0.455	0.534	0.287	0.478	0.231

The eigenvalues in *s*-plane are presented in Figure 4.3. The degree of stability, i.e., the

minimum distances of the eigenvalues to the imaginary axis, of the non-traditional TMD

system using stability maximization criterion is the maximum, which indicates that the

free vibration response will decay the most quickly in the system. The degree of stability

in the WSB case is the second largest, and since the other two eigenvalues (-1.289+2.953*j*,

-1.289-2.953*j*) in the WSB case are far away from the imaginary axis, they are not

presented in the figure.

For response time history analyses, an SDOF primary structure with a period of 4

seconds and a damping ratio of 0.2, attached by traditional and non-traditional TMDs

with a mass ratio of 0.1, is considered. Two representative types of pulse motions (Makris,

1997), shown in Figure 4.4, are used as the excitations.
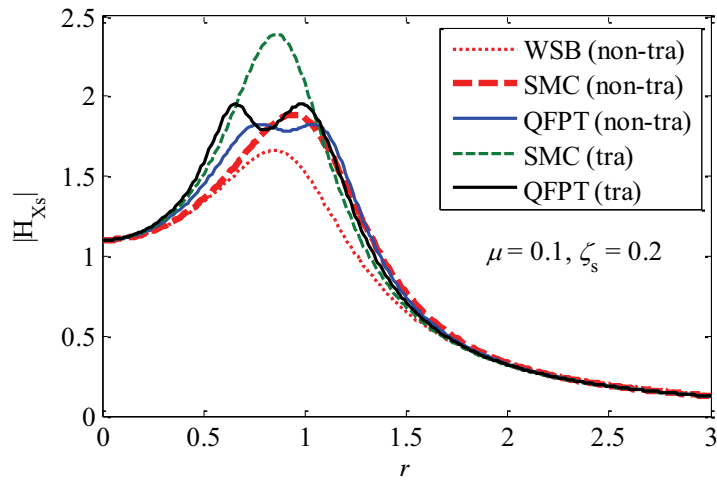
(a) relative displacement of primary structure
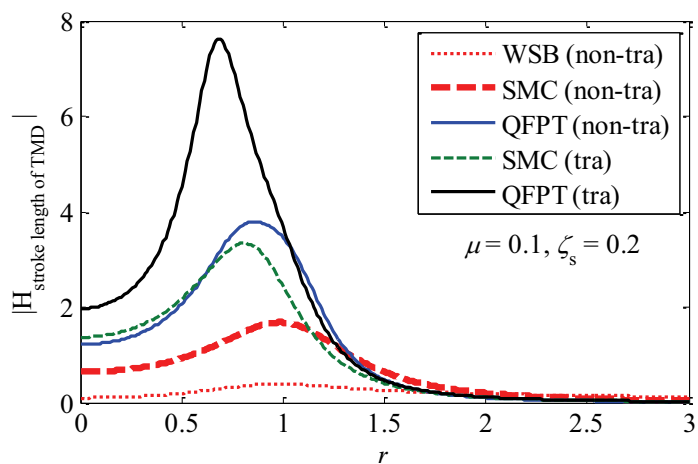
(b) stroke length of TMD

Figure 4.2 Magnitudes of FRFs from harmonic acceleration input to relative displacement

of primary structure and stroke length of TMD ($r=\omega/\omega_s$)
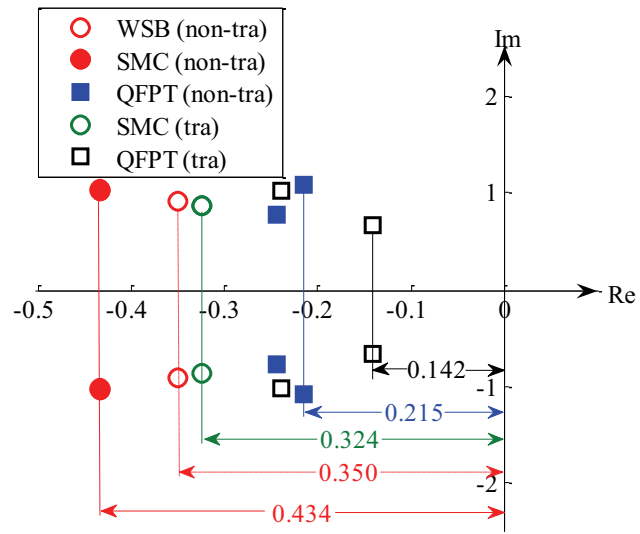
Figure 4.3 Eigenvalues in *s*-plane
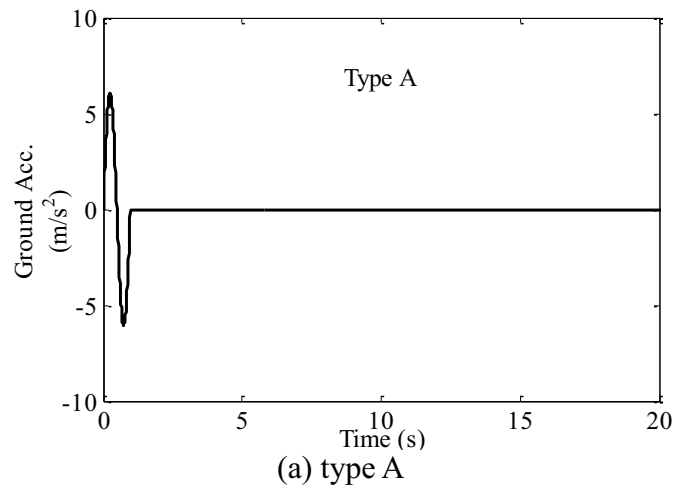
(a) type A
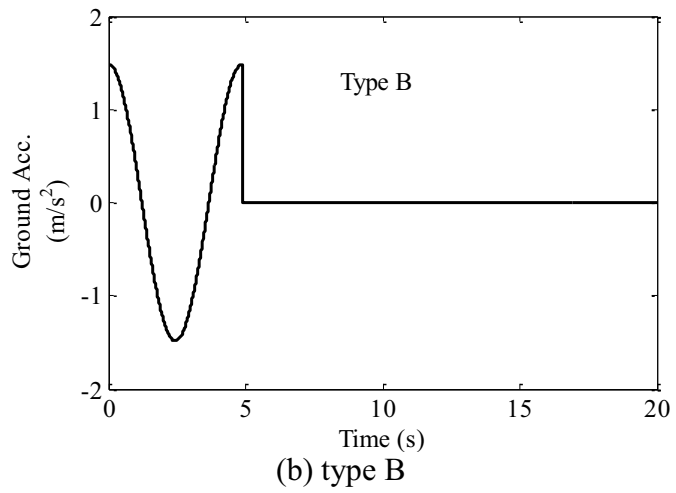
(b) type B

Figure 4.4 Two types of pulse motions

The time histories for the relative displacement of the primary structure and stroke length of TMD are shown in Figures 4.5 and 4.6, respectively. The maximum relative displacement of the primary structure as well as the stroke length of the TMD in the non-traditional TMD attached system designed by the method in Chapter 3 (WSB) are the minimum, among the five systems. These figures verify that the responses of the primary structure attached by the non-traditional TMD employing the stability maximization criterion (SMC) decay the most quickly, because the responses stop nearly at the same time in the SMC based and the WSB based non-traditional TMD systems though the maximum responses in the former system are larger than those in the latter system. SMC is still recommended as a design criterion because the required stiffness and damping coefficient are smaller than those in the WSB based system.

4.5 Conclusions

In this chapter, the design method for non-traditional TMDs using the stability maximization criterion is discussed. It is found that a non-traditional TMD provides better performance than a traditional TMD designed either by the quasi-fixed points theory or the stability maximization criterion. In the non-traditional TMD system designed by the stability maximization criterion, the degree of stability is the largest, i.e., the free vibration response decays the most quickly, and the stroke length of the TMD is the second smallest in comparison with the other four systems (non-traditional TMD system designed by the method proposed in Chapter 3, non-traditional TMD system designed by the quasi-fixed points theory, traditional TMD system designed by the stability maximization criterion, and traditional TMD system designed by the quasi-fixed

points theory). Though the non-traditional TMD attached system designed by the method proposed in Chapter 3 achieves the minimum values of the maximum relative displacement of the primary structure as well as the stroke length of the TMD among the five systems, SMC is still recommended as a design criterion for non-traditional TMD system because smaller stiffness and damping coefficient than those in WSB are required.
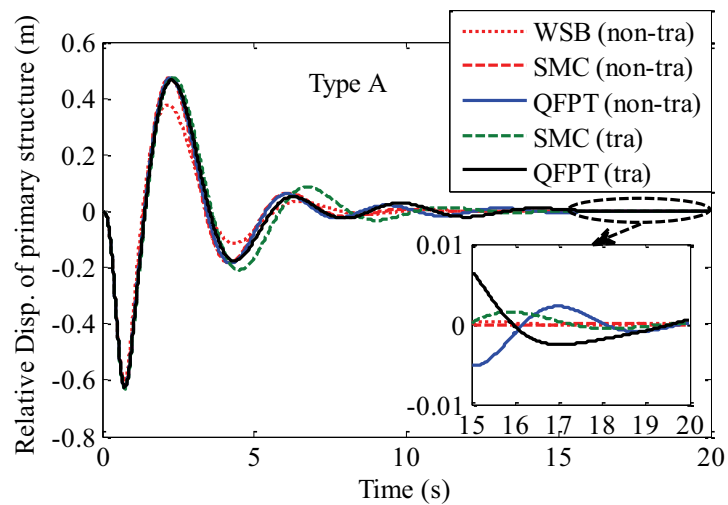
(a) under Type A pulse motion
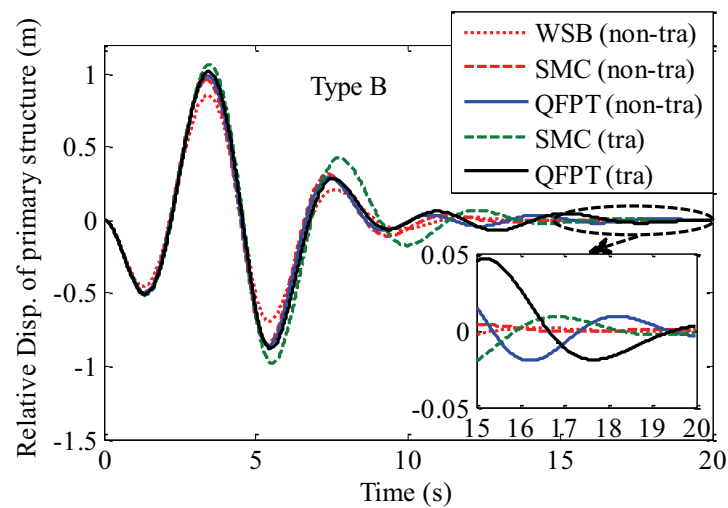
(b) under Type B pulse motion

Figure 4.5 Response time histories of relative displacement of primary structure
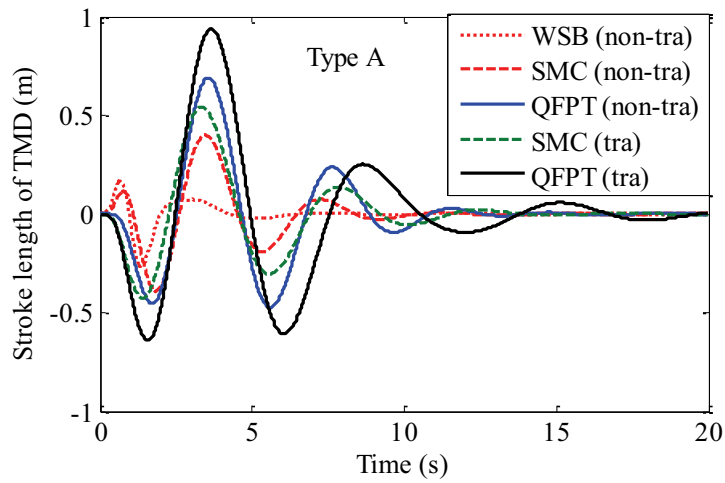
(a) under Type A pulse motion
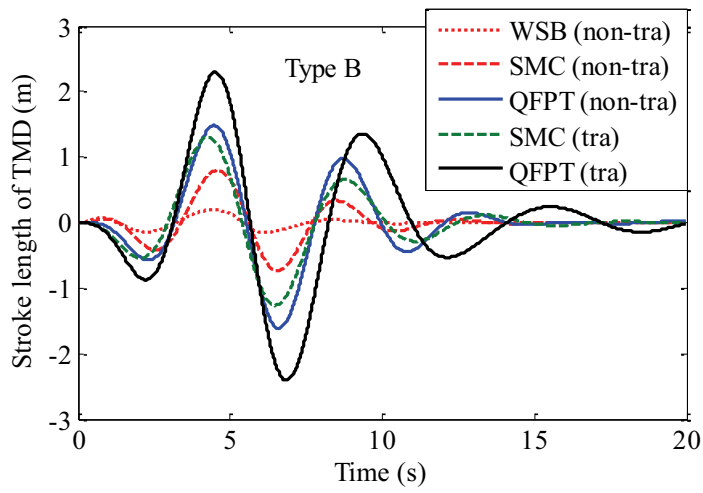
(b) under Type B pulse motion

Figure 4.6 Response time histories of stroke length of TMD

5. SEISMIC PERFORMANCE OF FLOOR SYSTEM WITH TUNED MASS DAMPER FUNCTION

5.1 Introduction

Human safety and comfortability are two main concerns for seismic design of building structures. A floor isolation system (FIS) and a tuned mass damper (TMD) are two common devices to reduce dynamic responses of equipments or structures. FIS (e.g., Iwan, 1978; Lambrou and Constantinou, 1994; Iemura and Taghikhany, 2004; Fujimoto, 2005; Cui *et al.*, 2010) is effective in reducing floor accelerations, and is commonly used to ensure human comfortability or protect important equipments. However, excessive displacements of isolation floors could damage the FIS and overturn equipments during high-amplitude and long period ground motions, e.g., near-fault excitations (Fan *et al.*, 2009). Increasing damping can reduce displacements of isolation floors at the expense of increasing inertia forces sustained by equipments (Gavin and Zaicenco, 2007). Active (Lu *et al.*, 2011) or semi-active (Fan *et al.*, 2009; Gavin and Zaicenco, 2007) devices can be incorporated into conventional isolation systems to improve the performance of FIS, and such systems may be adaptive to a wide range of excitations with different characteristics. However, both active and semi-active systems require sensing, computation and actuation units, and they are more complicated and may require more maintenance than passive systems. Furthermore, FIS has been seldom designed accounting for the reduction of seismic responses of main structures under strong earthquakes.

A TMD is a simple and reliable control device, and is usually installed on the top of a high-rise building (Sladek and Klingner, 1983; Soong and Dargush, 1997; Okhovat *et al.*,

2006). Other simple passive dampers, such as viscous, friction or visco-elastic dampers, rely on relative motions between the two components they are mounted to dissipate vibration energy. A TMD relies only on vibrations of one component it is attached to, and thus it does not need to be fastened to other component and would be effective even in systems with small shear deformations. However, a TMD usually requires a large mass for better control effect (Rana and Soong, 1998; De Angelis *et al.*, 2012). A TMD with a large mass ratio has been found to be able to function properly even if its parameters shift away from the optimally designed values. In this regard, a larger mass ratio TMD would be robust with respect to the changes in the structural properties (Hoang *et al.*, 2008). From this point of view, those non-conventional TMD systems in which a part of a building is utilized as a TMD for vibration control have been proposed by some researchers, such as mega subconfiguration system (Feng and Mita, 1995), roof garden TMD system (Matta and De Stefano, 2009), sliding roof system (Tian *et al.*, 2008), segmented upper storeys system (e.g. Chey *et al.*, 2010) and shading fin mass damper system (Fu and Johnson, 2011). Moreover, these TMDs can still retain the structural or architectural functions of the buildings. A single-tuned mass damper (STMD) installed on the top floor is usually used to control the fundamental vibration mode of a building, which indicates that an STMD system is effective only when the dominant frequency of a narrow-banded earthquake excitation is near the fundamental frequency of the structure. Thus it is not always effective in reducing vibrations induced by various kinds of earthquakes. On the other hand, multiple-tuned mass dampers (MTMDs) have been confirmed to be robust for earthquake ground motions with wide spectrum of frequency components and be able to moderately reduce peak responses even under impulsive

earthquakes (Chen and Wu, 2001). MTMDs have been recently employed to solve multimodal vibration problems in bridge engineering (e.g. Daniel *et al.*, 2012).

This chapter presents a new type of vibration control system utilizing TMD floors, which takes advantages of both the benefits of FIS and MTMDs, but does not require additional masses for TMDs. In the presented TMD floor system (TMDFS), the floors themselves serve as TMDs, and thus can achieve larger mass ratio of TMDs than that of a conventional TMD system. Moreover, multi vibration modes of a building can be controlled by installing such TMD floors in different storeys. In addition, it is demonstrated that TMD floors have a merit in that the accelerations of TMD floors are smaller than those of main structure storeys. Therefore, TMDFS can achieve very satisfactory control effect in an innovative way, as described in the following sections.

5.2 Proposed Floor System with Tuned Mass Damper Function

5.2.1 Formulation of tuned mass damper floor system

There are several approaches to realize the proposed TMDFS. For example, a main structure can be composed of primary beams, columns, bracings and sliding bearings. Floor slabs serving as TMDs can be connected with sliding bearings using stiffness and damping devices. (However, with such TMD floor slabs implemented, frame beams would have no constraint from the floor slabs. To prevent such an inconvenient situation and ensure the floor in-plane rigidity, diagonal bracings would be installed into the locations of TMD floor slabs and some side spans as shown in Figure 5.1, for example.) In TMDFS, there are some gaps between the TMD floor slabs and frame. Those gaps

could be filled with a kind of elastic material, such as polyisobutylene-based intumescent rubber (Chiba *et al.*, 2003) which owns fireproof characteristics and can deform in accordance with the deformation of an object it is adhered to, as shown schematically in Figure 5.2. Waterproof problem can also be solved if the interfaces among the floor slabs, the elastic materials and the frame are carefully handled.
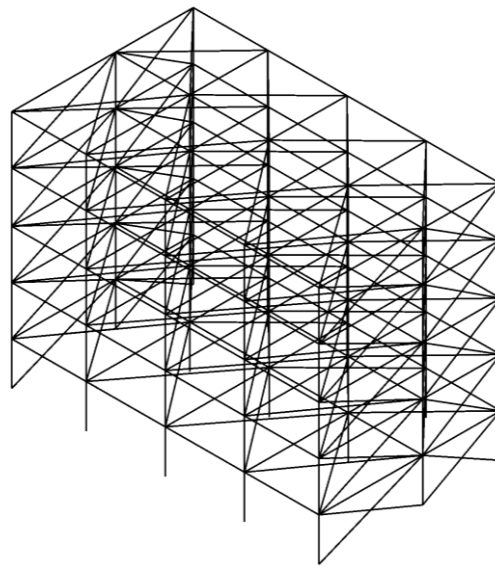
Figure 5.1 Frame with bracings
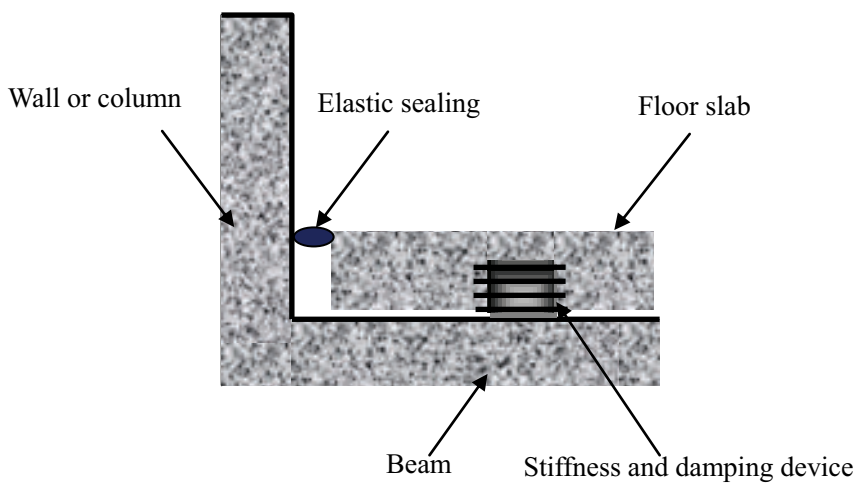
Figure 5.2 Illustration of connection between main structure and floor slab

The mathematical model is shown in Figure 5.3 considering an *N*-storey building with *N*-degree-of-freedom (*N*-DOF). A number of TMD floors are connected to the frames of a building at the locations of supposed-to-be-floors with linear stiffness (spring) and linear viscous damping (dashpot). M_n (*n*=1, 2, …, *N*) in the figure denotes the *n*-th lumped mass of the main structure, but does not include the mass of the *n*-th floor if that floor serves as a TMD. If the *n*-th floor is an ordinary floor (not a TMD floor), M_n includes the floor mass as well.
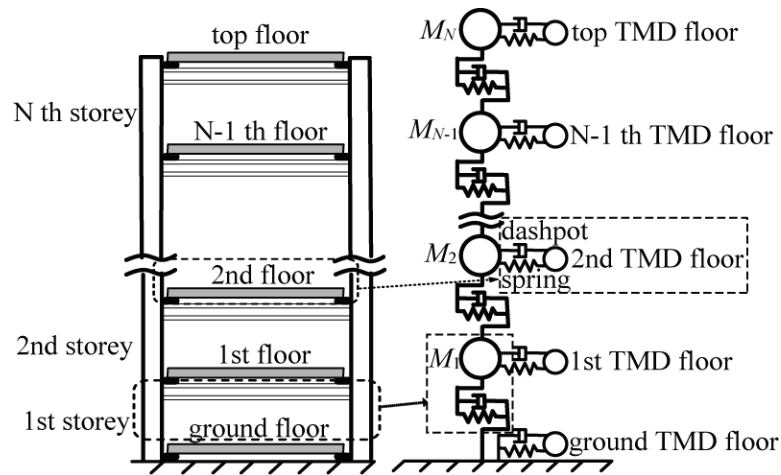
Figure 5.3 Schematic model of TMDFS for an *N*-DOF structure

Suppose *p* storeys are equipped with TMD floors in a damped *N*-DOF lumped-mass elastic structure excited by a ground acceleration of a_g, the equation of motion for the passively controlled system can be described as

$$\mathbf{M\ddot{x}} + \mathbf{C\dot{x}} + \mathbf{Kx} = -\mathbf{ME}a_g \tag{5.1}$$

with $\mathbf{x}$, $\mathbf{\dot{x}}$ and $\mathbf{\ddot{x}}$, respectively, the (*N*+*p*)×1 displacement, velocity and acceleration vectors of the system relative to the ground. $\mathbf{M}$, $\mathbf{C}$ and $\mathbf{K}$ are the (*N*+*p*)×(*N*+*p*) mass,

damping and stiffness matrices, respectively. They are written as

$$\mathbf{M} = \begin{bmatrix} \mathbf{M}_{s\,N \times N} & \mathbf{0}_{N \times p} \\ \mathbf{0}_{p \times N} & \mathbf{0}_{p \times p} \end{bmatrix} + \sum_{i=1}^{p} m_{\mathrm{T}i} \mathbf{a}_i \mathbf{a}_i^{\mathrm{T}}, \quad \mathbf{C} = \begin{bmatrix} \mathbf{C}_{s\,N \times N} & \mathbf{0}_{N \times p} \\ \mathbf{0}_{p \times N} & \mathbf{0}_{p \times p} \end{bmatrix} + \sum_{i=1}^{p} c_{\mathrm{T}i} \mathbf{b}_i \mathbf{b}_i^{\mathrm{T}},$$

$$\mathbf{K} = \begin{bmatrix} \mathbf{K}_{s\,N \times N} & \mathbf{0}_{N \times p} \\ \mathbf{0}_{p \times N} & \mathbf{0}_{p \times p} \end{bmatrix} + \sum_{i=1}^{p} k_{\mathrm{T}i} \mathbf{b}_i \mathbf{b}_i^{\mathrm{T}},$$

where $\mathbf{M}_s$, $\mathbf{C}_s$ and $\mathbf{K}_s$ are respectively the $N \times N$ mass, damping and stiffness

matrices of the structure, and the superscript T denotes the transpose of a matrix or

vector; $m_{\mathrm{T}i}$, $c_{\mathrm{T}i}$ and $k_{\mathrm{T}i}$ are respectively the mass, damping coefficient and stiffness

of the i-th TMD floor; $\mathbf{a}_i = \begin{bmatrix} \mathbf{0}_{1 \times (N+i-1)} & 1 & \mathbf{0}_{1 \times (p-i)} \end{bmatrix}^{\mathrm{T}}$ and

$\mathbf{b}_i = \begin{bmatrix} \mathbf{0}_{1 \times (loc_i - 1)} & -1 & \mathbf{0}_{1 \times (N+i-loc_i-1)} & 1 & \mathbf{0}_{1 \times (p-i)} \end{bmatrix}^{\mathrm{T}}$ are $(N+p) \times 1$ location vectors, and loc_i

represents the location of the i-th TMD floor; and $\mathbf{E}$ is a $(N+p) \times 1$ unit vector if a ground

motion is considered as the excitation.

Suppose that common reinforced concrete buildings are concerned, the average

self-weight of the buildings is approximately 12.0kN/m^2 (Nishitani and Matsui, 2001).

The value is obtained based on the assumption that all the weights of beams, columns,

slabs, exterior/interior walls and live loads, etc., are on the floor slabs. On the other hand,

the value of real slab weight would be around 5.0kN/m^2 if only the weight of slab and

live loads are considered (Nishitani and Matsui, 2001). Accordingly, the mass ratio of

such a floor to the corresponding main structure storey mass can be roughly estimated as

5.00/(12.00-5.00)=0.71. If TMD floors are practically integrated into a building system,

most of the parts of the extra floor supporting mechanisms which are fixed to the main

structure, such as bracings, sliding bearings and damping devices, are unmovable. Thus their weights are roughly counted as the weight of the main structure herein. Based upon such consideration, the mass ratio μ of each TMD floor is assumed to be 0.5, and the mass of the i-th TMD floor is written as $m_{\mathrm{T}i} = \mu M_i$.

5.2.2 Eigenvalue-problem and anti-resonance

Under the zero initial condition, Laplace transform of Equation (5.1) gives

$$\mathbf{X}(s) = (\mathbf{M}s^2 + \mathbf{C}s + \mathbf{K})^{-1} \cdot (-\mathbf{M}\mathbf{E}) \cdot A_{\mathrm{g}}(s) = \mathbf{G}(s) \cdot (-\mathbf{M}\mathbf{E}) \cdot A_{\mathrm{g}}(s) = \mathbf{H}(s) \cdot A_{\mathrm{g}}(s) \quad (5.2)$$

where $\mathbf{G}$ is the dynamic flexibility matrix, and $\mathbf{H}$ is the transfer function vector; $\mathbf{X}(s)$ and $A_{\mathrm{g}}(s)$ are the Laplace transforms of $\mathbf{x}$ and a_{g}, respectively.

The standard eigenvalue-problem (Humar, 2002) of the TMD floor integrated system is

$$\begin{bmatrix} -\mathbf{M}^{-1}\mathbf{C} & -\mathbf{M}^{-1}\mathbf{K} \\ \mathbf{I} & \mathbf{0} \end{bmatrix} \mathbf{v} = s\mathbf{v} \quad (5.3)$$

Because the coefficient matrix is real, the eigenvalues as well as the corresponding eigenvectors $\mathbf{v}$ are either real or complex conjugate pairs. The system natural frequencies, $0 \le \omega_1 < \omega_2 < \cdots < \omega_{N+p}$, are the absolute values of the eigenvalues. Suppose $\mathbf{v}_i$ is the $2(N+p) \times 1$ eigenvector corresponding to the i-th eigenvalue, and the last $N+p$ elements should be selected so as to form the displacement eigenvector $\mathbf{q}_i$. The i-th participation vector $\mathbf{r}_i$ can be obtained as $\mathbf{r}_i = \beta_i \mathbf{q}_i$, where β_i is the i-th participation factor defined

as $\beta_i = \dfrac{\mathbf{q}_i^{\mathrm{T}} \mathbf{M} \{1\}_{(N+p)\times 1}}{\mathbf{q}_i^{\mathrm{T}} \mathbf{M} \mathbf{q}_i}$. The corresponding mass matrix normalized eigenvectors, $\mathbf{e}_i$,

satisfying $\mathbf{e}_i^{\mathrm{T}} \mathbf{M} \mathbf{e}_i = 1$ ($i = 1, 2, \ldots, N+p$), which are used in this chapter, can be

obtained by

$$\mathbf{e}_i = \frac{\mathbf{r}_i}{\sqrt{\mathbf{r}_i^{\mathrm{T}} \mathbf{M} \mathbf{r}_i}} \tag{5.4}$$

The element $G_{lk}(s)$ in $\mathbf{G}(s)$ is the complex amplitude of the structural response of the

l-th DOF with a unit harmonic force applied at the k-th DOF. The anti-resonances of the

system corresponding to $G_{nn}(s)$ ($n = 1, 2, \ldots, N$) (Preumont, 2011) can be obtained by

$$G_{nn}(s) = 0 \tag{5.5}$$

where $G_{nn}(s)$ denotes the n-th diagonal element. It should be noted that the solutions of

Equation (5.5) are complex values with small real parts for lightly damped systems. The

anti-resonance frequencies herein denoted as $\bar{\omega}_i$ ($i = 1, 2, \ldots, N+p-1$) are the imaginary

parts of s.

5.2.3 Frequency response functions

In the frequency domain, the frequency response function (FRF) vector $\mathbf{H}(j\omega)$ for

relative displacements to the ground can be written as

$$\mathbf{H}(j\omega) = (-\omega^2 \mathbf{M} + j\omega \mathbf{C} + \mathbf{K})^{-1} \cdot (-\mathbf{M} \mathbf{E}) \tag{5.6}$$

$\mathbf{H}(j\omega)$ includes $N+p$ elements, and each of the first N elements of $\mathbf{H}(j\omega)$, i.e., $H_{Xs_n}(j\omega)$ ($n=1,2,\ldots,N$), denotes the FRF of the displacement of the n-th DOF relative to the ground, and each of the other p elements, i.e., $H_{XTMD_i}(j\omega)$ ($i=1,2,\ldots,p$), is the FRF of the displacement of the i-th TMD floor relative to the ground.

The FRF, $H_{Xs(drift)_n}(j\omega)$, of the n-th inter-storey drift displacement can be thus obtained by

$$H_{Xs(drift)_n}(j\omega) = H_{Xs_n}(j\omega) - H_{Xs_{n-1}}(j\omega) \tag{5.7}$$

where $n=1,2,\ldots,N$, and $H_{Xs_0}(j\omega)=0$.

The FRF vector, $\mathbf{H}_A(j\omega)$, of absolute accelerations can be obtained as

$$\mathbf{H}_A(j\omega) = -\omega^2\mathbf{H}(j\omega) + \mathbf{E} = (-\omega^2\mathbf{M} + j\omega\mathbf{C} + \mathbf{K})^{-1} \cdot (j\omega\mathbf{C} + \mathbf{K}) \tag{5.8}$$

Each element in $\mathbf{H}_A(j\omega)$, i.e., $H_{A_n}(j\omega)$ ($n=1,2,\ldots,N+p$), denotes the FRF of the absolute acceleration of the n-th DOF of the main structure for $n \le N$ and of the i-th TMD floor for $n=N+i$ ($i=1,2,\ldots,p$).

5.3 Fundamental Experimental Test

5.3.1 Description of experimental test configuration

An experimental test structure is a one-storey one-bay frame with a TMD floor attached to the roof as shown in Figure 5.4. Two plexiglas plates with a size of

300.00×150.00×5.00(mm) are used as the roof and foundation of the main frame, and two 300.00×100.00×0.50(mm) aluminum plates are used as columns. As shown in Figure 5.5, another plexiglas plate with a size of 140.00×200.00×5.00(mm) representing the TMD floor is connected to the roof by a linear ball slide. The linear ball slide LSP 2080 is manufactured by the THK Corporation. Each side of the TMD floor is connected to the roof with two extension coil springs, each with a stiffness of 7.00N/m, in series. The airpot dashpot 2KS56 manufactured by the Airpot Corporation, a damping adjustable dashpot, connects between the TMD floor and the roof of the main frame to provide damping. The test structure is rigidly attached to the shaking table, and accelerometers are placed on the basemat, roof and TMD floor to record the lateral accelerations. The masses of the test structure components are given in Table 5.1. The mass ratio between the TMD floor and the main frame is 0.51, which meets the assumption in Section 5.2.1.

Table 5.1 Masses of components of test structure

	Components	Mass (g)
Main frame	Frame (includes one-half of columns, node plates, bolts, and roof Plexiglas)	561.11
	Slide base & bolts	55.33
	Spring node plates & bolts	57.42
	Dashpot node plate & bolts	23.67
	One-half of dashpot	4.25
	Accelerometer	25.00
	Sum	726.78
TMD floor	Slide block	122.50
	Spring node plates & bolts	29.82
	Dashpot node plates & bolts	25.70
	One-half of dashpot	4.25
	Accelerometer	25.00
	Plexiglas plate	165.10
	Sum	372.37
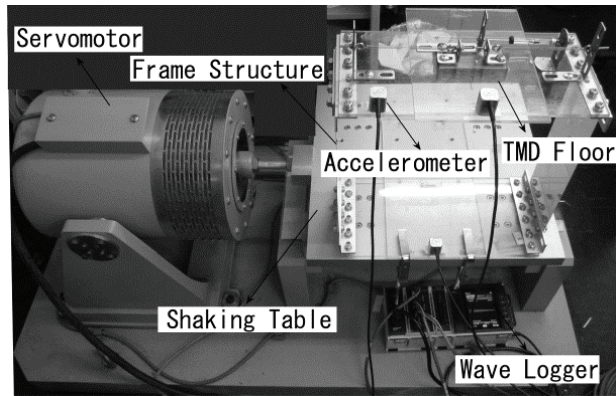
(a) Photograph
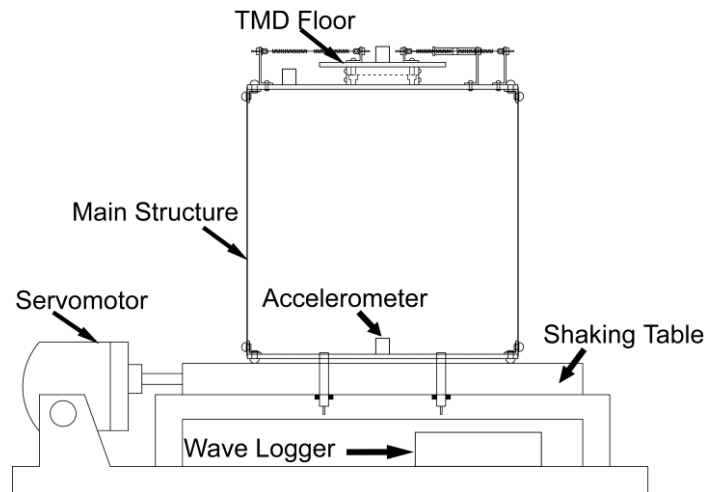
(b) Illustration

Figure 5.4 Panoramic view of experiment model
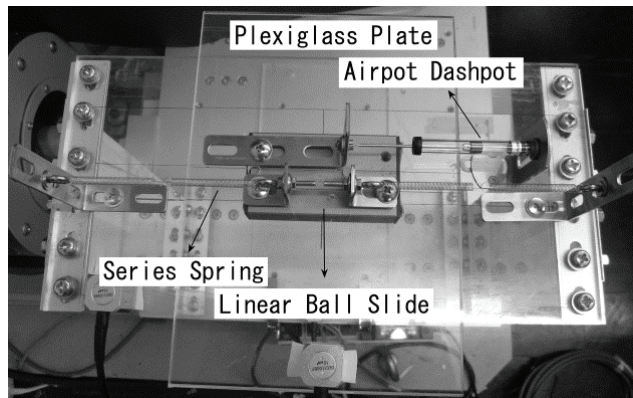
(a) Photograph
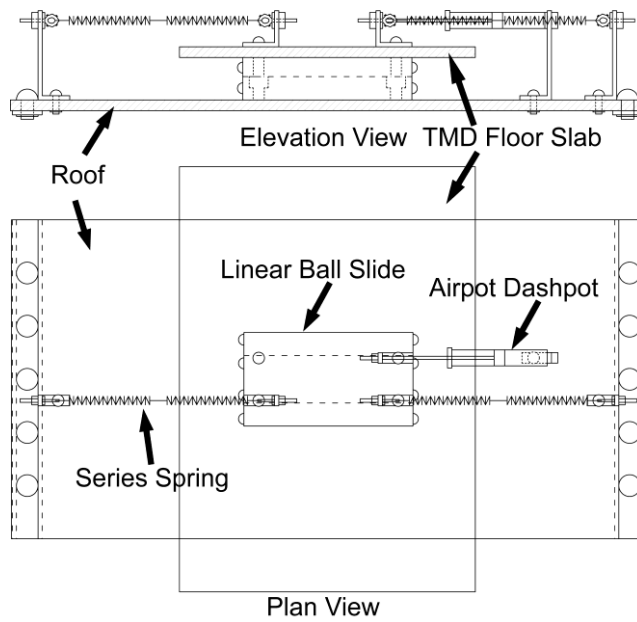
(b) Illustration

Figure 5.5 Close-up view of TMD floor

5.3.2 System identification of test structure

Firstly, free vibration experiment of the test structure is carried out when the TMD floor is fixed on the roof of the main frame. The black solid line in Figure 5.6 represents the free vibration response of the test structure, and the red dashed lines are the envelop lines. The identified parameters of the test structure are listed in Table 5.2.
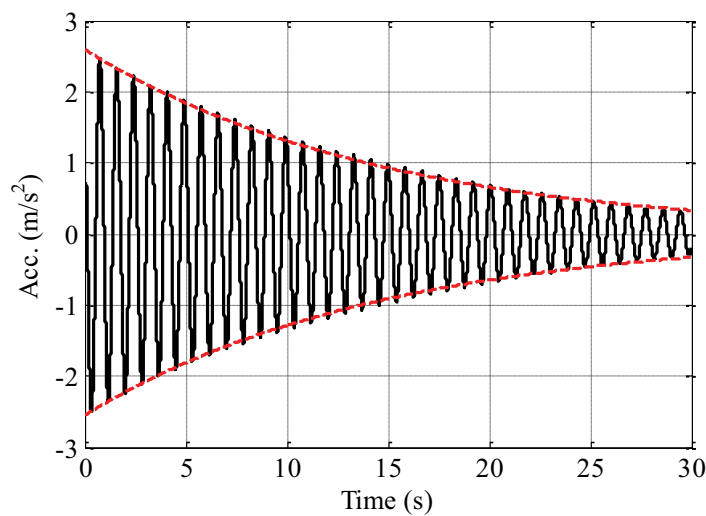
Figure 5.6 Free vibration response

Table 5.2 Identified parameters of test structure

Parameter	Value
Fundamental frequency (Hz)	1.19
Damping ratio	0.92×10^{-2}
Stiffness of columns (N/s)	61.00
Damping coefficient (Ns/m)	0.15

Then the identification test of the TMD floor is carried out by fixing the TMD floor directly on the shaking table as shown in Figure 5.7. A harmonic excitation at the frequency of 2.00Hz is applied as the input. At this step, the damping of the airpot dashpot is set to be zero. Figure 5.8 shows the hysteresis of the inertia force, and Figures

5.9 and 5.10 give the relationships between the friction force provided by the linear ball slide, and the relative displacement, the relative velocity of the TMD floor, respectively. The displacement and velocity data are the integrations of the obtained acceleration data by using a numerical integration algorithm with high accuracy (Chen *et al.*, 2010) which is shown in Appendix C. It can be found from the figures that the slide provides a friction force of 0.10N, and the stiffness of the TMD floor provided by the extension coil springs is 7.53N/m.
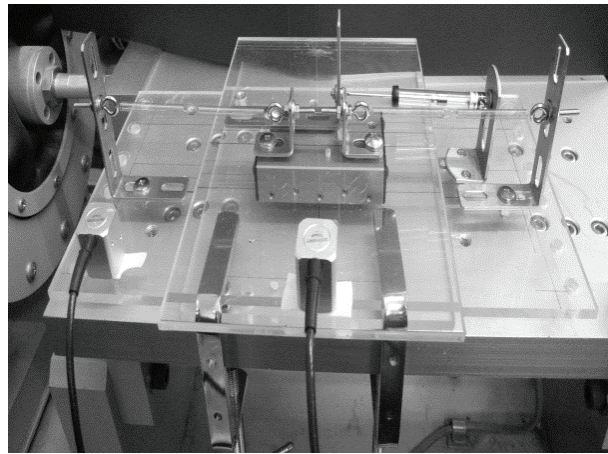
Figure 5.7 TMD floor identification test
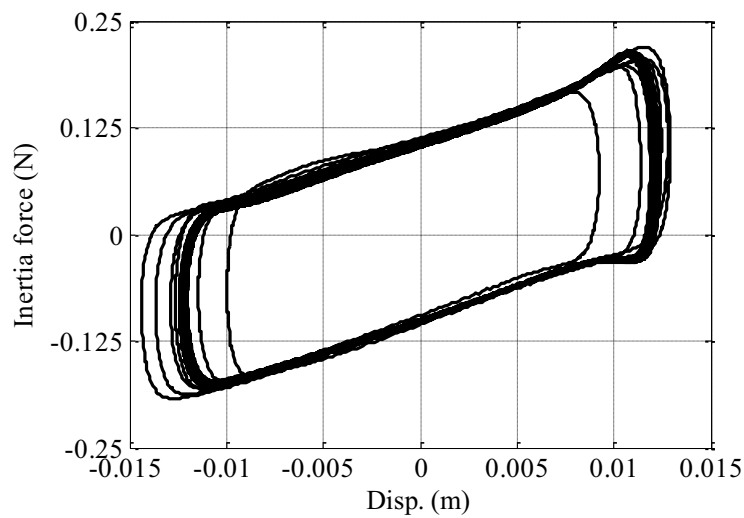
Figure 5.8 Inertia force hysteresis
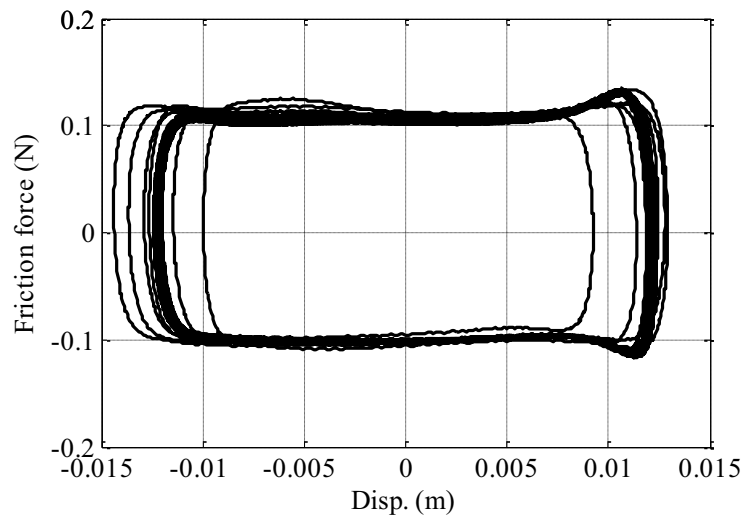
Figure 5.9 Relationship between friction force and displacement
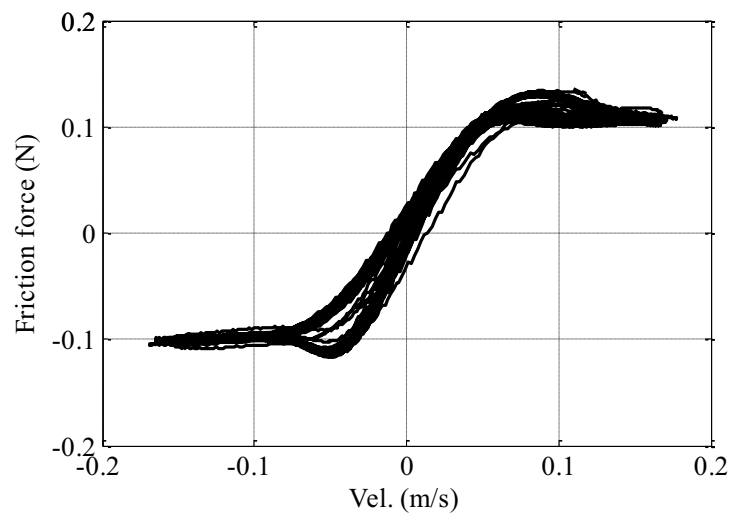
Figure 5.10 Relationship between friction force and velocity

The Stribeck friction model (Olsson *et al.*, 1998) is adopted herein as the analytical model to simulate the friction of the linear ball slide.

$$F = \begin{cases} F_{\mathrm{D}}\,\mathrm{sgn}\,(v) & \text{if } v \neq 0 \\ F_{\mathrm{e}} & \text{if } v = 0 \text{ and } |F_{\mathrm{e}}| < F_{\mathrm{S}} \\ F_{\mathrm{S}}\,\mathrm{sgn}\,(F_{\mathrm{e}}) & \text{otherwise} \end{cases} \tag{5.9}$$

with F_{D}: the dynamic friction (equal to 0.10N herein); F_{e}: the external force; and F_{S}: the static friction which is supposed to be equal to the dynamic friction of 0.10N herein; and v is the relative velocity of the TMD floor.

Figure 5.11 gives the comparison between the test result and the simulation result of the absolute accelerations of the TMD floor. It can be found that they agree well with each other. Accordingly, the stiffness of the TMD floor and the friction model are verified to be validated.
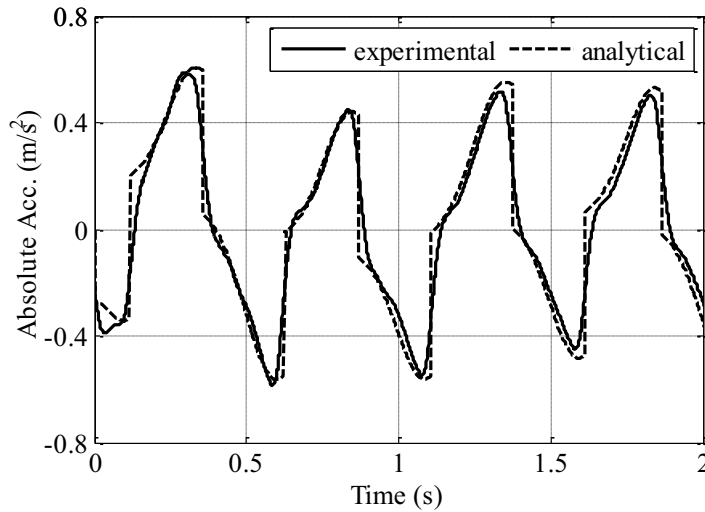
Figure 5.11 Comparison of experimental and analytical responses

5.3.3 Optimum design of tuned mass damper floor parameters in test

Damage of a building structure is deeply related to the values of inter-storey drift displacements. Thus the objective function for the optimization of TMD floor design parameters herein is defined as

$$J = \text{Max.} \left| H_{\text{Xs(drift)}}(j\omega) \right| \tag{5.10}$$

Based on the identified parameters of the main frame and the TMD floor, the optimum parameters are $\upsilon^{\text{opt}} = 0.56$ and $\zeta^{\text{opt}} = 0.41$ according to the gradient-based optimization method. Hence, the stiffness and the damping coefficient required for the TMD floor are $k_{\text{T}}^{\text{opt}} = 9.74\text{N/m}$ and $c_{\text{T}}^{\text{opt}} = 1.56\text{Ns/m}$.

Figure 5.12 schematically presents the spring connection between the TMD floor and the roof floor of the main frame, where l_0 is the original length of the coil extension springs 1, 2, 3, 4. Suppose k is the stiffness of the springs and Δl is the initial tensile length of the springs. When $t=0$, the resultant force imposed on m_{T} is F=0N. When $t=t'$, the force imposed on m_{T} by springs 1 and 2 is $F_{\text{left}}=k(\Delta l+x/2)$, and the force imposed on m_{T} by springs 3 and 4 is $F_{\text{right}}=k(\Delta l-x/2)$, then the resultant force $F=F_{\text{left}}-F_{\text{right}}= k(\Delta l+x/2)-k(\Delta l-x/2)=kx$. Accordingly, the stiffness of each coil extension spring should equal the required stiffness of the TMD floor. In order to keep the springs in the extension state, Δl should be larger than the expected maximum displacement of m_{T}. Due to the constraint of product types by considering the suitable dimension, allowable loading and maximum extension length, four extension coil springs with the stiffness of 7.00N/m are used for connecting the TMD floor and the roof floor, as mentioned in Section 5.3.1. And the

identified stiffness of the TMD floor provided by the springs is 7.53N/m, which is a little different from the theoretical value 7.00 N/m.
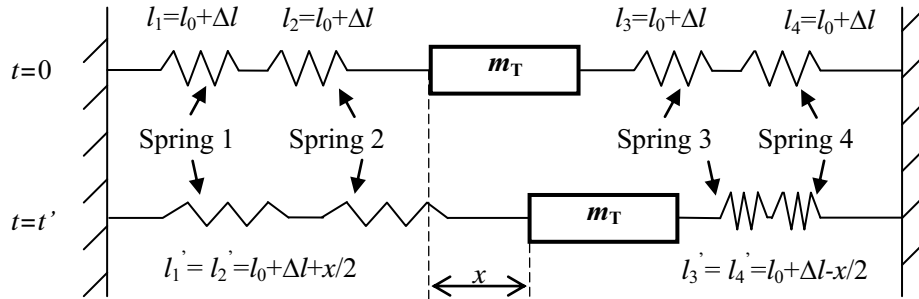
Figure 5.12 Spring connection

Since the stiffness of the TMD floor provided by the springs, i.e., k_{T}, is a predetermined constant, only the corresponding optimization variable, i.e., the optimum damping coefficient $c_{\text{T}}^{\text{opt}}$, should be 1.53Ns/m. However, due to the fact that the identified stiffness of the coil springs (k_{T}) which is 7.53N/m, is different from the required optimal value $k_{\text{T}}^{\text{opt}}$, the TMD floor is not theoretically optimum but sub-optimum. Figure 5.13 (a) and (b) give the magnitudes of the FRFs for the drift displacement of the main frame, and the absolute acceleration of the fixed/TMD floor, respectively. The black dashed lines display the FRF magnitudes of the fixed floor system, and the blue and red solid lines represent the FRF magnitudes for the optimum ($k_{\text{T}}^{\text{opt}}$ =9.74N/m and $c_{\text{T}}^{\text{opt}}$ =1.56Ns/m) and sub-optimum ($k_{\text{T}}^{\text{sub-opt}}$ =7.53N/m and $c_{\text{T}}^{\text{sub-opt}}$ =1.53Ns/m) cases, respectively. It can be found that the value of the objective function in the sub-optimum case is 0.040 which is larger than that in the optimum case (0.035). If the structure is subjected to a random excitation containing infinitely many frequencies, then the responses over all frequencies

is also of interest besides the response at the resonant frequency. Accordingly, the 2-norm values of the FRF magnitudes are given in Table 5.3. It can be found that the value of $\|H_{Xs(drift)}\|_2$ in the sub-optimum case is very close to that in the optimum case, and the value of $\|H_{A(floor)}\|_2$ in the sub-optimum case is even smaller than that in the optimum case due to the trade-off relationship between the responses of the main structure and TMD. Accordingly, the sub-optimum values of the parameters adopted in the practical experimental model are still reasonable.
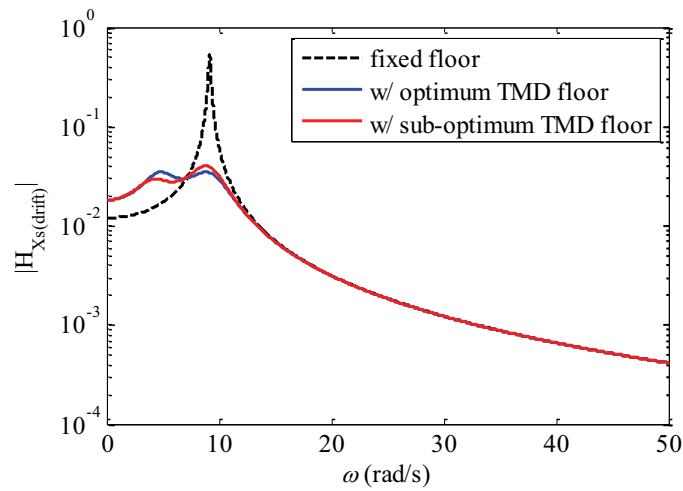
(a) drift displacement of main frame
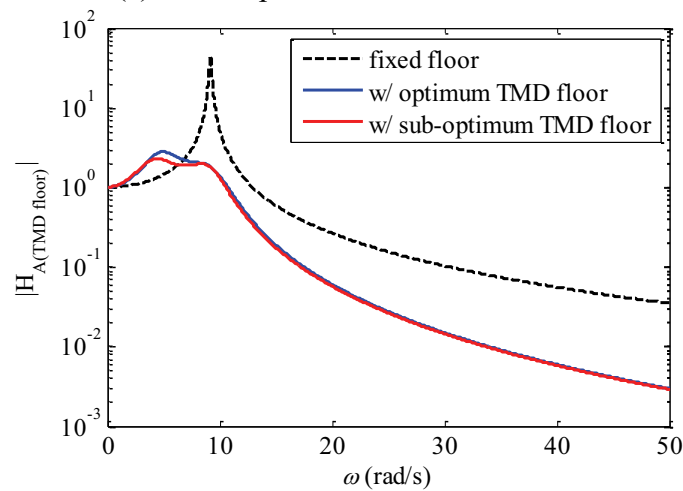
(b) absolute acceleration of floor

Figure 5.13 FRF magnitudes of structural responses

Table 5.3 2-norm value of FRF magnitudes

	Fixed floor	Optimum TMD floor	Sub-optimum TMD floor
$\|H_{Xs(drift)}\|_2$	3.00	0.9861	0.9941
$\|H_{A(floor)}\|_2$	252.22	64.20	57.99

The linear ball slide provides friction, and the equivalent linear viscous damping coefficient of the friction can be approximately estimated by

$$c_{Tf} = \frac{4F_D}{\pi \omega X}$$ (5.11)

where ω and X denote the circular frequency of response and displacement amplitude, respectively.

The constrained maximum stroke of the slide is 50mm which will be used as X, and the natural circular frequency of the main frame is 9.16rad/s which will be used as ω, and thus according to Equation (5.11) the equivalent linear viscous damping coefficient of the slide friction (c_{Tf}) is found approximately 0.28Ns/m. Correspondingly, the damping provided by the airpot dashpot (c_{Td}) should be 1.25Ns/m to achieve c_T^{opt}. By carrying out a number of tests and corresponding identification analyses with different adjustments of the airpot dashpot, the optimum position of the orifice has been determined, which can provide the optimum damping coefficient of 1.25Ns/m. The damping force hysteresis of the airpot and the absolute acceleration history of the TMD floor, obtained from the test, are compared with those of the analytical results as shown in Figures 5.14 and 5.15, respectively. It can be found that they agree well with each other, which further demonstrates the validity of the identified parameters and simulation method. It is noted that as the influence of the friction which is nonlinear, the hysteresis loops are no longer ellipses and the acceleration history is no longer harmonic wave even in the analytical

122

results, though the model is subjected to a harmonic excitation.
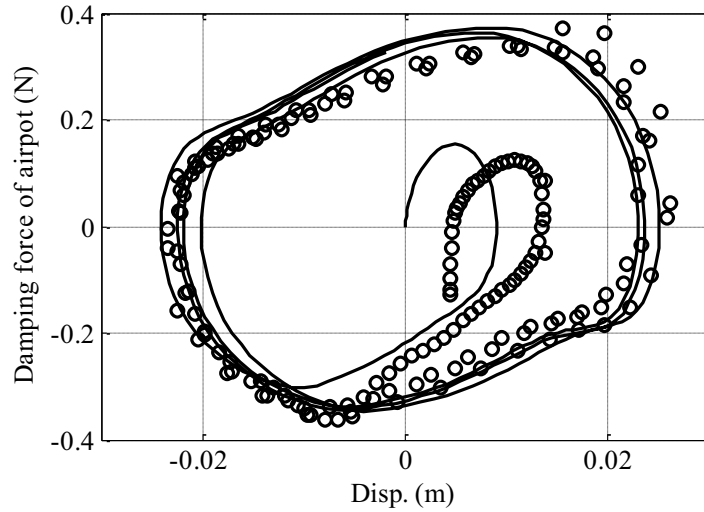
Figure 5.14 Airpot damping force hysteresis: '○' experimental, '—' analytical.
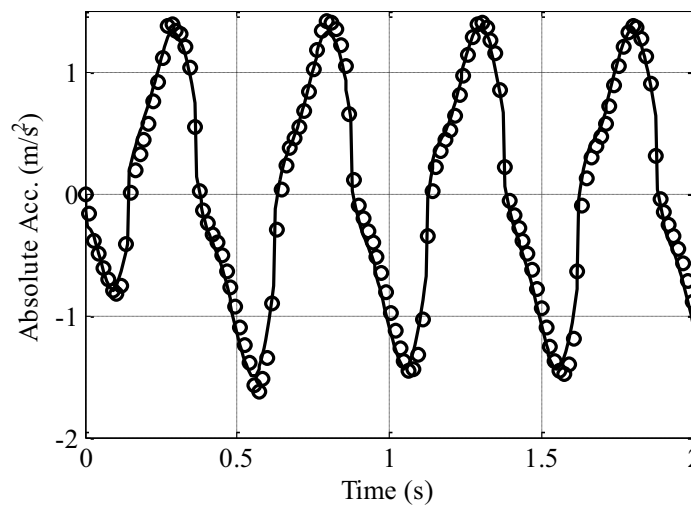
Figure 5.15 Absolute acceleration of TMD floor: '○' experimental, '—' analytical.

5.3.4 Experimental results and discussion

To investigate the seismic performance of the test structure with the TMD floor integrated,

the responses of the main frame and the TMD floor are studied under the three scaled earthquake records: the 1940 Imperial Valley (El Centro Array 6, NS component, referred to as El Centro in the following), the 1995 Kobe (JMA, NS component) and the 1992 Landers (LCN, 260 component), which are chosen as representatives of distinct classes of earthquakes. The three acceleration time histories which the shaking table reproduced are shown in Figure 5.16.

Figures 5.17-5.19 display the comparison results between the experimental and simulated absolute accelerations of the main frame and the TMD floor. The numerical results under all the three earthquake excitations compare well with the experimental results. Furthermore, it can be found that the accelerations of the TMD floor are smaller than those of the main frame for all the cases.

Figure 5.20 gives the experimental result comparisons with respect to the inter-storey drift displacement of the main frame between the case of fixed floor and the case of TMD floor. Figure 5.21 shows the corresponding comparison with respect to the absolute accelerations of the floor between the two cases. It is worth noting that the predominant periods of El Centro, JMA Kobe and LCN Landers are 0.56s, 0.86s and 4.15s (Adrian, 2000), respectively, and the former two are close to 0.69s which is the natural period of the main frame. Thus, the seismic performance of the test structure with the single TMD floor integrated is more significant under El Centro and JMA Kobe than that under LCN Landers.
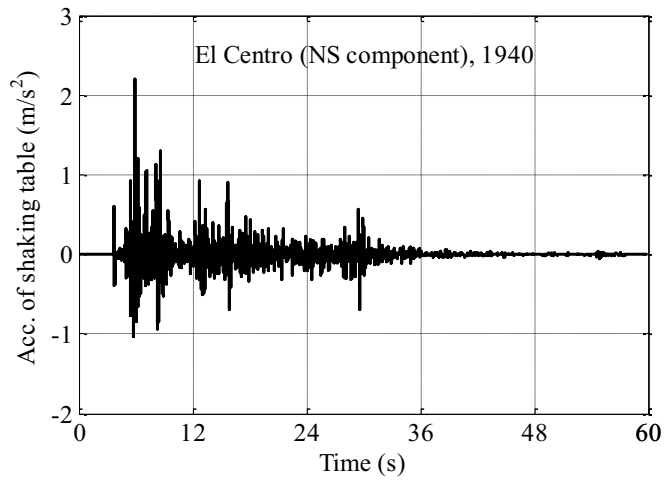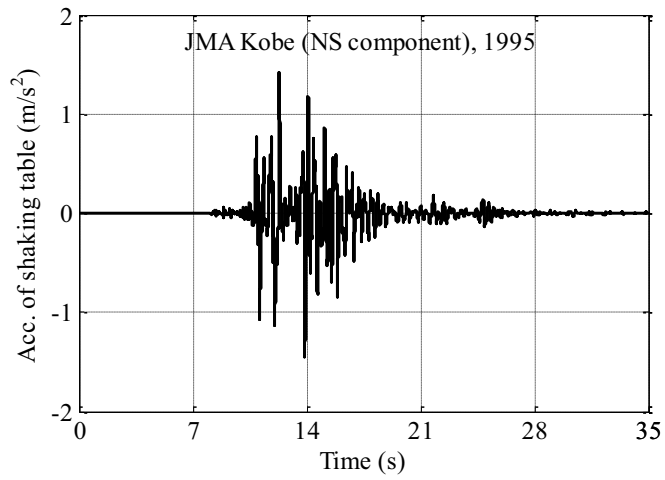
(a) El Centro NS

(b) JMA Kobe NS
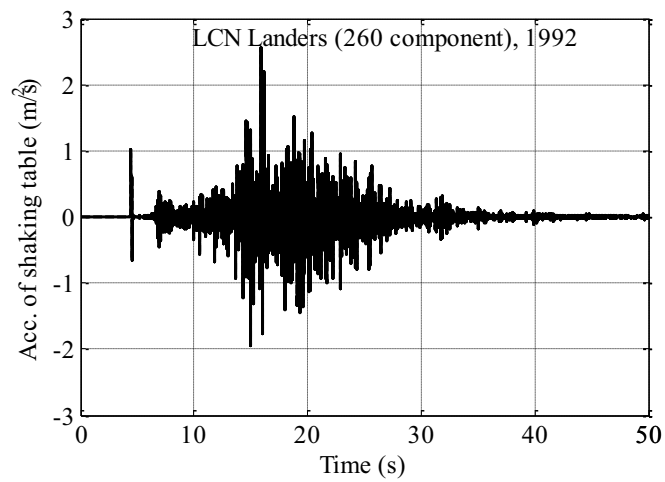
(c) LCN Landers 260

Figure 5.16 Inputs of shaking table
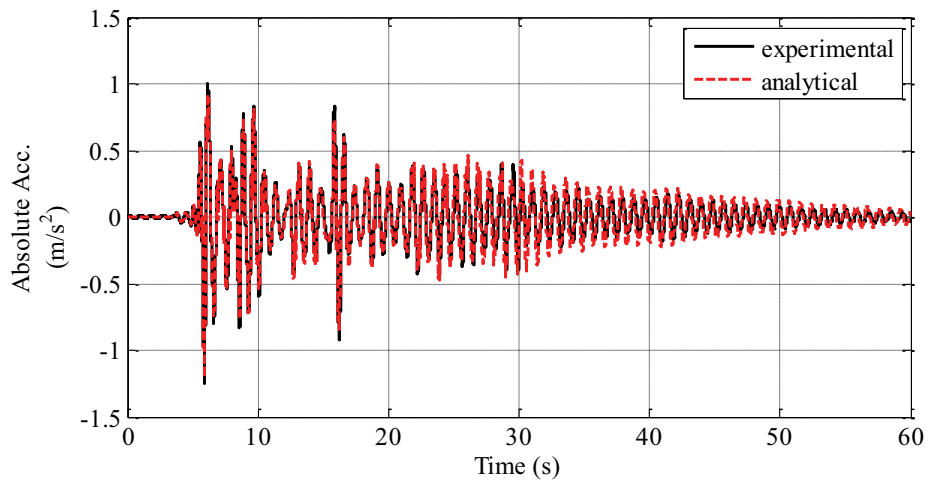
(a) Main frame
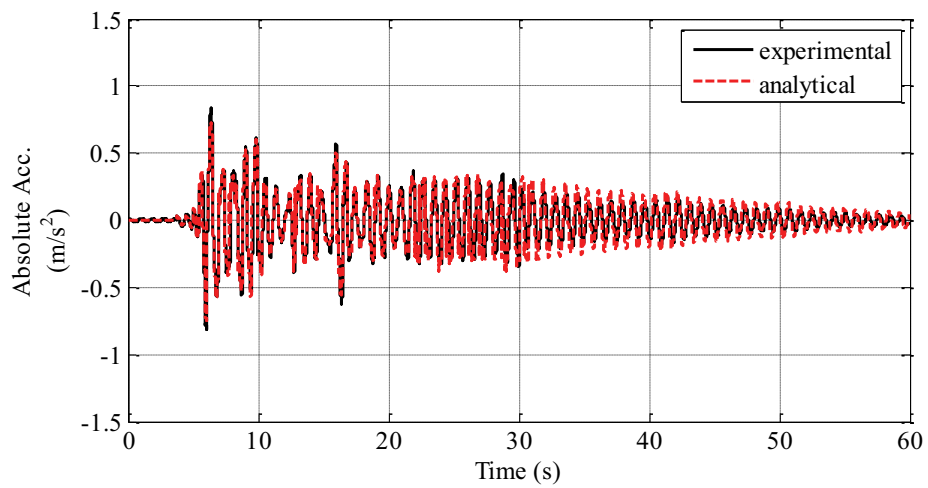
(b) TMD floor

Figure 5.17 Experimental and analytical absolute accelerations under El Centro
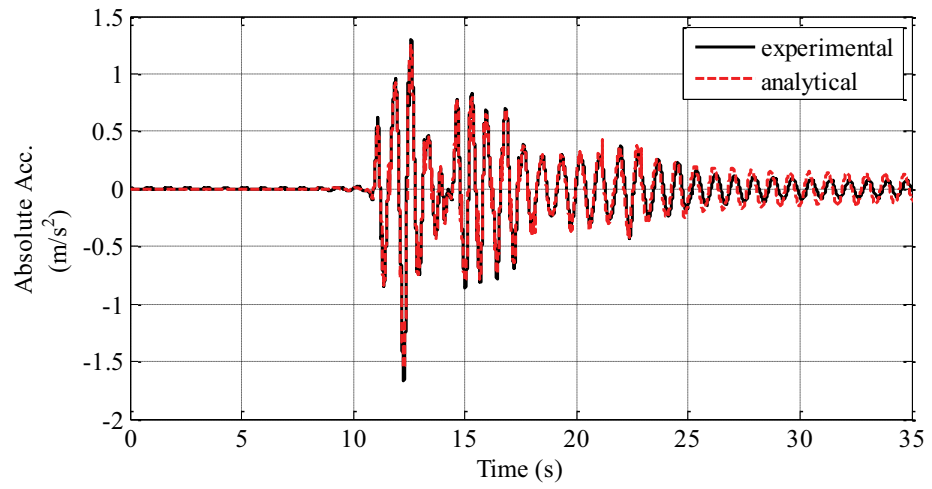
(a) Main frame
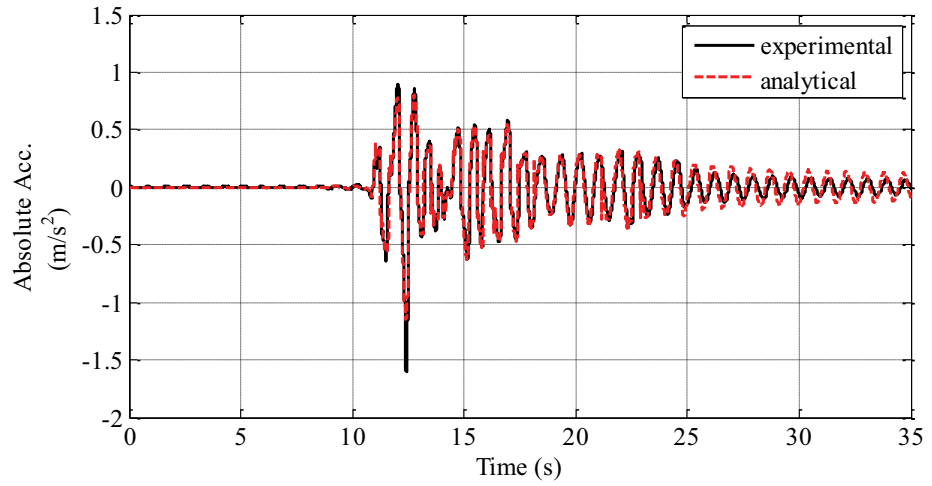
(b) TMD floor

Figure 5.18 Experimental and analytical absolute accelerations under JMA Kobe
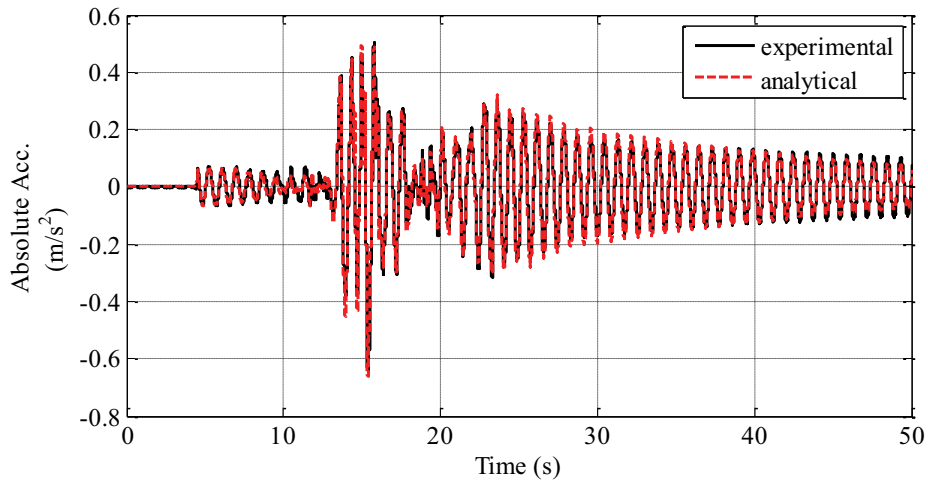
(a) Main frame
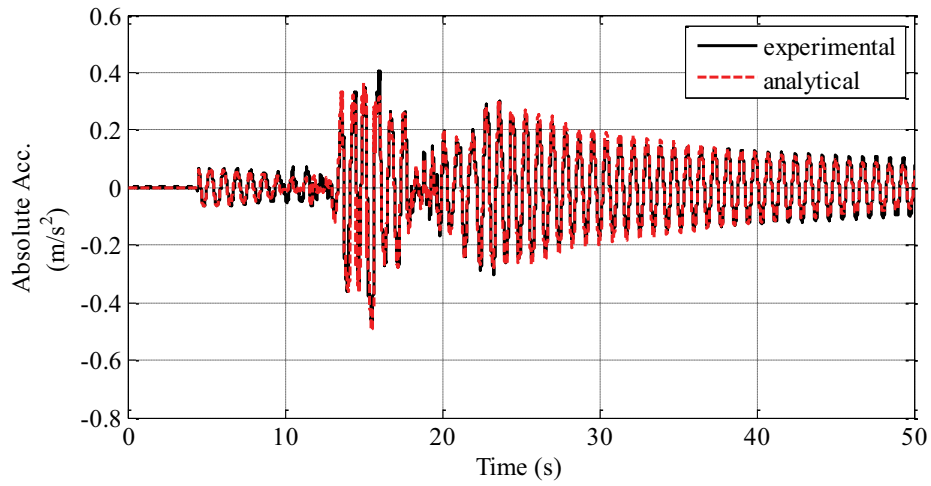
(b) TMD floor

Figure 5.19 Experimental and analytical absolute accelerations under LCN Landers

(a) El Centro NS

Max (fixed) = 0.039
Max (TMD) = 0.018
Reduction ratio = 54.27%

RMS (fixed) = 0.012
RMS (TMD) = 0.0034
Reduction ratio = 70.51%

fixed floor
TMD floor

(b) JMA Kobe NS

Max (fixed) = 0.044
Max (TMD) = 0.024
Reduction ratio = 46.66%

RMS (fixed) = 0.017
RMS (TMD) = 0.0041
Reduction ratio = 76.02%

fixed floor
TMD floor

(c) LCN Landers 260

fixed floor
TMD floor

Max (fixed) = 0.010
Max (TMD) = 0.010
Reduction ratio = 0.028%
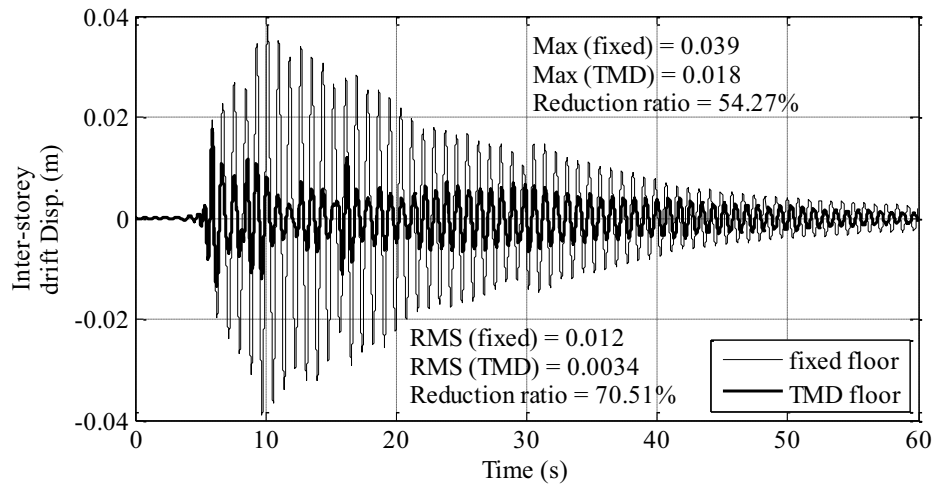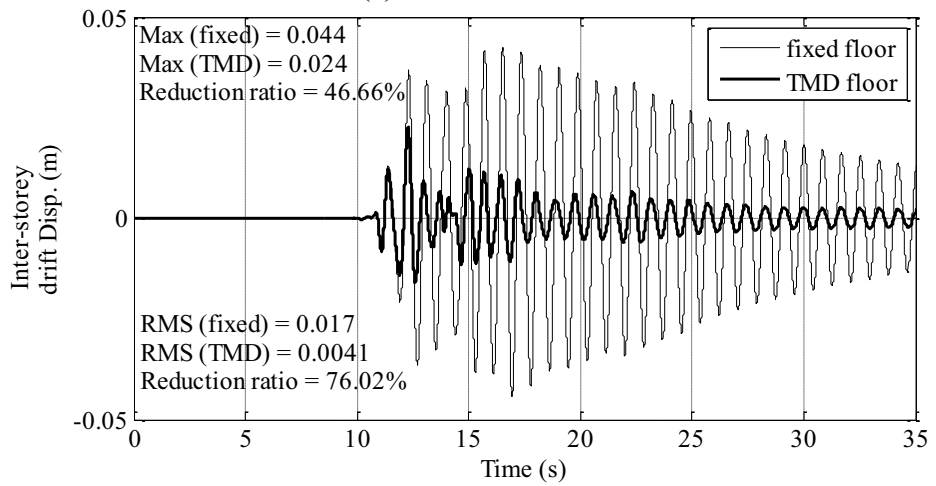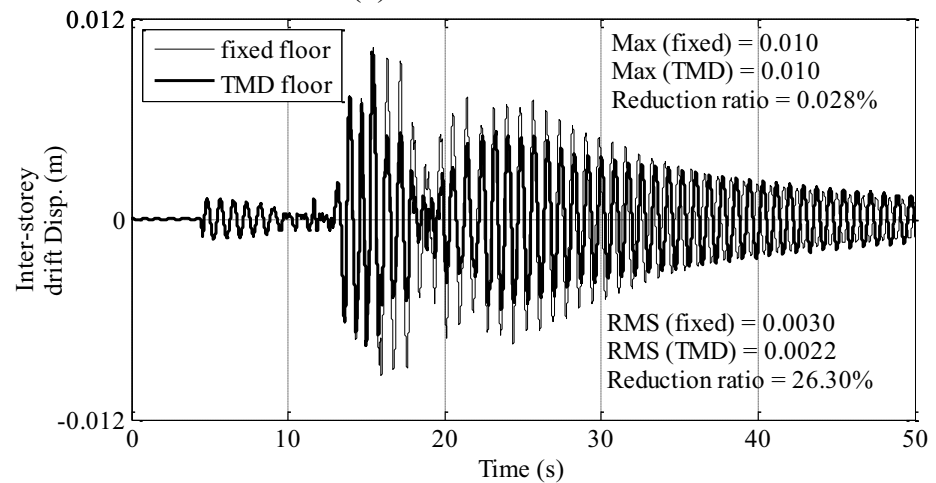
RMS (fixed) = 0.0030
RMS (TMD) = 0.0022
Reduction ratio = 26.30%

Figure 5.20 Inter-storey drift displacements of main frame
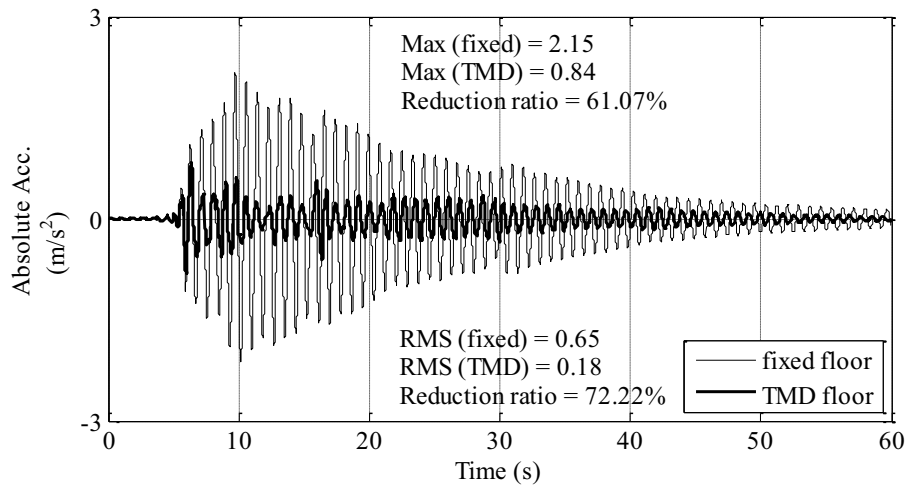
(a) El Centro NS
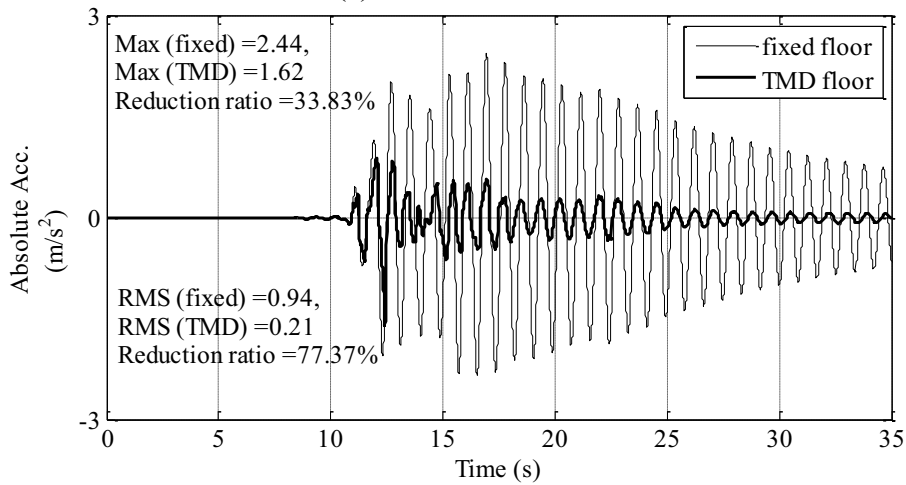
(b) JMA Kobe NS
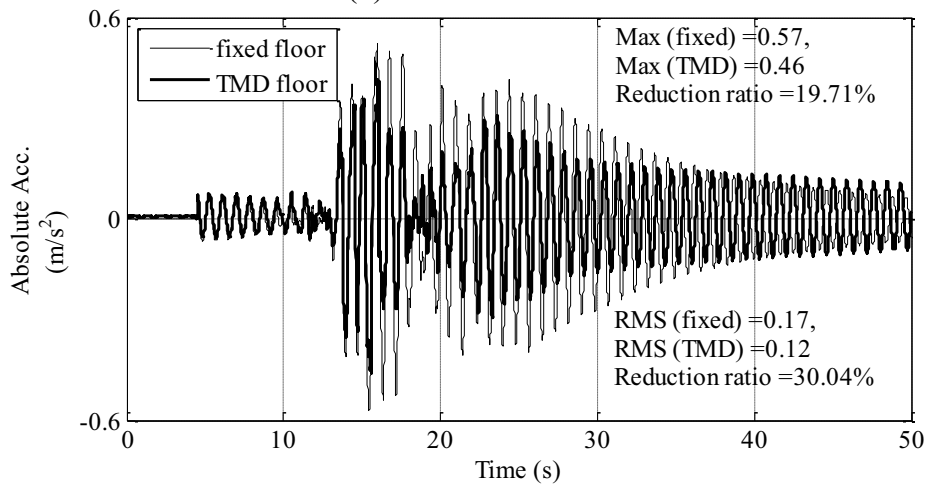
(c) LCN Landers 260

Figure 5.21 Absolute accelerations of floor

130

Table 5.4 compares the response reduction ratios between the analytical and experimental results with respect to the maximum (Max) and root mean square (RMS) values of the inter-storey displacements and floor absolute accelerations under the three seismic excitations. It can be found that the response reduction ratios of the experimental results are close to those of the analytical results, which verifies the validity of the analytical model and method.

<div align="center">Table 5.4 Comparison of response reduction ratios</div>

			analytical	experimental
El Centro	Inter-storey Disp.	Max	54.93%	54.27%
		RMS	69.75%	70.51%
	Floor absolute Acc.	Max	66.27%	61.07%
		RMS	70.42%	72.22%
JMA Kobe	Inter-storey Disp.	Max	48.66%	46.66%
		RMS	76.75%	76.02%
	Floor absolute Acc.	Max	53.23%	33.83%
		RMS	77.69%	77.37%
LCN Landers	Inter-storey Disp.	Max	5.41%	0.028%
		RMS	25.93%	26.30%
	Floor absolute Acc.	Max	14.73%	19.71%
		RMS	27.22%	30.04%

5.4 Optimum Design of Multiple Tuned Mass Damper Floors Integrated Structural System

5.4.1 Optimum parameters of tuned mass damper floors

Considering an N-storey building, the objective function for the optimization of TMD floor design parameters is set as follows

$$J = \text{Max.}\left(\text{Max.}\left| H_{Xs(drift)_1}(j\omega) \right|, \text{Max.}\left| H_{Xs(drift)_2}(j\omega) \right|, \ldots, \text{Max.}\left| H_{Xs(drift)_N}(j\omega) \right| \right) \tag{5.12}$$

where $\text{Max.}\left| H_{Xs(drift)_n}(j\omega) \right|$ $(n = 1, 2, \ldots, N)$ denotes the maximum magnitude of the FRF

of the inter-storey drift displacement for the *n*-th storey.

By using the gradient-based optimization method as mentioned in Section 2.3, the optimization problem herein can be formulated so as to search the optimal set of the design variables, tuning ratio, υ, i.e., the frequency ratio of the TMD to main structure, and damping ratio ζ_T, over an admissible domain with the objective function *J*.

5.4.2 Optimum locations of tuned mass damper floors

If not all the floors in a building can serve as TMDs due to certain reasons, e.g. construction cost constraints, the optimum attachment locations of TMD floors need to be determined. In general, the anti-nodal location of a single mode is taken as a priori for the attachment location (e.g., Rana and Soong, 1998; Daniel *et.al.*, 2012). However, this single mode approach loses accuracy for the cases of large mass TMDs attached systems with closely spaced natural frequencies, while the multimode approach proposed by Petit *et.al.*, (2009) can solve these problems. Therefore, the multimode approach is applied to search the optimum TMD floor locations.

Each TMD can only be tuned to a single mode, and the procedure for reducing the *i*-th resonance mode is presented in the flowchart in Figure 5.22. The neighboring anti-resonances are a representation of the activity of the neighboring modes, and a high activity of the neighboring modes has a negative effect on the vibration reduction of the *i*-th mode. Accordingly, the multimode approach combines the information about the eigenvector of the mode to be controlled with knowledge about the neighboring anti-resonances, as shown in the flowchart (Figure 5.22).
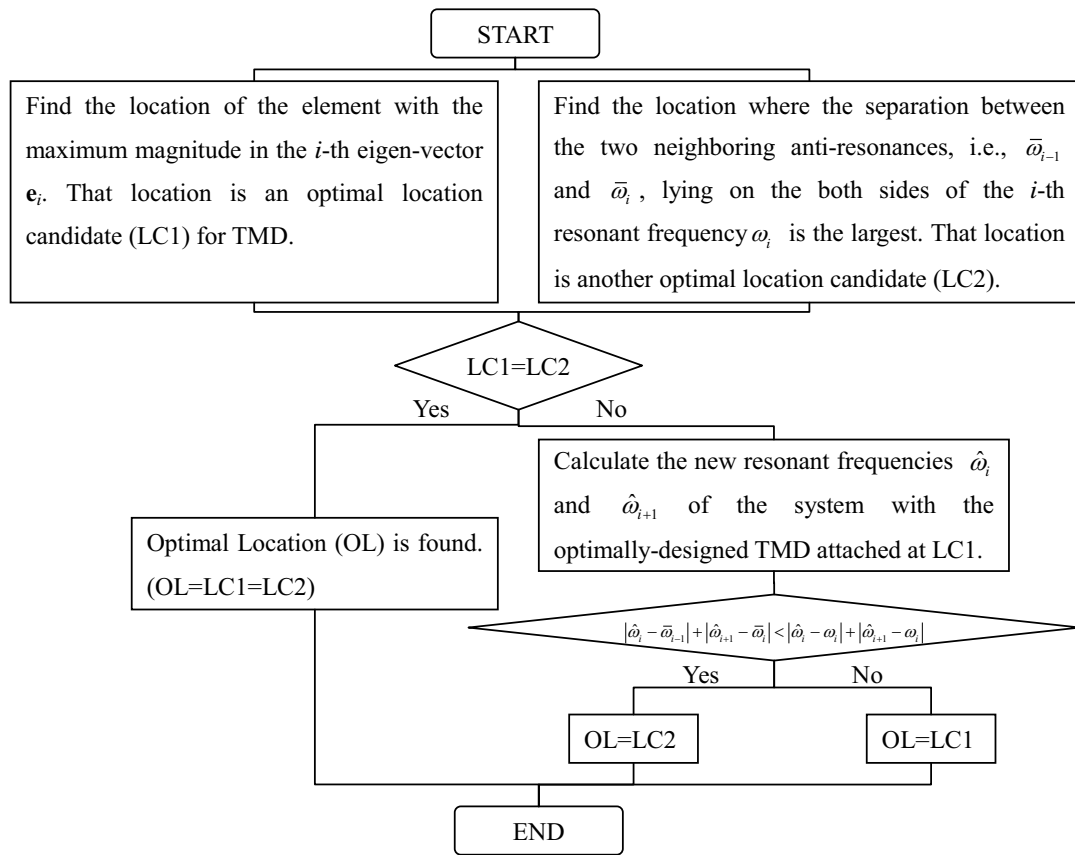
Figure 5.22 Flowchart of multimode approach

5.4.3 Numerical examples

(1) Mid-rise building

In conducting numerical simulations, a six-storey building is considered firstly, and the parameters are listed in Table 5.5. The first modal damping ratio is assumed to be 0.01, and the damping matrix is proportional to the stiffness matrix.

Table 5.5 Parameters of six-storey building

Storey	Mass [$\times 10^3$ kg]	Stiffness [$\times 9.8 \times 10^2$ kN/m]
6th	87.10	26.00
5th	79.30	26.40
4th	79.00	29.90
3rd	78.10	30.50
2nd	78.20	36.30
1st	78.10	67.20

The following two cases for the building are studied. One is the case in which all the floors can serve as TMDs, including the ground floor. And the other one is the case in which only three floors can be used as TMDs.

① **All floors serving as tuned mass dampers**

For simplicity, the design parameters for all TMDs in this case are assumed to be same, i.e., only one set of υ^{opt} and $\zeta_{\text{T}}^{\text{opt}}$ needs to be determined. The gradient-based optimization method as mentioned in Section 2.3 is applied with the objective function as defined in Section 5.4.1. The optimization results are υ^{opt}=0.70 and $\zeta_{\text{T}}^{\text{opt}}$=0.40, and the frequency of a TMD floor is calculated according to $\omega^{\text{opt}} = \upsilon^{\text{opt}} \cdot \omega_{1}$, where ω_{1} denotes the first modal natural circular frequency of the uncontrolled building. The stiffness and damping coefficient of the i-th TMD floor are then obtained as $k_{\text{T}i} = m_{\text{T}i} \left(\omega^{\text{opt}} \right)^{2}$ and $c_{\text{T}i} = 2m_{\text{T}i}\omega^{\text{opt}} \zeta_{\text{T}}^{\text{opt}}$, respectively. The inter-storey drifts of the main structure and absolute accelerations of TMD floors are defined as the two main performance indices in this study. Figure 5.23 (a)-(c) shows the magnitudes of the FRFs from the ground acceleration to the inter-storey drifts, the absolute accelerations of the TMD floors and the absolute accelerations of the main structure, respectively. It can be seen from Figure 5.23 (a) that the FRF magnitude for the third storey drift is the maximum at the fundamental frequency, and the two peak values are identical to each other. Thus the gradient-based optimization method of designing TMDs is verified to be effective for damped MDOF main structure and specified objective functions. Figure 5.23 (b) and (c) show that the FRF magnitudes of accelerations for both the TMD floors and main structure storeys at the fundamental

frequency increase as the height increases. For the comparison of (b) and (c), Figure 5.23 (d) shows the magnitude ratio of the FRFs of the TMD floor acceleration to main structure acceleration. The relationships between the acceleration FRF magnitude ratio and input frequency are the same for all the floors since the same design parameters are adopted for all the TMD floors in this case. Thus the same curves are obtained in Figure 5.23 (d). The FRF magnitudes of TMD floor accelerations are even smaller than those of the controlled main structure storey accelerations in most of the frequency ranges except for the ranges with small input frequencies (approximately smaller than the fundamental frequency of the uncontrolled building). This fact indicates that the merit of FIS can be achieved in TMDFS though the objective function of the optimum design framework in this study does not take explicitly the floor accelerations into consideration.
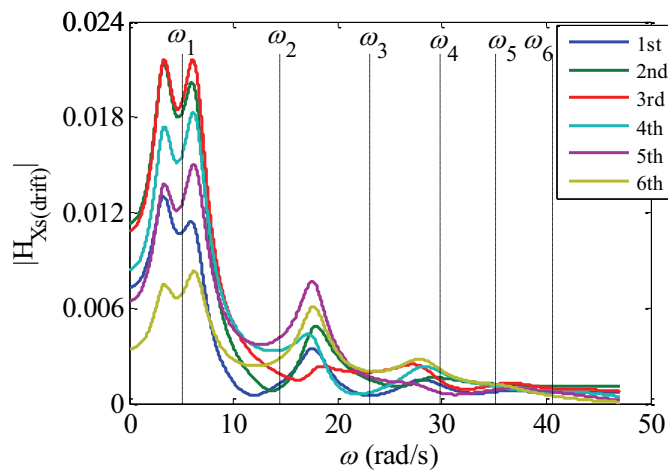
(a) inter-storey drifts of main structure

Figure 5.23 FRF magnitudes from ground accelerations to structural responses

($\omega_1 \sim \omega_6$ are natural circular frequencies of uncontrolled building)

135
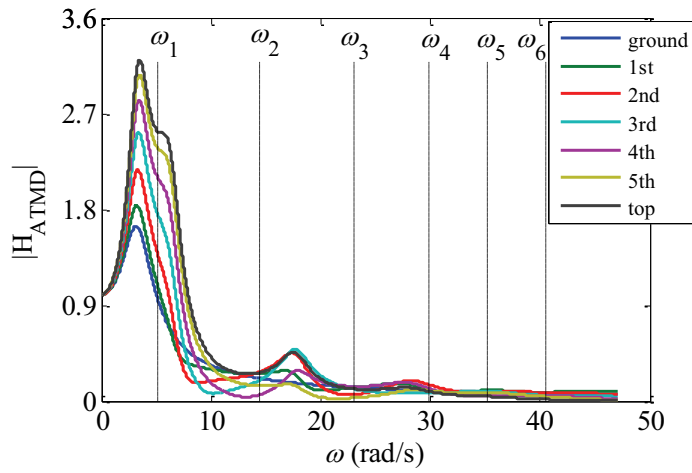
(b) absolute accelerations of TMD floors
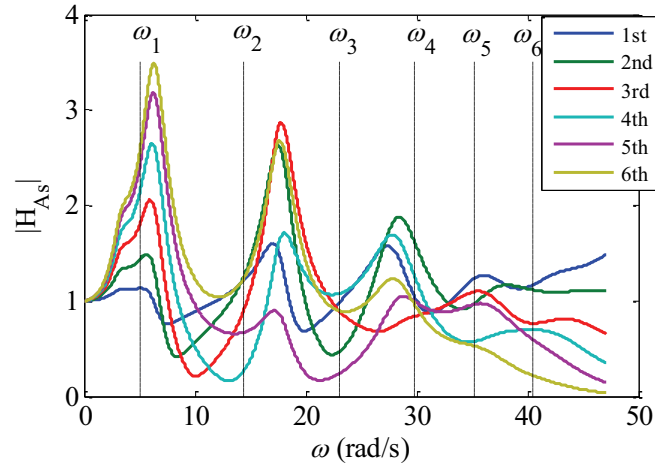
(c) absolute accelerations of main structure
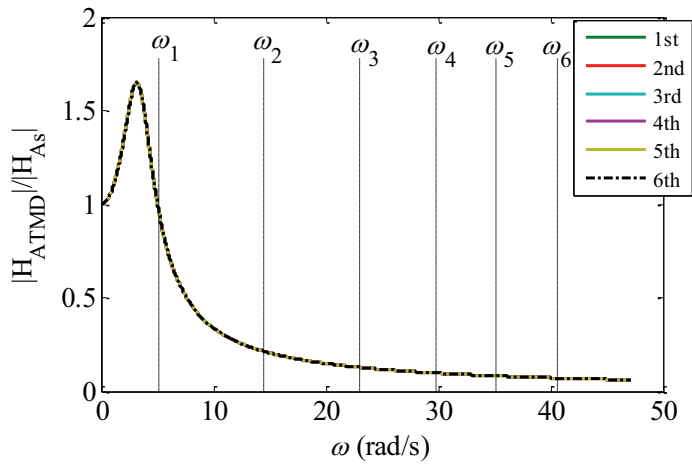
(d) ratio of (b) and (c)

Figure 5.23 Continued

136

To further demonstrate the seismic performance of TMDFS, the performance of the six-storey building with the TMDFS is studied with respect to the following six representative un-scaled earthquake records:

i. El Centro (NS component), 1940;

ii. JMA Kobe (NS component), 1995;

iii. Northridge (NS component), 1994;

iv. LCN Landers (260 component), 1992;

v. TCU068 Chi-chi (EW component), 1999;

vi. TKY007 Tohoku (EW component), 2011.

The peak responses of the TMDFS subjected to the above six seismic excitations are presented in Figure 5.24 (a)-(l). The figures (a, c, e, g, i, k) show the peak values of the inter-storey drift displacements of the storeys, and the figures (b, d, f, h, j, l) show the peak values of the absolute accelerations of the TMD floors. In the figures, the dotted lines represent the responses of the un-controlled case (fixed floor system with the first modal damping ratio of 0.01); the solid lines indicate the responses of the TMDFS; and the dashed lines portray the responses of the fixed floor system in which damping devices are implemented in each storey with the same damping coefficient as the damping devices between the TMD floors and the corresponding storeys in TMDFS. In the figures (b, d, f, h, j, l), "floor 0" denotes the ground floor which is utilized as a TMD floor as well (referred to Figure 5.3). Though the ground TMD floor has no control effect for mitigating the vibration response of the main structure, its acceleration is smaller than the input ground motion PGA, as seen from the figures. For the other two cases than the

TMDFS, the ground floor peak acceleration is equal to the input ground motion PGA. From Figure 5.24, it is apparent that the TMDFS achieves the most significant control effect in terms of both the inter-storey drift displacements of the main structure and the absolute accelerations of the floors under all the six seismic excitations. In addition, Figure 5.25 presents the peak values of the stroke length of the TMD floors in TMDFS, and it can be found that the maximum stroke length of the TMD floors under the six seismic excitations i-vi is 0.12m, 0.34m, 0.50m, 0.32m, 0.40m and 0.068m, respectively, which are acceptable values in practical applications. Comparing with the control effects of the single TMD floor integrated system in the experiment, the multiple TMD floors integrated system is also effective for LCN Landers, though the predominant period of the excitation is far away from the fundamental period of the six-storey building (without considering floors) which is 1.00s, and this fact reflects the advantage of MTMDs.
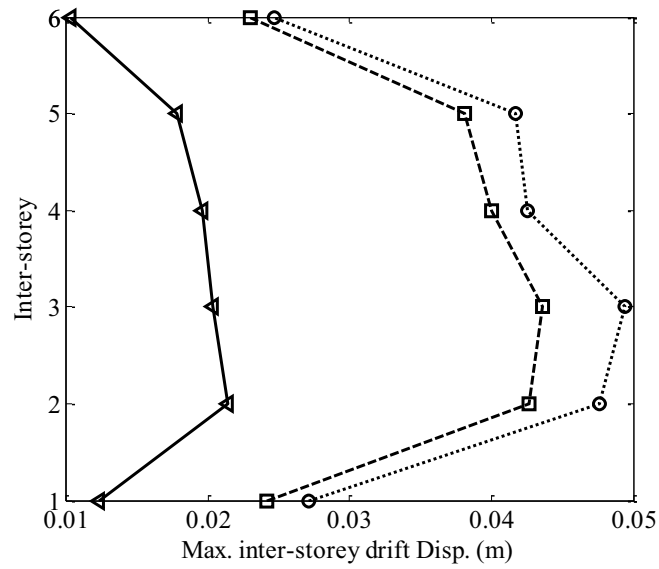
(a) under El Centro
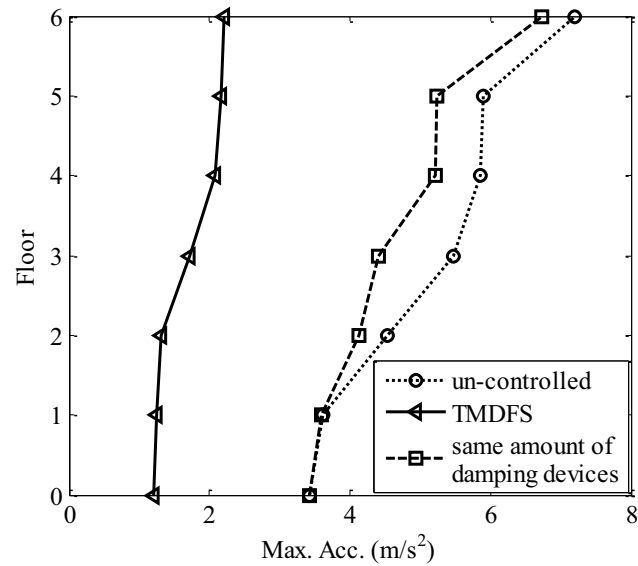
(b) under El Centro

Figure 5.24 Peak responses of six-storey building in different cases: (a, c, e, g, i, k) inter-storey drift displacements of storeys; (b, d, f, h, j, l) absolute accelerations of TMD floors; (a, b) El Centro; (c, d) JMA Kobe; (e, f) Northridge; (g, h) LCN Landers; (i, j) TCU068 Chi-chi; and (k, l) TKY007 Tohoku.
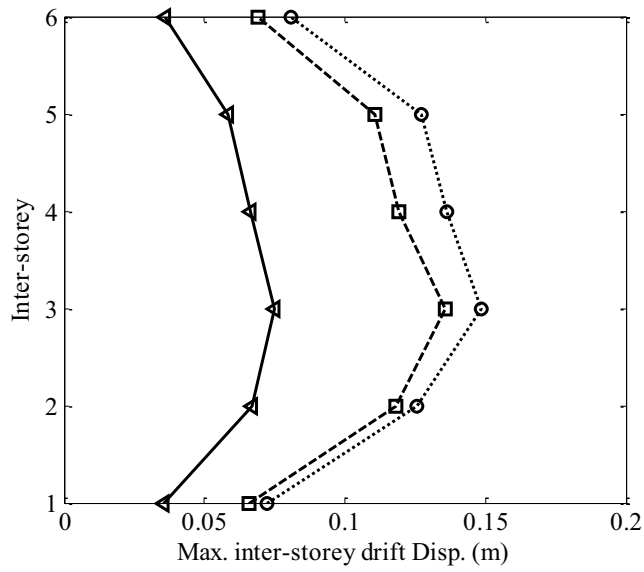
(c) under JMA Kobe
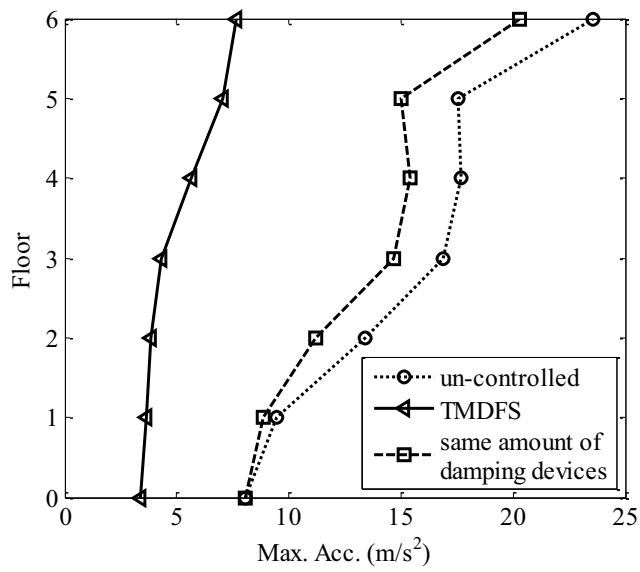
(d) under JMA Kobe

Figure 5.24 Continued
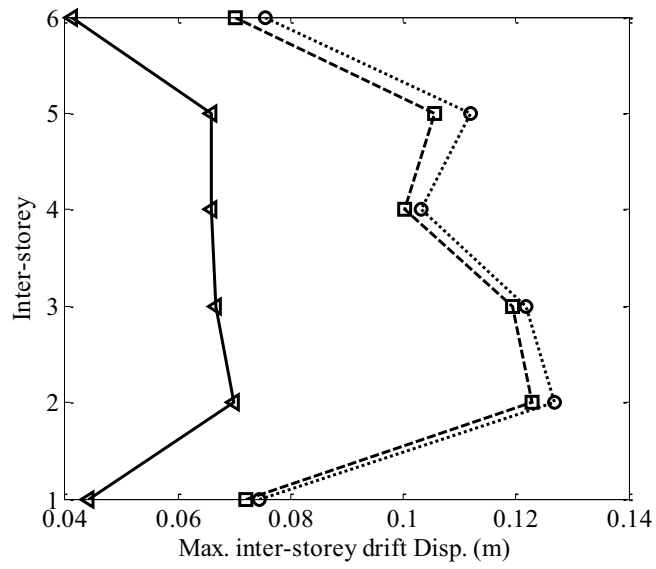
(e) under Northridge
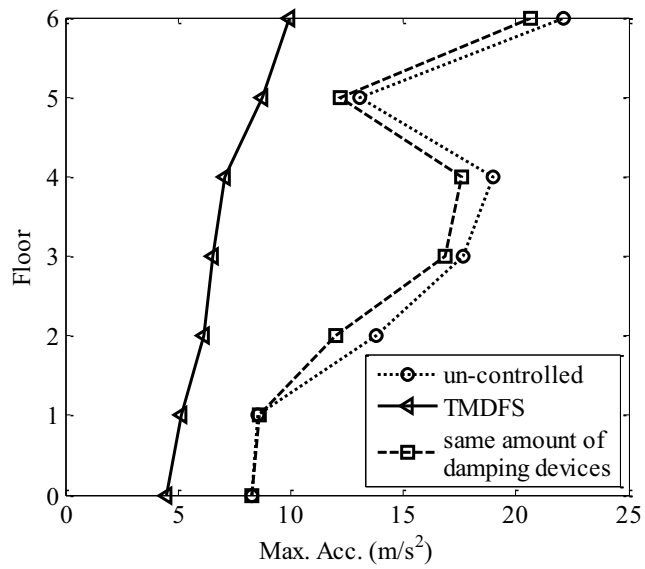
(f) under Northridge

Figure 5.24 Continued
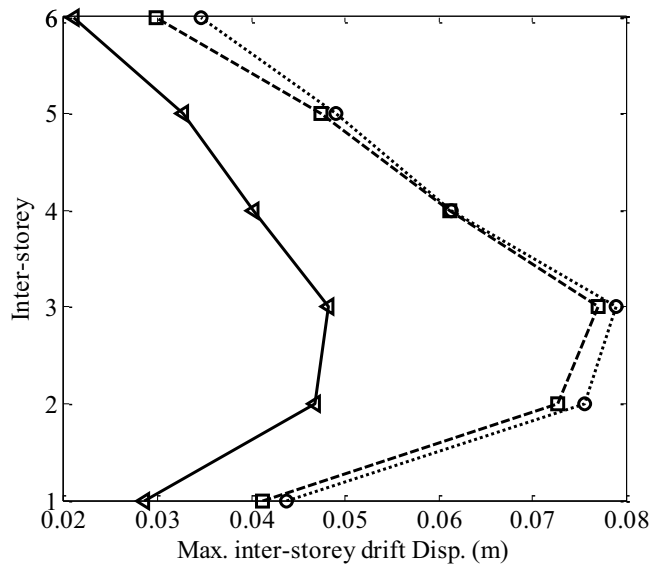
(g) under LCN Landers
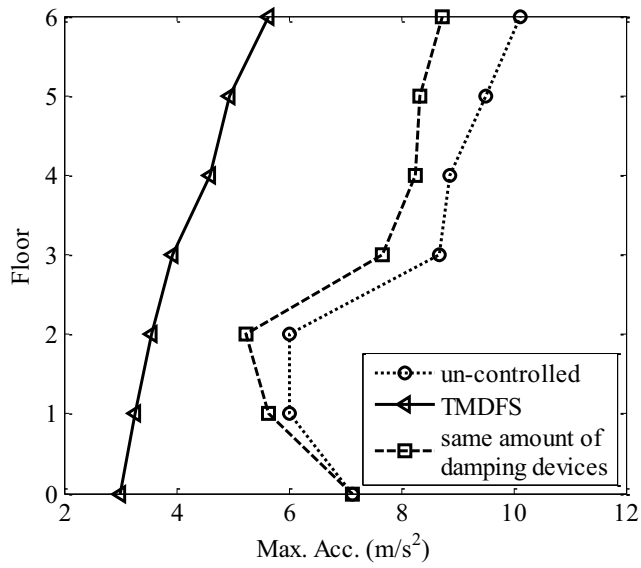
(h) under LCN Landers

Figure 5.24 Continued
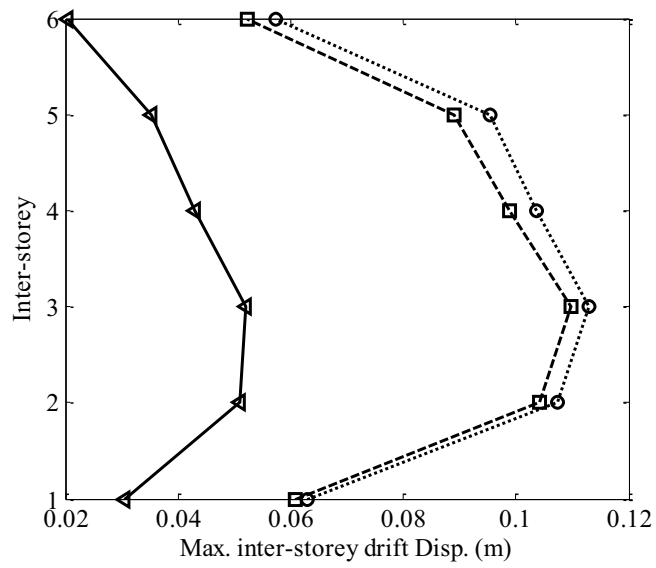
(i) under TCU068 Chi-chi
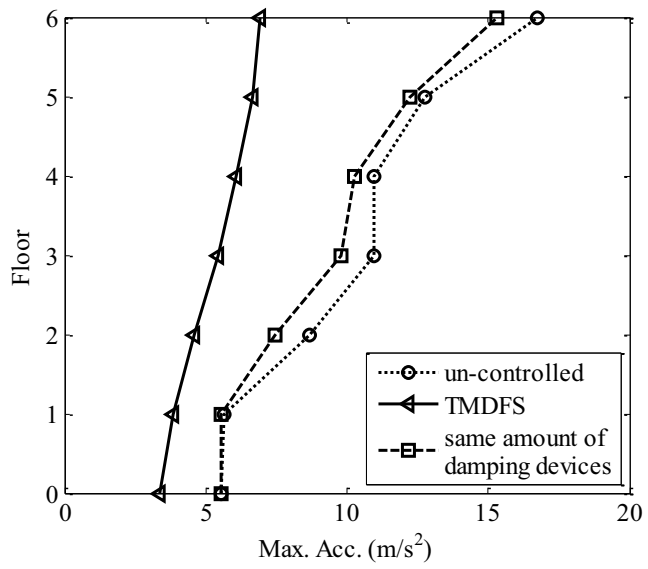
(j) under TCU068 Chi-chi

Figure 5.24 Continued
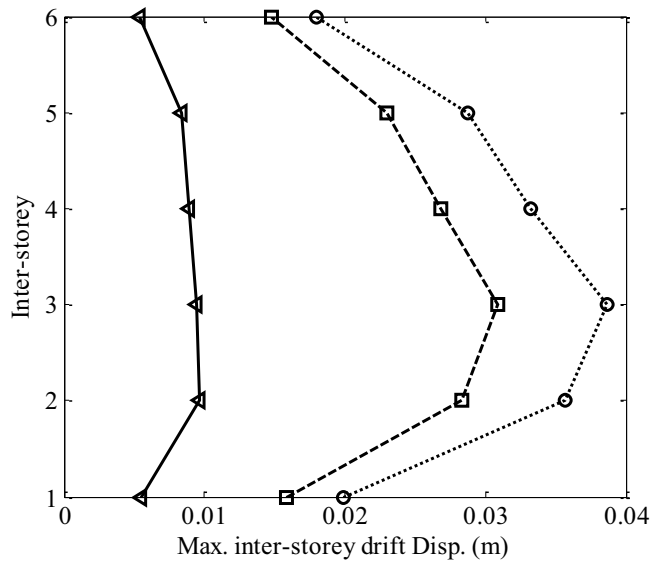
(k) under TKY007 Tohoku
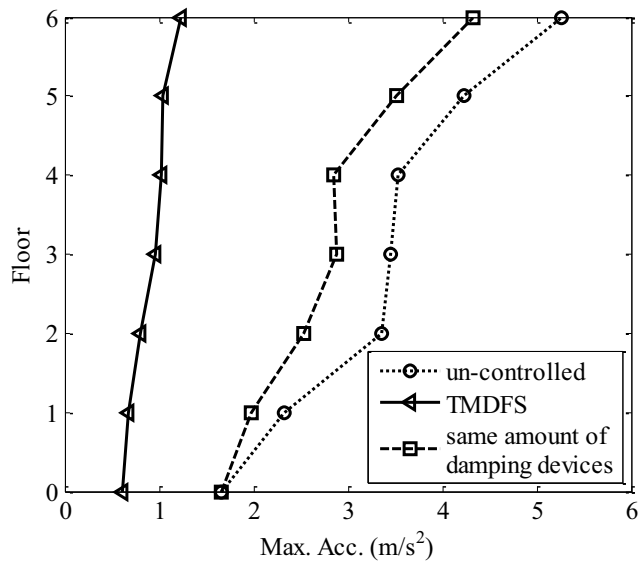
(l) under TKY007 Tohoku

Figure 5.24 Continued
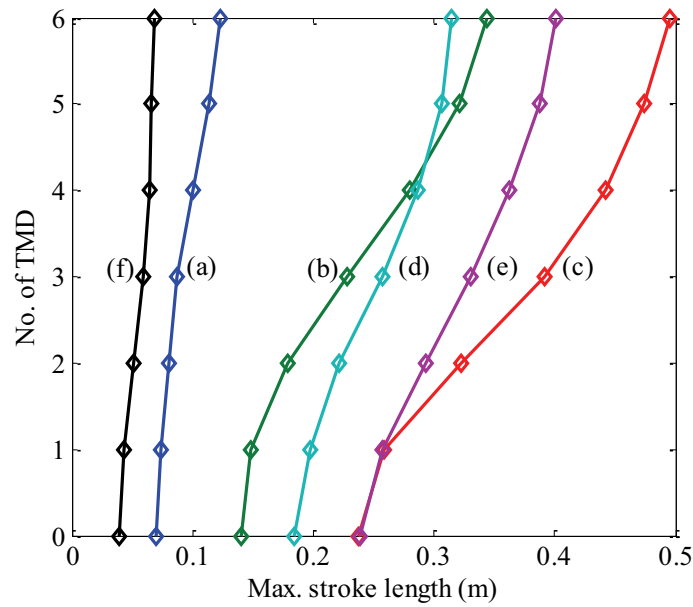
Figure 5.25 Peak stroke length of TMD floors: (a) El Centro; (b) JMA Kobe; (c) Northridge; (d) LCN Landers; (e) TCU068 Chi-chi; and (f) TKY007 Tohoku.

② **Partial floors serving as tuned mass dampers**

In the following, the case in which only three floors of the building are used as TMDs is studied, and the multimode approach mentioned in Section 5.4.2 is adopted to specify the optimal locations of the TMD floors. It can be observed from Figure 5.23 that the peak values based upon the two performance indices are much larger at the first modal frequency than those at higher modal frequencies, and decrease gradually as the mode order increases. Accordingly, the first mode should be controlled beforehand. The modal natural circular frequencies and their corresponding mass matrix normalized eigenvectors of the first three modes for the uncontrolled six-storey building are shown in Figure 5.26.
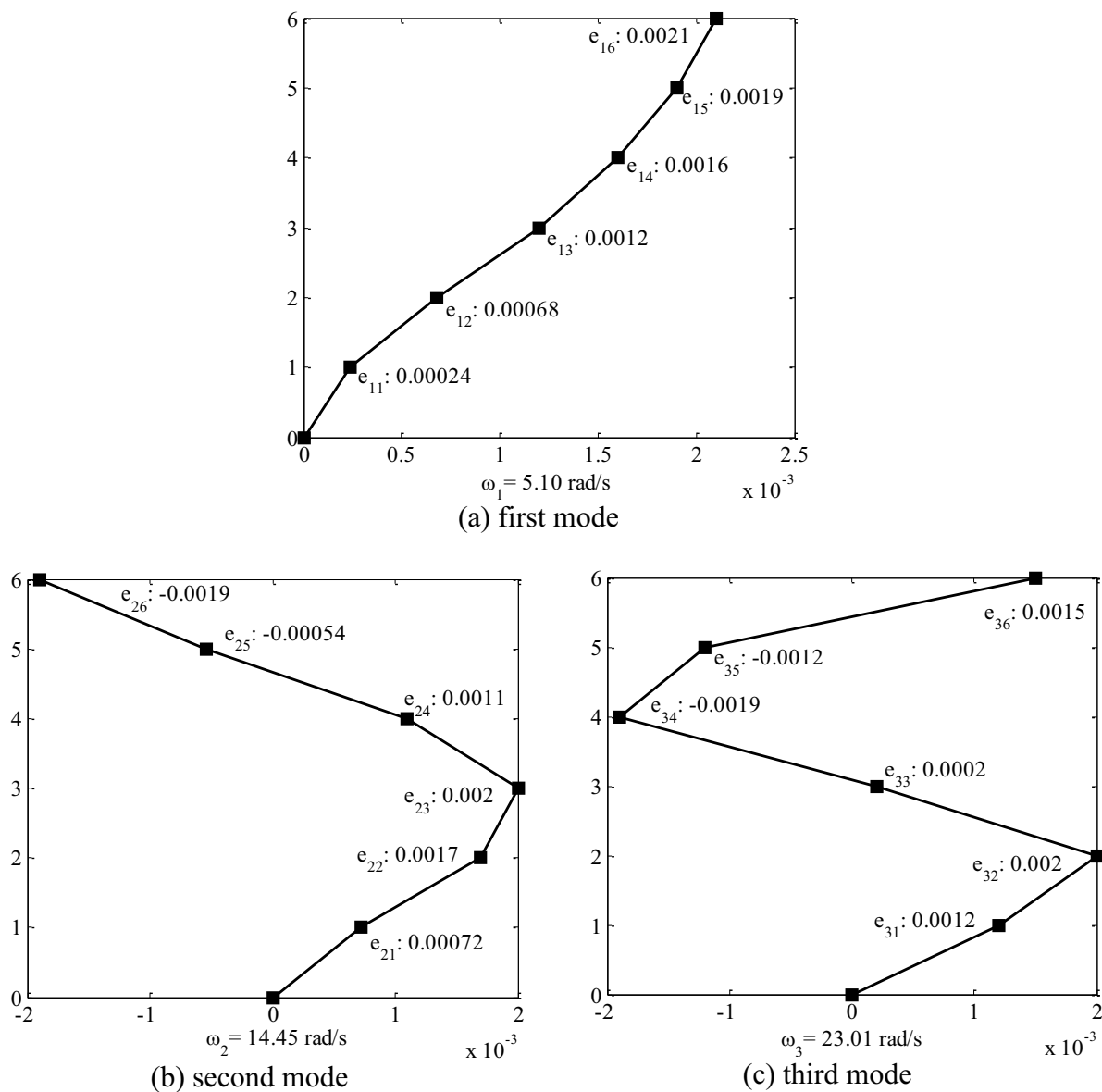
Figure 5.26 Modal natural circular frequencies and mass matrix normalized eigenvectors

of uncontrolled six-storey building

When the first modal response is considered, LC1 for the first TMD floor should be the

top floor according to the procedure of the multimode approach. The anti-resonances

neighboring to the first natural frequency ω_1 are [5.51 6.46 8.08 10.76 13.40 10.91]

(rad/s) for the six locations, respectively. Accordingly, LC2 for the first TMD floor is the

fifth storey, which is different from LC1. So the optimal location (OL) should be further determined. If the first TMD floor is located on the top floor, the optimization results are obtained as υ_1^{opt}=0.92 and ζ_{T1}^{opt}=0.23 by using the gradient-based optimization method presented in Section 2.3. For the structure with the top floor served as TMD, the new first and second resonant frequencies $\hat{\omega}_1$ and $\hat{\omega}_2$ are 4.30 and 5.82 (rad/s), respectively. As the original first resonant frequency ω_1 and the neighboring anti-resonance $\bar{\omega}_1$ corresponding to the top location are 5.10 and 10.91 (rad/s), respectively, the magnitude of $|\hat{\omega}_2 - \bar{\omega}_1|$ is 5.09 rad/s, which is larger than the magnitude of $|\hat{\omega}_1 - \omega_1| + |\hat{\omega}_2 - \omega_1|$ that equals 1.52 rad/s. Accordingly, LC1 defines OL, i.e., the top floor is OL for the first TMD floor.

Then OL of the second TMD floor has to be determined for reducing the original second mode vibration which corresponds to the new third mode of the one-TMD-floor-attached system. As the damping matrix with the damping of the first TMD integrated is non-proportional, the resulting mass matrix normalized eigenvectors are complex. Herein, the magnitudes of the first six elements corresponding to the six DOF main storeys of the eigenvectors are presented, because only the magnitudes are required in the multimode approach. The magnitudes of the new eigenvector corresponding to the third mode of the main structure with the top floor serving as a TMD are obtained as [0.00078 0.0018 0.0019 0.00082 0.0010 0.0021]^T. The third floor is LC1 because the third element in the vector is the second maximum next to the sixth element, since the top floor has already served as the first TMD. Table 5.6 lists the neighboring anti-resonances lying on the both sides of the third resonant frequency, ω_2' (corresponding to the second modal natural

147

circular frequency of the uncontrolled building), of the main structure with the top floor serving as the first TMD. It can be concluded that LC2 for the second TMD floor is the third floor because the separation between the neighboring anti-resonances of the third location is the maximum. LC1 and LC2 are the same, and thus the third floor should serve as the second TMD. The optimum parameters for the second TMD obtained by the gradient-based optimization method are υ_2^{opt}=0.27 and $\zeta_{\text{T2}}^{\text{opt}}$=0.17.

Table 5.6 Neighboring anti-resonances for mode 3 of one-TMD-floor-attached system (ω_2'=15.39 rad/s)

Locations	1	2	3	4	5	6
Anti-resonances (rad/s)	6.25-16.71	7.32-19.55	9.25-23.59	12.62-17.46	13.40-21.12	10.91-20.84
Separation (rad/s)	10.46	12.23	14.34	4.84	7.72	9.93

Finally, OL of the third TMD floor will be determined for controlling the original third mode which corresponds to the new fifth mode of the two-TMD-floor-attached system. As the magnitudes of the new eigenvector corresponding to the fifth mode of the main structure with the top and third floors serving as TMDs are [0.0012 0.0019 0.00015 0.0021 0.00060 0.0020]$^{\text{T}}$, LC1 of the third TMD should be the fourth floor. Table 5.7 lists the neighboring anti-resonances lying on the both sides of the fifth resonant frequency, ω_3'' (corresponding to the third modal natural circular frequency of the uncontrolled building), of the main structure with the top and third floors serving as TMDs. LC2 of the third TMD floor should be the fourth floor, which is the same as LC1. Accordingly, the third TMD floor is determined to be the fourth floor, and the optimization parameters for the third TMD are υ_3^{opt}=0.15 and $\zeta_{\text{T3}}^{\text{opt}}$=0.22.

Table 5.7 Neighboring anti-resonances for mode 5 of two-TMD-floor-attached system
(ω_3'' =24.02 rad/s)

Locations	1	2	3	4	5	6
Anti-resonances (rad/s)	17.81-26.27	20.57-31.20	23.59-24.32	18.54-30.53	21.12-24.96	21.06-29.47
Separation (rad/s)	8.46	10.63	0.73	11.99	3.84	8.41

To verify the validity of the multimode approach, the control effect for the case of the second floor, which is the anti-nodal location of the third mode shape (referring to Figure 5.26 (c)), serving as the third TMD is compared with that for the case of the fourth floor serving as the third TMD. The optimization results are $\upsilon_{3'}^{\mathrm{opt}}$ =0.16 and $\zeta_{T3'}^{\mathrm{opt}}$ =0.16 if the second floor serves as the third TMD floor. Figure 5.27 shows the magnitudes of the two FRFs, i.e., FRFs of the inter-storey drift of the third storey and the absolute acceleration of the top floor. They have the maximum magnitudes for FRFs of inter-storey drifts and absolute accelerations, respectively, among all the storeys. In the figure, the solid lines correspond to the case in which the fourth floor serves as the third TMD, while the dashed lines display the case in which the second floor serves as the third TMD. From the figures, it is apparent that the third TMD achieves much better control effect at the fourth floor location than at the second floor location.

The control effect of the TMDFS will be illustrated by Figures 5.28 and 5.29. Figure 5.28 (a)-(l) shows the FRF magnitudes of the inter-storey drift displacements and floor absolute accelerations. In the figure, the dotted lines represent the single TMD floor case in which only the top floor serves as the TMD, the dashed lines display the case in which the top and third floors serve as two TMDs, and the solid lines indicate the case in which the top, third and fourth floors serve as three TMDs. It can be seen from the figures that,
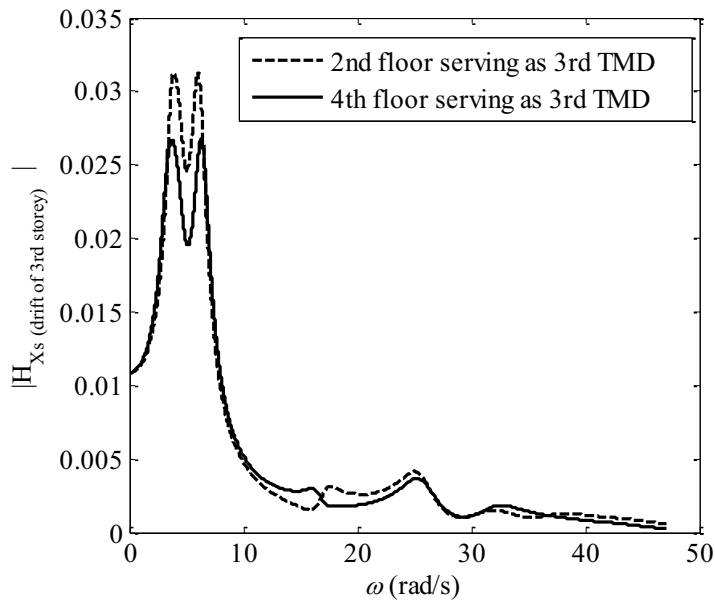
(a) inter-storey drift displacement of third storey
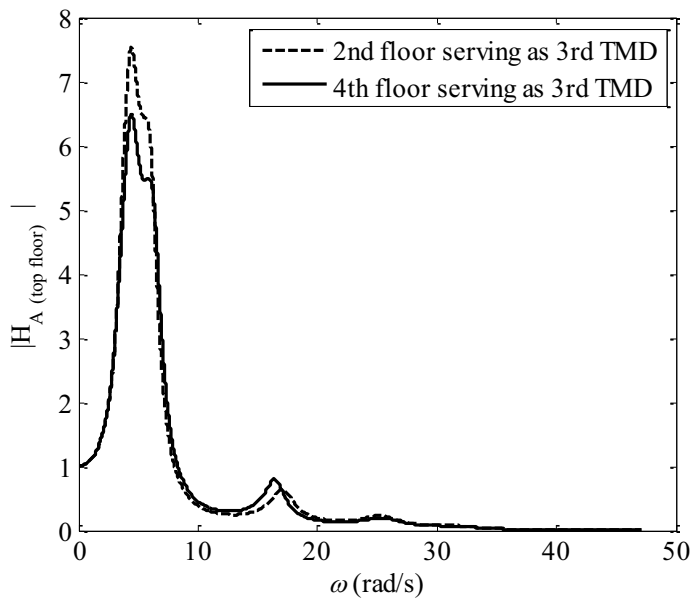
(b) absolute acceleration of top floor

Figure 5.27 Magnitudes of FRFs for two performance indices

the peak magnitudes of the FRFs of the inter-storey drift displacements at the first three

modal frequencies have been mitigated for all the storeys, and the maximum magnitudes

of the FRFs for inter-storey drift displacements decrease as the number of TMD floors increases. On the other hand, the FRF magnitudes of the absolute accelerations for the top, third and fourth floors, which serve as TMDs in the three-TMD-floor-attached system, are mitigated significantly with wide suppression bandwidths achieved in the frequency range.

Figure 5.29 gives responses of the three different TMD floor systems (i.e., with one TMD floor, with two TMD floors and with three TMD floors), as well as the un-controlled system, subjected to the above mentioned six seismic excitations. The figures (a, e, i, m, q, u) portray the maximum inter-storey drift displacements of storeys; the figures (b, f, j, n, r, v) show the maximum displacements of the main structure for all the stories relative to the ground; the figures (c, g, k, o, s, w) display the maximum absolute accelerations of the floors; and the figures (d, h, l, p, t, x) present the corresponding root mean square values of the absolute accelerations. From the figures, it can be found that the control effect for the inter-storey drifts achieved by the three-TMD-floor-attached system is the best among the four systems under all the six excitations. And the maximum absolute accelerations of the third, fourth and top floors which serve as TMDs in the three-TMD-floor-attached system are all smaller than those in the other three systems under all the excitations. As far as the root mean square values of the absolute accelerations of all the floors are concerned, the three-TMD-floor-attached system generally achieves the most satisfactory control effect among the four systems.
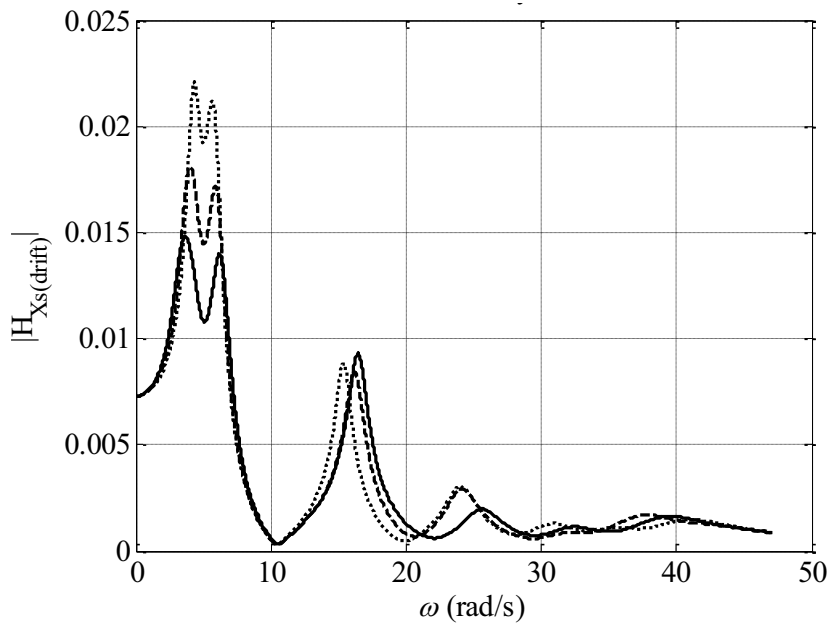
(a) 1st storey
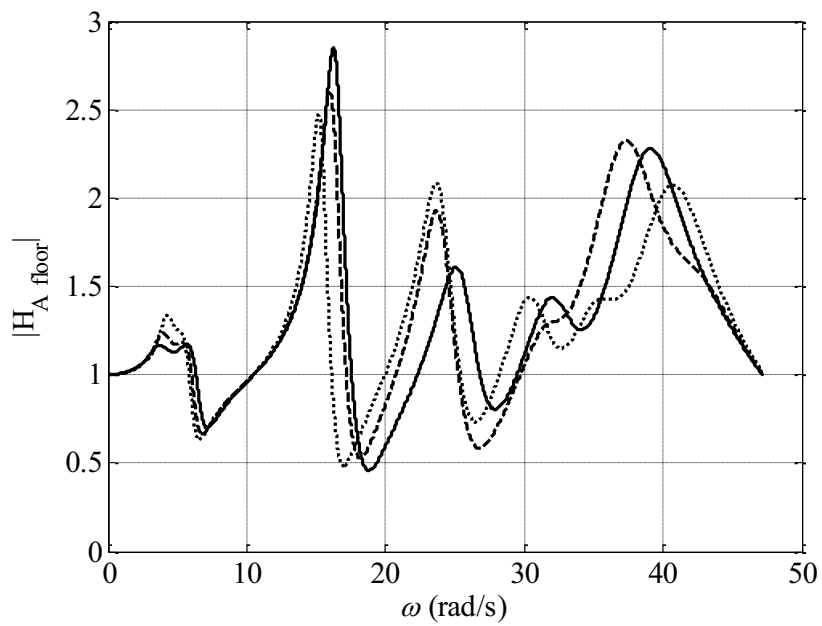
(b) 1st floor

Figure 5.28 FRF magnitudes: (a, c, e, g, i, k) inter-storey drift displacements; (b, d, f, h, j, l) absolute accelerations; '····' top floor serving as one TMD floor; '---' top and 3rd floors serving as two TMD floors; and '—' top, 3rd and 4th floors serving as three TMD floors.
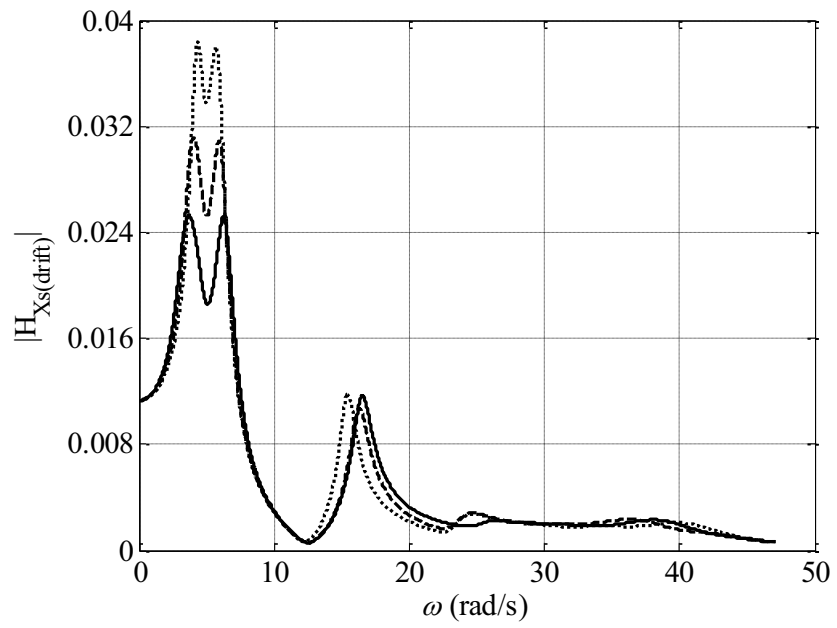
(c) 2$^{\text{nd}}$ storey
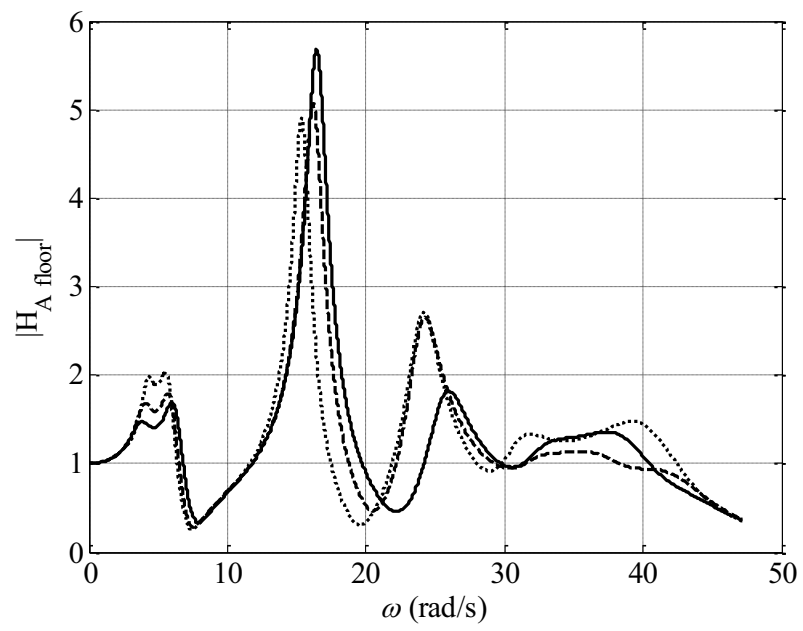
(d) 2$^{\text{nd}}$ floor

Figure 5.28 Continued

153
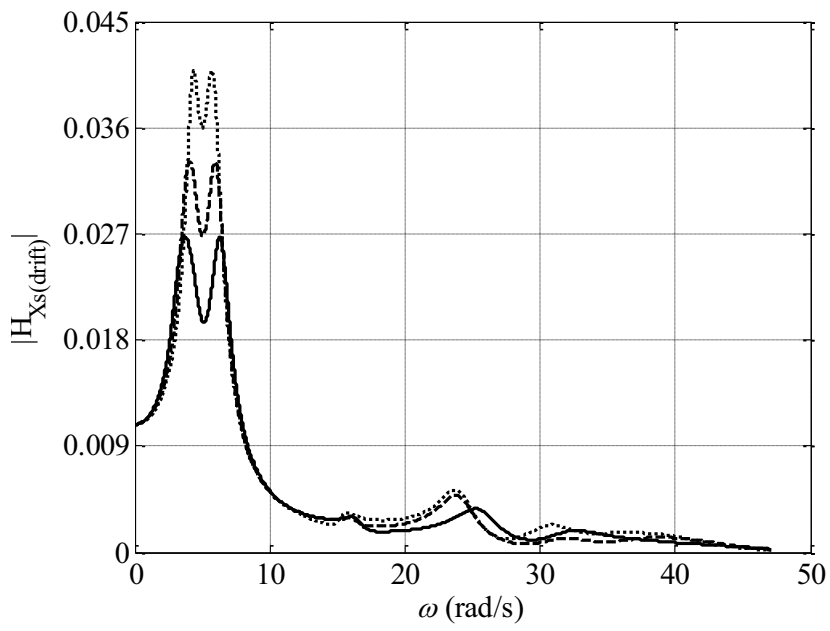
(e) 3rd storey
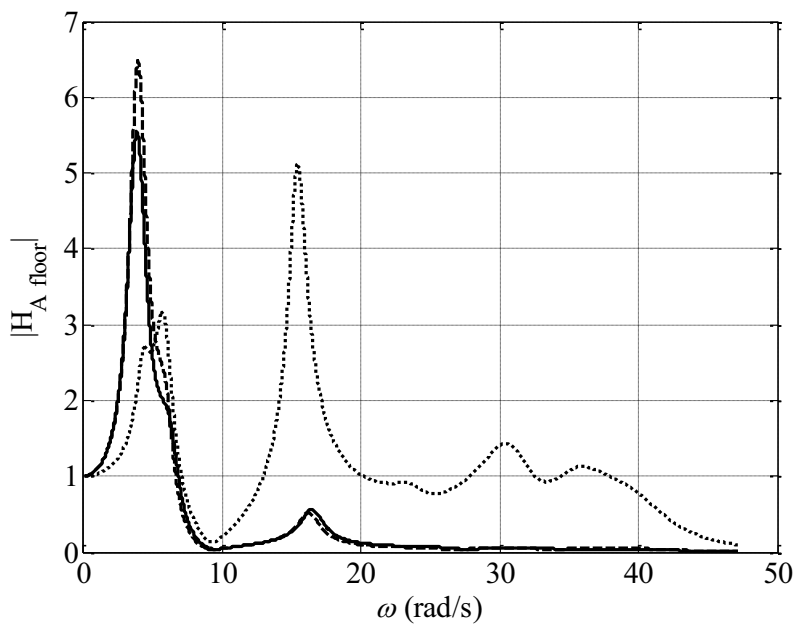
(f) 3rd floor

Figure 5.28 Continued
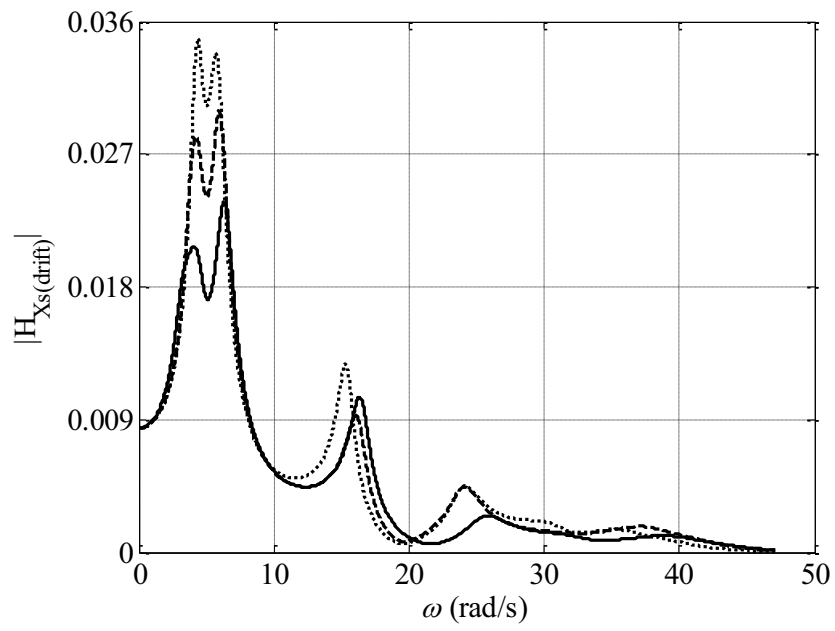
(g) 4th storey
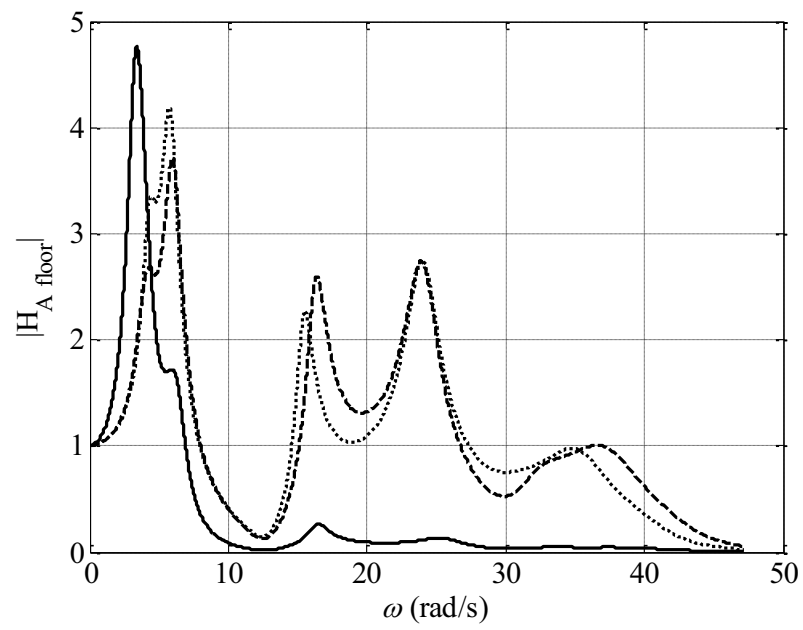
(h) 4th floor

Figure 5.28 Continued

155
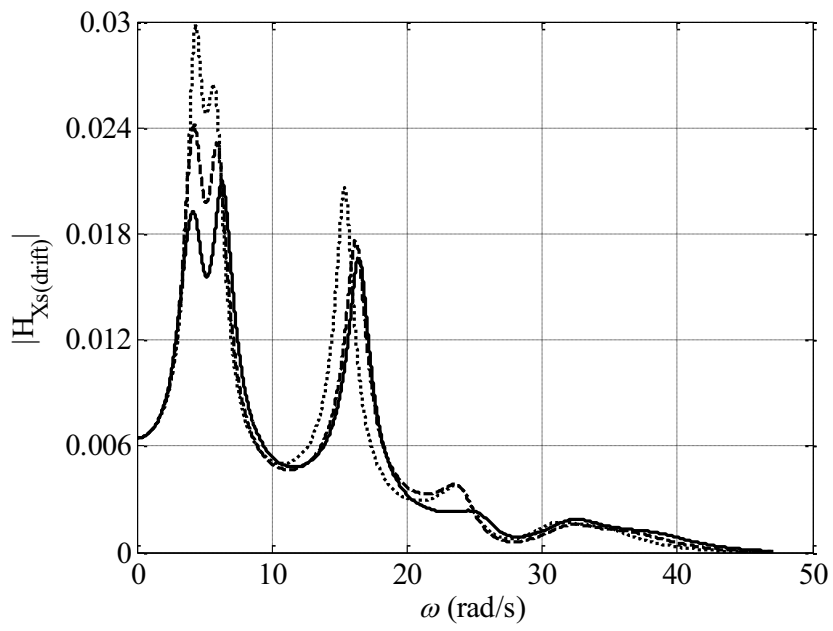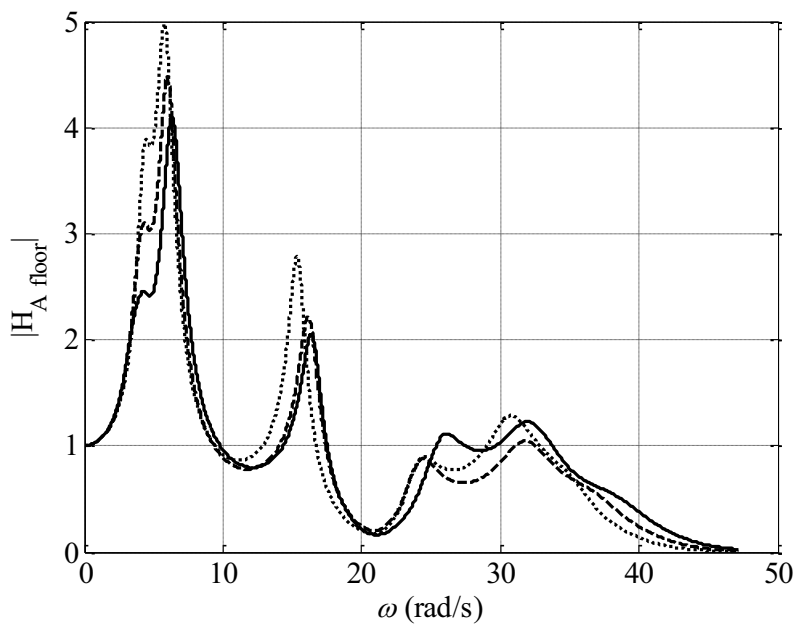
(i) 5th storey

(j) 5th floor

Figure 5.28 Continued

156
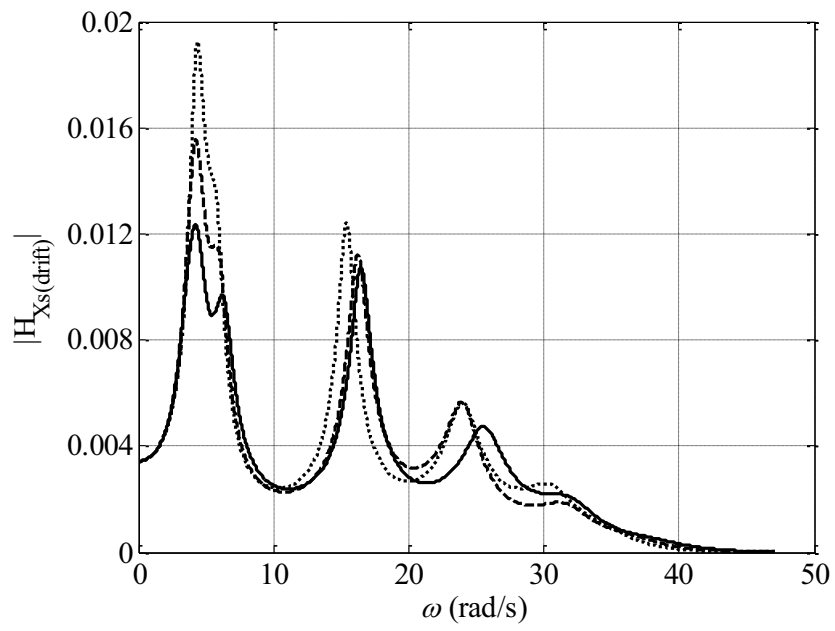
(k) 6th storey
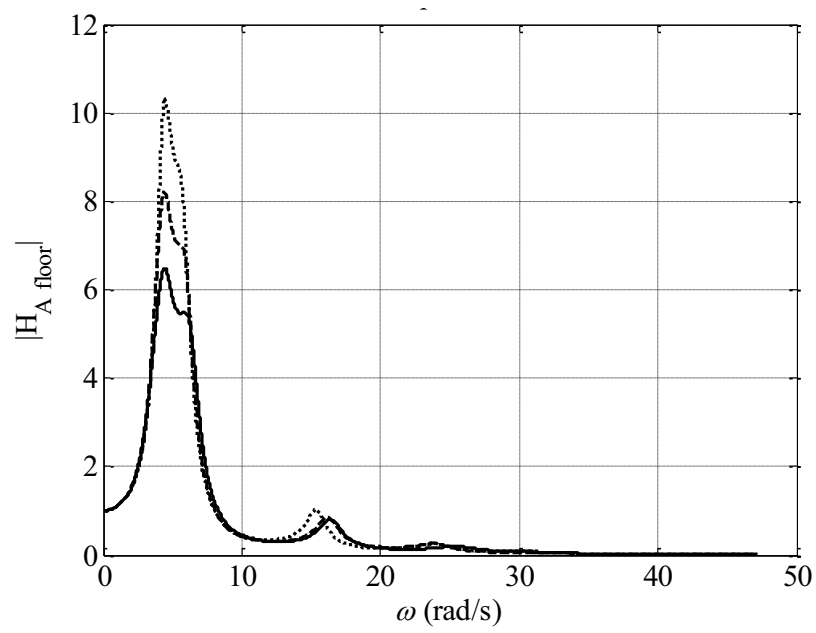
(l) top floor

Figure 5.28 Continued
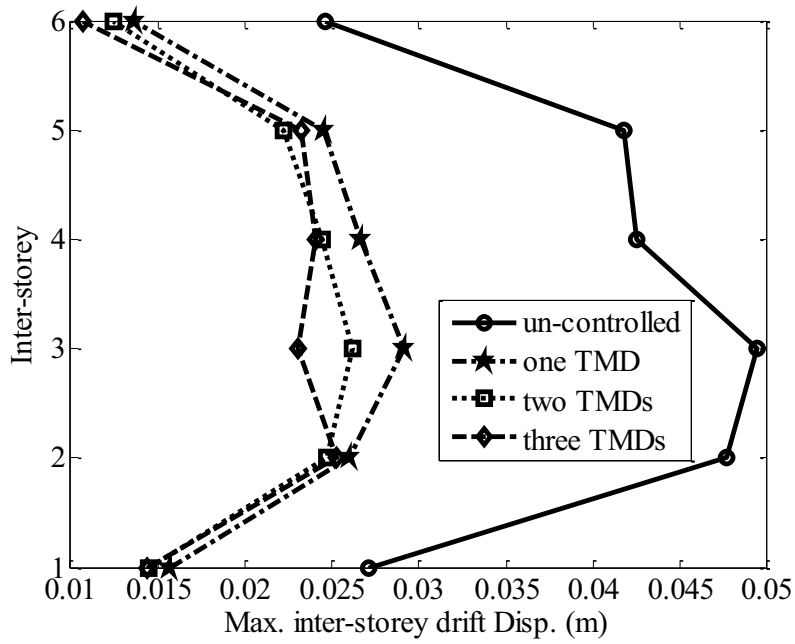
(a) maximum inter-storey drift displacements of storeys
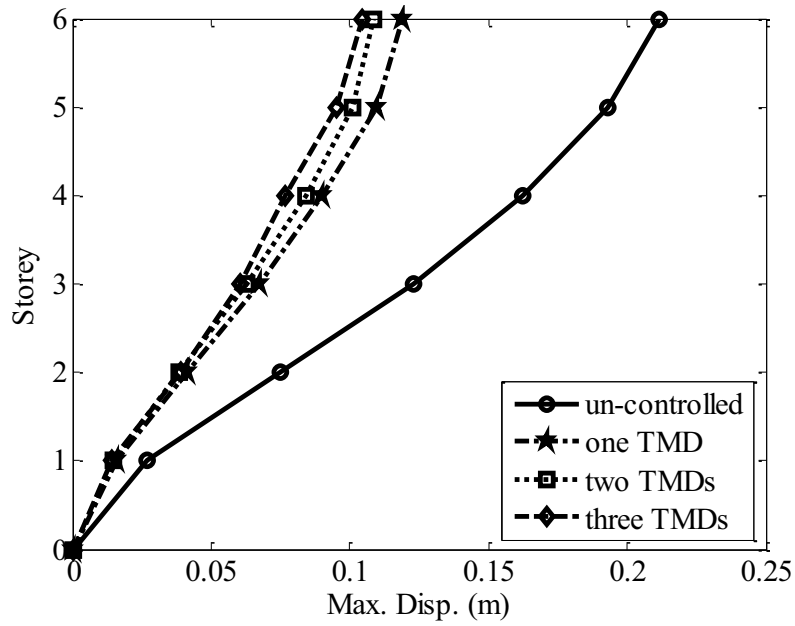
(b) maximum displacements of storeys relative to ground

Figure 5.29 Responses of different systems under El Centro
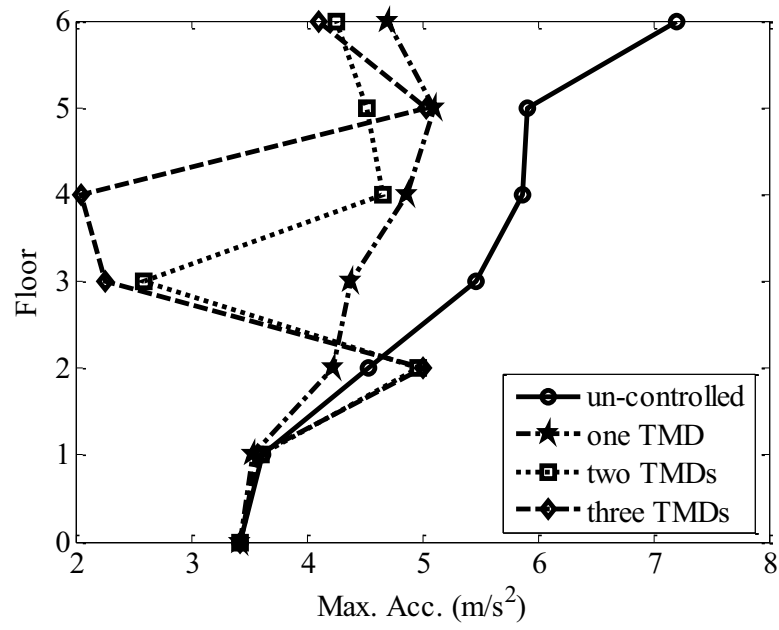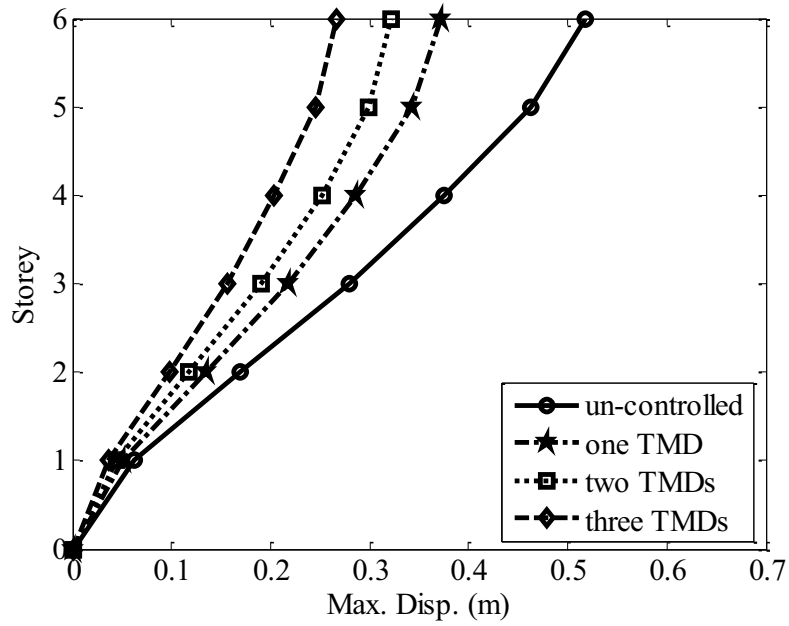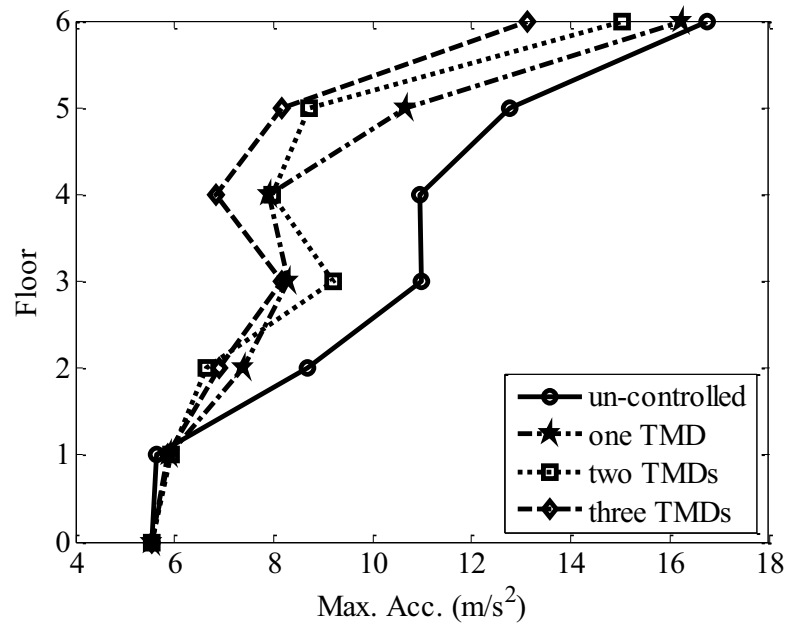
(c) maximum absolute accelerations of floors
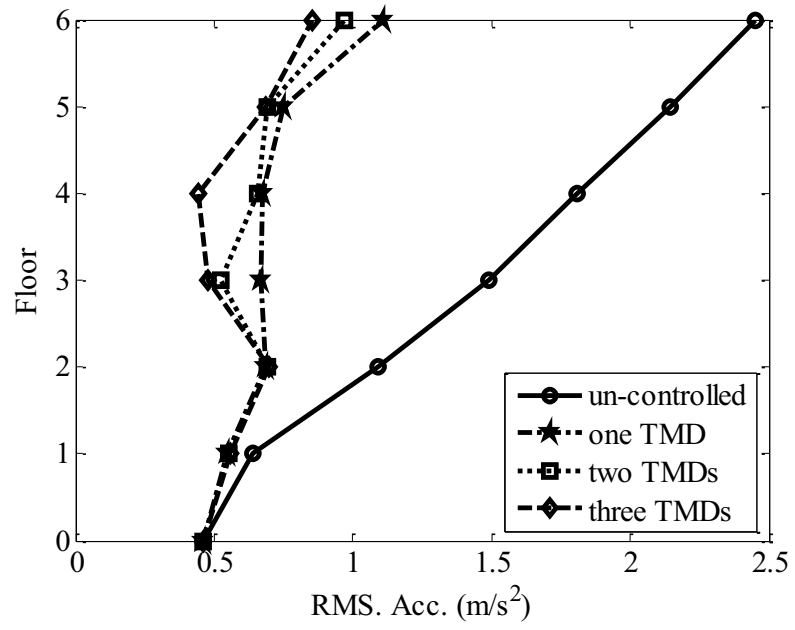
(d) root mean square values of absolute accelerations of floors

Figure 5.29 Continued
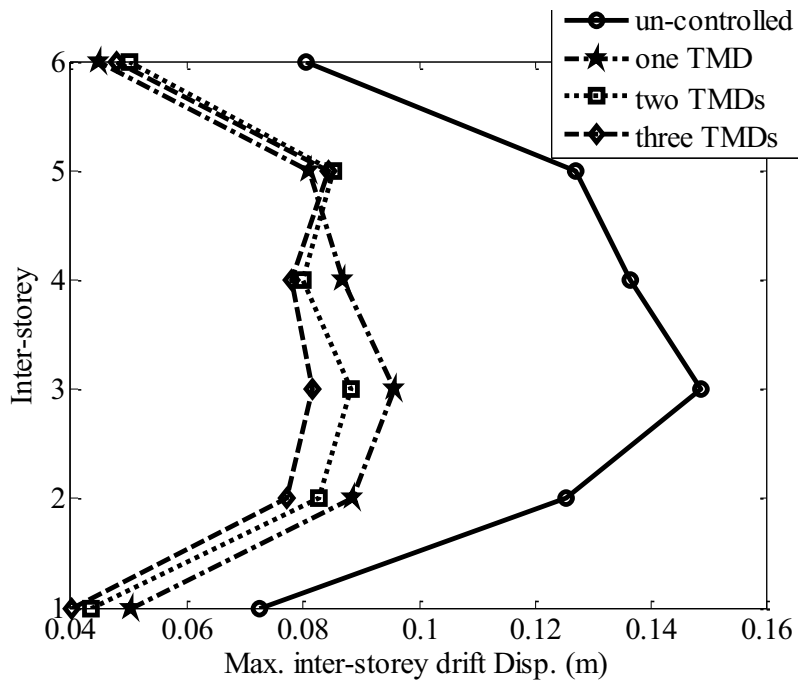
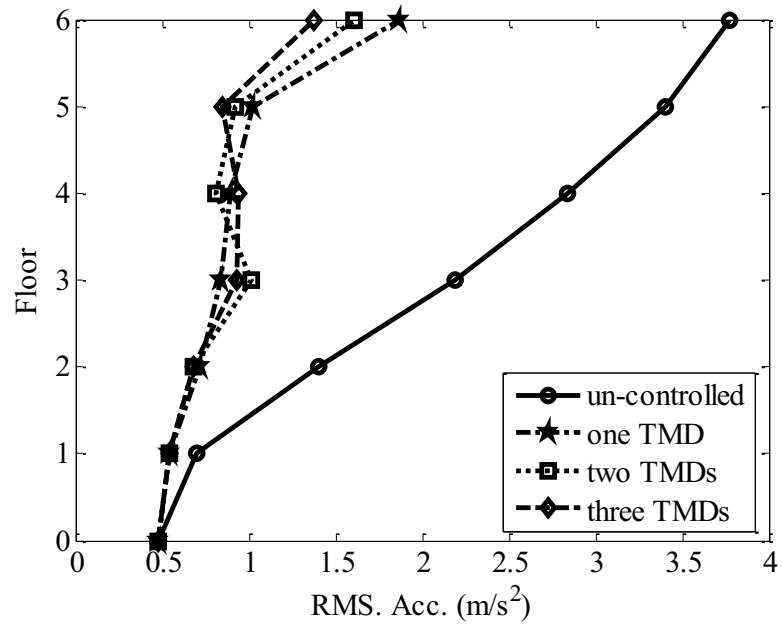(a) maximum inter-storey drift displacements of storeys
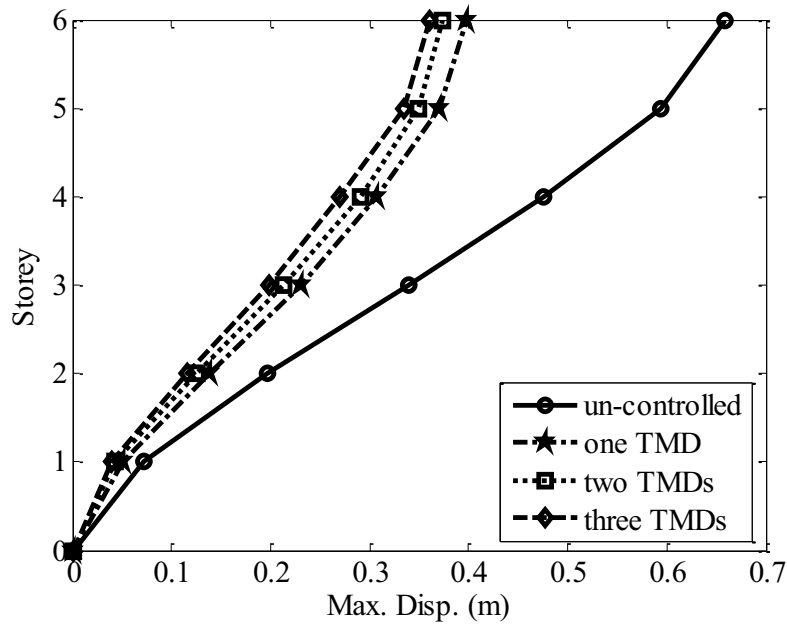
(b) maximum displacements of storeys relative to ground

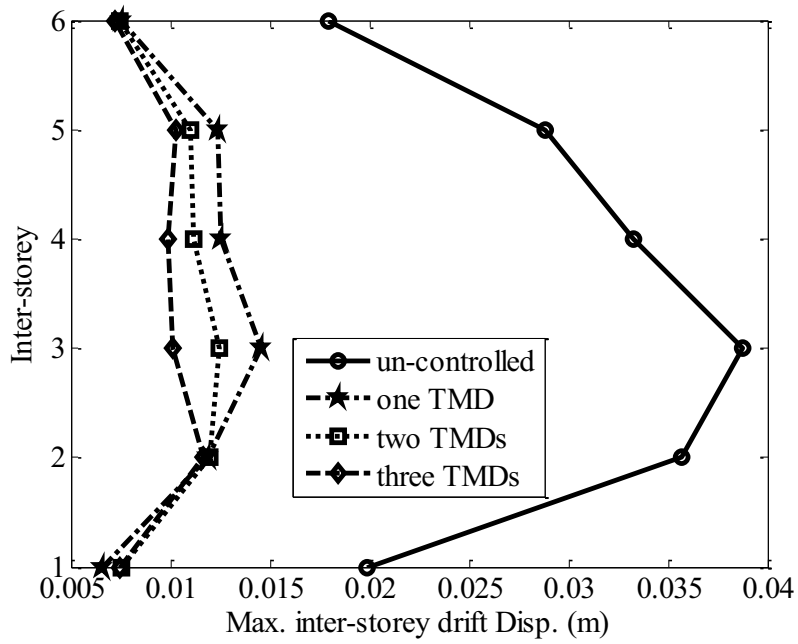Figure 5.30 Responses of different systems under JMA Kobe
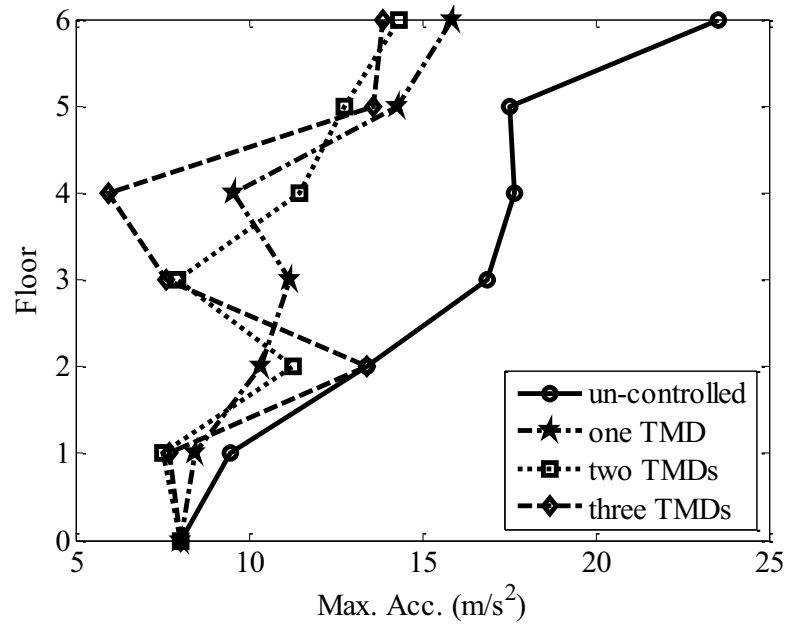
(c) maximum absolute accelerations of floors
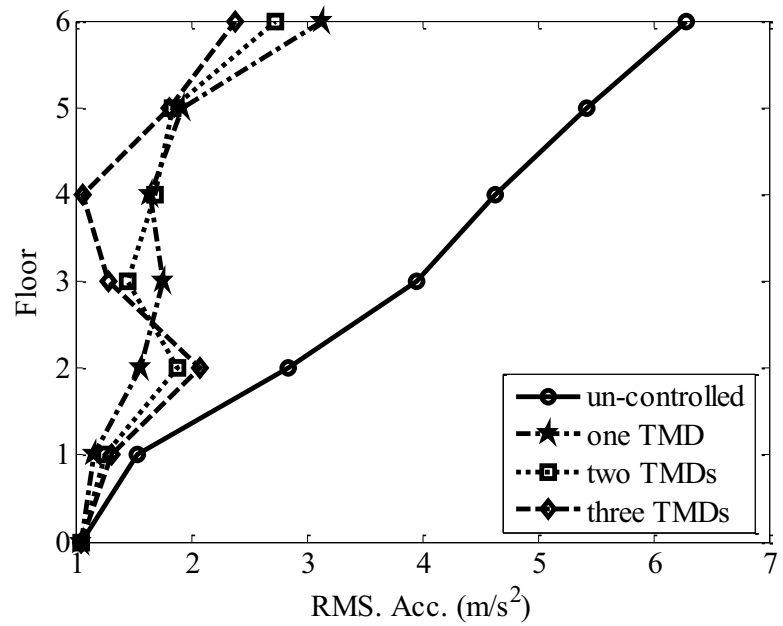
(d) root mean square values of absolute accelerations of floors

Figure 5.30 Continued
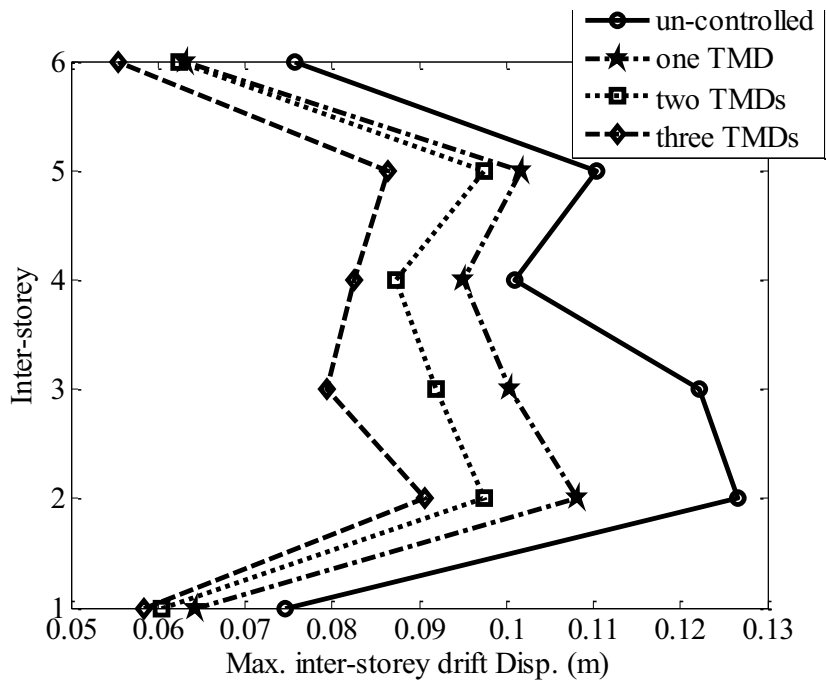
(a) maximum inter-storey drift displacements of storeys
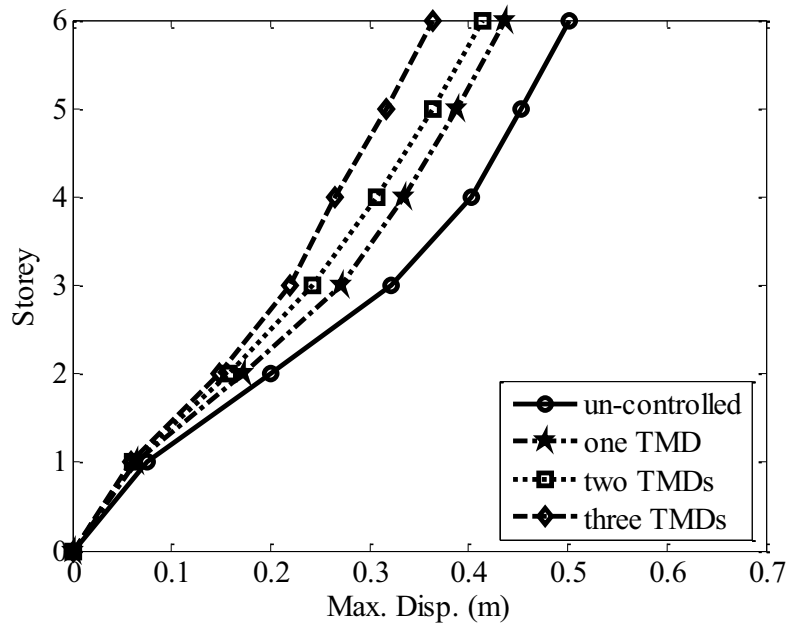
(b) maximum displacements of storeys relative to ground

Figure 5.31 Responses of different systems under Northridge
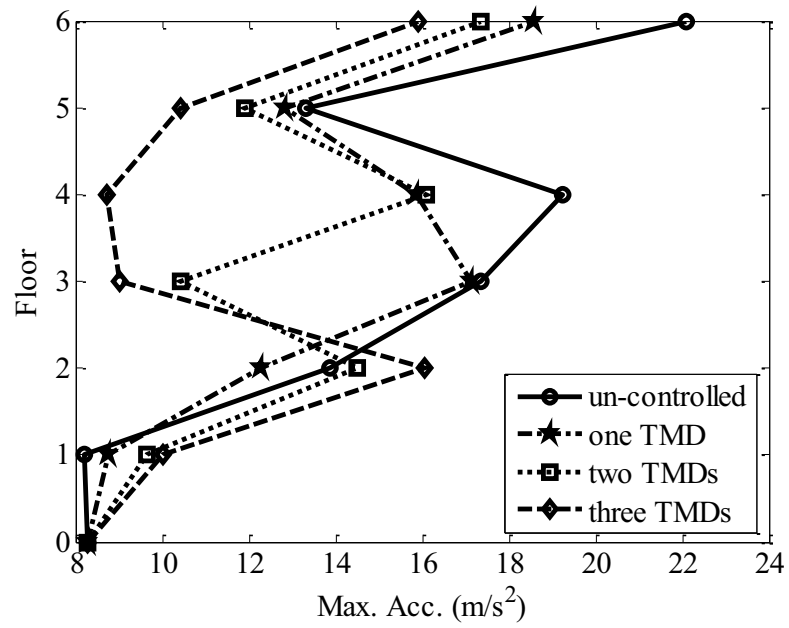
162

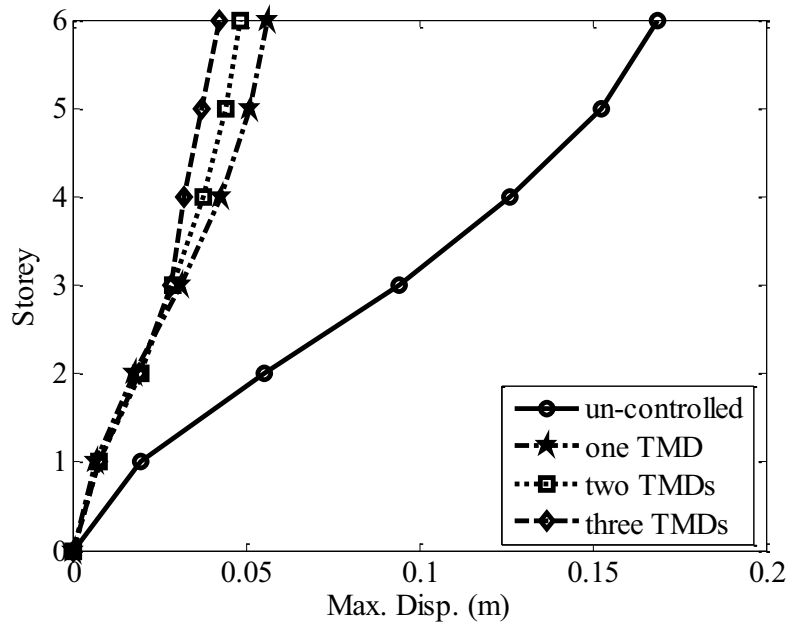(c) maximum absolute accelerations of floors
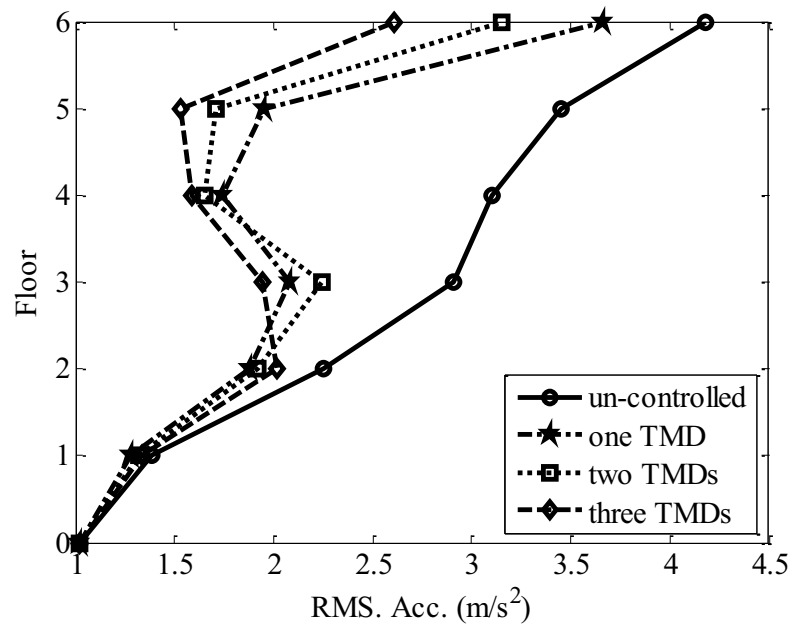
(d) root mean square values of absolute accelerations of floors
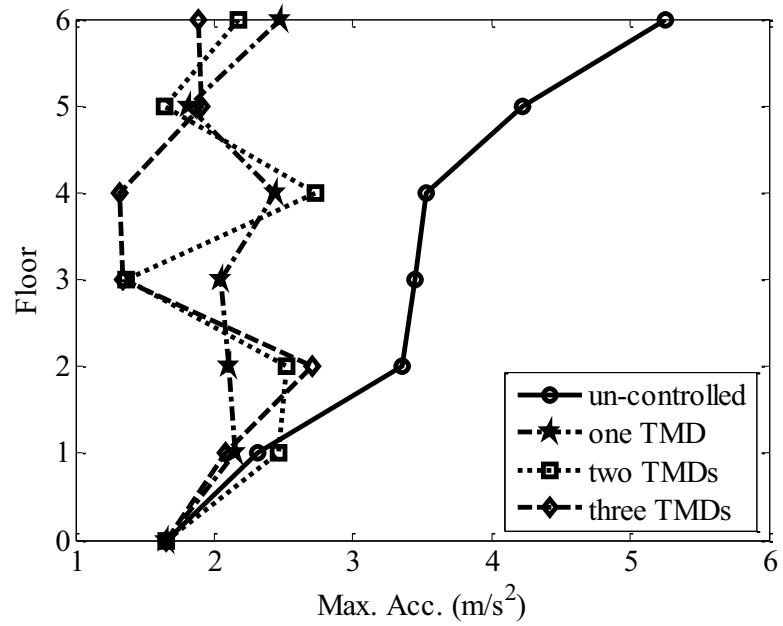
Figure 5.31 Continued
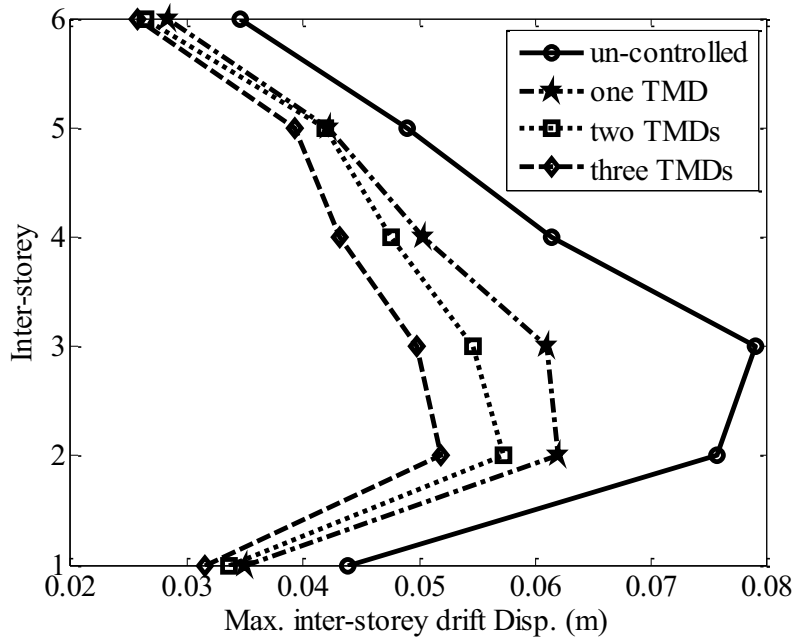
(a) maximum inter-storey drift displacements of storeys
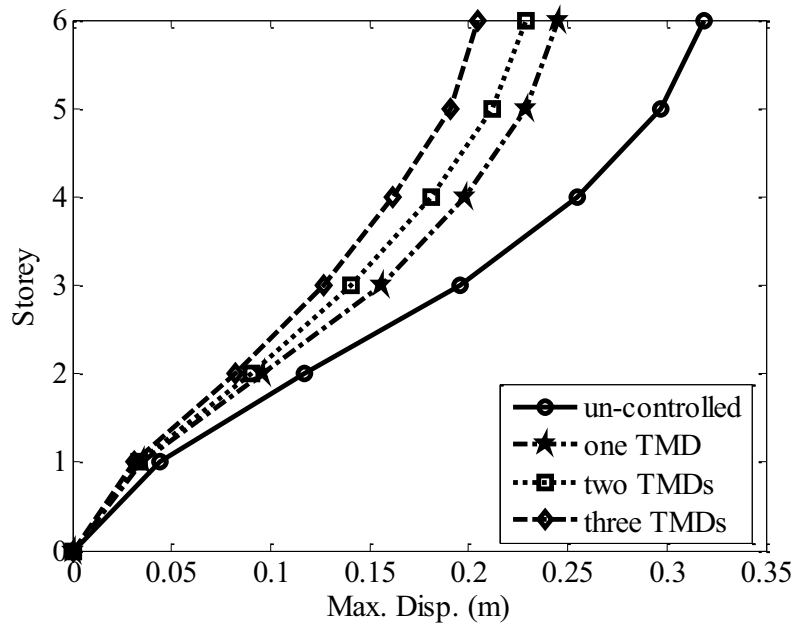
(b) maximum displacements of storeys relative to ground

Figure 5.32 Responses of different systems under LCN Landers
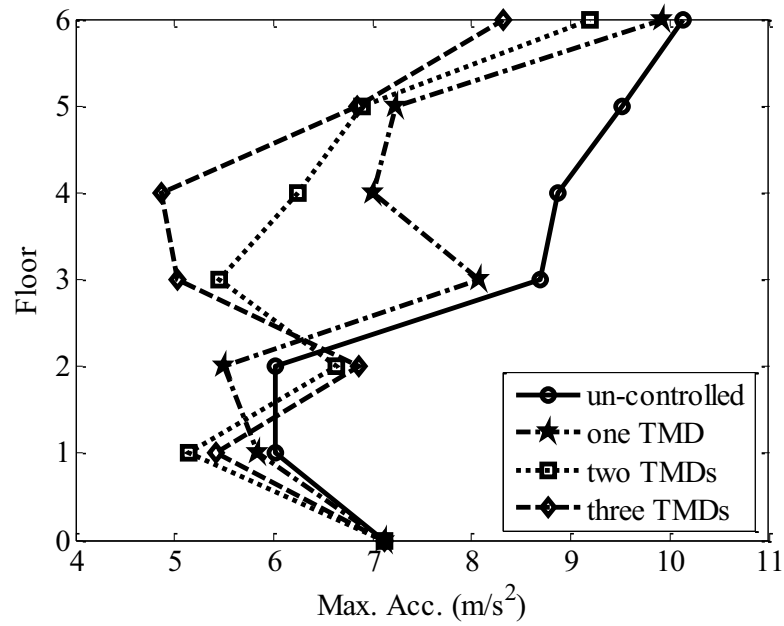
(c) maximum absolute accelerations of floors
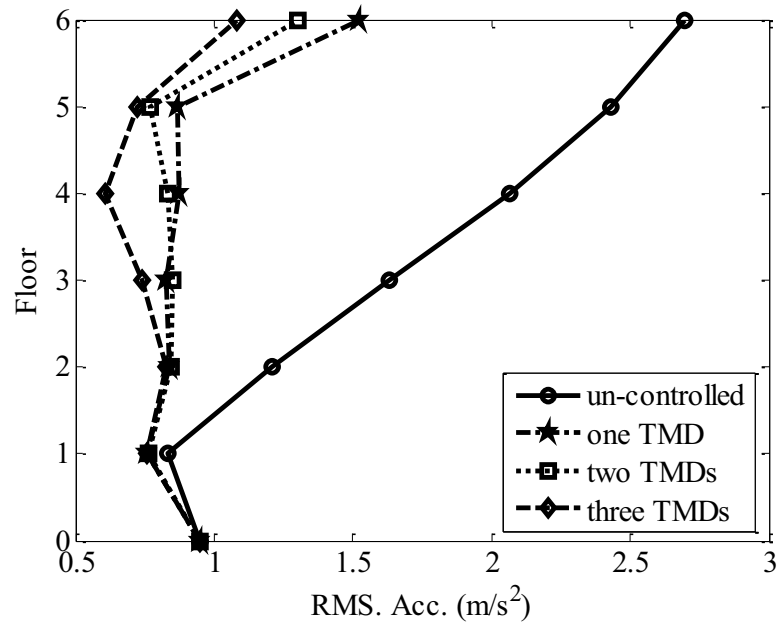
(d) root mean square values of absolute accelerations of floors

Figure 5.32 Continued
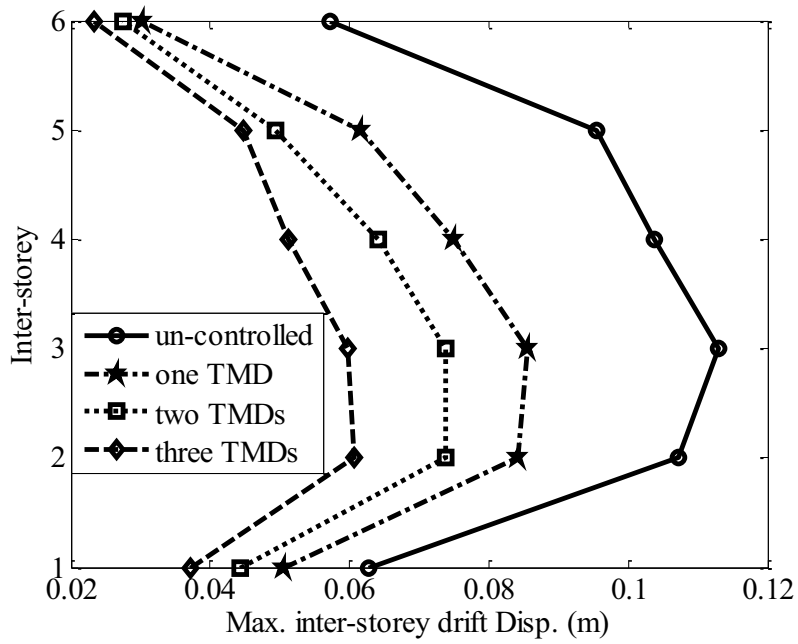
(a) maximum inter-storey drift displacements of storeys

(b) maximum displacements of storeys relative to ground

Figure 5.33 Responses of different systems under TCU068 Chi-chi

166

(c) maximum absolute accelerations of floors

(d) root mean square values of absolute accelerations of floors

Figure 5.33 Continued

(a) maximum inter-storey drift displacements of storeys

(b) maximum displacements of storeys relative to ground

Figure 5.34 Responses of different systems under TKY007 Tohoku
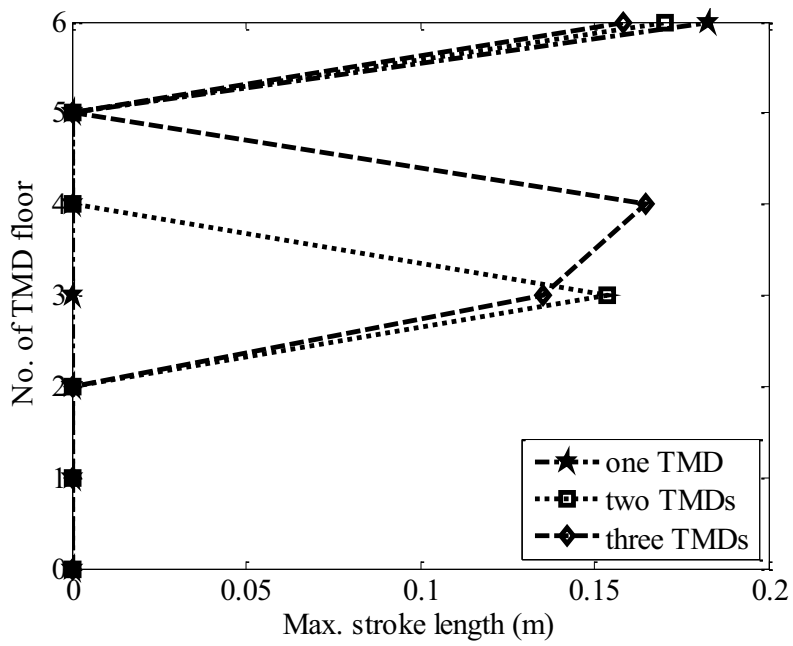
(c) maximum absolute accelerations of floors
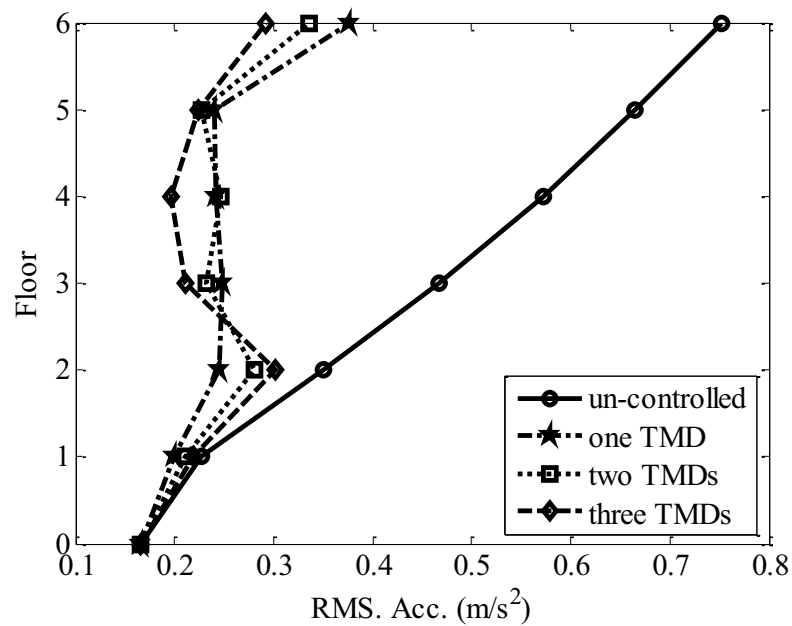
(d) root mean square values of absolute accelerations of floors

Figure 5.34 Continued

Figure 5.35 presents the maximum stroke length of TMD floors in the three TMDFSs. It can be seen from the figures that the maximum stroke length of a TMD floor can be mitigated if floors in other storeys are further utilized as TMDs.
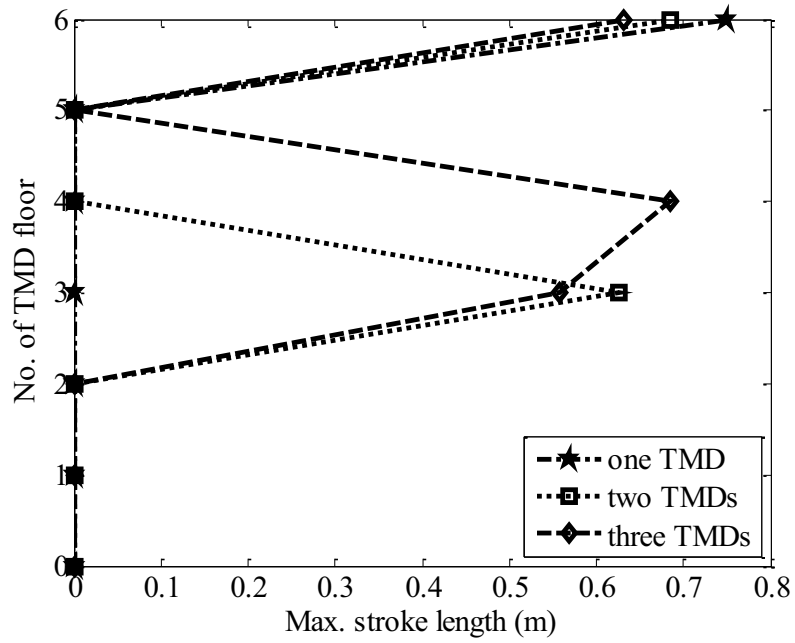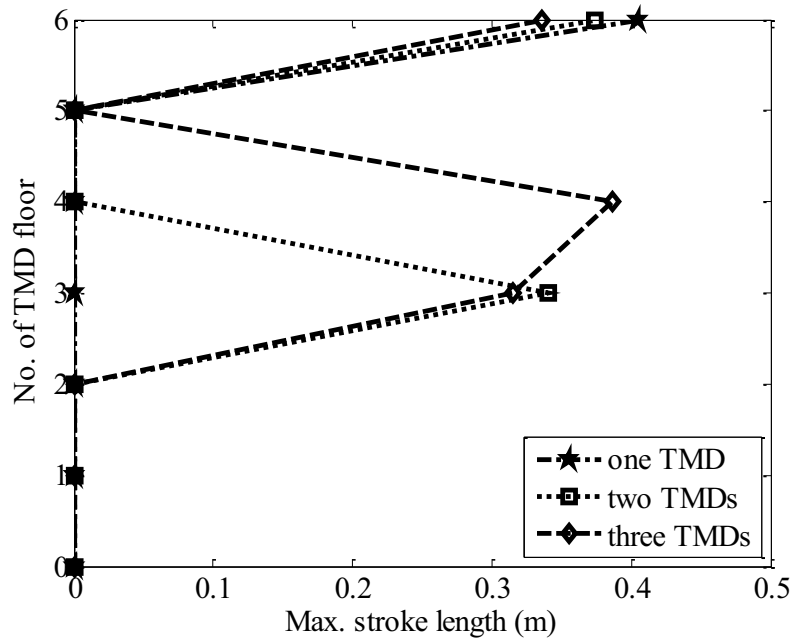
(a) El Centro
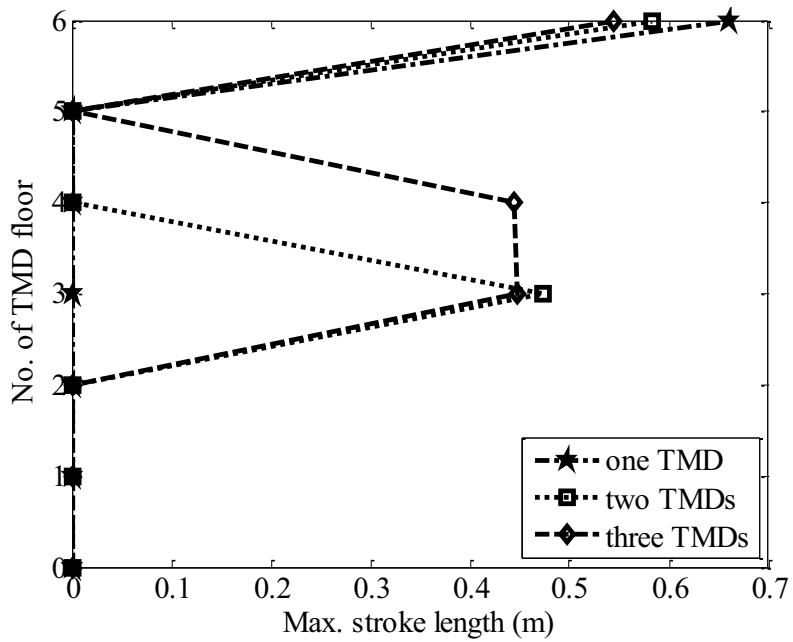
(b) JMA Kobe

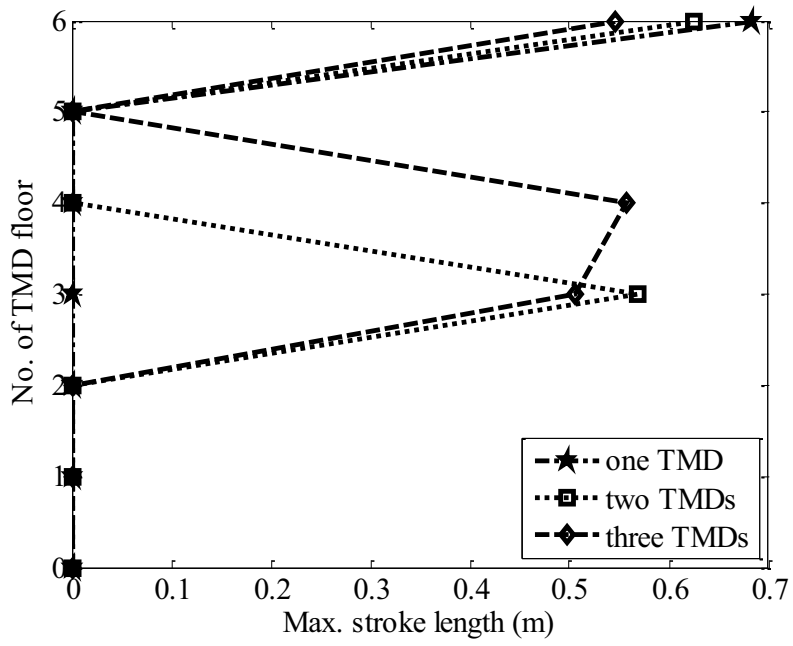Figure 5.35 Peak stroke length of TMD floors in three TMDFSs
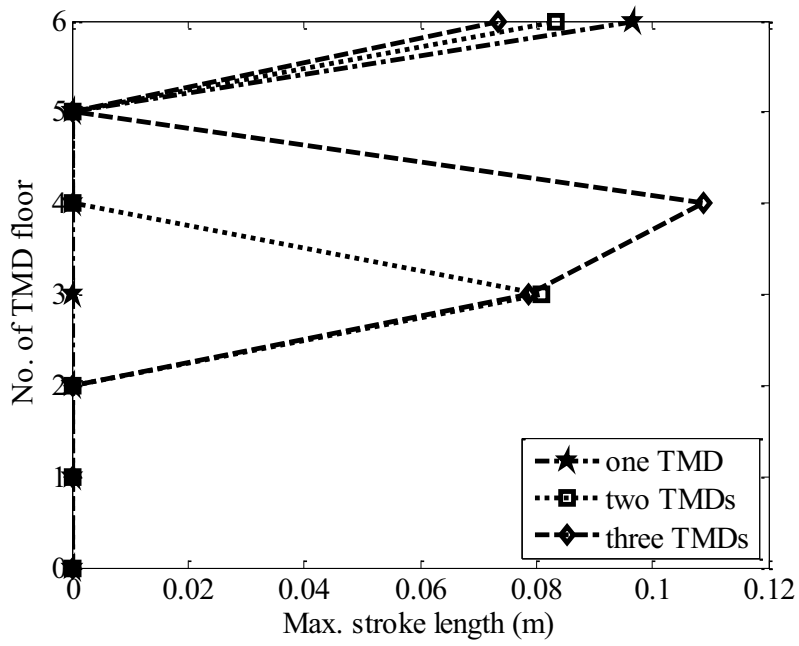
(c) Northridge

(d) LCN Landers

Figure 5.35 Continued

(e) TCU068 Chi-chi

(f) TKY007 Tohoku

Figure 5.35 Continued

(2) High-rise building

In addition to the aforementioned six-storey building, a twenty-storey building which is representative of high-rise buildings is also analyzed. The mass and stiffness parameters of the twenty-storey building are listed in Appendix D, and the damping matrix is assumed to be proportional to the stiffness matrix with the first modal damping ratio of 0.02. The peak responses of the twenty-storey building with all the floors serving as TMDs are compared with those of the uncontrolled fixed floor building and the fixed floor building equipped with the same amount of damping devices as TMDFS, as displayed in Appendix E. Figure 5.36 presents the maximum stroke length of the TMD floors in TMDFS for the six excitations, and it can be found that the global maximum stroke length achieves 0.76m which is a relatively large value.
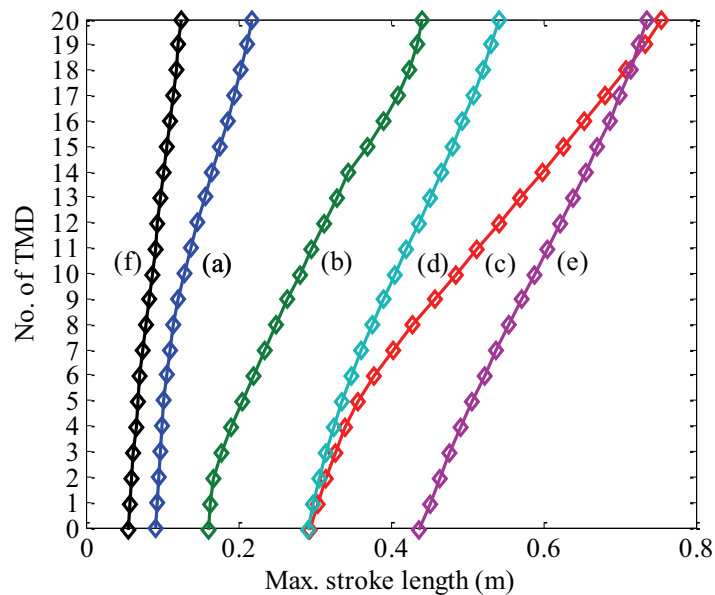
Figure 5.36 Peak stroke length of TMD floors: (a) El Centro; (b) JMA Kobe; (c) Northridge; (d) LCN Landers; (e) TCU068 Chi-chi; and (f) TKY007 Tohoku.

The aforementioned TMDFS is designed by the gradient-based optimization method via H_∞ criterion (denoted as Hinf TMDFS in the following), i.e., with the objective function set as Equation (5.12), of which the objective is virtually the same as the fixed or quasi-fixed points theory. As stroke length of TMDs designed via the stability maximization criterion (SMC) is much smaller than that of TMDs designed by the quasi-fixed points theory according to the discussion in Chapter 4, a second TMDFS is designed via the SMC (denoted as SMC TMDFS in the following), i.e., using the gradient-based optimization method with the objective function set as the maximum value of the real parts of the eigenvalues of the MDOF TMDFS, as shown in the following equation.

$$J = \text{Max.}\big(\text{Re}(\lambda_1), \text{Re}(\lambda_2), \ldots, \text{Re}(\lambda_{N+p})\big) \tag{5.13}$$

where $\lambda_i \ (i = 1, 2, \ldots, N + p)$ are the i-th eigenvalue of the TMDFS, and p equals N for the case that all the floors serve as TMDs.

A third TMDFS is designed by the approximate formula proposed by Sadek *et.al.* (1997) for MDOF primary structures, which is denoted as Sadek TMDFS in the following.

Additionally, a fourth TMDFS is designed by the gradient-based optimization method with the objective function set as the maximum value of the 2-norm values of the FRF magnitudes for the inter-storey drift displacements (denoted as H2 TMDFS in the following) as follows

$$J = \text{Max.}\left(\left\|H_{\text{Xs(drift)}_1}(j\omega)\right\|_2, \left\|H_{\text{Xs(drift)}_2}(j\omega)\right\|_2, \ldots, \left\|H_{\text{Xs(drift)}_N}(j\omega)\right\|_2\right) \tag{5.14}$$

where $\left\|\mathrm{H}_{\mathrm{Xs(drift)}_n}(j\omega)\right\|_2$ $(n=1,2,\cdots,N)$ denotes the 2-norm value of the FRF magnitude

of the n-th inter-storey drift displacement.

The optimum parameters of the four TMDFSs designed via four different criteria are

given in Table 5.8.

Table 5.8 Optimum parameters of TMD floors for twenty-storey building via different design criteria

Optimum parameters	Hinf	H2	Sadek	SMC
υ	0.69536	0.71162	$\dfrac{1}{1+\mu_1\Phi_{n1}}\left(1-\zeta_{s1}\sqrt{\dfrac{\mu_1\Phi_{n1}}{1+\mu_1\Phi_{n1}}}\right)$	0.80494
ζ_T	0.40043	0.31429	$\Phi_{n1}\left(\dfrac{\zeta_{s1}}{1+\mu_1}+\sqrt{\dfrac{\mu_1}{1+\mu_1}}\right)$	0.59356

Notes:
1. μ_1 is the mass ratio of the TMD mass to the generalized mass of the primary structure for the fundamental mode for a unit modal participation factor, and it is equal to 0.03406 for each TMD floor of the twenty-storey building in this case.
2. Φ_{n1} is the amplitude of the first mode of vibration for a unit modal participation factor computed at the location of the n-th TMD, and it equals 0.05612, 0.10914, 0.16748, 0.23065, 0.29816, 0.36881, 0.44235, 0.51847, 0.59670, 0.67644, 0.75821, 0.84176, 0.92561, 1.00963, 1.09295, 1.17359, 1.25126, 1.32434, 1.39078 and 1.44759 from bottom to top, respectively, in this case.
3. ζ_{s1} is the first mode damping ratio of the twenty-storey building which equals 0.02 in this case.

The degree of stability of the four TMDFSs is displayed in Figure 5.37, and the SMC

TMDFS achieves the maximum degree of stability, which indicates that the free vibration

of the SMC TMDFS decays the most quickly.

The free vibration response time histories of the displacement of the top storey relative to

the ground and the absolute acceleration of the top floor in the aforementioned four

TMDFSs as well as those of the un-controlled building under the six seismic excitations
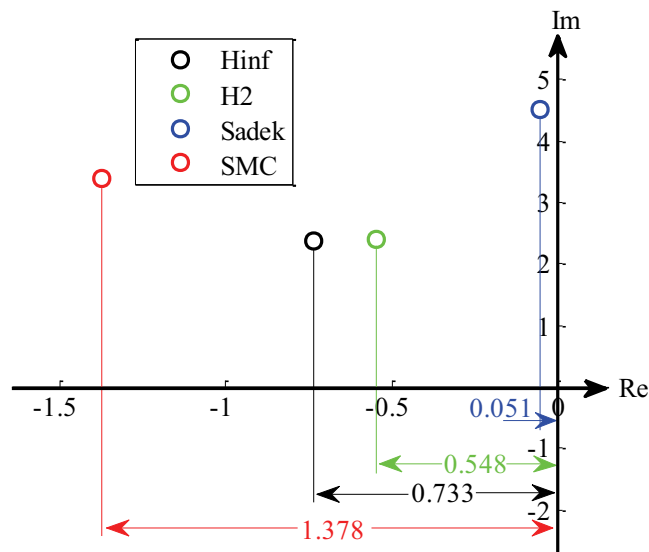
Figure 5.37 Degree of stability of four TMDFSs

are presented in Appendix F, which verifies that the free vibration responses of the SMC TMDFS decay the most quickly under all the six excitations.

The maximum stroke length of the TMD floors in the four TMDFSs is shown in Appendix G, and it can be found that the stroke length in the SMC TMDFS is generally smaller than that in other three TMDFSs. The global maximum stroke length in the SMC TMDFS is 0.57m, which is 25% smaller than the global maximum stroke length in the Hinf TMDFS.

The comparison of the peak responses of the inter-storey drift displacements and floor absolute accelerations for the four TMDFSs are presented in Appendix H. It can be found that the peak responses in the SMC TMDFS are generally larger than those in the Hinf and H2 TMDFSs. However, the SMC is also recommended as the design criterion for high-rise TMDFSs, because stroke length can be mitigated considerably and also

vibration can stop the most quickly.

5.5 Conclusions

This chapter proposes a new vibration control system with TMD floors integrated. The focus of this study is the investigation the fundamental effectiveness of the TMD floor integrated system for protecting building structures subjected to earthquake ground motions.

A test structure with single TMD floor integrated is experimentally investigated on a shaking table. System identification tests are performed to identify the parameters of the experimental main frame and the stiffness and damping of the experimental TMD system. The Stribeck friction model is verified to be suitable for simulating the friction force provided by the linear ball slide used in the TMD system. The orifice of the airpot dashpot is adjusted to the optimal position so as to provide the optimal damping coefficient based on the H_∞ optimization solution. The test structure is subjected to three representative earthquakes, and the experimental results demonstrate that the performance of the TMD floor system is satisfactory in terms of reducing the inter-storey drift displacements of the main frame as well as achieving small floor accelerations. Furthermore, the numerical simulations are in good agreement with the experimental results.

Multiple TMD floors integrated system, which takes advantages of both the benefits of

floor isolation systems and multiple tuned mass dampers, is also studied by numerical analyses. The parameter values of TMD floors are optimally determined with respect to the tuning ratio and damping ratio via the H_∞ criterion. With such optimally designed parameters, the TMD floors do not only serve as normal floors but also mitigate the responses of the main structure. Both the absolute accelerations of floors and the inter-storey drift displacements of storeys can be significantly mitigated. The performance of the TMD floor system has been demonstrated to be effective for different types of seismic excitations. A multimode approach is employed to select the optimum locations of TMD floors if not all the floors can serve as TMDs. In addition, a twenty-storey TMDFS is designed via the stability maximization criterion for achieving small stroke length of TMD floors and quick decay of building free vibration. The above fundamental study indicates that the proposed TMD floor system has a great potential of achieving very satisfactory, innovative vibration control performance for building structures.

6. CONCLUSIONS

This study has formulated frameworks for the optimal design of traditional and non-traditional tuned mass dampers (TMDs), and proposed innovative structural control schemes of applying TMDs to mitigating seismic vibration of base-isolated buildings and high-rise buildings, which are vulnerable to long period ground motions. The main conclusions are listed in the following.

(1) A gradient-based optimization method to obtain the optimal parameters of a traditional TMD attached to a highly damped primary structure is proposed.

(2) A hybrid control strategy based on the combination of a passive TMD and a semi-active variable slip-force level damper (VSFLD) is applied to a base-isolated structure. Through numerical simulations of the hybrid-controlled system under different types of ground excitations, the performance of the hybrid control strategy is verified to be superior compared with TMD based passive control and VSFLD based semi-active control, especially for protecting base-isolated structures from low-frequency resonance induced by long period ground motions.

(3) The conventional design method based on the quasi-fixed points theory cannot provide the global minimum value of the maximum FRF magnitude of a primary structure response in a non-traditional TMD system, where dashpot is connected between the tuned mass and the ground.

(4) An optimum design method of non-traditional TMDs to obtain wider suppression bandwidths in the frequency domain has been proposed. The control effect of the optimally designed non-traditional TMD integrated to a base-isolated structure is significantly improved compared with the optimally designed traditional TMD, in particular in terms of significant reduction of TMD stroke length.

(5) The design method for non-traditional TMDs via the stability maximization criterion is discussed. Non-traditional TMDs provide better performance than traditional TMDs designed by either the quasi-fixed points theory or the stability maximization criterion. The free vibration response decays the most quickly in the non-traditional TMD system designed by the stability maximization criterion.

(6) A new vibration control system with multiple TMD floors integrated is proposed, where the benefits of both floor isolation systems and multiple tuned mass dampers are retained. Both the absolute accelerations of floors and the inter-storey drifts of storeys can be significantly mitigated in this new system. Larger mass ratios of TMDs than the conventional TMD systems can be realized by utilizing floors of a building as TMDs. The performance of the TMD floor system has been demonstrated to be superior under different types of seismic excitations. The seismic performance has also been demonstrated by a shaking table experiment using a scaled model. Numerical simulation is carried out, and the results compare with the experimental results with favorable accuracy. The TMDFS designed via the stability maximization criterion can achieve smaller stroke length of TMD floors and quicker decay of free vibration than the

TMDFSs designed via H_∞ or H_2 criterion.

Publications

[1] Xiang P, Nishitani A. Hybrid structural control based on the combination of tuned mass damper and variable slip-force level damper. *Proceedings of the 15th World Conference on Earthquake Engineering*. Lisbon, Portugal, September, 2012.

[2] Xiang P, Nishitani A. Optimum design of non-traditional TMD via stability maximization criterion. *Summaries of Technical Papers of Annual Meeting AIJ*. Hokkaido, Japan, August, 2013.

[3] Xiang P, Nishitani A. Fundamental study on control effect of TMD floor system under seismic excitation. *Journal of Structural and Construction Engineering, Architectural Institute of Japan* 2013; 78(694):2093-2101.

[4] Xiang P, Nishitani A. Optimum design for more effectiveness tuned mass damper system and its application to base-isolated buildings. *Structural Control and Health Monitoring* 2014; 21(1):98-114.

[5] Xiang P, Nishitani A. Seismic vibration control of building structures with multiple TMD floors integrated. *Earthquake Engineering and Structural Dynamics*. (Article in press, published online: 10 OCT 2013, DOI: 10.1002/eqe.2379)

REFERENCES

Abe M, Fujino Y. (1994). Dynamic characterization of multiple tuned mass dampers and some design formulae. *Earthquake Engineering and Structural Dynamics*; 23(8):813-835.

Abe M, Kimura S, Fujino Y. (1996). Control laws for semi-active tuned liquid column damper with variable orifice opening. *Proceedings of the 2nd International Workshop on Structural Control*, International Association for Structural Control, Hong Kong.

Abe M. (1996). Semi-active tuned mass dampers for seismic protection of civil structures. *Earthquake Engineering and Structural Dynamics*; 25(7):743-749.

Adrian RM. (2000). Near-fault seismic site response. *[D].Berkeley: University of California*.

Aldemir U. (2003). Optimal control of structures with semiactive-tuned mass dampers. *Journal of Sound and Vibration*; 266(4):847-874.

Ali MM, Moon KS. (2007). Structural developments in tall buildings: current trends and future prospects. *Architectural Science Review*; 50(3):205-223.

Anh ND, Nguyen NX. (2012). Extension of equivalent linearization method to design of TMD for linear damped systems. *Structural Control and Health Monitoring*; 19(6):565-573.

Anh ND, Nguyen NX. (2013). Design of non-traditional dynamic vibration absorber for damped linear structures. *Proceedings of the Institution of Mechanical Engineers, Part C: Journal of Mechanical Engineering Science*.

Ankireddi S, Yang TY. (1996). Simple ATMD control methodology for tall buildings subject to wind loads. *Journal of Structural Engineering*; 122(1):83-91.

Asami T, Hosokawa Y. (1995). Approximate expression for design of optimal dynamic

absorbers attached to damped linear systems. *Journal of the Japan Society of Mechanical Engineers*; 61(583):915-921. (in Japanese)

Asami T, Nishihara O, Baz AM. (2002). Analytical solutions to H_∞ and H_2 optimization of dynamic vibration absorbers attached to damped linear systems. *Journal of Vibration and Acoustics*; 124(2):284-295.

Asami T, Nishihara O. (2003). Closed-form exact solution to H_∞ optimization of dynamic vibration absorbers (application to different transfer functions and damping systems). *Journal of Vibration and Acoustics*; 125(3):398-405.

Bakre SV, Jangid RS. (2007). Optimum parameters of tuned mass damper for damped main system. *Structural Control and Health Monitoring*; 14:448-470.

Banerji P, Murudi M, Shah AH, Popplewell N. (2000). Tuned liquid dampers for controlling earthquake response of structures. *Earthquake Engineering and Structural Dynamics*; 29(5):587-602.

Bekdas G, Nigdeli SM. (2011). Estimating optimum parameters of tuned mass dampers using harmony search. *Engineering Structures*; 33(9):2716-2723.

Bekdas G, Nigdeli SM. (2013). Mass ratio factor for optimum tuned mass damper strategies. *International Journal of Mechanical Sciences*; 71:68-84.

Brock JE. (1946). A note on the damped vibration absorber. *Transactions of the American Society of Mechanical Engineers*; 68(4):A284.

Brozer A, Altay G. (2013). Hybrid tracking controller with attached tuned mass damper. *Structural Control and Health Monitoring*; 20(3):337-353.

Chang J, Soong TT. (1980). Structural control using active tuned mass dampers. *Journal of Engineering Mechanical Division, ASCE*; 106:1081-1088.

Chang ML, Lin CC, Ueng JM, Hsieh KH, Wang JF. (2010). Experimental study on adjustable tuned mass damper to reduce floor vibration due to machinery. *Structural Control and Health Monitoring*; 17(5):532-548.

Chen G, Wu J. (2003). Experimental study on multiple tuned mass dampers to reduce seismic responses of a three-storey building structure. *Earthquake Engineering and Structural Dynamics*; 32(5):793-810.

Chen GD, Wu JN. (2001). Optimal placement of multiple tune mass dampers for seismic structures. *Journal of Structural Engineering, ASCE*; 127(9):1054-1062.

Chen WZ, Wang BW, Hu XY. (2010). Acceleration signal processing by a numerical integration. *Journal of Huazhong University of Science and Technology (Natural Science Edition)*; 38(1):1-4. (in Chinese)

Cheung YL, Wong WO. (2009). Design of a non-traditional dynamic vibration absorber. *Journal of the Acoustical Society of America*; 126(2):564-567.

Cheung YL, Wong WO. (2011). H_2 optimization of a non-traditional dynamic vibration absorber for vibration control of structures under random force excitation. *Journal of Sound and Vibration*; 330(6):1039-1044.

Cheung YL, Wong WO. (2011). H-infinity optimization of a variant design of the dynamic vibration absorber-Revisited and new results. *Journal of Sound and Vibration*; 330(16): 3901-3912.

Cheung YL, Wong WO, Cheng L. (2012). Minimization of the mean square velocity response of dynamic structures using an active-passive dynamic vibration absorber. *Journal of Acoustical Society of America*; 132(1):197-207.

Chey MH, Chase JG, Mander JB, Carr AJ. (2010). Semi-active tuned mass damper

building systems: application. *Earthquake Engineering and Structural Dynamics*; 39(1):69-89.

Chiba M, Hori N, Takahashi K. (2003, 7). Study on fireproof cover sysem of rubber bearing for base isolation: Part 5 Durability estimation of polyisobutylene-based resin for fireproof cover system. *Summaries of technical papers of Annual Meeting Architectural Institute of Japan*, A-2, Fire safety, off-shore engineering and architecture, information systems technology, 195-196. (in Japanese)

Crandall SH, Mark WD. (1963). *Random Vibrations in Mechanical Systems*. Academic Press, New York.

Cui SL, Bruneau M, Kasalanati A. (2010). Behavior of bidirectional spring unit in isolated floor systems. *Journal of Structural Engineering, ASCE*; 136(8):944-952.

Daniel Y, Lavan O, Levy R. (2012). Multiple-tuned mass dampers for multimodal control of pedestrian bridges. *Journal of Structural Engineering, ASCE*; 138(9):1173-1178.

Davidon WC. (1959). Variable metric method for minimization. A.E.C. Research and Development Rept; ANL-5990.

De Angelis M, Perno S, Reggio A. (2012). Dynamic response and optimal design of structures with large mass ratio TMD. *Earthquake Engineering and Structural Dynamics*; 41(1):41-60.

Den Hargot JP. (1956). *Mechanical Vibrations*. 4th edition, McGraw-Hill, New York.

Desu NB, Deb SK, Dutta A. (2006). Coupled tuned mass dampers for control of coupled vibrations in asymmetric buildings. *Structural Control and Health Monitoring*; 13(5):897-916.

Fan YC, Loh CH, Yang JN, Lin PY. (2009). Experimental performance evaluation of an

equipment isolation using MR dampers. *Earthquake Engineering and Structural Dynamics*; 38(3):285-305.

Feng MQ, Mita A. (1995). Vibration control of tall buildings using mega subconfiguration. *Journal of Engineering Mechanics, ASCE*; 121(10): 1082-1088.

Fletcher R, Powell MJD. A rapidly convergent descent method for minimization. *The Computer Journal* 1963; 6:163-168.

Frahm H. (1911). Device for damping vibrations of bodies. U.S. Patent No. 989958:3576-3580.

Fu TS, Johnson EA. (2011). Distributed mass damper system for integrating structural and environmental controls in buildings. *Journal of Engineering Mechanics, ASCE*; 137(3): 205-213.

Fujimoto S. (2005). Studies on development of seismic isolation floors for industrial facilities. *Memoirs of Shonan Institute of Technology*; 39(1):37-48. (in Japanese)

Fujino Y, Sun LM, Pacheco BM, Chaiseri P. (1992). Tuned liquid damper (TLD) for suppressing horizontal motion of structures. *Journal of Engineering Mechanics*, *ASCE*; 118(10):2017-2030.

Gao H, Kwok KCS, Samali B. (1997). Optimization of tuned liquid column dampers. *Engineering Structures*; 19(6):476-486.

Gavin HP, Zaicenco A. (2007). Performance and reliability of semi-active equipment isolation. *Journal of Sound and Vibration*; 306(1-2):74-90.

Geem ZW, Kim JH, Loganathan GV. (2001). A new heuristic optimization algorithm: Harmony search. *Simulation*;76(2):60-68.

Ghosh A, Basu B. (2007). A closed-form optimal tuning criterion for TMD in damped

structures. *Structural Control and Health Monitoring*; 14(4):681-692.

Hadi MN, Arfiadi Y. (1998). Optimum design of absorber for MDOF structures. *Journal of Structural Engineering*; 124(11):1272-1280.

Hahnkamm E. (1932). Die Dämpfung von Fundamentschwingungen bei veränderlicher Erregerfrequenz. *Ingenieur-Archiv*; 4:192-201. (in German)

Heaton TH, Hall JF, Wald DJ, Halling MW. (1995). Response of high-rise and base-isolated buildings to a hypothetical M_w 7.0 blind thrust earthquake. *Science*; 267, 206-211.

Hisada Y. (2004). Strong ground motion in near source area and earthquake damage. *Proceedings of Architectural Institute of Japan*, Hokkaido, Japan. (in Japanese)

Hoang N, Warnitchai P. (2005). Design of multiple tuned mass dampers by using a numerical optimizer. *Earthquake Engineering and Structural Dynamics*; 34(9):125-144.

Hoang N, Fujino Y, Warnitchai P. (2008). Optimal tuned mass damper for seismic applications and practical design formulas. *Engineering Structures*; 30(3):707-715.

Holland JH. (1975). *Adaptation in Natural and Artificial Systems*. University of Michigan Press, Ann Arbor MI.

Hrovat D, Barak P, Rabins M. (1983). Semi-active versus passive or active tuned mass dampers for structural control. *Journal of Engineering Mechanics Division*, *ASCE*; 109:691-705.

Humar JL. (2002). *Dynamics of Structures, 2nd edition*. A.A. Balkema.

Iemura H, Taghikhany T. (2004). Optimum design of resilient sliding isolation system to protect equipments. *13th World Conference on Earthquake Engineering*, Vancouver BC,

Canada; Paper No. 1362.

Igusa T, Xu K. (1994). Vibration control using multiple tuned mass dampers. *Sound and Vibration*; 175(4):491-503.

Inoue T, Sato E, Sakai H, Fukuyama K, Nakashima M, Furukawa S, Kobayashi K, Kakehi A. (2010). Outline of shaking table test for improvement of seismic performance in medical facility. *Proceedings of Architectural Institute of Japan*, No.21039:77-78. (in Japanese)

Itou A, Fujitani H, Kido S, Nagae T. (2009). Semiactive control of isolated floor in the building excited by long period earthquake ground motion. *Research report of Architectural Institute of Japan Kinki Branch-2016*. (in Japanese)

Iwan WD. (1978). The earthquake design and analysis of equipment isolation systems. *Earthquake Engineering and Structural Dynamics*; 6(6):523-534.

Jagadish KS, Prasad BKR, Rao PV. (1979). The inelastic vibration absorber subjected to earthquake ground motions. *Earthquake Engineering and Structural Dynamics*; 7(4):317-326.

Joshi AS, Jangid RS. (1996). Optimum parameters of multiple tuned mass dampers for base-excited damped systems. *Journal of Sound and Vibration*; 202(5):657-667.

Kareem A, Kline S. (1995). Performance of multiple mass dampers under random loading. *Journal of Structural Engineering*, *ASCE*; 121(2):348-361.

Kaynia AM, Biggs JM, Veneziano D. (1981). Seismic effectiveness of tuned mass dampers. *Journal of the Structural Division*, *ASCE*; 107(8):1465-1484.

Kelly JM. (1999). The role of damping in seismic isolation. *Earthquake Engineering and Structural Dynamics*; 28(1):3-20.

Kwok KCS, MacDonald PA. (1990). Full-scale measurement of acceleration response of Sydney Tower. *Engineering Structures*; 12(3):153-162.

Kwon SD, Park KS. (2004). Suppression of bridge flutter using tuned mass dampers based on robust performance design. *Journal of Wind Engineering and Industrial Aerodynamics*; 92(11):919-934.

Lambrou V, Constantinou MC. (1994). Study of seismic isolation systems for computer floors. *Technical Report NCEER-94-0020*, National Center for Earthquake Engineering Research, State University of New York, Buffalo, NY.

Lee CL, Chen YT, Chung LL, Wang YP. (2006). Optimal design theories and applications of tuned mass dampers. *Engineering Structures*; 28(1):43-53.

Lee CS, Goda K, Hong HP. (2012). Effectiveness of using tuned-mass dampers in reducing seismic risk. *Structure and Infrastructure Engineering: Maintenance, Management, Life-Cycle Design and Performance*; 8(2):141-156.

Leung AYT, Zhang H, Cheng CC, Lee YY. (2008). Particle swarm optimization of TMD by non-stationary base excitation during earthquake. *Earthquake Engineering and Structural Dynamics*; 37(9):1223-1246.

Leung AYT, Zhang HJ. (2009). Particle swarm optimization of tuned mass dampers. *Engineering Structures*; 31(3):715-728.

Li CX. (2000). Performance of multiple tuned mass dampers for attenuating undesirable oscillations of structures under the ground acceleration. *Earthquake Engineering and Structural Dynamics*; 29(9):1405-1421.

Li Q, Fan JS, Nie JG, Li QW, Chen Y. (2010). Crowd-induced random vibration of footbridge and vibration control using multiple tuned mass dampers. *Journal of Sound*

and Vibration; 329(19):4068-4092.

Li S, Xie LL. (2007). Progress and trend on near-field problems in civil engineering. *Acta Seismologica Sinica*; 20(1):105-114.

Liu KF, Liu J. (2005). The damped dynamic vibration absorbers: revisited and new result. *Journal of Sound and Vibration*; 284(3-5):1181-1189.

Liu KF, Coppola G. (2010). Optimal design of damped dynamic vibration absorber for damped primary systems. *Transaction of the Canadian Society for Mechanical Engineering*; 34(1):119-135.

Loh CH, Chao CH. (1996). Effectiveness of active tuned mass damper and seismic isolation on vibration control of multi-storey building. *Journal of Sound and Vibration*; 193(4):773-792.

Lu LY, Lin GL, Lin CC. (2011). Absolute-energy-based active control strategies for linear seismic isolation systems. *Structural Control and Health Monitoring*; 18(3):321-340.

Luft RW. (1979). Optimum tuned mass dampers for buildings. *Journal of the Structural Division*, *ASCE*; 105(12):2766-2772.

Makris N. (1997). Rigidity-plasticity-viscosity: can electrorheological dampers protect base-isolated structures from near-source ground motions. *Earthquake Engineering and Structural Dynamics*; 26(5):571-591.

Mathews JH. (1992). *Numerical Methods for Mathematics, Science, and Engineering*. 2nd edition, Prentice Hall, London.

Matta E, De Stefano A. (2009). Seismic performance of pendulum and translational roof-garden TMDs. *Mechanical Systems and Signal Processing*; 23(3):908-921.

McNamara RJ. (1977). Tuned mass dampers for buildings. *Journal of the Structural*

Division, *ASCE*; 103(9): 1785-1798.

Minagawa K, Fujita S, Omi T, Shinno K, Yamagata K, Miyano H. (2011). Research and development of tuned mass damper using impact force for environment vibration and earthquakes, *Journal of the Japan Society of Mechanical Engineers*; 77(780):2982-2992. (in Japanese)

Mitchell R, Kim Y, El-Korchi T, Cha YJ. (2012). Wavelet-neuro-fuzzy control of hybrid building-active tuned mass damper system under seismic excitations. *Journal of Vibration and Control*; 19(12):1881-1894.

Morison J, Karnopp D. (1973). Comparison of optimized active and passive vibration absorber. *Proceedings of the 14th Annual Joint Automatic Control Conference*; Columbus, OH:932-938.

Murakami K, Kitamura H, Ozaki H, Teramoto T. (2000). Design and analysis of a building with the middle-story isolation structural system. *Twelfth World Conference of Earthquake Engineering*, Auckland, New Zealand; Paper No. 0857.

Nagarajaiah S. (2009). Adaptive passive, semiactive, smart tuned mass dampers: identification and control using empirical mode decomposition, Hilbert transform, and short-term fourier transform. *Structural Control and Health Monitoring*; 16(7-8):800-841.

Natsiavas S. (1992). Steady state oscillations and stability of non-linear dynamic vibration absorbers. *Journal of Sound and Vibration*; 156(2):227-245.

Nishihara O, Matsuhisa H. (1997). Design and tuning of vibration control devices via stability criterion, *Preprint of Japan Society of Mechanical Engineers*; 97-10-1:165-168. (in Japanese)

Nishimura H, Yoshida K, Shimogo T. (1989). Optimal dynamic vibration absorber for multi-drgree-of-freedom systems (Theoretical consideration in the case of random input). *JSME International Journal*, Ⅲ; 32(3):373-379.

Nishitani A [Author], Matsui G [Supervisor]. (2001). *Reinforced Concrete Building Structures Fundamentals, revised edition*. Kajima Publishing Company. (in Japanese)

Nishitani A, Nitta Y, Itoh A, Ikeda Y. (2000). Semiactive variable-friction damper control with simple algorithms. *Proceedings of the 2000 American Control Conference*; 1: 503-507.

Nishitani A, Inoue Y. (2001). Overview of the application of active/semiactive control to building structures in Japan. Earthquake Engineering and Structural Dynamics; 30(11):1565-1574.

Nishitani A, Nitta Y, Ikeda Y. (2003). Semiactive structural-control based on variable slip-force level damper. *Journal of Structural Engineering*; 129(7):933-940.

Nishitani A, Nitta Y, Wakahara C. (2009). Artificial nonlinearity in structural control: Its original concept survey and significance in semiactive control scheme. *Structural Control and Health Monitoring*; 16:17-31.

Nissen JC, Popp K, Schmalhorst B. (1985). Optimization of a non-linear dynamic vibration absorber. *Journal of Sound and Vibration*; 99(1):149-154.

Okhovat MR, Rahimian M, Ghorbani-Tanha AK. (2006). Tuned mass damper for seismic response reduction of Tehran Tower. *4th International Conference on Earthquake Engineering*, Taipei, Taiwan; Paper No. 132.

Olsson H, Astrom KJ, de Wit CC, Gafvert M, Lischinsky P. (1998). Friction models and friction compensation. *European Journal of Control*; 4(3):176-195.

Ormondroyd J, Den Hargot JP. (1928). The theory of the dynamic vibration absorber. *Transactions of the American Society of Mechanical Engineers*; 50(7):9-22.

Palazzo B, Petti L, De Ligio M. (1997). Response of base isolated systems equipped with tuned mass dampers to random excitations. *Journal of Structural Control*; 4(1):9-22.

Pan P, Zamfirescu D, Nakashima M, Nakayasu N, Kashiwa H. (2005). Base-isolation design practice in Japan: Introduction to the post-Kobe approach. *Journal of Earthquake Engineering*; 9(1):147-171.

Park J, Reed D. (2001). Analysis of uniformly and linearly distributed mass dampers under harmonic and earthquake excitation. *Engineering Structures*; 23(7):802-814.

Petit F, Loccufier M, Aeyels D. (2009). On the attachment location of dynamic vibration absorbers. *Journal of Vibration and Acoustics, ASME*; 131(3):034501-1 - 034501-8.

Petti L, Giovanni G, De Luliis M, Palazzo B. (2010). Small scale experimental testing to verify the effectiveness of the base isolation and tuned mass dampers combined control strategy. *Smart Structures and Systems*; 6(1):57-72.

Pinkaew T, Lukkunaprasit P, Chatupote P. (2003). Seismic effectiveness of tuned mass dampers for damage reduction of structures. *Engineering Structures*; 25(1):39-46.

Pourzeynali S, Lavasani HH, Modarayi AH. (2007). Active control of high rise building structures using fuzzy logic and genetic algorithms. *Engineering Structures*; 29(3):346-357.

Preumont A. (2011). *Vibration Control of Active Structures: An Introduction, 3rd edition*. Springer.

Rana R, Soong TT. (1998). Parametric study and simplified design of tuned mass dampers. *Engineering Structures*; 20(3):193-204.

Ren MZ. (2001). A variant design of the dynamic vibration absorber. *Journal of Sound and Vibration*; 245(4):762-770.

Ribakov Y. (2010). Reduction of structural response to near fault earthquakes by seismic isolation columns and variable friction dampers. *Earthquake Engineering and Engineering Vibration*; **9**(1):113-122.

Roffel AJ, Lourenco R, Narasimhan S, Yarusevych S. (2011). Adaptive compensation for detuning in pendulum tuned mass dampers. *Journal of Structural Engineering*, *ASCE*; 137(2):242-251.

Rüdinger F. (2006). Optimal vibration absorber with nonlinear viscous power law damping and white noise excitation. *Journal of Engineering Mechanics*, *ASCE*; 132(1):46-53.

Sadek F, Mohraz B, Lew HS. (1998). Single- and multiple- tuned liquid column dampers for seismic applications. *Earthquake Engineering and Structural Dynamics*; 27(5):439-463.

Sadek F, Mohraz B, Taylor AW, Chung RM. (1997). A method of estimating the parameters of tuned mass dampers for seismic applications. *Earthquake Engineering and Structural Dynamics*; 26(6):617-635.

Sakai F, Takaeda S. (1989). Tuned liquid column damper- New type device for suppression of building vibrations. *Proceedings International Conference on High Rise Buildings*, Nanjing, China.

Setareh M, Hanson R. (1992). Tuned mass dampers to control floor vibration from humans. *Journal of Structural Engineering*, *ASCE*; 118(3):741-762.

Shi YD, Sato E, Hoki K, Kurata M, Nakashima M. (2012). Development of semi-active

controlled floor isolation system for equipment protection. *Proceedings of Architectural Institute of Japan*, No.21268:535-536.

Singh MP, Singh S, Moreschi LM. (2002). Tuned mass dampers for response control of torsional buildings. *Earthquake Engineering and Structural Dynamics*; 31(4):749-769.

Sladek JR, Klingner RE. (1983). Effect of tuned-mass dampers on seismic response. *Journal of the Structural Division*, *ASCE*; 109(8):2004-2009.

Soong TT, Dargush GF. (1997). *Passive Energy Dissipation Systems in Structural Engineering*. Wiley, Chichester, United Kingdom.

Strasberg M, Feit D. (1996). Vibration damping of large structures induced by attached small resonant structures. *Journal of Acoustical Society of America*; 99(1):335-344.

Sueoka T, Torii S, Tsuneki Y. (2004). The application of response control design using middle-story isolation system to high-rise building. *Thirteenth World Conference on Earthquake Engineering*, Vancouver, Canada; Paper No. 3457.

Sun LM, Fujino Y, Pacheco BM, Isobe M. (1989). Nonlinear waves and dynamic pressure in rectangular TLD- Simulation and experimental verification. *Japan Society of Civil Engineers, Journal of Structural Engineering/Earthquake Engineering*; 6(2):251-262.

Tajimi H. (1965). *Introduction to Structural Dynamics (Kenchiku shindogaku)*. Corona, Tokyo, Japan. (in Japanese)

Takewaki I, Murakami S, Fujita K, Yoshitomi S, Tsuji M. (2011). The 2011 off the Pacific coast of Tohoku earthquake and response of high-rise buildings under long-period ground motions. *Soil Dynamics and Earthquake Engineering*; 31(11):1511-1528.

Tamura Y, Kousaka R, Modu V. (1992). Practical application of nutation damper for suppressing wind-induced vibrations of airport towers. *Journal of Wind Engineering and Industrial Aerodynamics*; 43:1919-1930.

Taniguchi T, Kiureghian AD, Melkumyan M. (2008). Effect of tuned mass damper on displacement demand of base-isolated structures. *Engineeing Structures*; 30:3478-3488.

Tian ZC, Qian JR, Zhang LM. (2008). Slide roof system for dynamic response reduction. *Earthquake Engineering and Structural Dynamics*; 37(4):647-658.

Tigli OF. (2012). Optimum vibration absorber (tuned mass damper) design for linear damped systems subjected to random loads. *Journal of Sound and Vibration*; 331(13):3035-3049.

Tsai HC, Lin GC. (1993). Optimum tuned-mass dampers for minimizing steady-state response of support-excited and damped structures. *Earthquake Engineering and Structural Dynamics*; 22:957-973.

Tsai HC. (1995). The effect of tuned-mass dampers on the seismic response of base-isolated structures. *International Journal of Solids and Structures*; 32(8/9):1195-1210.

Udwadia FE, Tabaie S. (1981). Pulse control of single degree of freedom system. *Journal of Engineering Mechanical Division*, *ASCE*; 107:997-1009.

Vakakis AF, Manevitch LI, Gendelman O, Bergman, LA. (2003). Dynamics of linear discrete systems connected to local, essentially non-linear attachments. *Journal of Sound and Vibration*; 264(1):559-577.

Villaverde R. (1985). Reduction in seismic response with heavily-damped vibration

absorbers. *Earthquake Engineering and Structural Dynamics*; 13(1):33-42.

Villaverde R, Koyama LA. (1993). Damped resonant appendages to increase inherent damping in buildings. *Earthquake Engineering and Structural Dynamics*; 22(6):491-507.

Villaverde R, Martin SC. (1995). Passive seismic control of cable-stayed bridges with damped resonant appendages. *Earthquake Engineering and Structural Dynamics*; 24(2):233-246.

Wakahara T, Ohyama T, Fujii K. (1992). Suppression of wind-induced vibration of a tall building using tuned liquid damper. *Journal of Wind Engineering and Industrial Aerodynamics*; 43(1-3):1895-1906.

Warburton GB. (1982). Optimum absorber parameters for various combinations of response and excitation parameters. *Earthquake Engineering and Structural Dynamics*; 10(3):381-401.

Wirsching PH, Campbell GW. (1973). Minimal structural response under random excitation using the vibration absorber. *Earthquake Engineering and Structural Dynamics*; 2(4):303-312.

Wong WO, Cheung YL. (2008). Optimal design of a damped dynamic vibration absorber for vibration control of structure excited by ground motion. *Engineering Structures*; 30(1):282-286.

Wongprasert N, Symans MD. (2005). Experimental evaluation of adaptive elastomeric base-isolated structures using variable-orifice fluid dampers. *Journal of Structural Engineering*; 131(6):867-877.

Xu K, Igusa T. (1992). Dynamic characteristics of multiple substructures with closely

spaced frequencies. *Earthquake Engineering and Structural Dynamics*; 21(12):1059-1070.

Xu YL, Samali B, Kwok KCS. (1992). Control of along-wind response of structures by mass and liquid dampers. *Journal of Engineering Mechanics*, *ASCE*; 118(1):20-39.

Yalla SK, Kareem A. (2000). Optimum absorber parameters for tuned liquid column dampers. *Journal of Structural Engineering*, *ASCE*; 126(8):906-915.

Yamaguchi H. (1988). Damping of transient vibration by a dynamic absorber. *Transactions of the Japan Society of Mechanical Engineers*; 59(499):561-568. (in Japanese)

Yamaguchi H, Harnpornchai N. (1993). Fundamental characteristics of multiple tuned mass dampers for suppressing harmonically forced oscillations. *Earthquake Engineering and Structural Dynamics*; 22(1):51-62.

Yang JN, Danielians A, Liu SC. (1991). Aseismic hybrid control systems for building structures. *Journal of Engineering Mechanics*, *ASCE*; 117(4):836-853.

Ziyaeifar M, Noguchi H. (1998). Partial mass isolation in tall buildings. *Earthquake Engineering and Structural Dynamics*; 27(1):49–65.

Zuo L, Nayfeh SA. (2004). Minimax optimization of multi-degree-of-freedom tuned-mass dampers. *Journal of Sound and Vibration*; 272(3-5):893-908.

Zuo L, Nayfeh SA. (2005). Optimization of the individual stiffness and damping parameters in multiple-tuned-mass-damper systems. *Journal of Vibration and Acoustics*; 127(1):77-83.

Appendix A. STMD_design_fmincon.m

```
clc
clear
close all

mu=0.1;
NUM=10;
for n=1:NUM
    n
    x0 = [rand(1)/sqrt(mu); rand(1)];
    options = optimset('largescale', 'off');
    [x, optimindex, exitflag, output] = fmincon('STMD_design_objfun', x0, [-1 0; 0 -1; 1 0; 0 1],
    [-0.01; -0.01; 1/sqrt(mu); 1], [], [], [], [], 'mycon',options)

    optimresult(n) = optimindex;
    parameter(n,:) = x;
    result(i) = optimindex;
end

[optiresult, num] = min(result);
Optiparameter = parameter(num,:);
```

Appendix B. Flowchart for FRF magnitude calculation procedure

```
┌─────────────────────────────────────────────────────────────┐
│ Define sampling frequency (Sfreq=1/sampling time)             │
│ Define FFT size (Num=1.5 times of excitation length)          │
│ Import excitation and response time history data              │
└─────────────────────────────────────────────────────────────┘
                              │
                              ▼
              ┌──────────────────────────────────┐
              │ Calculate  Δf=Sfreq/Num           │
              │ Nyquist=Sfreq/2                    │
              └──────────────────────────────────┘
                              │
                              ▼
           ┌────────────────────────────────────────┐
           │ Calculate FFT of excitation and response │
           │ (FFT_e and FFT_r)                         │
           └────────────────────────────────────────┘
                              │
                              ▼
      ┌──────────────────────────────────────────────────────────┐
      │ Keep the first (Num/2+1) FFT elements and truncate the rest │
      │ (FFT_e=FFT_e(1:Num/2+1) and FFT_r=FFT_r(1:Num/2+1))         │
      └──────────────────────────────────────────────────────────┘
                              │
                              ▼
          ┌──────────────────────────────────────────────┐
          │ Scale: divide all the elements by FFT size      │
          │ (FFT_e=FFT_e/Num and FFT_r=FFT_r/Num)           │
          └──────────────────────────────────────────────┘
                              │
                              ▼
   ┌────────────────────────────────────────────────────────────────┐
   │ Fold: leave the first element unchanged and multiply all the      │
   │ other elements by 2                                                │
   │ (FFT_e(2:end)=FFT_e(2:end)×2 and FFT_r(2:end)=FFT_r(2:end)×2)      │
   └────────────────────────────────────────────────────────────────┘
                              │
                              ▼
          ┌──────────────────────────────────────────────┐
          │ Calculate the magnitudes of the complex spectra │
          │ (mFFT_e=abs(FFT_e) and mFFT_r=abs(FFT_r))       │
          └──────────────────────────────────────────────┘
                              │
                              ▼
              ┌──────────────────────────────────┐
              │ Calculate the FRF magnitudes       │
              │ (mFRF=mFFT_r./mFFT_e)              │
              └──────────────────────────────────┘
                              │
                              ▼
┌─────────────────────────────────────────────────────────────────────┐
│ Calculate the (Num/2+1) values of frequency series from 0 to Nyquist   │
│ frequency with the step of  Δf                                         │
│ (freq=linspace(0, fNyquist, Num/2+1))                                  │
└─────────────────────────────────────────────────────────────────────┘
                              │
                              ▼
                 ┌──────────────────────────────┐
                 │ Plot FRF magnitudes graph      │
                 └──────────────────────────────┘
```

Appendix C. Numerical integration algorithm of acceleration signal

Obtain velocity and displacement data from acceleration data by Trapezoidal Rule:

$$v(n) = 0 \ (n = 1)$$
$$d(n) = 0 \ (n = 1)$$
$$v(n) = v(n-1) + \frac{a(n-1) + a(n)}{2} \cdot \Delta t \ (2 \le n \le N)$$
$$d(n) = d(n-1) + \frac{v(n-1) + v(n)}{2} \cdot \Delta t \ (2 \le n \le N)$$

Calculate coefficients p_0, p_1, q_0, q_1 and q_2:

$$\begin{bmatrix} N & \sum_{i=1}^{N} t(i) \\ \sum_{i=1}^{N} t(i) & \sum_{i=1}^{N} (t(i))^2 \end{bmatrix} \begin{Bmatrix} p_0 \\ p_1 \end{Bmatrix} = \begin{Bmatrix} \sum_{i=1}^{N} v(i) \\ \sum_{i=1}^{N} (v(i) \cdot t(i)) \end{Bmatrix}$$

$$\begin{bmatrix} N-1 & \sum_{i=1}^{N-1} t(i) & \sum_{i=1}^{N-1} (t(i))^2 \\ \sum_{i=1}^{N-1} t(i) & \sum_{i=1}^{N-1} (t(i))^2 & \sum_{i=1}^{N-1} (t(i))^3 \\ \sum_{i=1}^{N-1} (t(i))^2 & \sum_{i=1}^{N-1} (t(i))^3 & \sum_{i=1}^{N-1} (t(i))^4 \end{bmatrix} \begin{Bmatrix} q_0 \\ q_1 \\ q_2 \end{Bmatrix} = \begin{Bmatrix} \sum_{i=1}^{N-1} v(i) \\ \sum_{i=1}^{N-1} (v(i) \cdot t(i)) \\ \sum_{i=1}^{N-1} (v(i) \cdot (t(i))^2) \end{Bmatrix}$$

Calculate the trend of error for velocity:
$$v_{error} = p_1 t + p_0$$

Calculate the trend of error for displacement:
$$d_{error} = q_2 t^2 + q_1 t + q_0$$

Calculate revised velocity by subtracting the trend of error:
$$v_r = v - v_{error}$$

Calculate revised displacement by subtracting the trend of error:
$$d_r = d - d_{error}$$

Appendix D. Parameters of twenty-storey building

Table A.1 Parameters of twenty-storey building

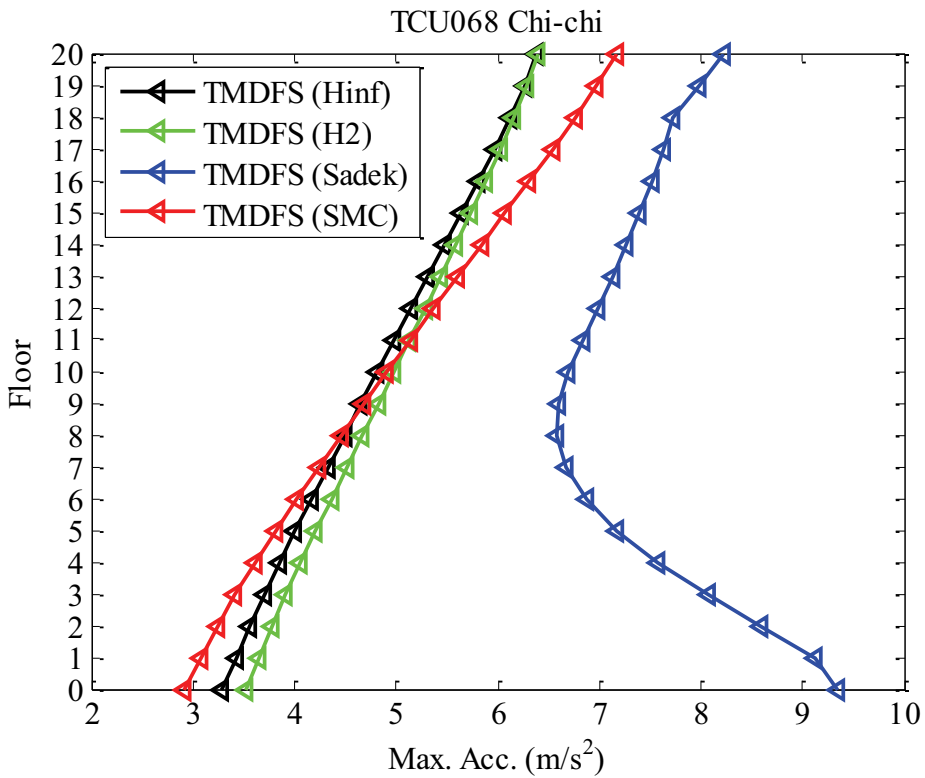| Storey	Mass [$\times 10^3$ kg]	Stiffness [$\times 10^4$ kN/m]
20th	980	34
19th	980	57
18th	980	76
17th	980	93
16th	980	109
15th	980	123
14th	980	138
13th	980	153
12th	980	167
11th	980	183
10th	980	199
9th	980	213
8th	980	228
7th	980	244
6th	980	261
5th	980	279
4th	980	303
3rd	980	332
2nd	980	368
1st	980	349

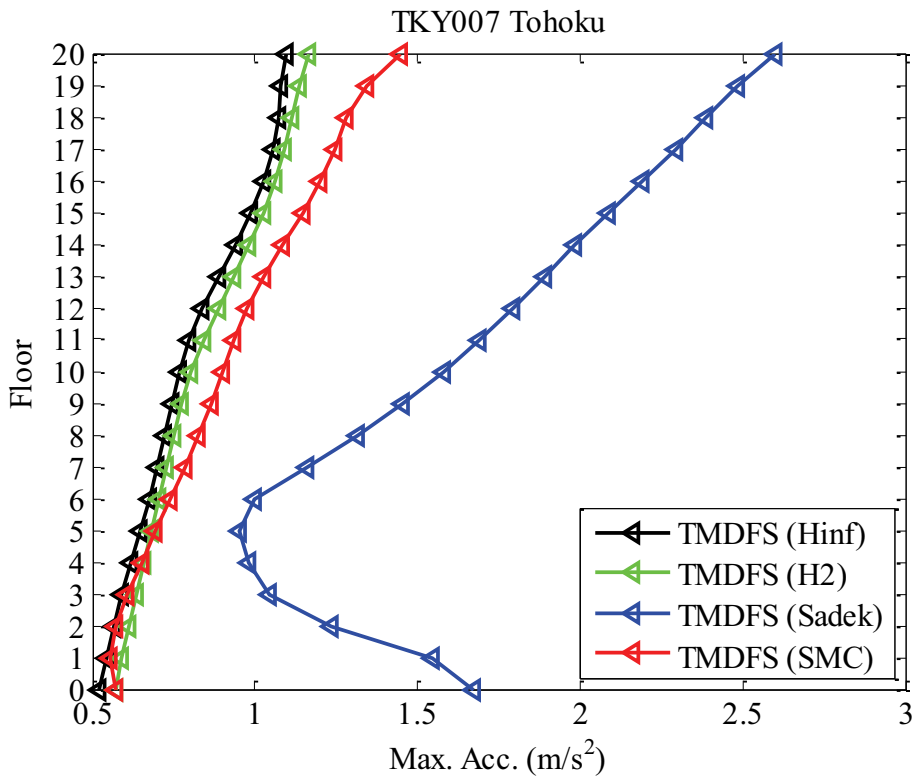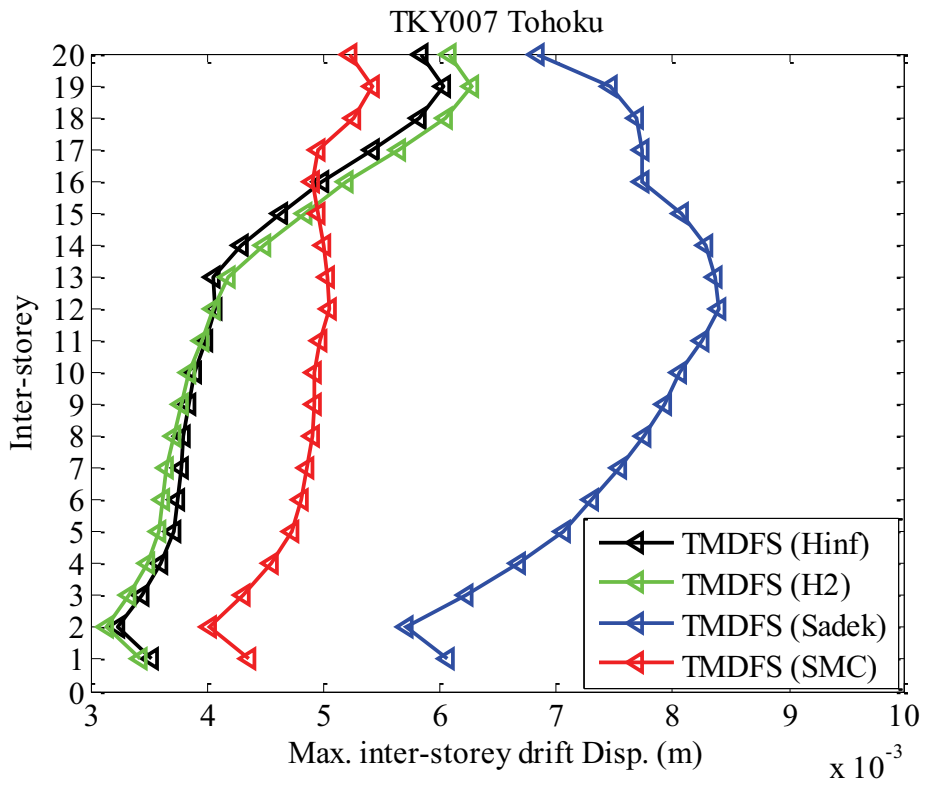**Appendix E. Peak responses of twenty-storey building in different systems**

JMA Kobe

Max. inter-storey drift Disp. (m)

JMA Kobe

Max. Acc. (m/s^2)

···◦··· un-controlled
—◁— TMDFS
- -☐- - same amount of
damping devices

208

TCU068 Chi-chi

TCU068 Chi-chi

un-controlled
TMDFS
same amount of
damping devices

209

TKY007 Tohoku

Max. inter-storey drift Disp. (m)

x 10⁻³

TKY007 Tohoku

Max. Acc. (m/s²)

- ⊙ ···· un-controlled
- ◁ — TMDFS
- ☐ --- same amount of damping devices
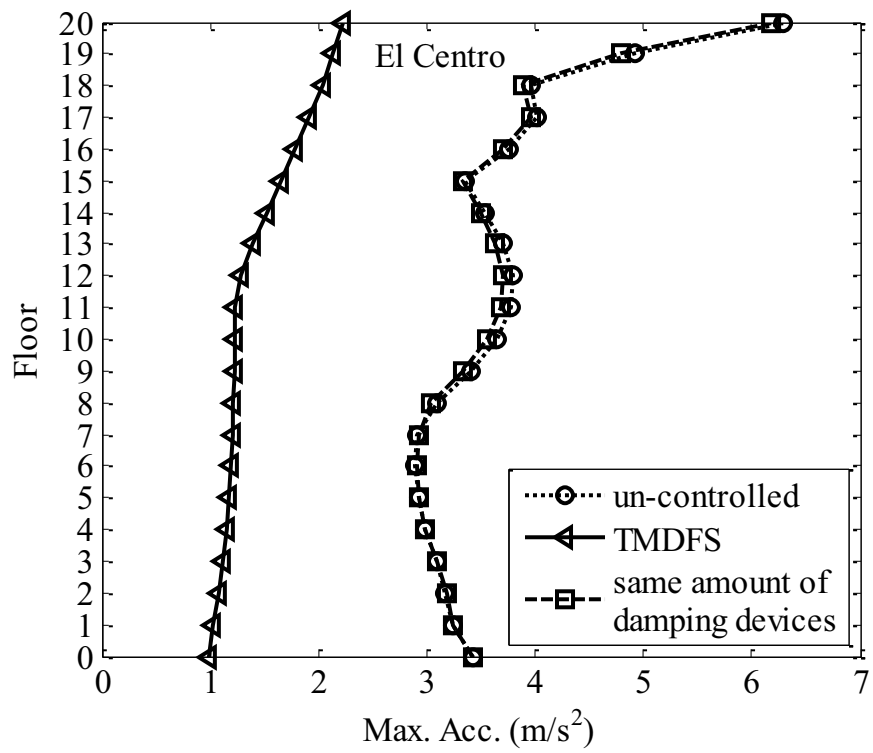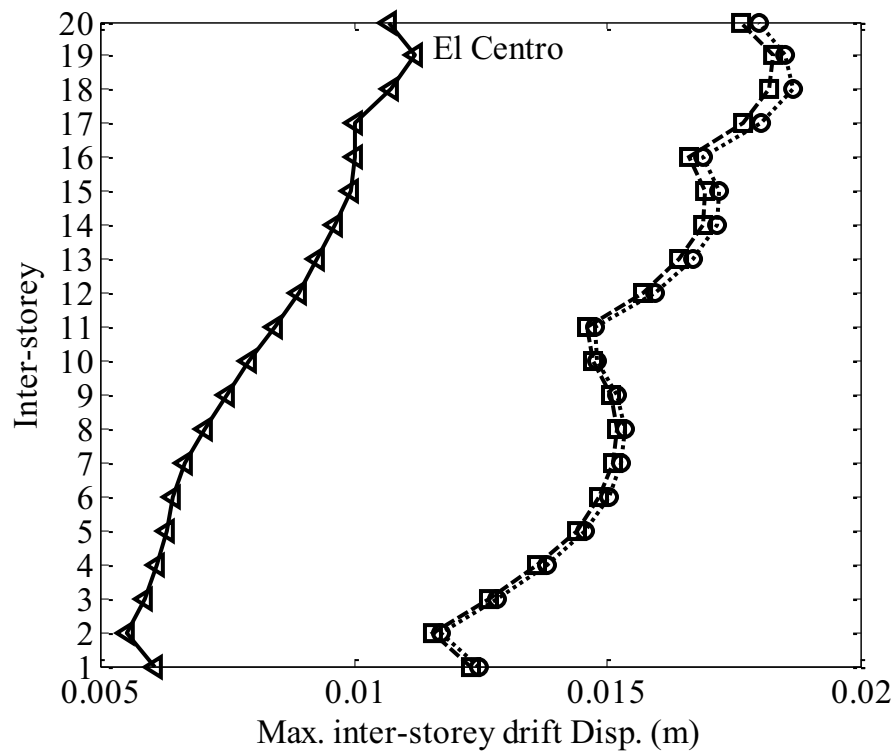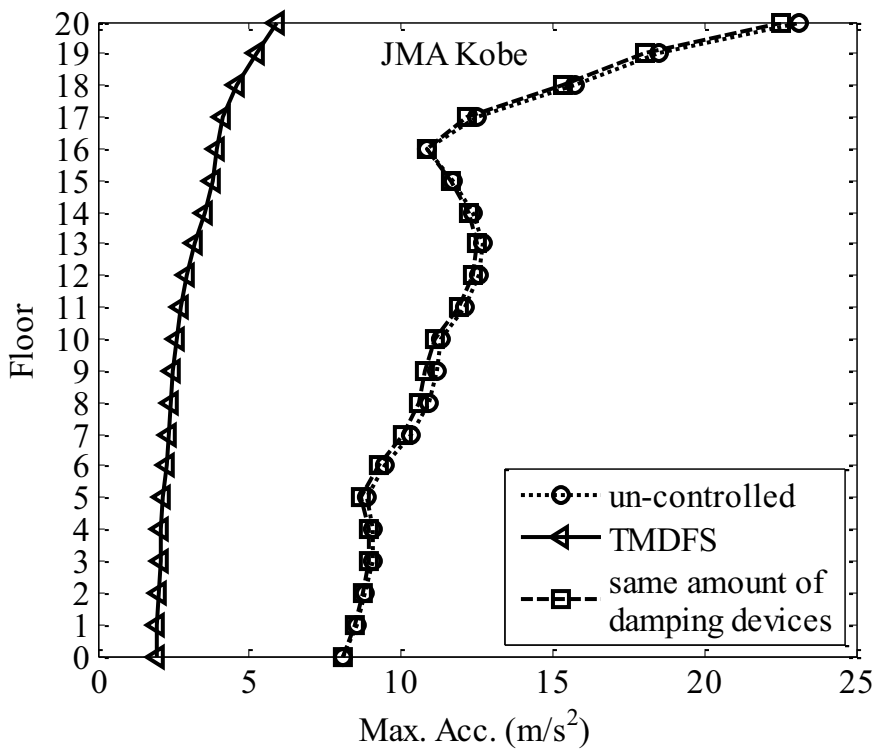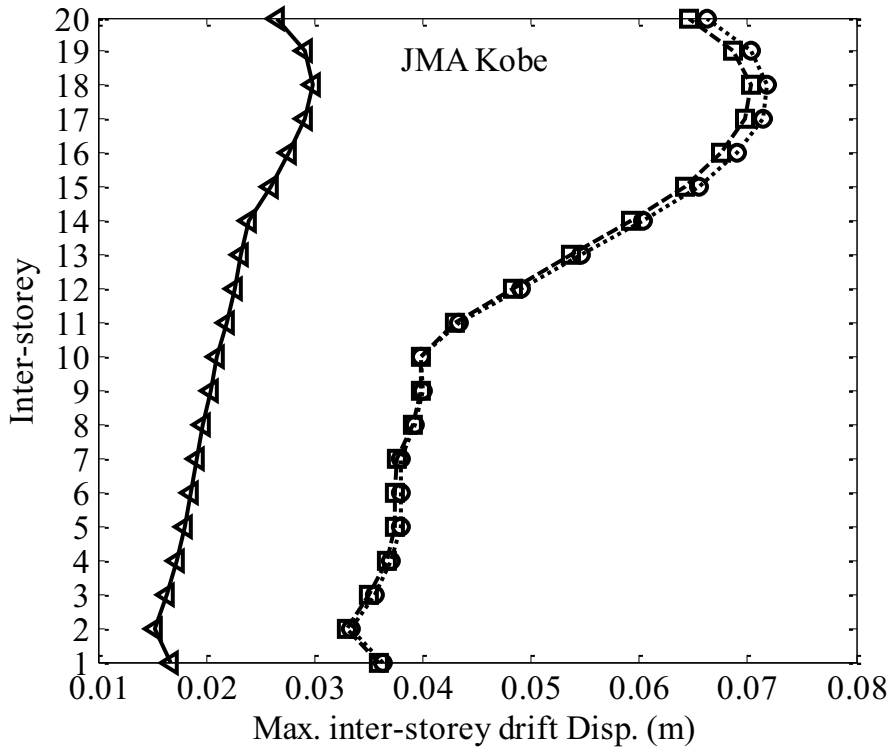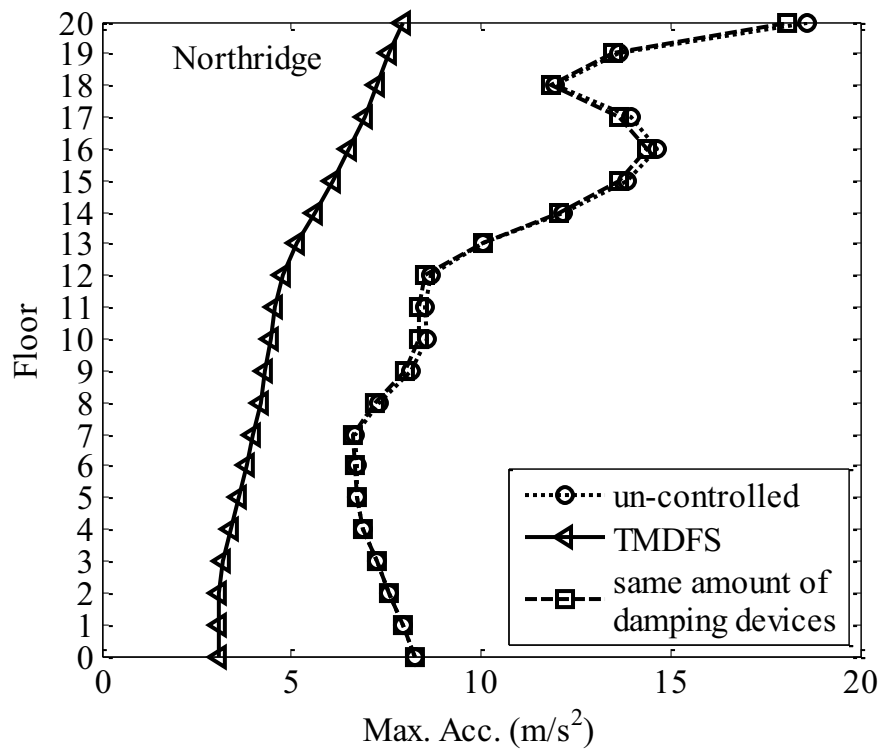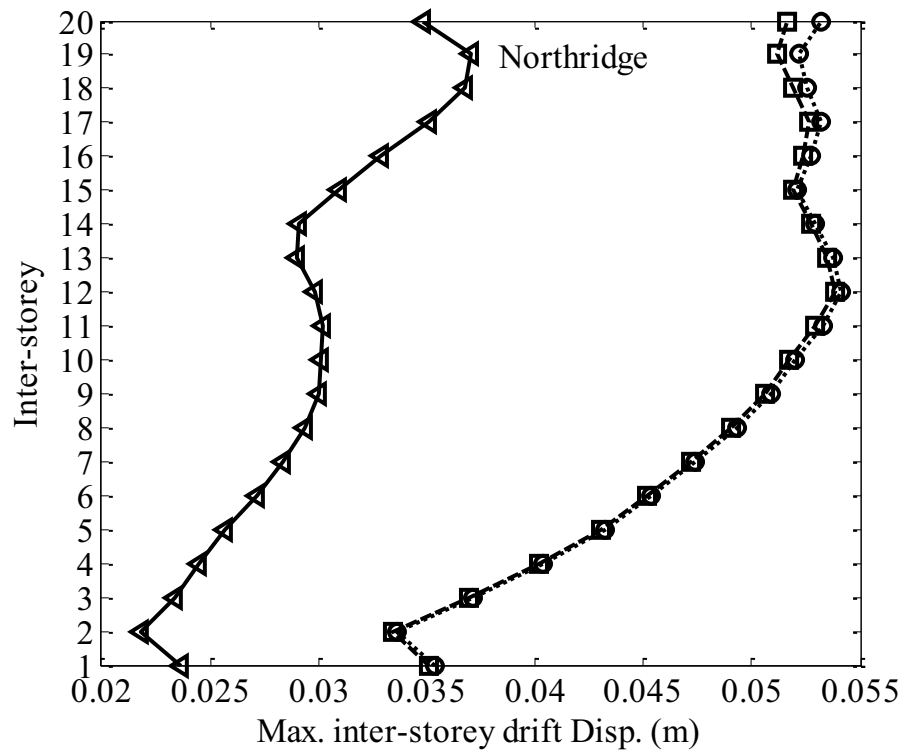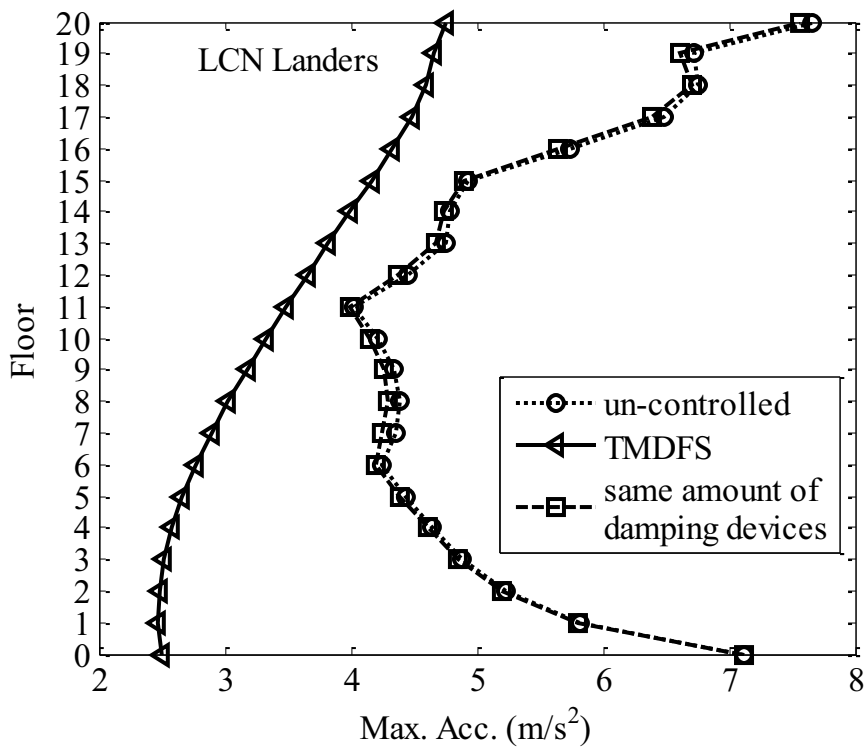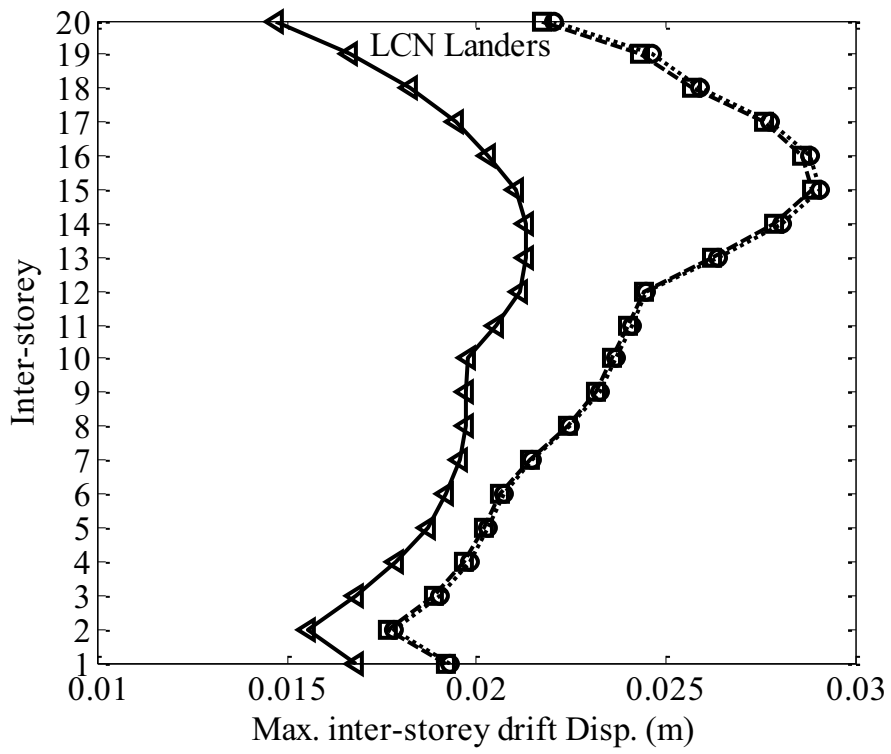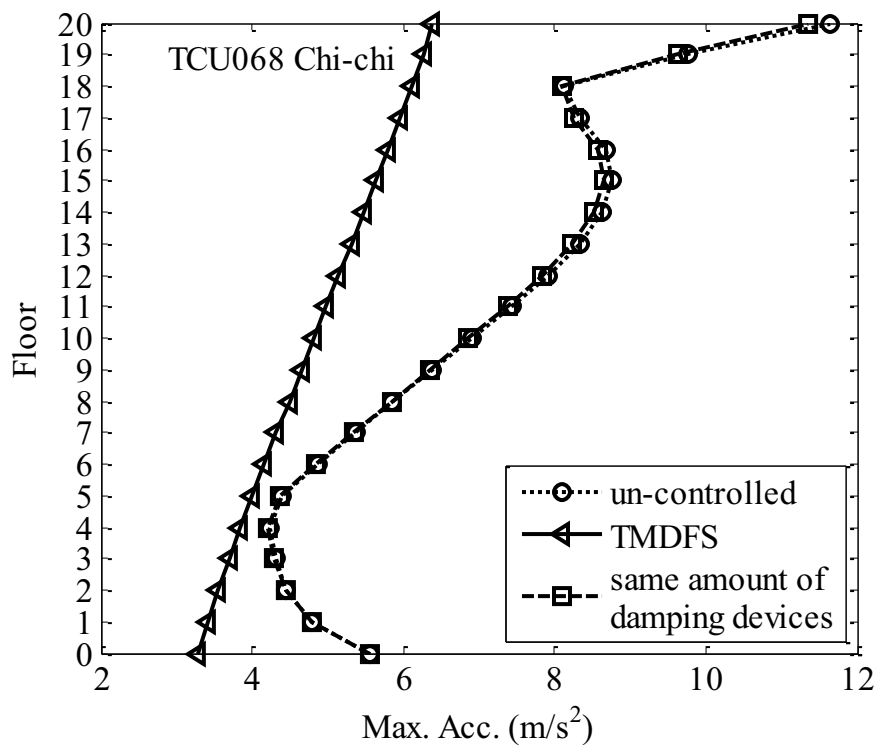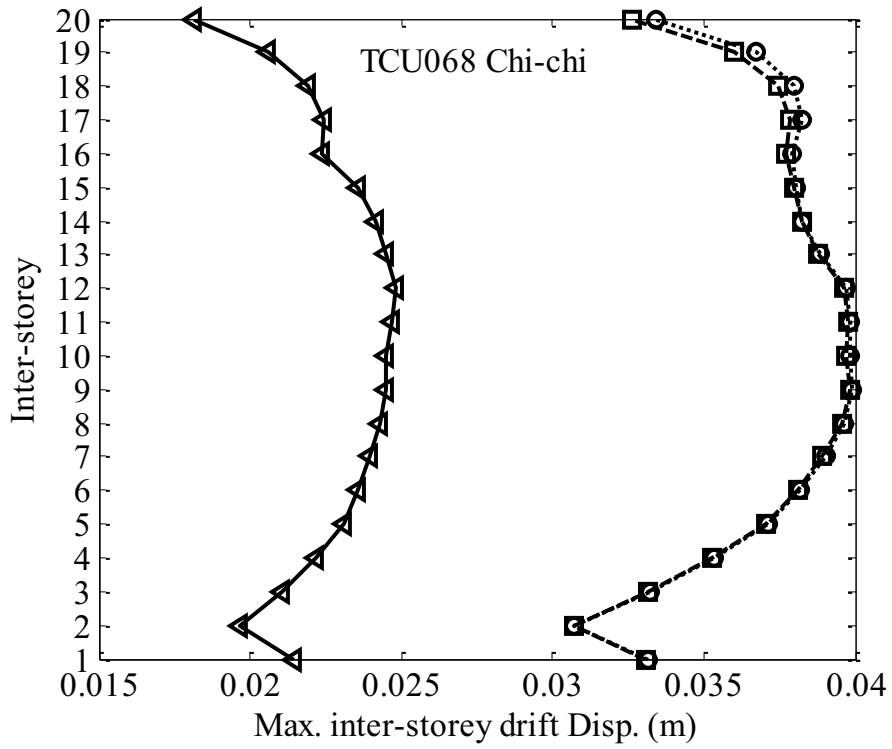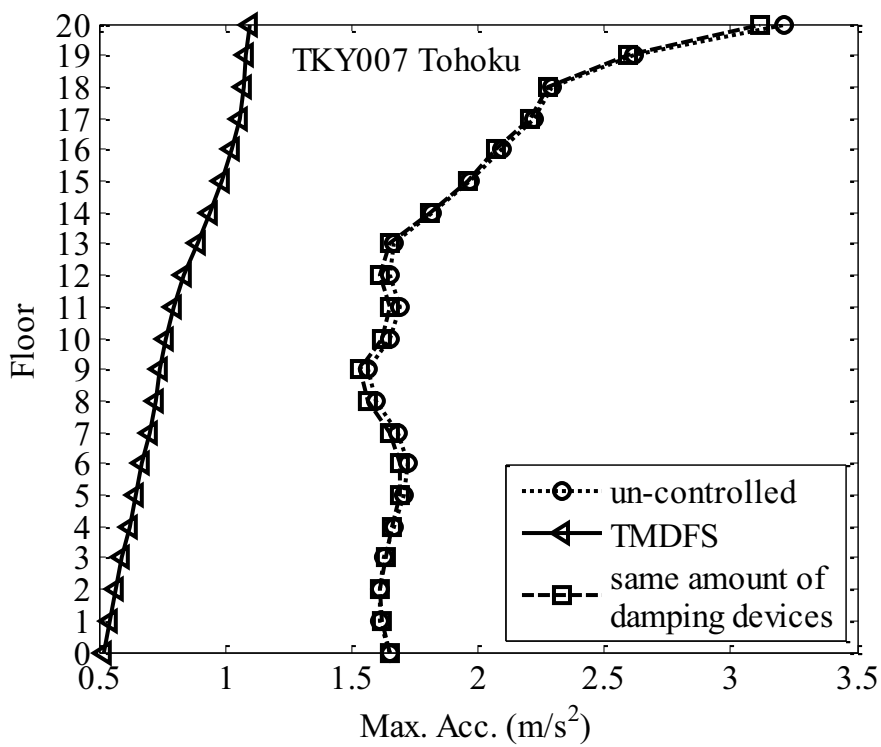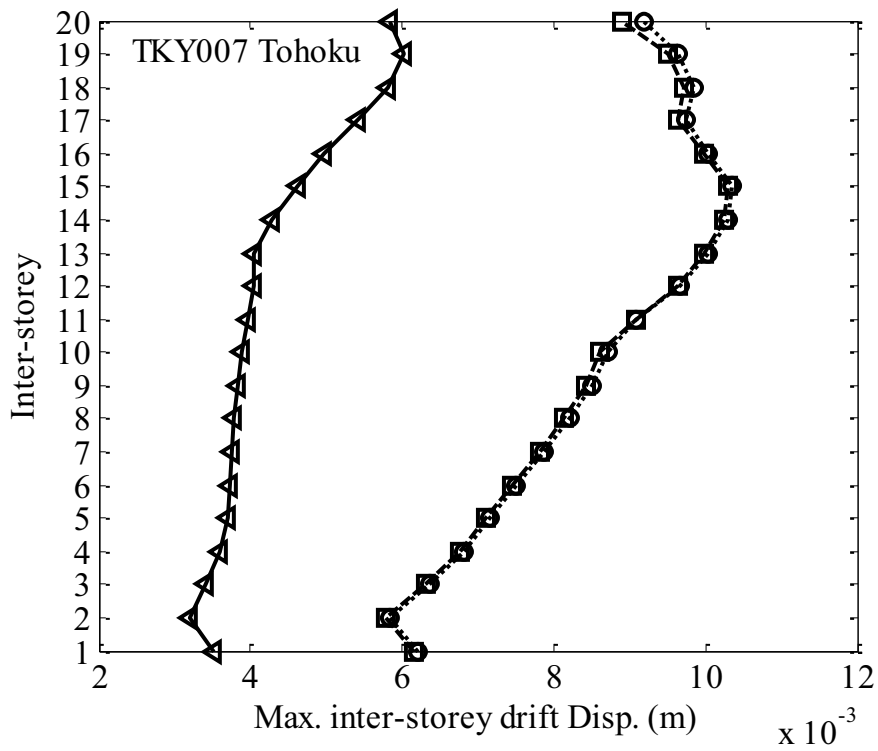
Appendix F. Free vibration responses of twenty-storey building in five systems

TCU068 Chi-chi

TCU068 Chi-chi

TKY007 Tohoku

TKY007 Tohoku
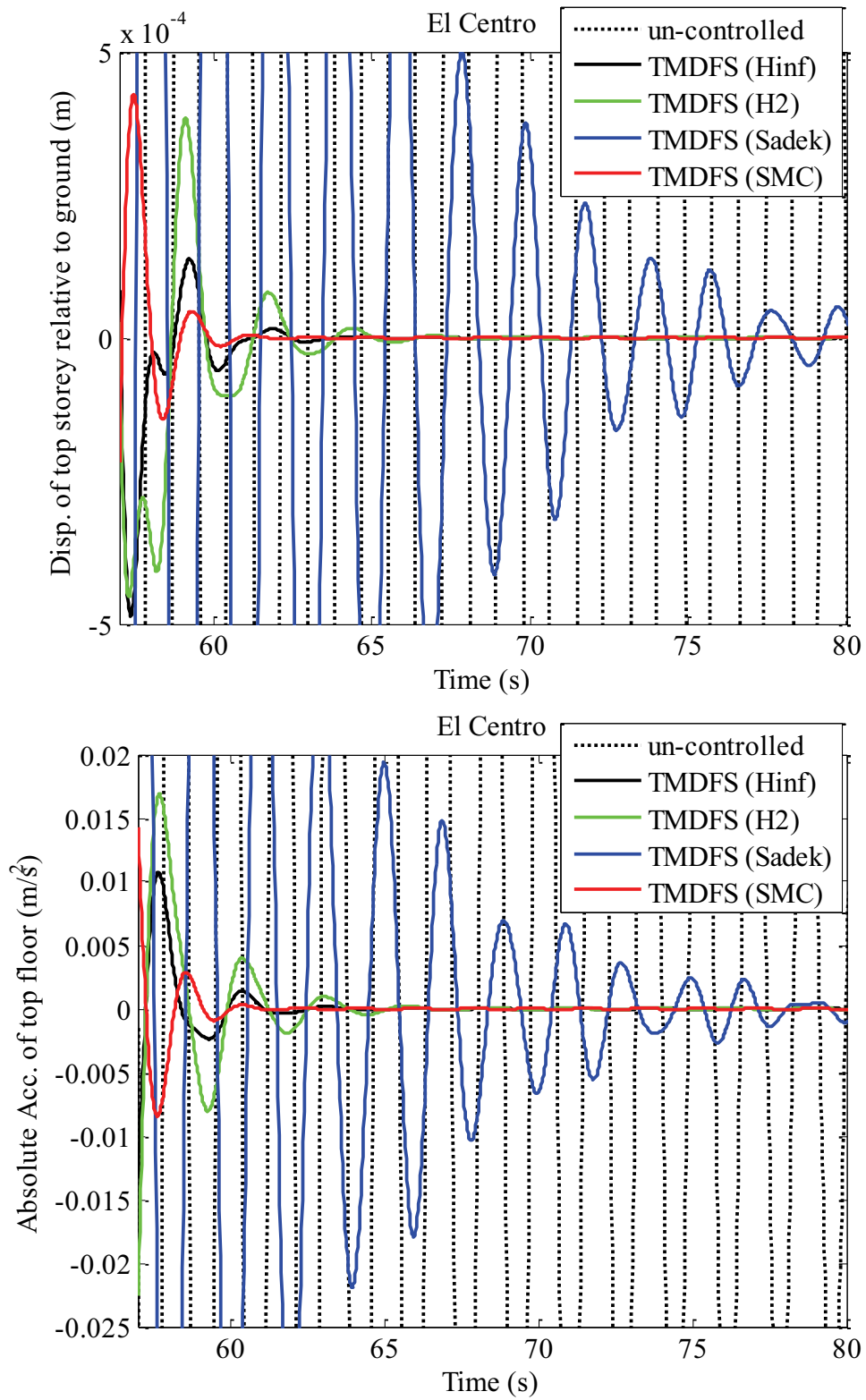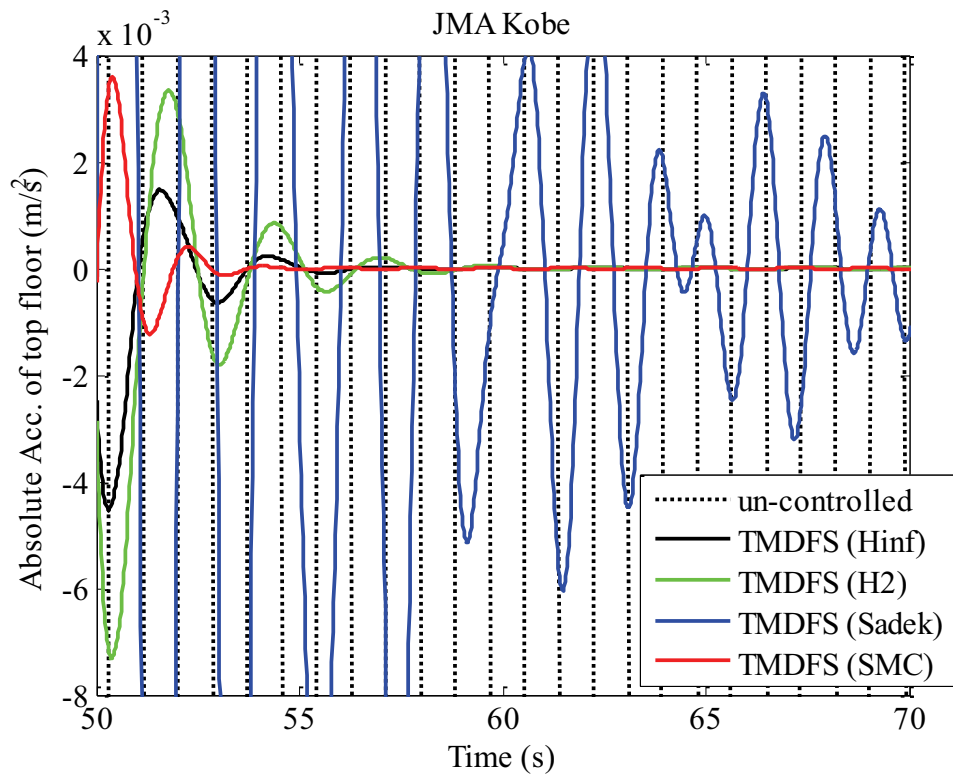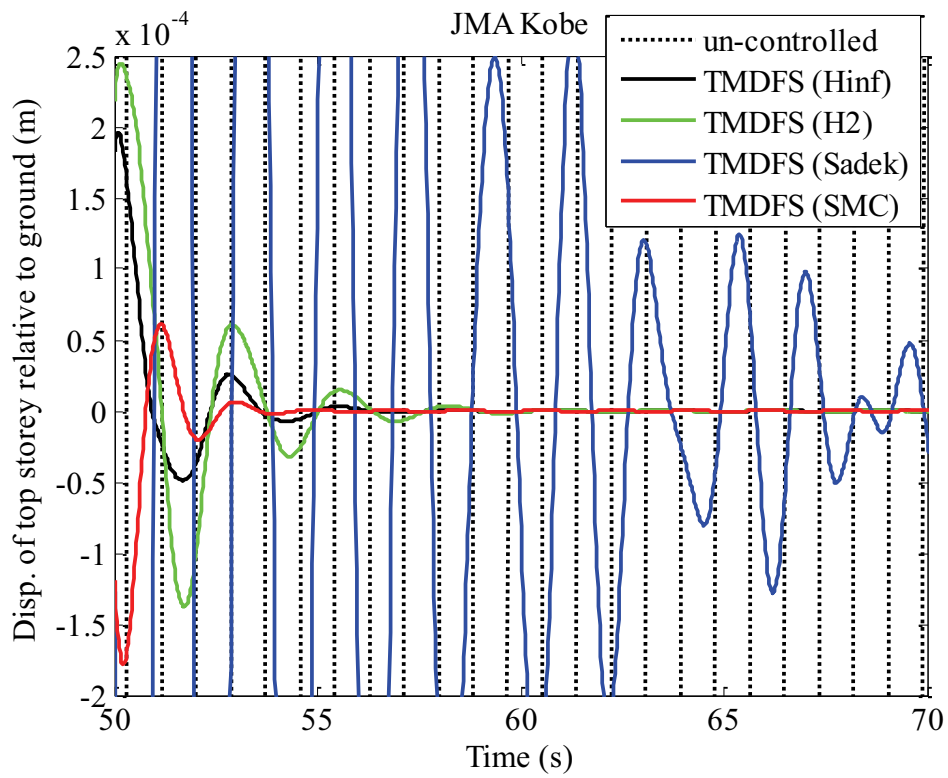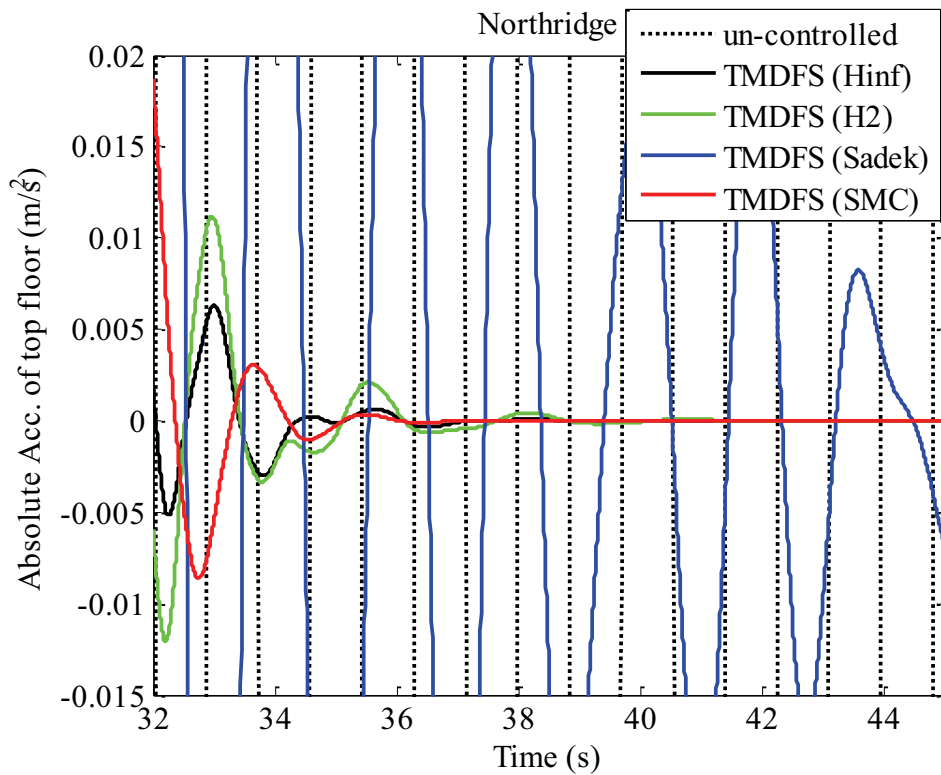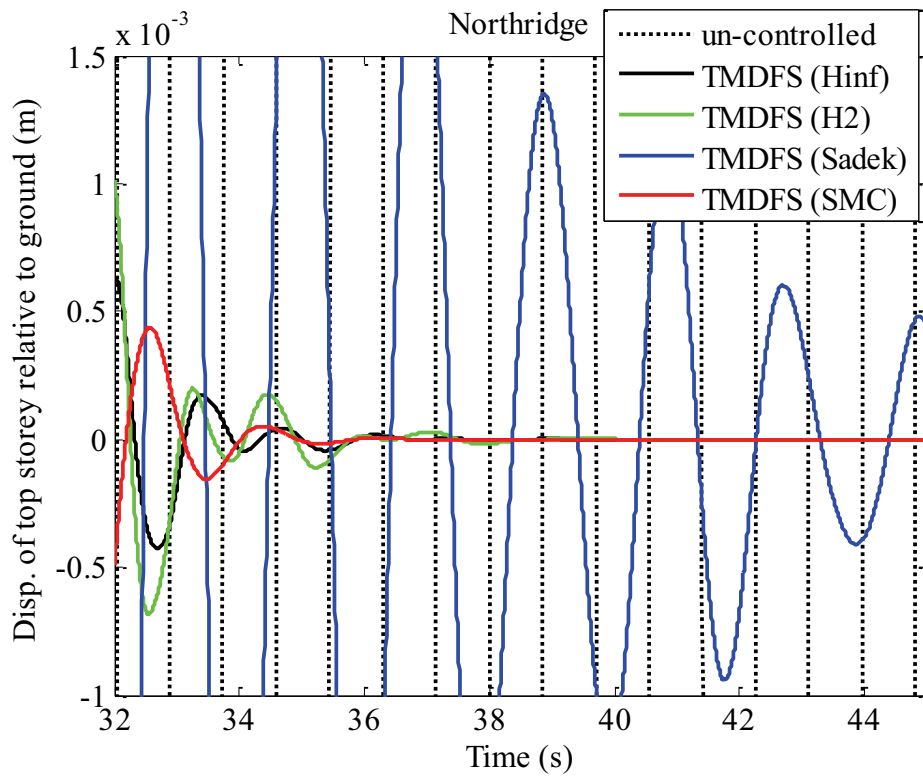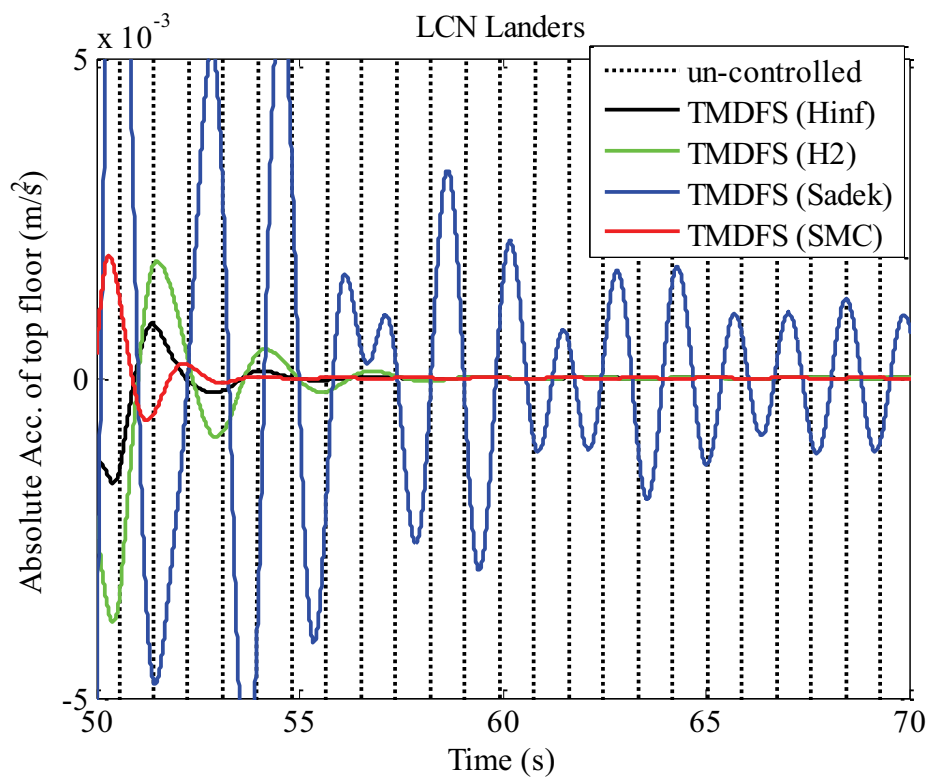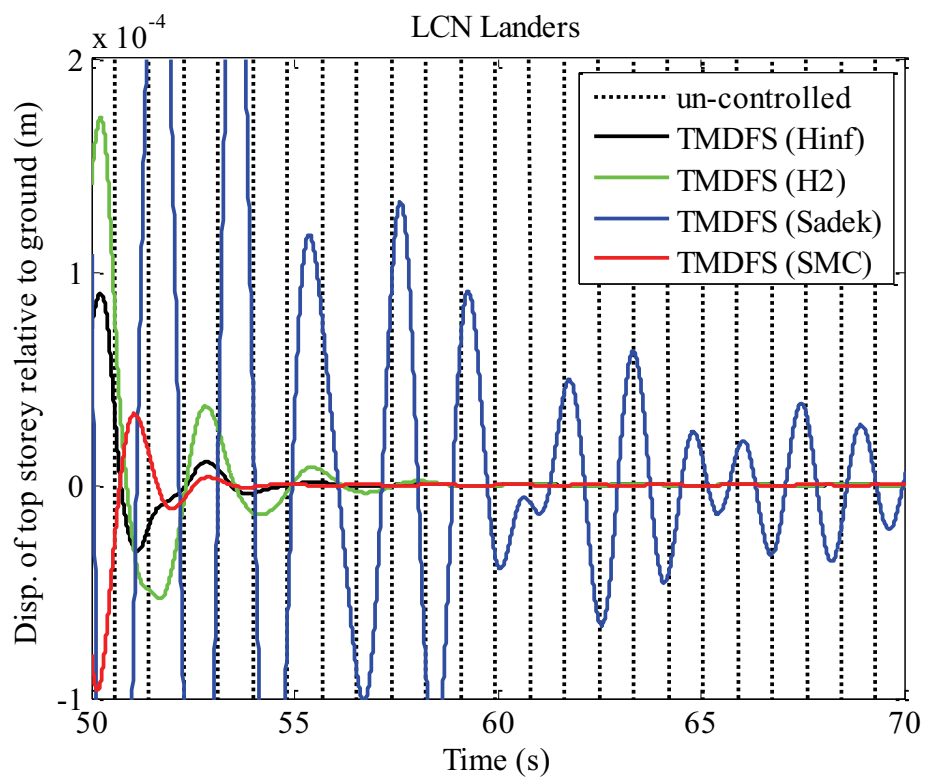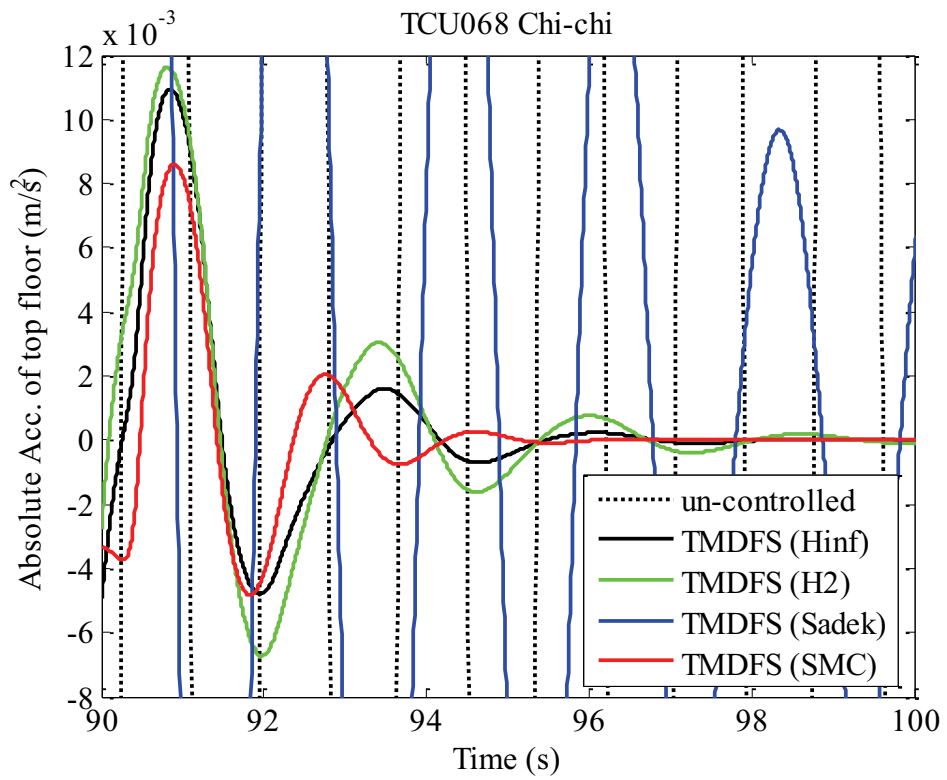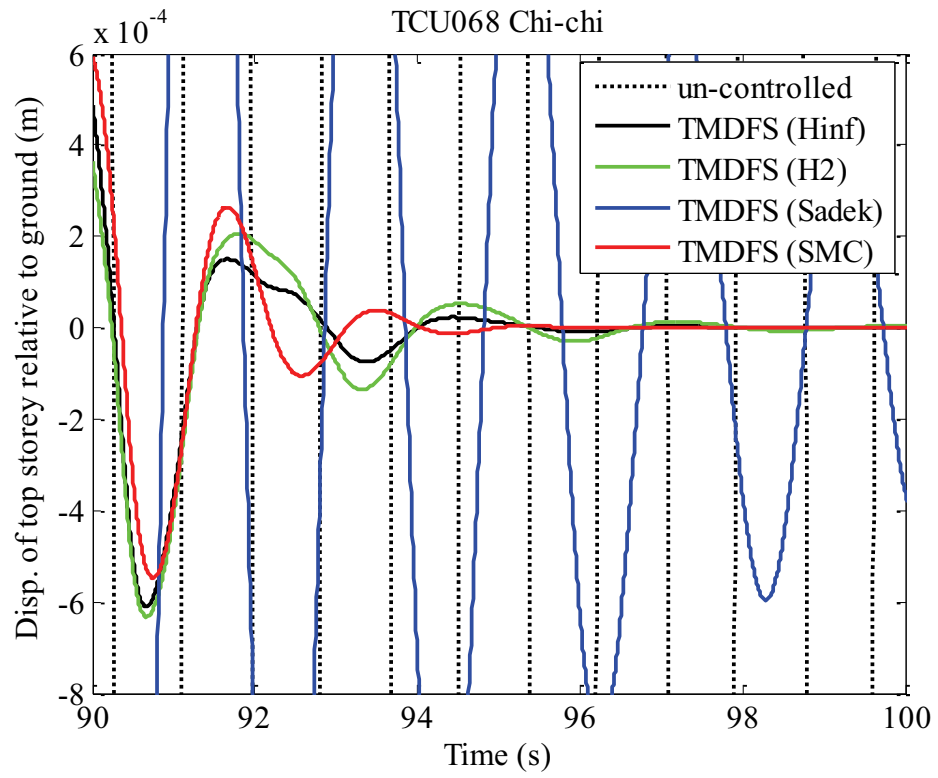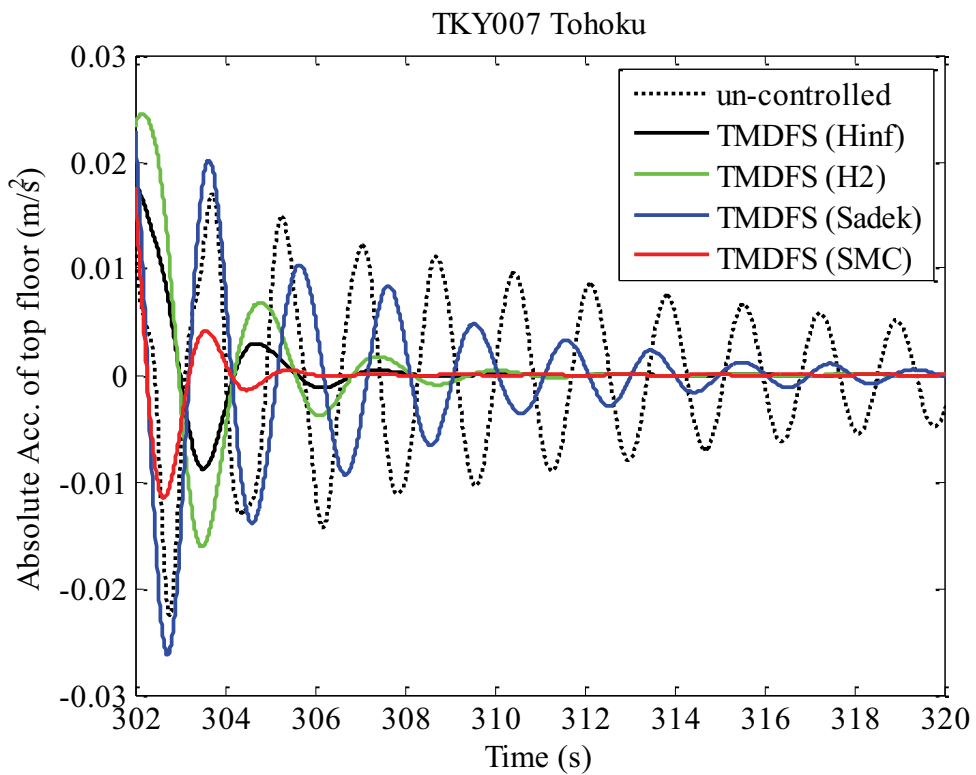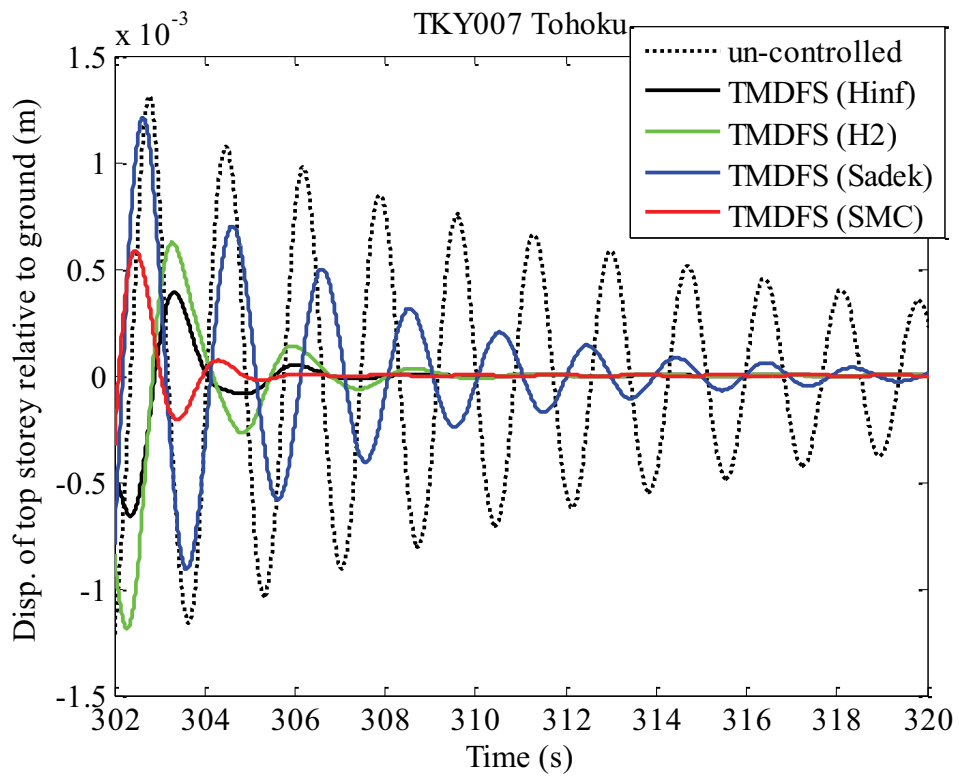
Appendix G. Maximum stroke length of TMD floors in four TMDFSs

El Centro

JMA Kobe

Northridge

LCN Landers

TCU068 Chi-chi

TKY007 Tohoku
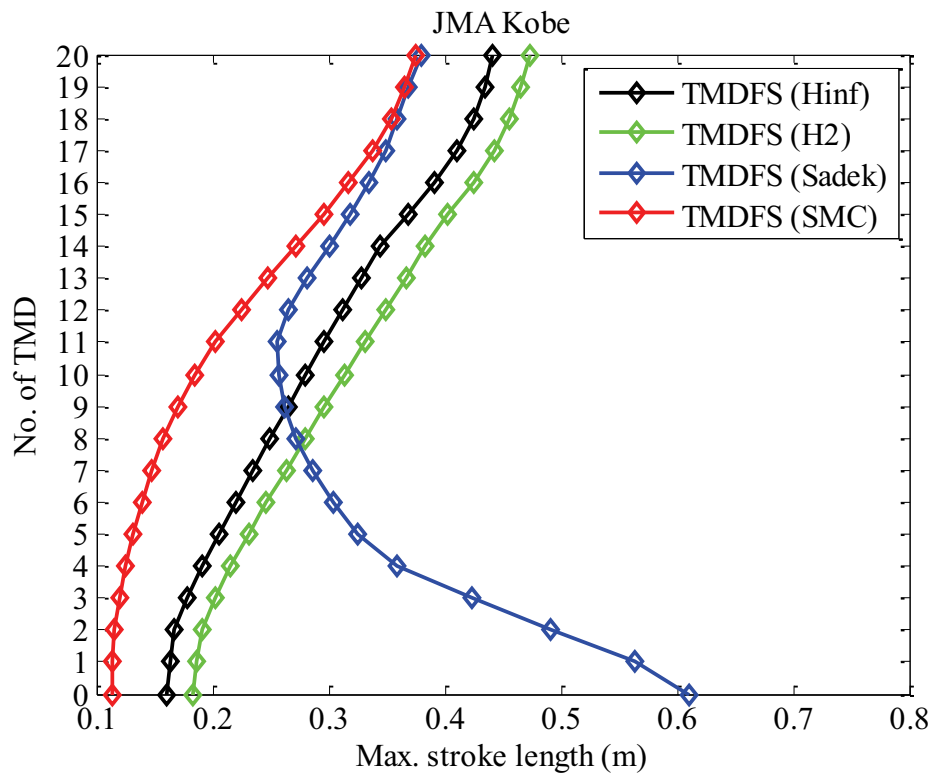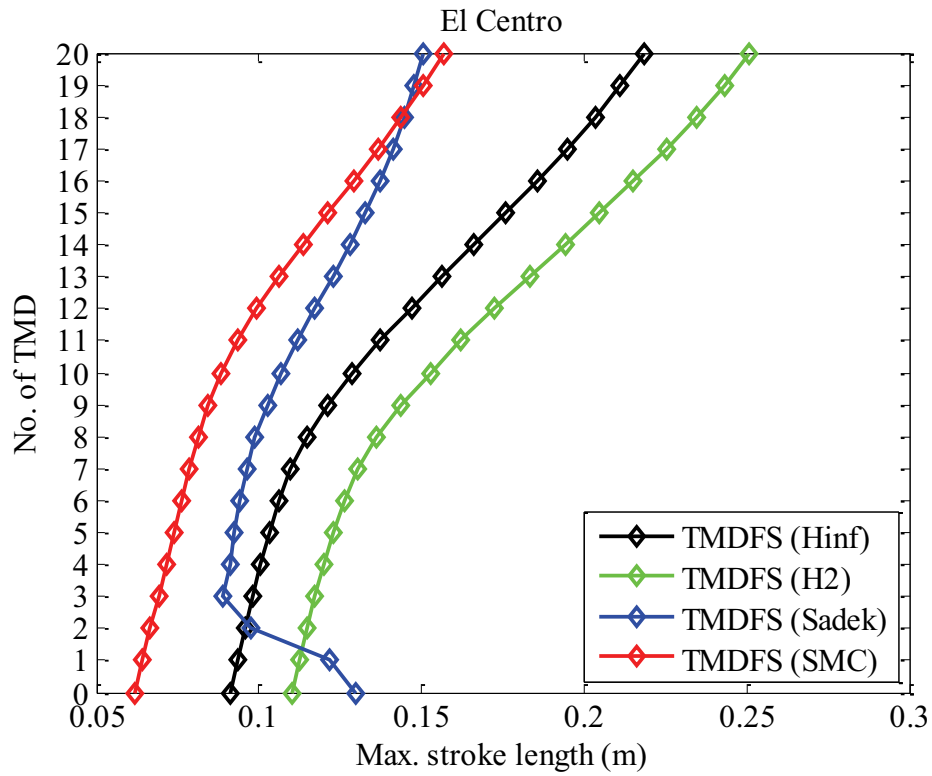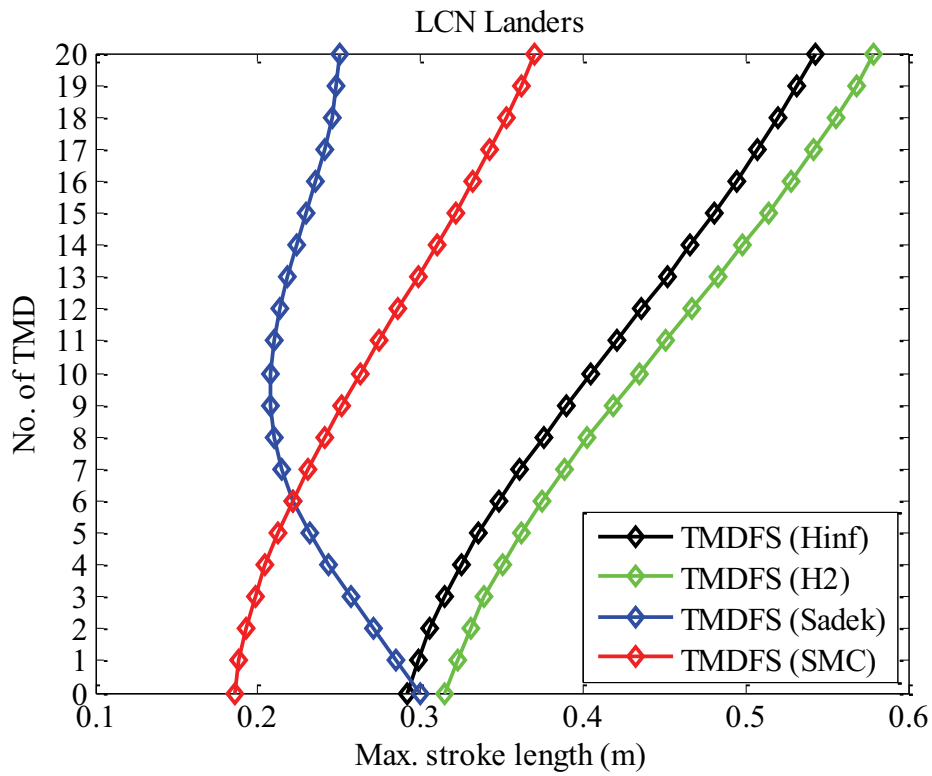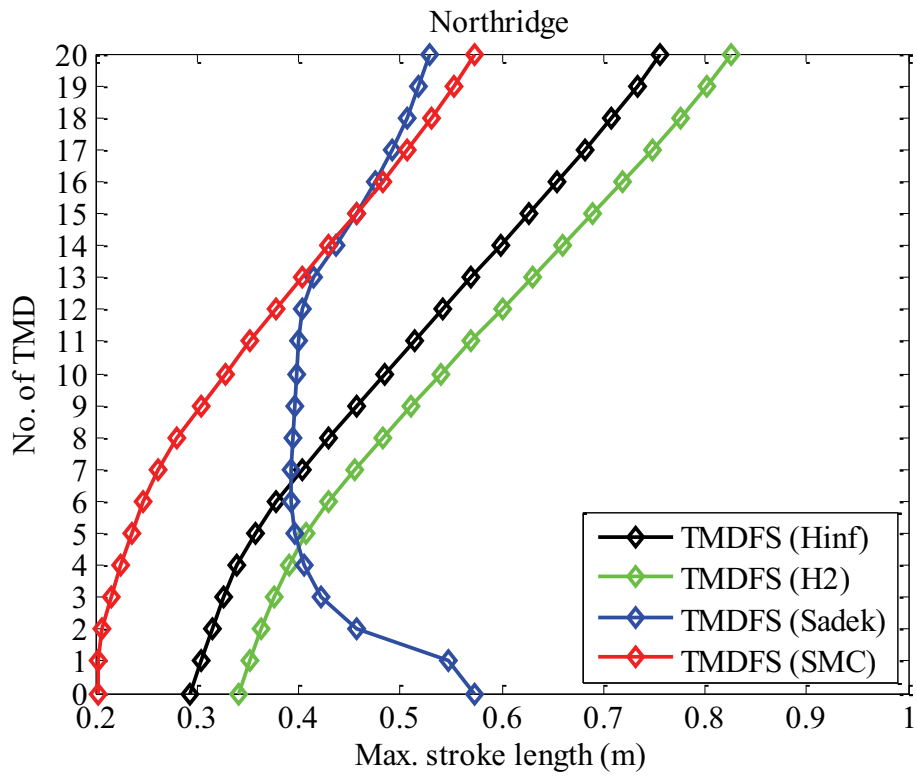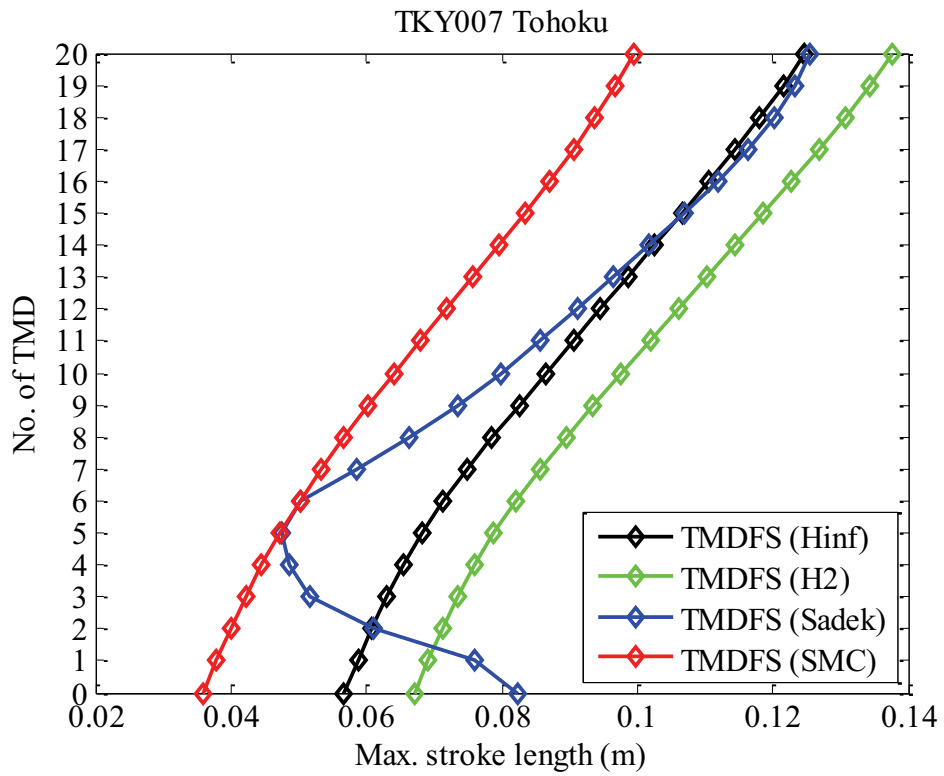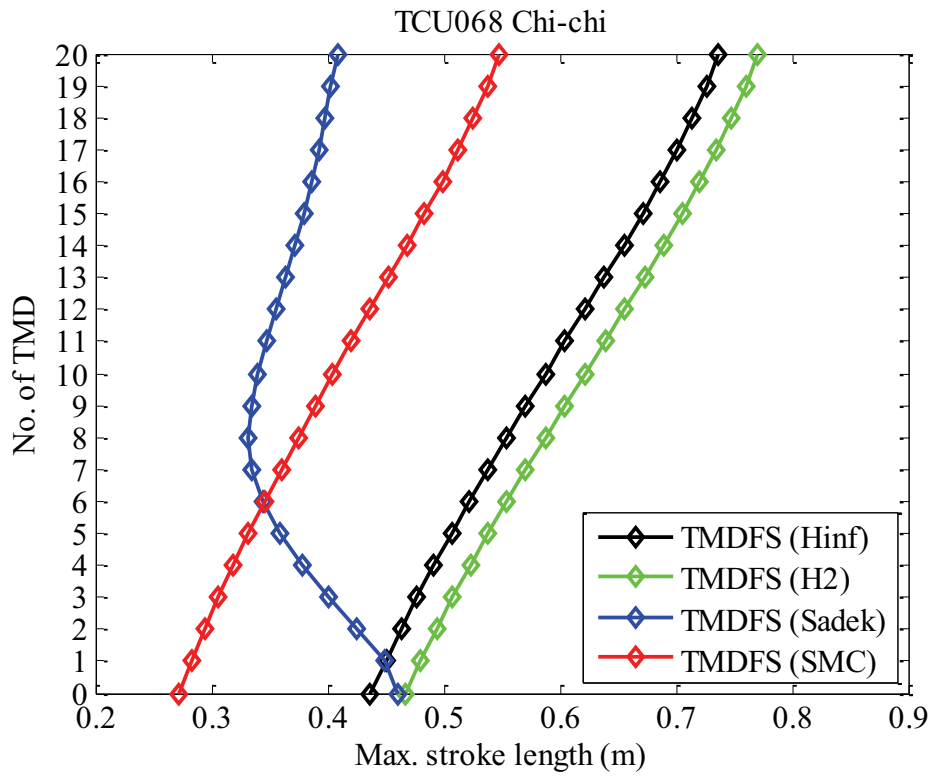
Appendix H. Peak responses of twenty-storey building in four TMDFSs

El Centro

El Centro

JMA Kobe

JMA Kobe

221

Northridge

Northridge

LCN Landers

LCN Landers

TCU068 Chi-chi

TCU068 Chi-chi

TKY007 Tohoku

TKY007 Tohoku

225

I would like to thank Professors Toshiro MAEDA, Satsuya SODA and Jun KANDA for serving on my dissertation examination committee.

Many thanks go to my parents and twin sister, for all their love, support and encouragement. Thanks also go to my friends for their support and understanding during all these years. I am also grateful to the China Scholarship Council (CSC) for the financial support of my Ph. D. study in Japan. Finally, I would like to express my love and gratitude to my husband LJ JIA for his support and understanding, and my lovely son ZY JIA for happiness he brings to my family.